
# CHARACTERISATION AND OPTIMISATION OF THE MECHANICAL PERFORMANCE OF PLANT FIBRE COMPOSITES FOR STRUCTURAL APPLICATIONS

*BY*

**DARSHIL UPENDRA SHAH**

**BENG (HONS)**

**THESIS SUBMITTED TO THE UNIVERSITY OF NOTTINGHAM**

**FOR THE DEGREE OF DOCTOR OF PHILOSOPHY**

**AUGUST 2013**

# ABSTRACT

**Characterisation and Optimisation of the Mechanical Performance of Plant Fibre Composites for Structural Applications**

***Darshil U Shah, BEng***

Plant fibres, perceived as environmentally sustainable substitutes to E-glass, are increasingly being employed as reinforcements in polymer matrix composites. However, despite the promising technical properties of cellulose-based fibres and the historic use of plant fibre composites (PFRPs) in load-bearing components, the industrial uptake of PFRPs in structural applications has been limited. In developing PFRPs whose mechanical properties are well-characterised, optimised and well-predicted, this thesis addresses the question: Can PFRPs replace E-glass composites (GFRPs) in structural applications?

Ensuring that the highest reinforcement potential is exploited, this research examines the mechanical properties of aligned PFRPs based on bast fibre yarns/rovings and thermoset matrices. Although aligned GFRPs are found to outperform aligned PFRPs in terms of absolute mechanical properties, PFRPs reinforced with flax rovings exhibit exceptional properties, with a back-calculated fibre tensile modulus of up to 75 GPa and fibre tensile strength of about 800 MPa.

To identify the processing window which produces composites with useful properties, the minimum, critical and maximum fibre volume fraction of PFRPs have been determined, and compared to that of synthetic fibre reinforced composites. The effect of fibre volume fraction on the physical and tensile properties of aligned PFRPs has also been investigated. Furthermore, micro-mechanical models have been developed and experimentally validated, to reliably predict the effect of (mis)orientation, in the forms of yarn twist/construction and off-axis loading, on the tensile properties of aligned PFRPs.

To provide a complete set of fatigue data on aligned PFRPs, the effect of various composite parameters on PFRP cyclic-loading behaviour has been illustrated through S-N lifetime diagrams. A constant-life diagram has also been generated to enable the fatigue design and life prediction of a PFRP component. At each stage, the fatigue performance of PFRPs has been compared to that of GFRPs.

Finally, in directly addressing the main theme, this thesis adopts a novel comparative case study approach to investigate the manufacture and mechanical testing of full-scale 3.5-meter composite rotor blades (suitable for 11 kW turbines) built from flax/polyester and E-glass/polyester. The study claims that under current market conditions, optimised plant fibre reinforcements are a structural, but not low-cost or sustainable, alternative to conventional E-glass reinforcements.

# ACKNOWLEDGEMENTS

The author is immensely indebted to his academic supervisors, Dr Peter Schubel, Dr Mike Clifford and Dr Peter Licence, for their guidance and support through the research degree.

The financial support of the Nottingham Innovative Manufacturing Research Centre (NIMRC) and the University of Nottingham Engineering Faculty Research Committee are gratefully acknowledged.

The author is thankful to the Faculty of Engineering and Polymer Composites Research Group (University of Nottingham) for the use of school and lab facilities. The technical support of Roger Smith, Geoffrey Tomlinson, Keith Dinsdale and Thomas Buss is gratefully acknowledged.

The author is grateful to the anonymous referees for their respective valuable comments on the manuscripts of journal papers. In addition, the author is thankful to his colleagues for their advice and assistance.

Finally, the author offers his gratitude to his family (mum, dad, Vihar) and friends who have supported and encouraged him throughout this work. In particular, the author is thankful to Krati, for her unconditional love and support at all times.

# CONTENTS

# 1 INTRODUCTION

Composites originated as biomaterials employing plant fibres as reinforcements. References have been made to the use of linen and hemp textiles as reinforcements of ceramics as early as 6500 BC [1]. The Egyptians have also been known to use grass and straw as reinforcing fibres in mud and clay bricks for the building of walls over 3000 years ago [2]. While synthetic fibres, specifically E-glass, dominate today's FRP market [3], awareness of the scarcity of non-renewable resources and a demand for environmental sustainability have led to a renewed and ever-increasing interest in biocomposites. This is reflected by the increasing number of publications on biocomposites during recent years, including books [1, 2, 4-7] and review articles [8-21].

Plant fibres, such as flax, sisal and bamboo, offer several economical, technical and ecological advantages over synthetic fibres in reinforcing polymer composites (Table 1.1). The wide availability, low cost, low density, high specific properties and eco-friendly image of plant fibres has portrayed them as prospective substitutes to traditional composite reinforcements, specifically E-glass [8, 22-26]. As 87% of the 8.7 million tonne global FRP market is based on E-glass composites (GFRPs) [3], plant fibres and their composites have a great opportunity for market capture.

Although the use of plant fibres (non-wood and non-cotton) in reinforced plastics has tripled to 45,000 tonnes over the last decade [1, 11, 25], plant fibre composites (PFRPs) make up only ~1.9% of the 2.4 million tonne EU FRP market (Fig. 1.1) [25]. Notably, the use of carbon fibre composites, globally and in the EU, is lower than the use of biocomposites and on the same level as the use of PFRPs (Fig. 1.1) [3, 25]. It is of interest to note that while PFRPs were developed and are viewed as alternatives to GFRPs [8, 26], they have mainly replaced wood fibre reinforced thermosets in the EU automotive industry [27, 28]. Up to 30% of these PFRPs are based on thermoset matrices, while the rest are based on thermoplastic matrices (Fig. 1.1) [27].

**Table 1.1. Comparison between plant and synthetic fibres [8, 23, 26, 29-31].**

| | Properties | Plant Fibres [a] | Glass Fibres [b] | Carbon Fibres [c] |
|---|---|---|---|---|
| Economy | **Annual global production [tonnes]** [d] | 31,000,000 | 4,000,000 | 55,000 |
| | **Distribution for FRPs in EU [tonnes]** [d] | Moderate (~60,000) | Wide (600,000) | Low (15,000) |
| | **Cost of raw fibre [£/kg]** | Low (~0.5-1.5) | Low (~1.3-20.0) | High (>12.0) |
| Technical | **Density [gcm$^{-3}$]** | Low (~1.35-1.55) | High (2.50-2.70) | Low (1.70-2.20) |
| | **Tensile stiffness [GPa]** | Moderate (~30-80) | Moderate (70-85) | High (150-500) |
| | **Tensile strength [GPa]** | Low (~0.4-1.5) | Moderate (2.0-3.7) | High (1.3-6.3) |
| | **Tensile failure strain [%]** | Low (~1.4-3.2) | High (2.5-5.3) | Low (0.3-2.2) |
| | **Specific tensile stiffness [GPa/gcm$^{-3}$]** | Moderate (~20-60) | Low (27-34) | High (68-290) |
| | **Specific tensile strength [GPa/gcm$^{-3}$]** | Moderate (~0.3-1.1) | Moderate (0.7-1.5) | High (0.6-3.7) |
| | **Abrasive to machines** | No | Yes | Yes |
| Ecological | **Energy demand of raw fibre [MJ/kg]** | Low (4-15) [e] | Moderate (30-50) | High (>130) |
| | **Renewable source** | Yes | No | No [f] |
| | **Recyclable** | Yes | Partly | Partly |
| | **Biodegradable** | Yes | No | No |
| | **Hazardous/toxic (upon inhalation)** | No | Yes | Yes |

[a] Includes bast, leaf and seed fibres, but does not include wood and grass/reed fibres.

[b] Includes E- and S-glass fibres.

[c] Includes PAN- and pitch-based carbon fibres.

[d] Estimated values for the year 2010, from [32] for global fibre production values and from [24, 25, 27] for values on the distribution of fibres for FRPs in EU.

[e] While the energy required in the cultivation of plant fibres is low (4-15 MJ/kg), further processing steps (*e.g.* retting and spinning) can significantly increase the cumulative energy demand, for instance, to up to 146 MJ/kg for flax yarn [10].

[f] Carbon fibres based on cellulosic precursors currently account for only 1-2% of the total carbon fibre market [33].

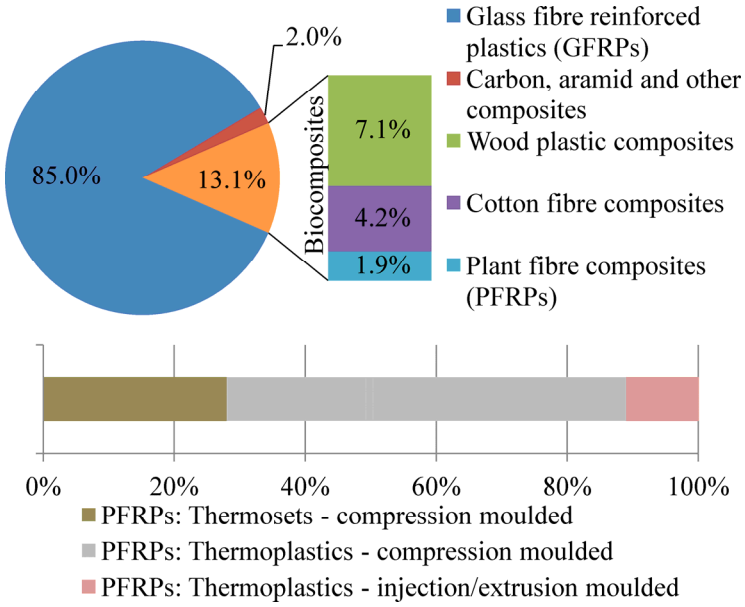


**Fig. 1.1. PFRPs, primarily manufactured via compression moulding, account for only ~1.9% of the 2.4 million tonne EU FRP market in 2010 [25, 27].**

By commercial application, over 95% of PFRPs produced in the EU are used for non-structural automotive components, which are manufactured primarily via compression moulding [10, 25, 27]. Other than automotive applications (for interior components such as door and instrumental panels) [1, 25, 31, 34], PFRPs are being considered for applications in:

*i)* construction and infrastructure (such as beams, roof panels, bridges) [1, 20, 21, 34-40],

*ii)* sports and leisure (for boat hulls, canoes, bicycle frames, tennis rackets) [1, 21, 27, 34, 36, 40],

*iii)* furniture and consumer goods (such as packaging, cases, urns, chairs, tables, helmets, ironing boards) [1, 21, 25, 27, 34, 36-40],

*iv)* pipes and tanks (for water drainage/transportation) [1, 14, 34, 35, 39-41], and

*v)* small-scale wind energy (as rotor blade materials) [42-46].

In many of these applications, plant fibres are being employed primarily as light, cheap and 'green' reinforcements, playing little or no structural role. Interestingly, this is different to what was envisaged in the mid-twentieth century, when the potential of plant fibres as structural reinforcing agents was acknowledged by

pioneers like Ford to manufacture the first 'green car' with an all-plastic-body using 70 wt% lignocellulosic fibres [47]. Ford was even able to demonstrate the strength and impact resistance of the material by famously taking a sledgehammer onto the car's deck lid [47]. At the same time, Aero Research Ltd developed Gordon Aerolite, a flax/phenolic composite, to replace light-alloy sheets for building the structural members of Spitfire fuselages for British military aircrafts during the Second Great War [48]. With Britain facing potential shortages of aluminium, Gordon Aerolite was then the most promising material for aircraft [48]. Furthermore, the structural potential of plant fibres is revealed by the fact that bast fibres (like flax, hemp and jute) are high in cellulose content (~60-80% of the dry chemical composition [22]) and native cellulose has remarkable tensile stiffness (138 GPa) and strength (>2 GPa) [1, 49, 50]. Therefore, investigating and eventually promoting the potential use of plant fibres in load-bearing composite components, as a possible replacement to E-glass, is a natural step ahead.

## 1.1 DESIGNING PFRPS FOR STRUCTURAL APPLICATIONS

While structural composites are required to sustain external loads in addition to self-support (like the shear web of a wind turbine blade) or play a principal role in supporting the structure of the final component (like the airframe of an aircraft), non-structural composites are primarily for aesthetic purposes enduring minimal loads (like the interior panels of a car). Hence, the 'make-up', that is the design and construction, of structural and non-structural composites is different.

One of the many advantages of composite materials, in general, is the possibility of tailoring material properties to meet different requirements. It is well-known that the macro-mechanical behaviour of heterogeneous FRPs depends on many factors; including the stress-strain behaviour of each phase (that is, the fibre and the matrix), the volumetric composition, the geometrical structure and arrangement of the phases, and the interface properties [51].

While the EU automotive industry has principally focussed on three bast fibres, namely flax, jute and hemp, for PFRP production [10, 11, 25, 52], noting their regional availability, other fibres like sisal [13], bamboo [53], cotton [54], coir [55]

and even banana leaf [56] have been shown to be suitable for such non-structural applications. However, as bast fibres themselves play a structural role in a plant, their morphology and mechanical properties make them most suitable for load-bearing applications. Bast fibres are abundant [15], producible with low environmental footprint [5], and due to their textile applications are readily available in the forms of semi-finished products (yarns/rovings, mats and aligned fabrics) [5]. In addition, as the fibre extraction processes for bast fibres for composites applications have been the subject of several studies (such as [1, 57-59]), advancements have been made to produce fibres with high aspect ratios, fewer defects and better mechanical properties. Therefore, this study employs bast fibres for PFRP manufacture. Being of natural origin, the properties of plant fibres are variable and inconsistent. On the other hand, structural components need to have highly controlled properties. Hence, it is necessary to consider the effect of bast fibre type on PFRP mechanical properties and to specifically investigate whether employing such fibres in the forms of yarns and fabrics could enable the production of PFRPs with consistent quality.

Currently, both thermosets and thermoplastics are used with plant fibres [27]. However, there is a general trend, particularly in the automotive industry, of diminishing use of thermoset matrices and increased use of thermoplastic matrices [3, 25, 27]. This is primarily because the latter are faster to process, are fabricated by a cleaner process (dry systems with no toxic by-products), are easier to recycle, and are less expensive (for high volume production). However, thermosets are high-performance matrices (due to the formation of a large cross-linked rigid three-dimensional molecular structure upon curing), form a better interface with hydrophilic plant fibres, have low processing temperatures and have low viscosities allowing manufacture with liquid composite moulding (LCM) processes, which are more suitable for larger geometrically-intricate components (like wind turbine blades). It should be noted that in terms of end-of-life disposal, the use of thermosetting matrices, rather than thermoplastic matrices, does not necessarily lower the eco-performance of the PFRP produced. This is because the addition of plant fibres can significantly reduce the recyclability and reusability of a thermoplastic system [10, 15, 60]. All PFRPs can be incinerated for energy recovery

or re-used as fillers; the additional option with thermoplastic-based PFRPs is that they can also be granulated and re-processed into extrusion/injection moulded components [10]. Notably, thermoplastic-based PFRPs that are recycled by remoulding into new parts exhibit severely deteriorated mechanical properties due to repeated thermal exposure [60]. In fact, the 'recyclability' of PFRPs is an altogether different and unresolved issue.

Thermosets are selected as the matrix materials for this study. Firstly, the effect of matrix type on fibre/matrix compatibility and therefore PFRP mechanical properties needs to be studied. In addition, as porosity (particularly matrix-related) is an unavoidable part of composites produced via LCM processes, special attention must be paid to its effect on PFRP mechanical properties. The importance of studying porosity rises as PFRPs reinforced with twisted yarns are known to experience issues with impregnation and wettability [61, 62]. While Madsen *et al.* [63-65] have studied the effect of porosity on the properties of bast fibre compression moulded thermoplastics in detail, investigations on the effect of porosity on the properties of thermoset-based PFRPs are limited.

Today, for composites applications, plant fibres are typically used in the form of non-woven mats (for compression moulding) or granules/pellets (for injection/extrusion moulding) [15, 25, 27]. As the fibres are discontinuous (short (< 3-30 mm) [1, 15, 66] or even sub-critical length (< 0.2-3 mm) [1, 66-68]) and randomly oriented, the mechanical properties of the resulting non-structural composite are dominated by the polymer matrix, rather than the strong and stiff fibres [8, 62, 65]. According to Krenchel's fibre orientation efficiency factor [69], employing randomly oriented fibres in two-dimension (non-woven mats) and three-dimension (granules/pellets) would reduce the reinforcing effect of the fibre (in terms of providing strength and stiffness) to 37.5% and 20.0% of its potential, respectively. Using short and sub-critical length fibres (with low aspect ratios) would slash the fibre length efficiency factor as well.

For load-bearing applications, the use of reinforcements in the form of continuous aligned fibres is essential as they preserve high efficiency factors (of length and

orientation), thus allowing the entire properties of the fibre to be exploited. As technical plant fibres are staple fibres with a discrete length, they need to be processed into yarns/rovings and then textile reinforcements; that is, a continuous product with highly controlled fibre orientation. As found by several researchers [65, 70, 71], including the author of this thesis, employing such plant fibre yarns/rovings for PFRP manufacture enables realising the true potential of plant fibres as reinforcing agents. However, specific considerations are necessary when utilising yarns for composites manufacture. Firstly, the conversion of plant stems to workable technical fibres, spun yarns and eventually fabrics introduces several degrees of defects, thus diminishing fibre mechanical properties [14, 22, 59]. Secondly, the intricate structure-property relations of a yarn have several direct implications on the resulting composites. In particular, the twist and compaction of the reinforcing yarn affect composite mechanical properties, resin impregnability, yarn permeability and wettability, and even void formation [61, 62]. These issues need to be systematically investigated for wide applicability of plant yarn reinforced composites.

The volumetric composition of a composite is known to have a significant and well-predicted effect on the composite properties. In many studies on PFRP mechanical properties, the volumetric composition of the composites is not well-characterised. While most researchers give estimates of fibre weight fraction, some state the fibre volume fraction assuming no porosity. While there are some well-documented studies on structure-property relationships in PFRPs, there have been no direct studies on determining the minimum, critical and maximum fibre volume fraction for PFRPs. In the automotive industry, random short fibre PFRPs are employed at fibre volume fractions ranging from 15 to 55% [25, 31]. Importantly, the critical fibre volume fraction, above which the reinforcing effect of the fibre is realised, for random short-fibre PFRPs is typically in excess of 25% and even up to 50% (interpreted from [72, 73]). In essence, the tensile strength of the matrix is higher than the tensile strength of the composite for many of these components. On the other hand, Madsen *et al.* [64, 74] have found that the maximum fibre volume fraction, above which poor impregnation and extensive void formation lead to reduced mechanical properties, is of the order of 50% for hemp yarn reinforced

composites but in the range of 33-46% for short random flax/jute reinforced composites. That is, the fibre volume fraction process window for PFRPs is much smaller than that for conventional FRPs. Hence, investigating structure-property relations in twisted yarn reinforced PFRPs for structural composites is imperative as it would enable identifying the range of fibre volume fractions that produce useful properties and provide models to predict the composite properties.

Generally, the measurement of uniaxial composite tensile properties is appropriate in analysing the reinforcing contribution of plant fibres. However, structural components may not only be subjected to uniaxial loads, but also to off-axis loads and even fatigue loads. Indeed, the mechanical behaviour of aligned PFRPs subjected to off-axis loads and cyclic loads has been only sparsely investigated. If PFRPs are to be seriously considered for structural applications, their response to off-axis loads and cyclic loads needs to be thoroughly investigated and documented. In addition, to predict the response of PFRPs exposed to such loads, models need to be developed.

Finally, while PFRPs are attractive for structural applications, studies have largely been based on lab-scale coupon testing and computational modelling. To date, there are only limited, if any, scientific studies that conclusively show the suitability of PFRPs over GFRPs for structural applications [75]. The performance of PFRPs in real full-scale structural applications needs to be ambitiously tested and analysed.

## 1.2 THESIS OBJECTIVES

The work described in this thesis has formed part of a Nottingham Innovative Manufacturing Research Centre (NIMRC) funded project entitled '*Sustainable manufacture of small wind turbine blades using natural fibre composites and optimal design tools*'.

The overall objectives of this thesis are to *i)* characterise, *ii)* optimise, and *iii)* achieve an improved understanding of, the mechanical properties of PFRPs for structural applications. Furthermore, using composite rotor blades as a case study, the question is addressed whether PFRPs are potential alternatives to GFRPs for structural applications.

Bast fibres (flax, hemp and jute) are selected as suitable reinforcements for this study, due to their mechanical properties and ready availability. To develop composites for load-bearing applications, this study concerns PFRPs based on continuous aligned reinforcements (unidirectional and multi-axial), fabricated from yarns/rovings, embedded in a thermoset matrix. A liquid composite moulding (LCM) process is employed for composite manufacture.

Components like small wind turbine (SWT) blades are subjected to various loading situations over their design life, including static and fatigue loading. Hence, the first logical step for the application of PFRPs in structural applications would be to experimentally investigate and characterise these several mechanical properties (particularly, static tensile and fatigue properties). Once the necessary benchmark is set, efforts can be made to optimise these properties by investigating the effects of a range of relevant composite parameters such as *i)* plant fibre yarn type and quality, *ii)* thermoset matrix type, *iii)* volumetric composition (fibre, matrix and void content), *iv)* reinforcing yarn structure, and *v)* textile architecture (ply orientation). This methodology would not only facilitate an improved understanding of the mechanical behaviour of PFRPs, but would also provide a systematic solution in developing simple mathematical and/or micro-mechanical models for predicting their properties. Eventually, the optimised material technologies would be applied in the manufacture of full-scale structural components and the developed predictive models could be employed to demonstrate the components' structural integrity.

## 1.3 THESIS OUTLINE

This thesis presents different aspects of the potential of plant fibres as reinforcements in structural polymer composites. The thesis consists of 8 chapters. This chapter, *Chapter 1*, gives a general introduction to the subject, in addition to the objectives and outline of the thesis. In providing a relevant background for the work described in this thesis, *Chapter 2* contains a general literature survey on technical plant fibres and their composites with useful mechanical properties for structural applications.

*Chapters 3-6* form the central part of the thesis, with each chapter having a short introduction and literature review concerning the specific issue. In *Chapter 3*, the

mechanical properties of plant yarn reinforced unidirectional thermoset matrix composites are studied and compared to that of GFRPs. Attention is also paid to the effect of plant fibre/yarn type and matrix type on the properties of the composites. In *Chapter 4*, structure-property relationships in plant yarn composites are investigated, specifically to determine the range of fibre volume fractions (that is, minimum, critical and maximum fibre content) that produce PFRPs with useful tensile properties. *Chapter 5* details the effect of orientation, in the form of *i)* reinforcing yarn twist and *ii)* ply orientation, on the tensile properties of flax yarn reinforced composites, with a focus on mathematical modelling of the experimental data. Furthermore, attention is paid to the non-linear tensile stress-strain response of plant fibres and their composites. *Chapter 6* evaluates the fatigue performance of various aligned PFRPs through lifetime (S-N) diagrams, comparing them to aligned GFRPs. The effect of *i)* plant fibre type/quality, *ii)* fibre content, *iii)* textile architecture, and *iv)* stress ratio, on PFRP cyclic loading behaviour is investigated. Constant life diagrams are produced to enable the fatigue life prediction of PFRP components subjected to cyclic loads.

To apply the results from *Chapters 3-6* (gathered through coupon testing) and demonstrate the potential of PFRPs for full-scale structural applications, *Chapter 7* details a case study on the structural integrity (static and fatigue) of a 3.5-meter SWT blade built from flax/polyester. A comparison of the manufacturing and mechanical properties of the flax blade and an identical E-glass blade is presented. Finally, *Chapter 8* presents the main conclusions and highlights topics for future work.

## 1.4 LIST OF PUBLICATIONS AND AWARDS

Several publications have arisen from the work described in this thesis. The dissemination has been in the form of peer-reviewed journal papers, conference papers and presentations, and through public engagement. A critical review article, derived from the literature survey in *Chapters 1 and 2*, and original research articles, based on *Chapters 4-7*, have been published in peer-reviewed journals. The novel research has also attracted numerous awards.

**Peer-Reviewed Journal Papers**

1. **Shah DU**, Schubel PJ, Licence P, Clifford MJ. Hydroxyethylcellulose surface treatment of natural fibres: the new 'twist' in yarn preparation and optimization for composites applicability. *Journal of Materials Science*, 2012, 47(6): p. 2700-2711.
2. **Shah DU**, Schubel PJ, Licence P, Clifford MJ. Determining the minimum, critical and maximum fibre content for twisted yarn reinforced plant fibre composites. *Composites Science and Technology*, 2012, 72: p. 1909-1917.
3. **Shah DU**, Schubel PJ, Clifford MJ. Modelling the effect of yarn twist on the tensile strength of unidirectional plant fibre yarn composites. *Journal of Composite Materials*, 2012, 47(4): p. 425-436.
4. **Shah DU**, Schubel PJ, Clifford MJ, Licence P. The tensile behaviour of off-axis loaded plant fibre composites: an insight on the non-linear stress-strain response. *Polymer Composites*, 2012, 33(9): p. 1494-1504.
5. **Shah DU**, Schubel PJ, Clifford MJ, Licence P. Fatigue life evaluation of aligned plant fibre composites through S-N curves and constant-life diagrams. *Composites Science and Technology*, 2013, 74: p. 139-149.
6. **Shah DU**, Schubel PJ, Clifford MJ. Can flax replace E-glass in structural composites? A small wind turbine blade case study. *Composites Part B: Engineering*, 2013, 52: p. 172-181.
7. **Shah DU**. Developing plant fibre composites for structural applications by optimising composite parameters: a critical review. *Journal of Materials Science*, 2013, 48 (18): p. 6083-6107.

**Conference Papers/Presentations**

1. **Shah DU**, Schubel PJ, Clifford MJ, Licence P, Warrior NA. Mechanical characterization of vacuum infused thermoset matrix composites reinforced with aligned hydroxyethylcellulose sized plant bast fibre yarns, in *4th International Conference on Sustainable Materials, Polymers and Composites (ECOCOMP 2011)*. 6-7 July 2011. Birmingham, UK.
2. **Shah DU**, Schubel PJ, Clifford MJ, Licence P, Warrior NA. Yarn optimisation and plant fibre surface treatment using hydroxyethylcellulose for the development of structural bio-based composites, in *18th International Conference on Composite Materials (ICCM-18)*. 21-27 August 2011. Jeju, South Korea.
3. **Shah DU**, Schubel PJ, Clifford MJ, Licence P. Fatigue characterisation of plant fibre composites for small-scale wind turbine blade applications, in *SAMPE*

*Europe Student Conference 2012 (in SAMPE Europe 33rd International Conference SEICO 12)*. 24-25 March 2012. Paris, France.

4. **Shah DU**, Schubel PJ, Clifford MJ, Licence P. Fatigue characterisation of plant fibre composites for small-scale wind turbine blade applications, in *5th Innovative Composites Summit (in JEC Asia 2012)*. 26-28 June 2012. Singapore.
5. **Shah DU**, Schubel PJ. Can flax replace E-glass in structural composites? A small wind turbine blade case study, in *5th International Conference on Sustainable Materials, Polymers and Composites (ECOCOMP 2013)*. 3-4 July 2013. Birmingham, UK.

#### Other Articles

1. **Shah DU**, Schubel PJ, Clifford MJ, Licence P. Fatigue characterisation of plant fibre composites for rotor blade applications, in *JEC Composites Magazine*. June 2012, No. 73: Special JEC Asia, p. 51-54.
2. **Shah DU**, Schubel PJ. Can flax replace E-glass in small wind turbine blades?, in *JEC Composites Magazine*, Jan-Feb 2013, No. 78: Feature Wind Energy, p. 29-33.

#### Awards

1. **Jan 2012: 'Composites Sustainability Award'** at SAMPE/BCS/IOM3 Annual UK Student Seminar, London (UK).
2. **Mar 2012: 'JEC Sustainable Solutions Award'** at SAMPE Europe Student Conference, Paris (France).
3. **May 2012: 'Research Impact Prize'** at University of Nottingham Faculty Postgraduate Research Event, Nottingham (UK).
4. **June 2013**: **'JEC Asia 2013 Innovation Award'** in the Biocomposites category, at JEC Asia 2013, Singapore (Singapore). This award is for research and development on the first natural fibre reinforced composite small wind turbine blade.

## 1.5 REFERENCES

1. Pickering K, ed. *Properties and performance of natural-fibre composites*. 2008. CRC Press LLC: Boca Raton.
2. Bledzki A, Sperber VE, Faruk O. *Natural wood and fibre reinforcement in polymers*, 2002: Rapra Technology Ltd.
3. Reux F. Worldwide composites market: Main trends of the composites industry, in *5th Innovative Composites Summit - JEC ASIA 2012*. 26-28 June 2012. Singapore.
4. Mohanty A, Misra M, Drzal LT, ed. *Natural fibers, biopolymers and biocomposites*. 2005. Taylor and Francis.

5. Franck R, ed. *Bast and other plant fibres*. 2005. CRC Press LLC: Boca Raton.
6. Chand N, Fahim M. *Tribology of natural fiber polymer composites*, 2008: Woodhead Publishing Ltd.
7. Wool R, Sun XS. *Bio-based polymers and composites*, 2005: Elsevier Science & Technology Books.
8. Wambua P, Ivens J, Verpoest I. Natural fibres: can they replace glass in fibre reinforced plastics? *Composites Science and Technology*, 2003, 63: p. 1259-1264.
9. Zini E, Scandola M. Green composites: An overview. *Polymer Composites*, 2011, 32(12): p. 1905-1915.
10. Summerscales J, Dissanayake N, Virk AS, Hall W. A review of bast fibres and their composites. Part 2 – Composites. *Composites Part A: Applied Science and Manufacturing*, 2010, 41(10): p. 1336-1344.
11. Shahzad A. Hemp fiber and its composites - A review. *Journal of Composite Materials*, 2012, 46(8): p. 973-986.
12. Dhanasekaran S, Balachandran G. Structural behavior of jute fiber composites - A review. *SAE Technical Paper*, 2008, 1: p. 2653.
13. Li Y, Mai Y, Ye L. Sisal fibre and its composites: A review of recent developments. *Composites Science and Technology*, 2000, 60(11): p. 2037-2055.
14. Bledzki A, Gassan J. Composites reinforced with cellulose based fibres. *Progress in Polymer Science*, 1999, 24: p. 221-274.
15. Faruk O, Bledzki AK, Fink HP, Sain M. Biocomposites reinforced with natural fibres: 2000-2010. *Progress in Polymer Science*, 2012, 37(11): p. 1552-1596.
16. John M, Thomas S. Biofibres and biocomposites. *Carbohydrate Polymers*, 2008, 71: p. 343-364.
17. Kalia S, Kaith BS, Kaur I. Pretreatments of natural fibers and their application as reinforcing material in polymer composites - a review. *Polymer Engineering and Science*, 2009, 49(7): p. 1253-1272.
18. Miao M, Finn N. Conversion of natural fibres into structural composites. *Journal of Textile Engineering*, 2008, 54(6): p. 165-177.
19. Ku H, Wang H, Pattarachaiyakoop N, Trada M. A review on the tensile properties of natural fiber reinforced polymer composites. *Composites Part B: Engineering*, 2011, 42: p. 856-873.
20. Dittenber D, Gangarao HVS. Critical review of recent publications on use of natural composites in infrastructure. *Composites Part A: Applied Science and Manufacturing*, 2012, 43: p. 1419-1429.
21. Kalia S, Dufresne A, Cherian BM, Kaith BS, Avérous L, Njuguna J, Nassiopoulos A. Cellulose-based bio- and nanocomposites: A review. *International Journal of Polymer Science*, 2011, doi:10.1155/2011/837875.
22. Lewin M. *Handbook of fiber chemistry*. Third ed, 2007. Boca Raton: CRC Press LLC.
23. Vuure A. Natural fibre composites: recent developments, in *Innovation for Sustainable Production (i-SUP)*. 2008. Bruges, Belgium.
24. Witten E, Schuster A. Composites market report: Market developments, challenges, and chances, 2010. Industrievereinigung Verstärkte Kunststoffe and Carbon Composites.
25. Carus M. Bio-composites: Technologies, applications and markets, in *4th International Conference on Sustainable Materials, Polymers and Composites*. 6-7 July 2011. Birmingham, UK.
26. Joshi S, Drzal LT, Mohanty AK, Arora S. Are natural fiber composites environmentally superior to glass fiber reinforced composites? *Composites Part A: Applied Science and Manufacturing*, 2004, 35: p. 371-376.

27. Carus M, Gahle C. Natural fibre reinforced plastics - material with future, 2008. nova-Institut GmbH: Huerth.
28. Bos H. *The potential of flax fibres as reinforcement for composite materials*. PhD, 2004. Technische Universiteit Eindhoven: Eindhoven, Netherlands.
29. John M, Anandjiwala RD. Recent developments in chemical modification and characterization of natural fiber-reinforced composites. *Polymer Composites*, 2008: p. 187-207.
30. Witten E. The composites market in Europe: Market developments, challenges, and opportunities, 2008. Industrievereinigung Verstärkte Kunststoffe.
31. Bledzki A, Faruk O, Sperber VE. Cars from bio-fibres. *Macromolecular Materials and Engineering*, 2006, 291: p. 449-457.
32. *FAOSTAT- Food and Agriculture Organization of the United Nations*. 07 August 2012 [cited 2012; Available from: http://faostat.fao.org/site/567/DesktopDefault.aspx?PageID=567#ancor.
33. Dumanli A, Windle AH. Carbon fibres from cellulosic precursors: a review. *Journal of Materials Science*, 2012, 47: p. 4236-4250.
34. Almaguer R. *Opportunities in natural fiber composites*, 2011. Lucintel: Las Colinas, USA.
35. Ticoalu A, Aravinthan T, Cardona F. A review of current development in natural fiber composites for structural and infrastructure applications, in *Southern Region Engineering Conference*. 11-12 November 2010. Toowoomba, Australia.
36. van Rijswijk K, Brouwer WD, Beukers A. Application of natural fibre composites in the development of rural societies, 2001. Delft University of Technology: Delft, Netherlands.
37. Fowler P, Hughes JM, Elias RM. Biocomposites: technology, environmental credentials and market forces. *Journal of the Science of Food and Agriculture*, 2006, 86: p. 1781-1789.
38. Sharma R, Raghupathy VP, Rao SS, Shubhanga P. Review of recent trends and developments in biocomposites, in *International Conference on Recent Developments in Structural Engineering*. August 30 - September 1 2007. Manipal, India.
39. Riedel U, Nickel J. Natural fibre-reinforced biopolymers as construction materials – new discoveries. *Die Angewandte Makromolekulare Chemie*, 1999, 272: p. 34-40.
40. Riedel U. Biocomposites: Long natural fiber-reinforced biopolymers. *Polymer Science: A Comprehensive Reference*, 2012, 10(18): p. 295–315.
41. Yu H, Kim SS, Hwang IU, Lee DG. Application of natural fiber reinforced composites to trenchless rehabilitation of underground pipes. *Composite Structures*, 2008, 86: p. 285–290.
42. Frohnapfel P, Muggenhamer M, Schlögl C, Drechsler K. Natural fibre composites for innovative small scale wind turbine blades, in *International Workshop on Small Scale Wind Energy for Developing Countries*. 15-17 November 2010. Pokhara, Nepal.
43. Brøndsted P, Holmes JW, Sørensen BF, Jiang Z, Sun Z, Chen X. Evaluation of a bamboo/epoxy composite as a potential material for hybrid wind turbine blades, 2008. Chinese Wind Energy Association.
44. Mikkelsen L, Bottoli F, Pignatti L, Andersen TL, Madsen B. Material selection and design aspects of small wind turbine blades, in *Indo-Danish Workshop on Future Composites Technologies for Wind Turbine Blades*. 2012. Delhi, India.
45. Qin Y, Xu J, Zhang Y. Bamboo as a potential material used for windmill turbine blades - A life cycle analysis with sustainable perspective, 2009. Roskilde University Center: Denmark.

46. Bottoli F, Pignatti L. Design and processing of structural components in biocomposite materials - Rotor blade for wind turbine cars, ed. Madsen B, Mikkelsen LP, Brondsted P, Andersen TL, 2011. Technical University of Denmark: Roskilde, Denmark.
47. *Auto body made of plastics resists denting under hard blows*, in *Popular Mechanics Magazine*, Dec 1941, Vol 76 No. 6. p. 12.
48. -. A Fighter Fuselage in Synthetic Material, Vol. 34, October 1945. Aero Research Limited: Duxford, Cambridge.
49. Sakurada I, Nukushina Y, Ito T. Experimental determination of the elastic modulus of crystalline regions in oriented polymers. *Journal of Polymer Science*, 1962, 57(165): p. 651-660.
50. Eichhorn S, Dufresne A, Aranguren M, et al. Review: current international research into cellulose nanofibres and nanocomposites. *Journal of Materials Science*, 2010, 45: p. 1-33.
51. Harris B. *Engineering composite materials*, 1999. London: The Institute of Materials.
52. Summerscales J, Dissanayake N, Virk AS, Hall W. A review of bast fibres and their composites. Part 1 – Fibres as reinforcements. *Composites Part A: Applied Science and Manufacturing*, 2010, 41(10): p. 1329-1335.
53. Okuba K, Fujii T, Yamamoto Y. Development of bamboo-based polymer composites and their mechanical properties. *Composites Part A: Applied Science and Manufacturing*, 2004, 35: p. 377-383.
54. Kamath M, Bhat GS, Parikh DV, Mueller D. Cotton fiber nonwovens for automotive composites. *International Nonwovens Journal*, 2005, 14(1): p. 34-40.
55. Harish S, Michael DP, Bensely A, Lal DM, Rajadurai A. Mechanical property evaluation of natural fiber coir composite. *Materials Characterization*, 2009, 60: p. 44-49.
56. Venkateshwaran N, Elayaperumal A. Banana fibre reinforced polymer composites - A review. *Journal of Reinforced Plastics and Composites*, 2010, 29: p. 2387-2396.
57. Weyenberg I, Ivens J, Coster A, Kino B, Baetens E, Verpoest I. Influence of processing and chemical treatment of flax fibres on their composites. *Composites Science and Technology*, 2003, 63: p. 1241-1246.
58. Thygesen A. *Properties of hemp fibre polymer composites - An optimisation of fibre properties using novel defibration methods and fibre characterisation*. PhD, 2006. The Royal Agricultural and Veterinary University of Denmark: Roskilde, Denmark.
59. Hanninen T, Thygesen A, Mehmood S, Madsen B, Hughes M. Mechanical processing of bast fibres: The occurrence of damage and its effect on fibre structure. *Industrial Crops and Products*, 2012, 39: p. 7-11.
60. Reussman T, Mieck P, Grützner R, Bayer R. The recycling of polypropylene reinforced with natural fibres. *Kunststoffe Plast Europe*, 1999, 89: p. 80-84.
61. Goutianos S, Peijs T. The optimisation of flax fibre yarns for the development of high-performance natural fibre composites. *Advanced Composites Letters*, 2003, 12(6): p. 237-241.
62. Goutianos S, Peijs T, Nystrom B, Skrifvars M. Development of flax fibre based textile reinforcements for composite applications. *Applied Composite Materials*, 2006, 13(4): p. 199-215.
63. Madsen B, Thygesen A, Lilholt H. Plant fibre composites - Porosity and volumetric interaction. *Composites Science and Technology*, 2007, 67: p. 1584-1600.
64. Madsen B, Thygesen, A, Liholt, H. Plant fibre composites - Porosity and stiffness. *Composites Science and Technology*, 2009, 69: p. 1057-1069.
65. Madsen B. *Properties of plant fibre yarn polymer composites - An experimental study*. PhD, 2004. Technical University of Denmark: Lyngby, Denmark.

66. Garkhail S, Heijenrath RWH, Peijs T. Mechanical properties of natural-fibre-mat-reinforced thermoplastics based on flax fibres and polypropylene. *Applied Composite Materials*, 2000, 7: p. 351-372.
67. Bos H, Mussig J, van den Oever MJA. Mechanical properties of short-flax-fibre reinforced compounds. *Composites Part A: Applied Science and Manufacturing*, 2006, 37: p. 1591-1604.
68. Awal A, Cescutti G, Ghosh SB, Mussig J. Interfacial studies of natural fibre/polypropylene composites using single fibre fragmentation test (SFFT). *Composites Part A: Applied Science and Manufacturing*, 2011, 42: p. 50-56.
69. Krenchel H. Fibre reinforcement. *Akademisk Forlag*, 1964: p. 16-22.
70. Weyenberg I, Chitruong T, Vangrimde B, Verpoest I. Improving the properties of UD flax fibre reinforced composites by applying an alkaline fibre treatment. *Composites Part A: Applied Science and Manufacturing*, 2006, 37: p. 1368-1376.
71. Baets J, Plastria D, Ivens J, Verpoest I. Determination of the optimal flax fibre preparation for use in UD-epoxy composites, in *4th International Conference on Sustainable Materials, Polymers and Composites*. 6-7 July 2011. Birmingham, UK.
72. Ghosh R, Reena G, Krishna AR, Raju BHL. Effect of fibre volume fraction on the tensile strength of Banana fibre reinforced vinyl ester resin composites. *International Journal of Advanced Engineering Sciences and Technologies*, 2011, 4(1): p. 89-91.
73. Sawpan M, Pickering KL, Fernyhough A. Analysis of mechanical properties of hemp fibre reinforced unsaturated polyester composites. *Journal of Composite Materials*, 2012, (In Press). doi:10.1177/0021998312449028.
74. Madsen B, Hoffmeyer P, Lilholt H. Hemp yarn reinforced composites – II. Tensile properties. *Composites Part A: Applied Science and Manufacturing*, 2007, 38: p. 2204-2215.
75. Staiger M, Tucker N. *Natural-fibre composites in structural applications*, in *Properties and performance of natural-fibre composites*, Pickering K, 2008. CRC Press LLC: Boca Raton.

# 2 BACKGROUND: PLANT FIBRES AND THEIR COMPOSITES*

This chapter aims to provide a broad understanding of plant fibres and their composites, specifically commenting on critical factors influencing the mechanical properties of plant fibre composites, thereby dictating their applicability in structural components. In essence, this chapter serves as a relevant background and literature review to the work described in this thesis.

## 2.1 COMPOSITES: A CONCERN FOR THE ENVIRONMENT?

Since the mid-20$^{th}$ century, research and engineering interest has been shifting from monolithic materials to composite materials (Fig. 2.1) [1]. Fibre reinforced plastics (FRPs) – produced through a synthetic assembly of a (typically, petroleum-derived) polymer matrix with (typically, man-made) reinforcing fibres – have several advantages, predictably a combination of the main properties of the constituents. Due to the light-weight and high-performance capacity of FRPs, they are increasingly being exploited in all areas of engineering applications: from the performance-driven aerospace and automotive industries, to the cost-driven consumer goods market [2].

While the total global production of fibre reinforced plastics (FRPs) amounted to 5.9 million tonnes in 1999 [2], this figure increased to 8.7 million tonnes in 2011 [2]. With the increasing consumption of FRPs, environmental concerns relating not only to the energy-intensive unsustainable production processes of the reinforcing synthetic fibres and plastics [3, 4], but also to the limited recyclability and end-of-life disposal options of the FRPs have been highlighted [5, 6]. The perceived scale of the problem has even led to stringent government legislations, such as the EU Directive on Landfill of Waste (Directive 99/31/EC) and the End-of-life Vehicle Directive (Directive 2000/53/EC), which are seen as barriers to the development or even

* This chapter is based on the peer-reviewed journal article:

Shah DU. Developing plant fibre composites for structural applications by optimising composite parameters: a critical review. *Journal of Materials Science*, 2013, 48(18): p. 6083-6107.

continued use of FRPs in some markets [5]. To alleviate some of the environmental issues associated with using synthetics in FRPs, there has been a resurgent interest in biocomposites. Materials from renewable resources are being developed to replace not only the reinforcing fibres but also the polymer matrix of composites [7-14]. This thesis is concerned with the development of plant fibres as reinforcements for FRPs. While it is acknowledged that the use of synthetic thermoset matrices, for instance, will produce bio-based composites that are not biodegradable or strictly recyclable, the presented research will nonetheless play a valuable role in the future increasing use of eco-materials.

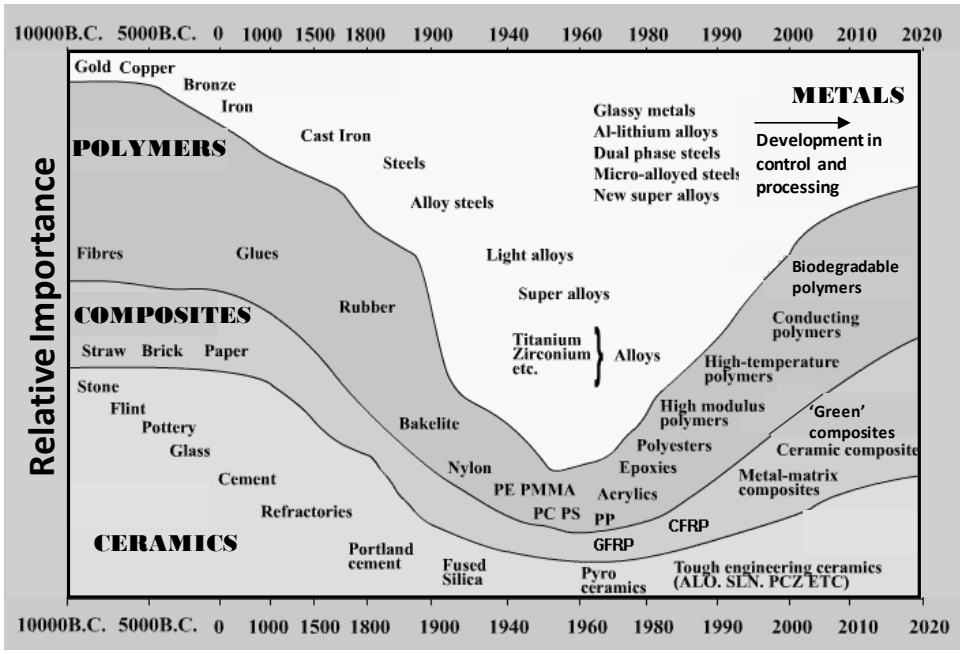


**Fig. 2.1: Brief timeline of engineering materials development (Adapted from [1])**

## 2.2 PLANT FIBRES: THE GLORY AND THE BLEMISHES

As discussed in *Chapter 1*, lignocellulosic fibres offer several economical, technical and ecological advantages over synthetic fibres, particularly E-glass (Table 1.1). Hence, plant fibre composites (PFRPs) were originally aimed at the replacement of E-glass composites (GFRPs), which lead today's FRP market [2]. Though the usage of PFRPs in commercial applications has increased annually over the past 15 years, today they are almost exclusively employed for non-structural interior automotive

applications, primarily as a replacement to wood fibre composites [15, 16]. This is attributable to the fact that the impressive theoretical properties of cellulose and cellulose-based fibres have been difficult to exploit in practice. Researchers who have worked with PFRPs agree that the major bottlenecks limiting their applications are: *i)* the inferior (often performance-limiting) and naturally variable mechanical properties of plant fibres, *ii)* the susceptibility of plant fibres and their composites to moisture ingress, and *iii)* the supposedly weak fibre/matrix interface in PFRPs impeding efficient property transfer of the fibres to the composite [17].

Nonetheless, there is a growing voice in the scientific community which suggests that the properties of plant fibres can be exploited for even load-bearing applications [11, 18-25]. Indeed, this is the objective and conclusion of this research study. With directed research on maximising and optimising the reinforcing contribution of plant fibres in polymer composites, significant headway has been made on the use of PFRPs for performance-demanding applications. The progress includes: *i)* fibre reinforcement development – from crop growth to fibre extraction and processing to reinforcement optimisation for composites applicability [9, 12, 21, 24-33], *ii)* composite manufacturing process development [9, 12, 16, 25, 34-37], and *iii)* composite property characterisation – for instance, as a function of composite parameters and loading conditions [8, 9, 12, 25]. This chapter will discuss some factors that require consideration in developing PFRPs for structural applications.

## 2.3 MATERIALS SELECTION CRITERIA FOR STRUCTURAL APPLICATIONS

During product development, materials selection is a process where a range of material properties are taken into consideration. Asbhy [38] describes a method to compare the relative performance of a variety of materials for a specific constructive element by using material *performance indices* – defined by the component function, objective and constraint – as design criteria. Generally, minimising material weight (density $\rho$) and/or cost are key objectives for industrial products. The key mechanical parameters, defined by the component function and constraint, are typically stiffness $E$ and strength $\sigma$. Following Asbhy [38], the critical material performance indices that need to be maximised for a beam/plate loaded in pure tension are specific tensile

stiffness $E/\rho$ and specific tensile strength $\sigma/\rho$. For a beam/plate loaded in bending mode, specific flexural stiffness $E^{1/3}/\rho$ and strength $\sigma^{1/2}/\rho$ need to be maximised. Material selection, on the basis of these performance indices, is best achieved by plotting the performance indices (which are typically a mathematical combination of material properties) on each axis of a *materials selection chart*, also known as an *Ashby plot*. Individual materials or material sub-classes appear as balloons, which define the range of their properties.

The Ashby plot in Fig. 2.2 compares the specific tensile performance of various natural fibres (from animals and plants) with synthetic fibres. It is observed that several plant fibres, including flax, hemp and jute, have better specific tensile stiffness than E-glass. On the other hand, specific tensile strength of plant fibres is consistently lower than that of synthetic fibres.

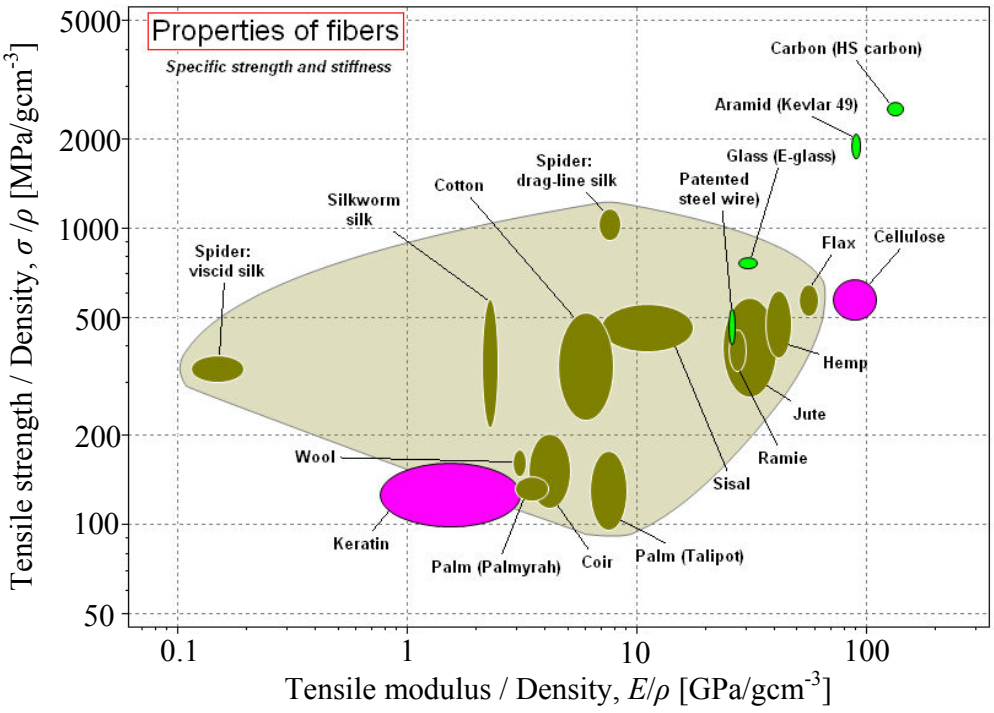


**Fig. 2.2. Ashby plot comparing the position of natural fibres against synthetic fibres with respect to specific tensile properties (from [39]).**

As the density of plant fibres (~1.30-1.55 $gcm^{-3}$) is approximately half of E-glass (2.60 $gcm^{-3}$), at the same fibre content PFRPs are significantly (30-40%) lighter than

GFRPs [19]. A lower density gives PFRPs a good chance to compete against GFRPs in terms of specific stiffness and strength. As the density of all plant fibres is fairly similar [30], there are minimal opportunities to reduce the density of PFRPs further. On the other hand, not only do plant fibre mechanical properties vary significantly and are strongly influenced by several factors [29, 40] (such as fibre chemical composition and structural morphology, plant growth conditions, fibre extraction and processing conditions), but composite mechanical properties are also dependent on several composite parameters (discussed in the next section). Hence, opportunities to maximise composite stiffness and strength are plentiful. To establish PFRPs as superior to GFRPs, with respect to the design criteria, PFRP mechanical properties need to be maximised.

## 2.4 COMPOSITE MATERIAL PARAMETERS

FRPs are heterogeneous materials, consisting of reinforcing fibres embedded in a continuous matrix. While the fibres provide strength and stiffness to the composite, the matrix transmits externally applied loads, via shear stresses at the interface, to the reinforcing fibres and protects the fibres from external damage. The advantage of coupling the two distinct constituents is that the high strength and stiffness of the fibres, which in practical situations would be difficult to realise, may be exploited.

Typically, composite properties are affected by the following parameters: *I)* the fibre properties, *II)* the volumetric composition (where the sum of the volume fraction of the fibres $v_f$, matrix $v_m$ and voids $v_p$ is unity, *i.e.* $v_f + v_m + v_p = 1$), *III)* the geometry of the fibres and the fibre/matrix interface properties, *IV)* the packing arrangement, orientation and stacking sequence of the fibre reinforcements, and *V)* the matrix properties. The effect of all these parameters is elegantly demonstrated by the fundamental equations in composites engineering: the generalised rule-of-mixtures (ROM) model for the tensile modulus $E_c$ (Eq. 2.1) and strength $\sigma_c$ (Eq. 2.2) of discontinuous fibre composites.

$$E_c = E_f v_f \eta_{lE} \eta_o + v_m E_m \qquad \text{Eq. 2.1}$$

$$\sigma_c = \sigma_f v_f \eta_{lS} \eta_o + v_m \sigma'_m \qquad \text{Eq. 2.2}$$

where, *I)* $E_f$ and $\sigma_f$ are the fibre modulus and fibre strength, *II)* $v_f$ and $v_m$ are the fibre and matrix volume fraction, *III)* $\eta_{lE}$ and $\eta_{lS}$ are the reinforcement length efficiency factors for stiffness and strength (incorporating the effect of fibre geometry and interfacial properties), *IV)* $\eta_o$ is the reinforcement orientation distribution factor (incorporating the effect of packing arrangement and orientation of the fibre reinforcements), and *V)* $E_m$ and $\sigma'_m$ are the matrix modulus and matrix tensile stress at the fibre failure strain. Note that the order of the parameters of Eq. 2.1 and Eq. 2.2 are homologous to the order of the composite parameters defined previously.

The basic assumptions of the above micromechanical models include: *i)* all fibres have identical geometry and properties, *ii)* homogenous and uniform distribution of fibres in the matrix, *iii)* iso-strain conditions within the composite, *iv)* ideal fibre/matrix interface, *v)* elastic deformation of the fibre and matrix, *vi)* no transverse deformations (*i.e.* ignore Poisson's contractions), *vii)* zero and maximum tensile stress at the fibre ends and centre, respectively, and *viii)* no effect of porosity content $v_p$ on composite properties (other than reducing $v_f$ and $v_m$). Although many of these simplifications and assumptions do not hold true for FRPs in general, the ROM model has proved to be adequate for the prediction/estimation of the properties of synthetic fibre composites and for the determination of the reinforcing potential of the fibres (by 'back-calculation').

The simplicity of the generalised ROM model implies that it has become a widely used model for PFRPs as well. Interestingly, as plant fibres are inherently discontinuous, the ROM model can be used for PFRPs even if plant yarns/rovings (*i.e.* 'continuous' reinforcements) are employed. Nonetheless, as plant fibres require specific considerations, recent pioneering work has led to a modified ROM model that has been shown to be more suitable for PFRPs [41, 42]. The modified ROM model, presented in Eq. 2.3 and Eq. 2.4, includes *i)* a factor of $(1 - v_p)^2$ to simulate the detrimental effect of porosity on the tensile properties of PFRPs [22, 43, 44], *ii)* a fibre diameter distribution factor $\eta_d$ to incorporate the effect of approximately linear ($E_f = E_{f0} - m \cdot d_f$) decline in fibre tensile modulus with increasing fibre diameter $d_f$ [34, 41, 42, 45, 46], and *iii)* a fibre area correction factor $\kappa$ to address the discrepancy between the true (non-circular, irregular and variable) cross-sectional area of the

fibre and the apparent circular cross-sectional area calculated by the measurement of the apparent fibre diameter [34, 41, 42, 47]. While these modifications to the general ROM model have been validated with experimental results on PFRPs in the relevant studies, they have been validated only for limited data sets. Therefore, the applicability of the modified ROM model to PFRPs needs to be investigated further.

$$E_c = \left(E_f v_f \eta_{lE} \eta_o \eta_d \kappa + v_m E_m\right)\left(1 - v_p\right)^2 \qquad \text{Eq. 2.3}$$

$$\sigma_c = \left(\sigma_f v_f \eta_{lS} \eta_o \kappa + v_m \sigma'_m\right)\left(1 - v_p\right)^2 \qquad \text{Eq. 2.4}$$

In Eq. 2.1 and Eq. 2.3, the length efficiency factor for stiffness $\eta_{lE}$ can be estimated by the Cox's shear lag model (Eq. 2.5) [48], where $l_f$ is the fibre length, $d_f$ is the fibre diameter, $G_m$ is the matrix shear stiffness, and $v_{f,max,FRP}$ is the maximum achievable fibre volume fraction (dependent on fibre packing geometry; *e.g.* $v_{f,max,FRP} = \pi/4$ for square-packing arrangement). In Eq. 2.2 and Eq. 2.4, the length efficiency factor for strength $\eta_{lS}$ is given by the Kelly-Tyson's model (Eq. 2.6) [49], where $l_c$ is the critical or ineffective fibre length. Sub-critical length fibres ($l_f < l_c$) will not carry the maximum load. If a composite has both sub-critical length ($l_f < l_c$) and super-critical length ($l_f > l_c$) fibres, Eq. 2.6 can be expressed as a summation of the contribution from different fibre lengths. It is useful to note that the critical fibre length is a function of the fibre tensile strength $\sigma_f$, the fibre diameter $d_f$, and the interfacial shear strength $\tau$ (Eq. 2.6). The length efficiency factors for stiffness and strength range between 0 (for $l_f << d_f$ or $l_f << l_c$) and 1 (for $l_f >> d_f$ or $l_f >> l_c$). This is graphically demonstrated in Fig. 2.3 using typical values for PFRPs. It can be inferred from the graphs that as $l_f \rightarrow 0.5$ mm ($l_f/d_f \rightarrow 25$), the length efficiency factors increase rapidly towards a value of about 0.80. Thereafter, the length efficiency factors asymptotically approach unity as fibre length (or fibre aspect ratio) increases. Fig. 2.3b also demonstrates the effect of interfacial properties on the length efficiency factor for strength $\eta_{lS}$; an increase in the fibre/matrix interfacial shear strength $\tau$ (and a subsequent decrease in the critical fibre length $l_c$) has a noticeable effect on $\eta_{lS}$ for short fibres ($l_f < 3$ mm), but a negligible effect on $\eta_{lS}$ if the fibre length is over 10 times the critical length (*i.e.* $l_f = 10l_c$) [50]. These observations are critical to selecting the reinforcement form.

$$\eta_{lE} = 1 - \frac{\tanh\left(\frac{\beta l_f}{2}\right)}{\frac{\beta l_f}{2}},\ \frac{\beta l_f}{2} = \frac{l_f}{d_f}\sqrt{\frac{2G_m}{E_f \ln\left(\sqrt{v_{f,\max,FRP}/v_f}\right)}},\ \eta_{lE} \in [0,1] \qquad \text{Eq. 2.5}$$

$$\eta_{lS} = \begin{cases} 1 - l_c/2l_f & for\ l_f \geq l_c \\ l_f/2l_c & for\ l_f \leq l_c \end{cases},\ l_c = \frac{\sigma_f d_f}{2\tau},\ \eta_{lS} \in [0,1] \qquad \text{Eq. 2.6}$$

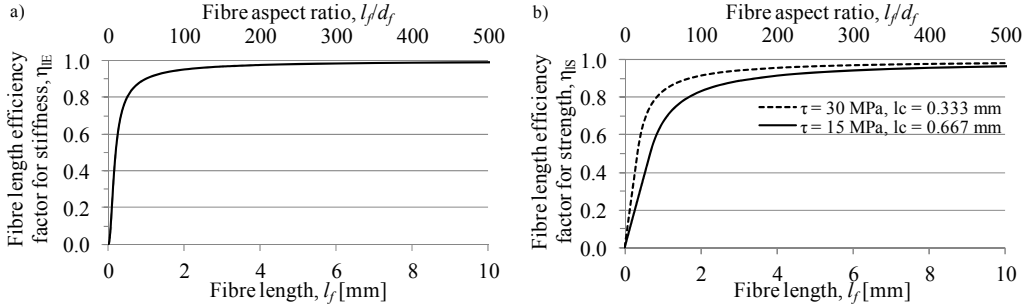


**Fig. 2.3. Predictions of the fibre length efficiency factors for a) stiffness $\eta_{lE}$ and b) strength $\eta_{lS}$, based on Cox's shear lag model (Eq. 2.5) and Kelly-Tyson's model (Eq. 2.6), respectively. Typical values for flax reinforced PFRPs are used in the calculations: $d_f$ = 20 µm, $G_m$ = 1 GPa, $E_f$ = 50 GPa, $v_{f,max,FRP}$ = π/4, $v_f$ = 0.30, $\sigma_f$ = 1000 MPa and $\tau$ = 30 MPa or 15 MPa ($l_c$ = 0.333 mm or 0.667 mm, respectively).**

The reinforcement orientation distribution factor $\eta_o$ in Eq. 2.1-2.4 can be estimated by the Krenchel orientation distribution factor (Eq. 2.7) [51], where $a_n$ is the fraction of fibre with orientation angle $\theta_n$ with respect to the axis of loading. The reinforcement orientation distribution factor ranges between 0 (fibres aligned transverse to the stress direction) and 1 (fibres aligned parallel to the stress direction).

$$\eta_o = \sum_n a_n \cos^4 \theta_n,\ \sum_n a_n = 1,\ \eta_o \in [0,1] \qquad \text{Eq. 2.7}$$

Although the fibre diameter distribution factor $\eta_d$ in Eq. 2.3 has not been formally defined [34, 46], it may be a complex function of the fibre structure [46] or be correlated to the probability density function of the fibre diameter [34, 45]. $\eta_d$ ranges between 0 and 1.

Coming to estimating the fibre area correction factor $\kappa$, while it is well known that the cross-section of plant fibres is variable, irregular and non-circular, only recently

have researchers quantitatively estimated the deviation of the fibre cross-section shape from circularity [42, 52, 53]. The studies suggest that calculating the cross-section area $A_C$, assuming a circular cross-section with an average fibre diameter $d_f$, overestimates the true cross-section area $A_T$ by a fibre area correction factor $\kappa$ $(A_C/A_T)$ of 1.42–2.55 [52-54]. Virk *et al.* [42] have shown that a fibre area correction factor of $\kappa$ = 1.42 for jute fibres offers a better prediction for the composite mechanical properties (than assuming circular fibre cross-section, *i.e.* $\kappa$ = 1).

Other than the fibre area correction factor $\kappa$, which is used to account for fibre area measurement discrepancies, all parameters in Eq. 2.1-2.4 can be maximised to achieve improvements in the mechanical properties of PFRPs, and FRPs in general. If $\eta_{lE}$, $\eta_{lS}$, $\eta_o$ and $\eta_d$ are taken to be unity, the generalised and modified ROM models (in Eq. 2.1-2.4) are equivalent to the Voigt 'upper bound' for continuous fibre composites.

## 2.5 PLANT FIBRES AS STRUCTURAL REINFORCEMENTS

### 2.5.1 Plant fibre type

There are five basic types of plant fibres, classified as follows: *i)* bast fibres, from the inner bark of the plant stems, *iii)* leaf fibres, *iv)* seed fibres, *v)* grass and reed fibres, and *vi)* all other fibres (including wood fibres). Examples of the different fibre types and their estimated annual global production values are shown in Table 2.1.

In terms of utilization, plant fibres can be classed as being from primary or secondary plants. Primary plants (like flax, sisal, cotton, bamboo, hardwood/softwood trees) are cultivated specifically for their fibre content, while fibres from secondary plants (like pineapple leaf, coir, oil palm (empty fruit bunch), bagasse, rice straw) are a by-product from some other primary utilization. Hence, although plant straws and stalks (secondary source) are a potentially larger source of fibre than even wood fibres (primary source) (Table 2.1), the former are predominantly used as livestock feed or bio-fuel [55-57].

Other than wood fibres (including flour and pulp), commercially useful fibres come mainly from the bast, leaf, and seed coverings of specific plants, whose principal

application lies in textiles. Notably, while the total global production of wood fibres and cotton exceeded 100 million tonnes and 20 million tonnes in 2010 (Table 2.1), respectively, the total global production of all bast, leaf and other seed fibres amounted to only ~5 million tonnes in the same year [30, 58]. Therefore, the significant consumption of wood and cotton fibres in FRP manufacture is not surprising. In fact, biocomposites accounted for ~13% of the 2.4 million tonne EU FRP market in 2010 (Fig. 1.1), of which 170,000 tonnes is attributable to wood fibre composites and 100,000 tonnes is attributable to cotton fibre composites [15, 59]. Only 45,000 tonnes of the biocomposites manufactured employed non-wood, non-cotton fibres [15, 59], primarily flax (64% of the market share), jute (11%), hemp (10%) and sisal (7%) [25].

**Table 2.1. Classification of plant fibres [12]. If data was available from the FAO database [58], the global production estimates ($10^3$ tonnes) for 2010 are given in brackets. The bottom-most row gives the estimated total global production quantity ($10^3$ tonnes; from [12, 58]) for each category.**

| **Bast** | **Core** | **Leaf** | **Seed** | | | | | **Grass/ Reed** | **Other** |
|---|---|---|---|---|---|---|---|---|---|
| | | | ***Fibres*** | ***Pod*** | ***Husk*** | ***Fruit*** | ***Hulls*** | | |
| Flax (622) | Flax | Sisal (361) | Cotton (23295) | | | | | Wheat | Wood |
| Jute (3056) | Jute | Pineapple | | Kapok (99) | | | | Corn | Roots |
| Hemp (214) | Hemp | Agave (34) | | | Coir (1058) | | | Rice | |
| Kenaf (500) | Kenaf | Banana | | | | Oil palm | | Bamboo (30000) | |
| Ramie (118) | | Abaca (95) | | | | | Rice | Bagasse (75000) | |
| (5000) | (8000) | (600) | | | (25000) | | | (>1000000) | (>100000) |

It should be noted, however, that wood and cotton fibres are used as 'fillers' in the plastics, with no reinforcing role, due to the short length (*i.e.* low aspect ratio) of the fibres (or particles, in the case of wood flour) [12, 60]. Nonetheless, the use of wood and cotton fibres for non-structural PFRPs has been attractive due to, *i)* the abundance of these low-cost fibres, *ii)* the weight savings that the resulting PFRPs provide, and *iii)* the improved green credentials of the material due to lower polymer

use [60]. The latter is attributable to the fact that raw plant fibre production requires <10-20% of the energy used in the production of the polymer matrix (*e.g.* 15 MJ/kg for hemp and 70-90 MJ/kg for polypropylene) [34, 59]. In fact, noting the regional availability of certain fibre types, there are an increasing number of studies which demonstrate that for such non-structural applications even fibres from secondary sources with poor mechanical properties (due to a lack of biological and evolutionary incentive) like rice straw [61, 62], coir [63], banana leaf [64], oil palm (empty fruit bunch) [65], and pineapple leaf [66], may be suitable.

Table 2.2 presents the physio-mechanical properties of different plant fibres. With some exceptions, it is observed that the tensile properties (absolute and specific) are in the following order: bast fibres > leaf fibres > seed fibres. In fact, only bast fibres have tensile stiffness and specific tensile properties comparable to E-glass (Table 2.2 and Fig. 2.2). Notably, the tensile strength of even bast fibres is considerably lower than that of E-glass.

**Table 2.2. Comparison of the mechanical properties of various plant fibres and E-glass. Sources include those listed and [8, 30].**

| | *Fibre* | *Density [gcm$^{-3}$]* | *Tensile modulus [GPa]* | *Specific tensile modulus [GPa/gcm$^{-3}$]* | *Tensile strength [MPa]* | *Specific tensile strength [MPa/gcm$^{-3}$]* | *Failure strain [%]* | *Source* |
|---|---|---|---|---|---|---|---|---|
| **Bast** | Flax | 1.45-1.55 | 28-100 | 19-65 | 343-1035 | 237-668 | 2.7-3.2 | [29] |
| | Hemp | 1.45-1.55 | 32-60 | 22-39 | 310-900 | 214-581 | 1.3-2.1 | [40] |
| | Jute | 1.35-1.45 | 25-55 | 19-38 | 393-773 | 291-533 | 1.4-3.1 | [29] |
| **Leaf** | Sisal | 1.40-1.45 | 9-28 | 6-19 | 347-700 | 248-483 | 2.0-2.9 | [67] |
| | Pineapple | 1.44-1.56 | 6-42 | 4-27 | 170-727 | 118-466 | 0.8-1.6 | [64, 66] |
| | Banana | 1.30-1.35 | 8-32 | 6-24 | 503-790 | 387-585 | 3.0-10.0 | [64] |
| **Seed** | Cotton | 1.50-1.60 | 5-13 | 3-8 | 287-597 | 191-373 | 6.0-8.0 | [68] |
| | Coir | 1.10-1.20 | 4-6 | 3-5 | 131-175 | 119-146 | 15.0-30.0 | [69] |
| | Oil palm | 0.70-1.55 | 3-4 | 2-4 | 248 | 160-354 | 25.0 | [9] |
| **Other** | Bamboo | 0.60-1.10 | 11-30 | 18-27 | 140-230 | 210-233 | 1.3 | [9] |
| | Wood pulp* | 1.30-1.50 | 40 | 26-31 | 1000 | 667-769 | 4.4 | [69] |
| | E-glass | 2.55 | 78.5 | 31 | 1956 | 767 | 2.5 | [70] |

* Particulate form of softwood pulp (produced using kraft separation method)

To observe the reinforcing effect of the different plant fibres in a composite, Table 2.3 presents typically reported mechanical properties of compression moulded polypropylene (PP) composites reinforced with randomly-oriented short-fibre mats.

**Table 2.3. Typically reported mechanical properties of compression moulded PP composites reinforced with various non-woven (randomly-oriented short-fibre) plant fibre mats. For comparison, the mechanical properties of neat PP and chopped strand E-glass mat reinforced PP are also given.**

| | *Fibre reinforcement* | *Fibre content*[*] *[wt%]* | *Tensile modulus [GPa]* | *Specific tensile modulus*[†] *[GPa/gcm$^{-3}$]* | *Tensile strength [MPa]* | *Specific tensile strength*[†] *[MPa/gcm$^{-3}$]* | *Source* |
|---|---|---|---|---|---|---|---|
| | PP | 0 | 0.7-1.7 | 1.1-1.9 | 19-35 | 21-39 | [40] |
| **Bast** | Flax | 40 | 8.8 | 8.0 | 57 | 52 | [71] |
| | Hemp | 40 | 6.9 | 6.3 | 52 | 47 | [17] |
| | Jute | 40 | 3.7 | 3.5 | 27 | 25 | [17] |
| **Leaf** | Sisal | 40 | 5.3 | 4.9 | 34 | 31 | [17] |
| | Pineapple | 20 | 0.6 | 0.6 | 32 | 32 | [72] |
| | Banana | 50 | 1.5 | 1.4 | 31 | 29 | [73] |
| **Seed** | Cotton | 30 | 1.9 | 1.8 | 27 | 26 | [74] |
| | Coir | 40 | 1.2 | 1.2 | 10 | 10 | [17] |
| | Oil palm | 40 | 0.7 | 0.7 | 8 | 8 | [75] |
| **Other** | Bamboo | 50 | 3.6 | 3.7 | 30 | 30 | [76] |
| | Wood fibre | 35 | 1.4 | 1.3 | 21 | 19 | [60] |
| | E-glass | 50 | 7.0 | 4.8 | 33 | 68 | [77] |
| | E-glass | 42 | 6.2 | 4.9 | 89 | 23 | [17] |

[*] Fibre content is approximate.

[†] Estimated values. Composite density is estimated assuming no porosity and using fibre densities in Table 2.2 and a density for PP of 0.91 gcm$^{-3}$.

Expectedly, it is observed that PP reinforced with bast fibres exhibit significantly superior mechanical properties in comparison to leaf and seed fibre reinforced PP. In fact, the tensile properties (absolute and specific) of leaf, seed and wood fibre reinforced PP is barely comparable to unreinforced PP. On the other hand, bast fibre reinforcements not only improve the tensile properties of the matrix considerably, but

the resulting composites can compete against even GFRPs in terms of (absolute and specific) tensile stiffness and strength. Therefore, if certain structural requirements need to be met, it is essential that bast fibres (or other selective fibres like sisal and bamboo) are used as reinforcements (not fillers) in FRPs. Perhaps, this is why composites reinforced with bast fibres are now replacing under-performing wood fibre composites and GFRPs in automotive applications [15].

### 2.5.2 Plant fibre structure

While it is clear from the previous section that bast fibres have superior mechanical properties in comparison to leaf and seed fibres, understanding the reasons behind this may prove useful in developing structural PFRPs.

One approach is considering the role of the fibre in the living plant [12]. Bast fibres (and some grass fibres like bamboo) provide rigidity and strength to the plant stems, so they would be ideal in stiffening/strengthening composites. Leaf fibres experience repetitive flexing from the wind, so they would be useful for toughening composites. As seed fibres have no structural role, they would not reinforce a plastic effectively.

A more fundamental and quantitative approach involves understanding the influence of the chemical and physical structure of plant fibres on their mechanical properties. Each elementary plant fibre is a single cell with an elongated thick cell wall surrounding a central luminal cavity (Fig. 2.4). While the cell wall is responsible for the structural integrity of the living plant, the luminal cavity facilitates transportation of nutrients. Although having a high aspect ratio, the cross-sectional shape and dimensions of the cells are highly variable [30]. Typically, elementary plant fibres are found in bundles (in the form of a technical fibre), where the middle lamella (a pectin layer) cements the cell walls of two adjoining cells together (Fig. 2.4).

As depicted in Fig. 2.4, the cell wall has a hierarchical structure, including a thin primary (P) cell wall, and a thick secondary (S) cell wall which exists in three sub-layers (S1, S2, S3). Typically, the primary cell wall accounts for less than 2% of the total cell wall thickness, while the secondary cell wall accounts for up to 90% of the total cell wall thickness [78]. Notably, the S2 cell wall is the main sub-layer, accounting for more than 80% of the total cell wall thickness [78]. The luminal

cavity is typically up to 25% of the total cross-sectional area for non-wood plant fibres [30, 79], and usually between 2-16% for bast fibres [78].

Plant fibres themselves can be referred to as composites as the cell wall composes of reinforcing oriented semi-crystalline cellulose microfibrils which are embedded in a two-phase (lignin-hemicellulose) amorphous matrix. The content of the three main polymers (*i.e.* cellulose, hemicellulose and lignin) is known to vary between plant fibre types [30]. The typical chemical composition of flax is given in Table 2.4.

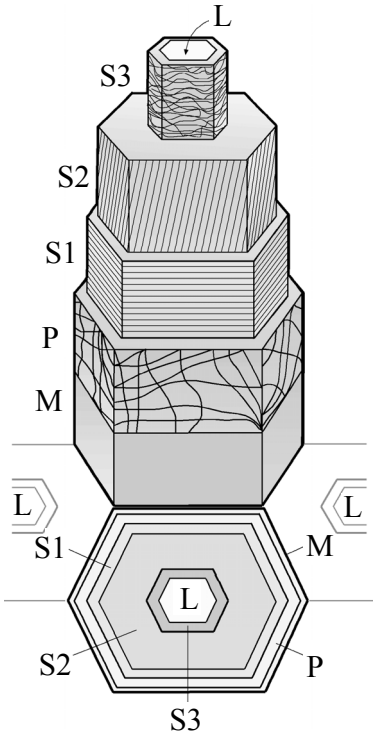


**Fig. 2.4. The structure of an elementary fibre (*i.e.* a unit cell) in a technical fibre bundle, where the middle lamella (M) glues adjacent cells together, and each unit cell composes of primary (P) and secondary (S) cell walls and a central lumen (L).**

Cellulose, a non-branched macromolecule (Fig. 2.5), is usually the major component of plant fibres (Table 2.4). Molecular chains of cellulose, comprising of about 10,000 pairs of covalent-bonded glucose units, are oriented in the fibre direction. Each repeating glucose unit contains three hydroxyl groups, which enables cellulose to form strong hydrogen bonds with its own chains to form fibrils, and with

neighbouring chains to form microfibrils [80]. It is well known that cellulose has both crystalline and amorphous regions, depending on whether the cellulose chains are held in a highly ordered (crystalline) structure due to intermolecular hydrogen bonding. Notably, crystalline and amorphous cellulose have very different mechanical properties; for instance, the tensile stiffness of crystalline cellulose (in the chain direction) is up to 15 times more than that of amorphous cellulose (Table 2.4). Furthermore, while amorphous cellulose is isotropic, the molecular linearity of crystalline cellulose makes it very anisotropic [78]. Flax fibres, for instance, comprise of 55-75 wt% cellulose, of which 53-70 % is crystalline (Table 2.4).

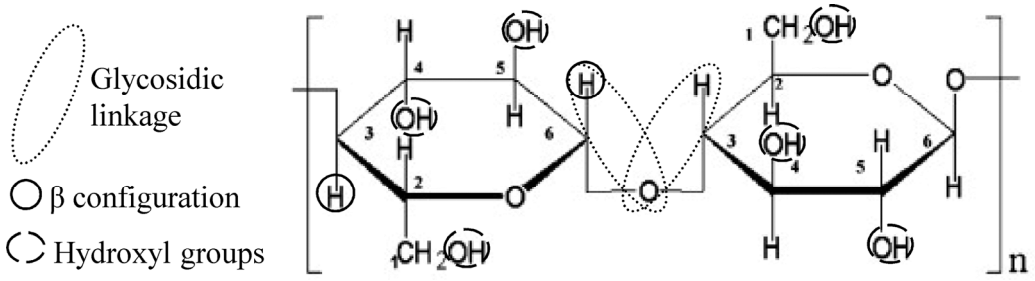


**Fig. 2.5. Molecular structure of cellulose [22].**

**Table 2.4. Typical chemical composition of flax fibre, alongside the density and tensile stiffness of the various constituents. From [30, 78].**

| | *Crystalline cellulose* | *Amorphous cellulose* | *Hemicellulose* | *Lignin* | *Pectin* |
|---|---|---|---|---|---|
| Content in flax [*wt%*] | 30-50 | 20-30 | 14-18 | 2-3 | 2-3 |
| Density [$gcm^{-3}$] | 1.6 | 1.42 | 1.4 | 1.4 | - |
| Tensile modulus [*GPa*] | 74-168 | 8-11 | 7-8 | 2-4 | - |

Cellulose microfibrils are helically wound around the cell wall, and thus are at an angle with respect to the fibre axis (Fig. 2.4). The cell walls also consist of heterogeneous, non-linear and highly-branched hemicellulose and lignin molecules. It is agreed that the hemicellulose molecules are hydrogen bonded to the cellulose

microfibrils and act as a cementing matrix between adjacent microfibrils. These structural cellulose/hemicellulose units are then encapsulated by a lignin matrix.

Importantly, both the chemical composition and the orientation of the cellulose microfibrils with respect to the fibre axis, vary between cell wall layers [30, 78]. As the S2 cell wall layer is the thickest, it is the microfibril angle (MFA) of the S2 cell wall that is of particular interest.

It is obvious that the chemical composition of a plant fibre would strongly affect its properties. For instance, the hydrophilic nature of cellulose and hemicellulose implies that plant fibres have a high moisture content (typically 5-15 wt% [10]) and the resulting composites have poor moisture resistance. Furthermore, it is known [79] that fibre chemical composition, cellulose crystallinity and density are correlated.

Four critical micro-structural parameters that affect the mechanical properties of plant fibres include: *i)* cellulose content, *ii)* cellulose crystallinity, *iii)* microfibril angle, and *iv)* fibre aspect ratio. Studies performed by McLaughlin and Tait [81] and Satyanarayana *et al.* [82, 83] conclude that these four parameters are strongly correlated to the tensile properties of plant fibres. Several studies on the prediction of plant fibre tensile properties also incorporate these four parameters [78, 84, 85].

Table 2.4 presents the typical tensile modulus of the different chemical constituents of a plant fibre. Crystalline cellulose has significantly better stiffness than all other constituents. In fact, even the transverse stiffness of crystalline cellulose (about 27 GPa [78]) is over 3 times higher than the stiffness of amorphous cellulose, hemicellulose and lignin. Hence, it is clear that not only high cellulose content, but high cellulose crystallinity is also desirable, when selecting plant fibres for use as reinforcements in structural applications. Furthermore, due to the highly anisotropic nature of crystalline cellulose, a low MFA is desirable so that the cellulose microfibrils are oriented in the fibre direction. Finally, several studies [84, 86] confirm that for a constant test gauge length, the tensile modulus and strength of a plant fibre increases with decreasing fibre diameter (*i.e.* increasing fibre aspect ratio). A higher fibre aspect ratio is also desirable for improved load transfer capability in a fibre reinforced composite.

Table 2.5 presents typical values of the four critical structural parameters for various plant fibres. It is found that bast fibres exhibit a high cellulose content (60-70 wt%) and crystallinity (50-90 %), low microfibril angle (<10°) and high aspect ratio. With some exceptions, leaf and seed fibres, exhibit lower cellulose content and crystallinity, higher microfibril angles (10-50°) and lower aspect ratios. Hence, the superior mechanical properties of bast fibres and their composites, observed in Table 2.2 and Table 2.3, is logical. Therefore, this research will focus on the utilisation of bast fibres, namely flax, hemp and jute, for structural composites applications.

**Table 2.5. Typical values of critical structural parameters for various plant fibres. Sources include those listed and [8, 23, 30, 82].**

| | *Fibre* | *Cellulose content* $v_x$ *[wt%]* | *Cellulose crystallinity [%]* | *MFA* $\theta$ *[°]* | *Aspect ratio* $l_f/d_f$ *[-]* | *Luminal porosity [%]* | *Source* |
|---|---|---|---|---|---|---|---|
| **Bast** | Flax | 64-71 | 50-90 | 5-10 | 1750 | 2-11 | [78] |
| | Hemp | 70-74 | 50-90 | 2-6 | 900 | 2-11 | [78, 87] |
| | Jute | 61-72 | 50-80 | 8 | 100 | 10-16 | |
| **Leaf** | Sisal | 66-78 | 50-70 | 10-25 | 100 | 10-22 | [67] |
| | Pineapple | 70-82 | 44-60 | 10-15 | 450 | 10-22 | [66] |
| | Banana | 44-64 | 45-55 | 10-12 | 150 | 35-53 | [64] |
| **Seed** | Cotton | 85-93 | 65-90 | 46 | 1000 | 5 | [88] |
| | Coir | 32-43 | 27-33 | 30-49 | 35 | 30-50 | [64] |
| | Oil palm | 40-50 | 20-30 | 42-46 | 100 | 5-10 | [65] |
| **Other** | Bamboo | 26-60 | 40-60 | 8-11 | 100 | | [76] |
| | Wood fibre* | 40-60 | 60-70 | 10-25 | 50 | 20-70 | [89] |

* Including softwoods and hardwoods.

It is noteworthy, that apart from the four micro-structural parameters identified previously, fibre cross-sectional shape and dimensions (particularly, fibre diameter and luminal porosity) are also thought to be important parameters in determining fibre mechanical properties [78, 82, 84, 85]. Table 2.5 presents typical values of surface area proportion of the lumen in different plant fibres; lower luminal porosity

would lead to better tensile properties. Several authors, for instance [34, 45, 46, 78, 84, 90], have reported that lower fibre diameter also leads to improved fibre tensile stiffness. While there is no ready explanation in literature to explain this phenomenon [78], Baley *et al.* [45, 84, 90] and Summerscales *et al.* [46] have hypothesised that this may be due to the lumen size increasing with fibre diameter. Placet *et al.* [78] and Gassan *et al.* [85] have also demonstrated through their models on the elastic properties of bast fibres that an only an increase in surface area proportion of the lumen (*i.e.* a reduction in the load-bearing area of the fibre), as a function of fibre diameter, could justify a decrease in fibre stiffness. However, both Placet *et al.* [78] and Summerscales *et al.* [46] acknowledge that this assumed relationship of increasing lumen size with increasing fibre diameter is not currently supported by morphological studies on hemp and jute fibres. Structural effects, such as the microfibril angle being a function of the fibre diameter, have been deemed unlikely to explain the diameter dependence of fibre modulus [46, 78].

Of interest is a recent analysis by Porter *et al.* [91] which shows that the fibre diameter plays a key role in determining fibre properties for both natural and synthetic polymer fibres. Applying Griffith observations, which combines fracture mechanics and inelastic deformations, to a variety of fibres, Porter *et al.* [91] find that the fibre fracture strength is directly proportional ($R^2 = 0.90$) to the square root of the ratio of the fibre stiffness to the fibre diameter, *i.e.* $\sigma_f = \sqrt{(G \cdot E_f / d_f)}$, where $G$ is the strain energy release rate (determined to be 1000 $Jm^{-2}$), for a large range of polymer fibres. As is suggested by the results of Porter *et al.* [91], for a given fibre (with a given characteristic fibre strength), the fibre stiffness would thus be characteristically inversely proportional to the fibre diameter. The latter is observed by Virk *et al.* [46], inspiring them to define a fibre diameter distribution factor $\eta_d$ for the modified ROM model (discussed in *Section 2.4*). Other than the diameter dependence of fibre tensile properties, Gassan *et al.* [85] have shown that the cross-sectional shape of the fibre may affect the fibre tensile properties. In fact, the tensile modulus is lower for circular cross-section shaped fibres than for elliptical cross-sectional shaped fibres [85]. This is possibly due to higher transverse fibre aspect ratio for elliptical cross-sectional shaped fibres.

### 2.5.3 Plant fibre processing

#### 2.5.3.1 Plant growth and fibre extraction

Plant fibres, even of the same type, have highly variable properties. The variability in properties can be ascribed to the variability in the previously described fibre micro-structural parameters. Indeed, even for a given plant fibre type, the fibre micro-structural parameters, which dictate the fibre quality, are themselves influenced by *i)* plant growth conditions (including, plant species, geographic location, climate, soil characteristics, crop cultivation), *ii)* fibre extraction and preparation (including, age of plant, fibre location in plant, type of retting method, decortification and carding processes), and *iii)* fibre processing (including, spinning to produce rovings from slivers and yarns from rovings, and production of mats and textile preforms from slivers/rovings/yarns). Several review articles and studies (for instance, [21, 23, 25-27, 29, 31, 92-94]) have discussed the influence of these factors on the fibre and composite properties. To ensure that the quality of their products is consistent (*i.e.* the variability in properties is within acceptable limits) and independent of plant growth conditions, suppliers of plant fibres/yarns typically use 'batch-mixing', across several crops/harvests/years.

Regarding optimising fibre extraction and processing, the resounding message of scientific studies is that an increasing number of mechanical processing steps leads to an increase in defect count (in the form of kink bands, for instance), a reduction in degree of polymerization of the cellulose chains, and a subsequent reduction in fibre mechanical properties [26, 92]. Minimally-processed fibres that have undergone retting and hackling produce high quality fibres and good quality composites [21, 25, 27]. However, to ensure full utilisation of fibre properties in a composite, a continuous and aligned reinforcement product is required. Once fibres have been carded or cottonised to produce a (typically coarse *i.e.* high linear density) sliver, rovings can be produced through a wet-spinning process, and yarns can produced through a dry-spinning process. Notably, the level of twist imparted to the product increases at each stage [21]. As will be discussed in depth in *Chapter 5*, increasing twist levels have various detrimental effects on composite properties, including

hindered resin impregnation, reduced wettability, increased intra-yarn void formation and a significant quantifiable drop in tensile properties, similar to an off-axis composite, due to increased fibre misorientation [19, 21, 95]. Interestingly, structure-property relations of twisted yarns imply that for the same twist level, yarns of fine count (low linear density) have a smaller diameter than heavier yarns. The result is that the twist angle in fine count yarns, and the induced reinforcement misorientation and subsequent reduction in composite properties, is smaller [21]. Therefore, to achieve a compromise between *i)* minimal fibre processing, *ii)* employing aligned/continuous reinforcements, and *iii)* limiting the detrimental effects of yarn twist, the order of preference for a reinforcement product is: slivers, followed by rovings, followed by fine-count yarns [21, 25].

Complementary to the studies on the effect of fibre processing on fibre and composite mechanical properties are life cycle assessment studies by Joshi *et al.* [3], Dissanayake *et al.* [34, 96-98], Steger [4] and Le Duigou *et al.* [99]. Dissanayake *et al.* [34, 96-98] quantified the energy required in the production of UK flax fibres, and found that while the energy required for cultivating plant fibres is low (4-15 MJ/kg of processed fibre), the use of agrochemicals and retting processes increases the energy consumption significantly (by 38-110 MJ/kg of processed fibre). An independent analysis by Le Duigou *et al.* [99] on French flax fibres, based on a different set of assumptions, provides a similar conclusion. Water retting is found to be least energy intensive, followed by dew retting and bio-retting [34, 96, 98]. Conversion from fibres to semi-products through textile processes increases the energy consumption further by 2-15 and 26-40 MJ/kg of processed fibre, for slivers and yarns respectively [34, 96]. The total energy required is 54-118 MJ/kg for flax sliver and 81-146 MJ/kg for flax yarn [34]. This compares to 55 MJ/kg for E-glass reinforcement mats and 90 MJ/kg for polypropylene fibres [34]. Hence, even in terms of minimising the environmental impact of plant fibre reinforcements, minimal processing is attractive.

#### 2.5.3.2 Fibre surface modification

The hydrophilic nature of plant fibres has led to the popular view, particularly amongst researchers of PFRPs, regarding the vulnerability of plant fibres and their

composites to moisture absorption and the poor compatibility of highly polar plant fibres with typically non-polar polymer matrices [17]. While the former is a concern for the long-term durability of PFRPs, the latter is a concern for the general mechanical performance of PFRPs. Not surprisingly, a significant amount of work has been undertaken, reviewed by several authors in [9, 23, 33, 100, 101], to explore various avenues in improving the fibre/matrix interfacial properties. The two fundamental routes are fibre surface physical/chemical modification and matrix modification. The former is usually preferred over the latter. The aim of physical modification techniques, such as plasma treatment or mercerisation, is to roughen the fibre surface topography and/or remove surface impurities (such as oils, waxes, pectin), enabling improved mechanical adhesion between the fibre and the matrix. In chemical modification techniques, a third material is introduced, as a compatibiliser or coupling agent, between the fibre and the matrix.

The question is: Is fibre surface modification necessary to achieve good mechanical properties in all PFRPs? In Section 2.4 it has been described that there is an ineffective fibre length below which the fibre does not carry the maximum load. The contribution of the fibre in reinforcing the composite (*i.e.* the length efficiency factor) is determined by the ratio of the critical fibre length to the reinforcing fibre length (Eq. 2.6). Notably, the critical fibre length is directly proportional to the ratio of the fibre tensile strength and fibre/matrix interfacial shear strength (Eq. 2.6). An interesting inference of these relationships is the following: assuming that *i)* a given plant fibre has the same diameter as E-glass (which is true in the case of flax [30]), and *ii)* a PFRP and GFRP are to be manufactured with reinforcing fibres of the same length, then for the critical fibre length (and thus length efficiency factor) to be the same in the PFRP and the GFRP, the ratio of the fibre strength to the interfacial shear strength needs to be the same in PFRP and the GFRP. In essence, as plant fibres have a lower tensile strength than E-glass, PFRPs require a proportionally lower interfacial shear strength than GFRPs. Therefore, the common notion that PFRPs have poor interfacial shear strength in comparison to GFRPs, is rather trivial.

$$\eta_{lS,plant} = \eta_{lS,Eglas} \Leftrightarrow l_{c,plant} = l_{c,Eglas} \Leftrightarrow \frac{\sigma_{plant} d_{plant}}{2\tau_{plant}} = \frac{\sigma_{Eglass} d_{Eglass}}{2\tau_{Eglass}} \Leftrightarrow \frac{\sigma_{plant}}{\tau_{plant}} = \frac{\sigma_{Eglass}}{\tau_{Eglass}}$$

The case for improving the interfacial shear strength of PFRPs (and thus employing fibre surface pre-treatments) becomes important when the reinforcing fibres are 'short', that is short in comparison to the critical fibre length. As was demonstrated in Section 2.4 (see Fig. 2.3), an increase in the interfacial strength from 15 MPa to 30 MPa (and a consequent reduction in the critical fibre length from 0.667 mm to 0.333 mm) leads to a significant increase in the length efficiency factor (from 0.667 to 0.833 for a constant fibre length of 1 mm). (Please refer to the typical values used for these calculations listed in the caption of Fig. 2.3). As a significant amount of research on PFRPs has focussed on short-fibre randomly oriented composites, based on the compression moulding of nonwovens (typically $l_f \approx$ 3-30 mm [9, 12, 102]) or the injection/extrusion moulding of pellets/granules (typically $l_f \approx$ 0.2-3 mm [9, 12, 102-104]), it is appreciable why some researchers report significant improvements in the mechanical properties of the resulting PFRPs if the fibres are pre-treated.

On the other hand, if the reinforcing fibres are 'long', that is more than 10 times the critical fibre length [50], improvements to the interfacial shear strength (through fibre surface pre-treatment) have negligible effect on the length efficiency factor (see Fig. 2.3). Essentially, as the fibres are carrying the maximum load over a majority of the fibre length, a reduction in the ineffective fibre length does not have a significant effect on the contribution of the fibre in reinforcing the composite. Therefore, it can be argued, that when considering PFRPs for structural applications, as long fibre reinforcements (typically $l_f >$ 30 mm) are used, the use of fibre surface modification is unnecessary. Indeed, PFRPs with impressive mechanical properties can be produced, without any active fibre surface treatment, by using an optimised reinforcement form (*i.e.* slivers or rovings) and high fibre volume fractions [21, 105] (demonstrated in *Chapter 3*). In fact, considering that *i)* fibre surface treatment techniques may employ expensive (*e.g.* silanes) and/or toxic (*e.g.* isocyanates) chemical reagents which tarnish the low-cost eco-friendly image of plant fibres [12], *ii)* unoptimised fibre treatments may slash the raw fibre tensile strength by up to 50%

[24], *iii)* there is a lack of consensus in literature on the surface treatment parameters to use (*e.g.* concentration of reagent, treatment time, temperature) to achieve improvements in PFRP mechanical properties [24], and *iv)* improvements in interfacial properties often lead to a reduction in impact and toughness performance (due to reduced fibre pull-out) [17], the use of fibre surface modification to potentially improve the mechanical properties of structural PFRPs is discouraged.

## 2.6 FIBRE VOLUME FRACTION

As already mentioned, the mechanical properties of a composite are dependent not only on the properties of the constituents, but more so on the volumetric composition of the composite. In fact, the fibre volume fraction $v_f$ is the single-most important factor in the rule of mixtures model (Eq. 2.1-2.4). For FRPs in general, improvements in most mechanical properties, including stiffness (tensile, flexural, compressive, shear) and strength (tensile, flexural, compressive, shear, impact), can be made by simply increasing the fibre volume fraction [50]. Indeed, several studies, particularly those employing aligned reinforcements, have shown this to be the case for PFRPs (such as [105-107]).

To produce PFRPs with high fibre content, it is generally suggested that due to the low compactability of plant fibre assemblies [12, 107], the plant fibre preforms need to be compacted using external force. As the literature survey in Table 2.6 reveals, compression moulding (including hot- and cold-pressing) has been the most popular method so far. It is being used for the manufacture of both thermoplastic- and thermoset-based PFRPs [9, 12]. Indeed, current commercial applications of PFRPs are primarily based on compression moulded components (Fig. 1.1) [15, 59]. In the case of liquid thermoset resins, a 'leaky mould' is typically used, where the excess resin is forced out during mould compaction [12].

From Table 2.6 it is clearly observed that amongst thermoset-based PFRPs, hand lay-up and vacuum infusion produce lower fibre content than compression moulding. Comparing hand layup and compression moulding techniques in the manufacture of flax/epoxy composites, Charlet *et al.* [108] find that the maximum achievable fibre volume fractions were ~15% and ~40%, respectively. While compression moulding

is suitable for high-volume part production at low-cycle times, the limitation with compression moulding is the component size that can be manufactured. Large structural components produced at a much lower rate, such as wind turbine blades, are typically manufactured through vacuum infusion, resin transfer moulding (RTM) or prepregging technology. The literature survey in Table 2.6 finds that fibre volume fractions achievable through RTM and prepregging technology (up to 50%) are comparable to compression moulding (up to 60%), noting that the latter is more prone to porosity-related issues [50].

## 2.7 ASHBY PLOT FOR PFRPS

The construction of a materials selection chart (*i.e.* Ashby plot) relies heavily on a large database that captures, and is representative of the variability in (*i.e.* range of), typical properties. To generate such a database, an extensive literature survey was conducted on the (absolute and specific) tensile properties of bast fibre reinforced PFRPs. The literature survey is partly presented in the form of Table 2.6. The wide-ranging database looks to particularly elucidate the effects of *i)* reinforcement geometry and orientation (pellets, short-random nonwovens, and long-aligned fibres for unidirectional and multiaxials), *ii)* matrix type (thermoplastic *vs.* thermoset), and *ii)* manufacturing technique (injection moulding, compression moulding, hand lay-up, vacuum infusion, resin transfer moulding and prepregging), on the tensile properties of bast fibre reinforced PFRPs. While the specific effects of each will be discussed in some detail in the following sections, here Ashby plots are presented for the PFRP materials (Fig. 2.6), showing the absolute and specific tensile strength plotted against the absolute and specific tensile stiffness, respectively. Note that the fibre volume fraction of the PFRPs may be dissimilar.

Ashby plots, such as the ones presented in Fig. 2.6, are very useful for four key reasons [38, 39]: *i)* they allow quick retrieval of the typical properties of a particular material, *ii)* they allow quick comparison of the properties of different materials, revealing their comparative efficiencies, *iii)* they facilitate the selection of the materials/manufacturing processes during the product design stage, and *iv)* they enable substitution studies exploring the potential of one material to replace another.

It is quite clear from the Ashby plots in Fig. 2.6 that PFRPs can be categorised into four distinct sub-groups, with increasing tensile properties in the following order: *i)* Injection-moulded PFRPs, whose mechanical properties are low and comparable to the matrix material, *ii)* PFRPs based on nonwoven reinforcements (randomly-oriented short fibres), *iii)* PFRPs based on textile reinforcements (woven and stitched biaxials, for instance) and *iv)* unidirectional PFRPs. It is also observed that tensile strength and stiffness tend to increase linearly with each other. Observing the variation in properties within each sub-group, it is found that thermoset-based PFRPs have better mechanical properties than thermoplastic-based PFRPs. Furthermore, the manufacturing technique can have a noticeable effect on PFRP mechanical properties, particularly in the case of unidirectional PFRPs.

The Asbhy plot in Fig. 2.6 can be expanded to include typical tensile properties of various GFRPs to enable a comparison between properties achievable with GFRPs and PFRPs. In fact, although the data has not been graphically shown in Fig. 2.6, the literature survey of Table 2.6 includes example tensile properties of GFRPs. The comparison reveals that when comparing short-fibre reinforced composites (*i.e.* injection moulded and nonwoven composites), PFRPs have better tensile modulus (specific and absolute) and comparable specific tensile strength than GFRPs. On the other hand, when comparing long-fibre reinforced composites (*i.e.* textile and unidirectional composites), PFRPs have better specific tensile modulus than GFRPs; the specific tensile strength of PFRPs is only up to half that of GFRPs.

Although the Asbhy plot in Fig. 2.6 suggests that unidirectional PFRPs, for instance provide 2 to 20 times better tensile properties than nonwoven PFRPs and up to 5 times better tensile properties than multiaxial PFRPs, this does not necessarily mean that unidirectional PFRPs would be preferred over the other materials for all structural applications. To truly enable substitution studies exploring the potential of one material to replace another, other material properties, such as cost and fatigue performance, may need to be taken into other, depending on the specific component function, objectives and constraint for a given application.

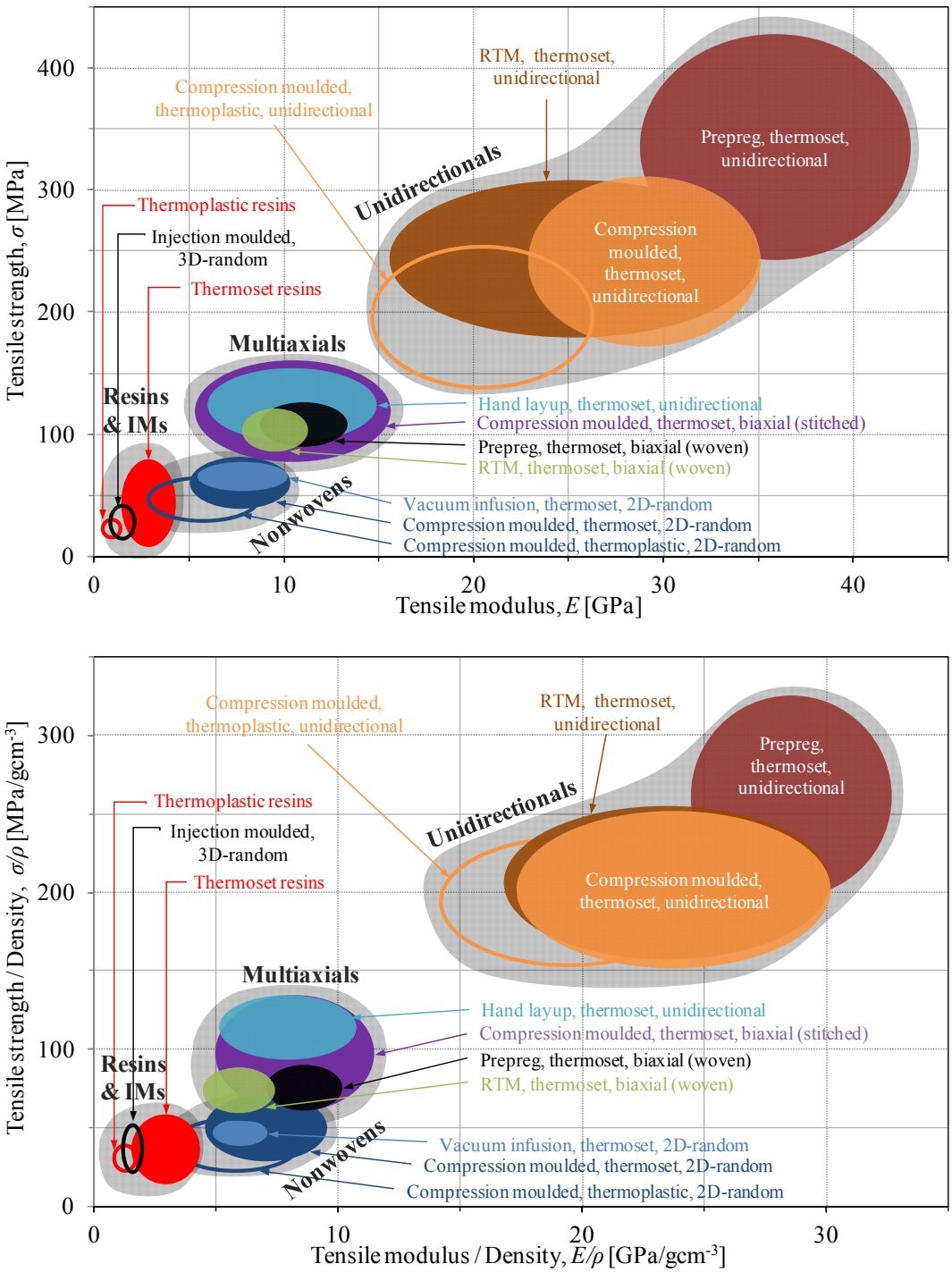


**Fig. 2.6. Typical tensile properties (absolute and specific) for PFRPs manufactured with thermoplastic/thermoset resins, short-random/long-aligned fibre reinforcements, and various manufacturing routes. Refer to the main text and Table 2.6 for more information, comparison with GFRPs, and the primary literature sources used in the production of this chart.**

**Table 2.6. Literature survey of typically reported mechanical properties of various PFRPs, specifically focussing on the effect of *i)* matrix type, *ii)* reinforcement form, *iii)* manufacturing technique, and *iv)* interface engineering, on PFRP mechanical properties. For comparison, the mechanical properties of the neat matrix and similarly manufactured GFRPs are also given.**

| *Manufacturing technique* | *Reinforcement form* | *Matrix type* | *Composite* | *Fibre content [a] [%]* | *Tensile modulus [GPa]* | *Specific tensile modulus [a] [GPa/gcm$^{-3}$]* | *Tensile strength [MPa]* | *Specific tensile strength [a] [MPa/gcm$^{-3}$]* | *Source* |
|---|---|---|---|---|---|---|---|---|---|
| - | - | Thermoplastic | PP [b] | 0 | 0.7-1.7 | 0.8-1.9 | 20-35 | 22-39 | |
| - | - | Thermoset | UP [b] | 0 | 1.4-4.7 | 1.2-3.9 | 12-75 | 10-63 | |
| - | - | Thermoset | Epoxy | 0 | 3.1-3.7 | 2.7-3.2 | 60-75 | 50-63 | |
| Injection moulding [c] | short fibre [e], 3D-random | Thermoplastic | Flax/PP | 30 wt | 1.7 | 1.6 | 27 | 26 | [109] |
| | | | Hemp/PP | 30 wt | 1.5 | 1.5 | 30 | 29 | [110] |
| | | | Flax/PP *5 wt% MAPP* [b] | 30 wt | 2.1 | 2.0 | 38 | 36 | [109] |
| | | | E-glass/PP | 30 wt | 2.2 | 1.5 | 49 | 35 | [109] |
| Compression moulding [d] | short fibre [e], 2D-random | Thermoplastic | Flax/PP | 40 v | 8.8 | 8.0 | 57 | 52 | [71] |
| | | | Jute/PP | 30 v | 3.7 | 3.6 | 27 | 26 | [17] |
| | | | Flax/PP *3.5 wt% MAPP* | 40 v | 8.6 | 7.8 | 68 | 62 | [71] |
| | | | E-glass/PP | 22 v | 6.2 | 4.8 | 89 | 69 | [17] |
| Compression moulding [d] | short fibre [e], 2D-random | Thermoset | Flax/UP | 21 wt | 11.0 | 8.7 | 80 | 63 | [111] |
| | | | Hemp/UP | 47 wt | 5.6 | 4.3 | 36 | 28 | [112] |
| | | | Hemp/UP *5% NaOH treated* | 46 wt | 7.5 | 5.8 | 46 | 35 | [112] |
| | | | E-glass/UP | 20 wt | 8.5 | 6.1 | 95 | 68 | [111] |

| *Manufacturing technique* | *Reinforcement form* | *Matrix type* | *Composite* | *Fibre content [a] [%]* | *Tensile modulus [GPa]* | *Specific tensile modulus [a] [GPa/gcm$^{-3}$]* | *Tensile strength [MPa]* | *Specific tensile strength [a] [MPa/gcm$^{-3}$]* | *Source* |
|---|---|---|---|---|---|---|---|---|---|
| Vacuum infusion | short fibre [e], 2D-random | Thermoset | Flax/UP | 30 v | 6.3 | 5.2 | 61 | 50 | [113] |
| | | | Jute/UP | 30 v | 8.0 | 6.3 | 50 | 39 | [113] |
| | | | Flax/epoxy *1% NaOH treated* | 22 v | 9.2 | 6.5 | 60 | 42 | [114] |
| | | | E-glass/UP | 30 v | 14.9 | 9.1 | 190 | 116 | [113] |
| Compression moulding [d] | long fibre [f], unidirectional | Thermoplastic | Flax/PP | 43 v | 26.9 | 23.6 | 251 | 220 | [43] |
| | | | Hemp/PP | 42 v | 21.1 | 18.2 | 215 | 185 | [22] |
| | | | Hemp/PP *0.2 wt% MAPP* | 40 v | 20.1 | 17.5 | 208 | 181 | [22] |
| | | | E-glass/PP | 35 v | 26.5 | 17.4 | 700 | 461 | [115] |
| Hand layup | long fibre [f], unidirectional | Thermoset | Flax/UP | 19 v | 6.5 | 5.2 | 150 | 120 | [108] |
| | | | Flax/UP | 28 v | 14.0 | 10.8 | 140 | 108 | [19] |
| Compression moulding [d] | long fibre [f], unidirectional | Thermoset | Flax/UP | 58 v | 29.9 | 23.0 | 304 | 233 | [116] |
| | | | Jute/UP | 56 v | 35.0 | 28.2 | 248 | 200 | [106] |
| | | | Jute/epoxy *26% NaOH treated* | 40 v | 24.0 | 18.8 | 220 | 172 | [117] |
| | | | E-glass/UP | 42 v | 30.6 | 16.9 | 695 | 384 | [116] |

| *Manufacturing technique* | *Reinforcement form* | *Matrix type* | *Composite* | *Fibre content* [a] *[%]* | *Tensile modulus [GPa]* | *Specific tensile modulus* [a] *[GPa/gcm$^{-3}$]* | *Tensile strength [MPa]* | *Specific tensile strength* [a] *[MPa/gcm$^{-3}$]* | *Source* |
|---|---|---|---|---|---|---|---|---|---|
| RTM (including vacuum infusion) | long fibre [f], unidirectional | Thermoset | Flax/epoxy | 42 v | 35.0 | 28.2 | 280 | 226 | [105] |
| | | | Flax/VE [b] | 37 v | 24.0 | 16.9 | 248 | 175 | [19] |
| | | | E-glass/epoxy | 48 v | 31.0 | 18.1 | 817 | 478 | [105] |
| Prepregging [g] | long fibre [f], unidirectional | Thermoset | Flax/epoxy | 42 v | 39.9 | 31.3 | 378 | 296 | [21] |
| | | | Flax/epoxy | 48 v | 32.0 | 24.7 | 268 | 207 | [24] |
| | | | E-glass/epoxy | 55 v | 39.0 | 18.6 | 1080 | 514 | [118] |
| Compression moulding [d] | long fibre [f], stitched balanced biaxial | Thermoset | Flax/epoxy [0, 90] | 44 v | 14.3 | 11.2 | 170 | 133 | [119] |
| | | | E-glass/epoxy [0, 90] | 43 v | 21.9 | 12.2 | 380 | 212 | [119] |
| | | | Flax/epoxy [±45] | 44 v | 6.5 | 5.1 | 79 | 62 | [119] |
| | | | E-glass/epoxy [±45] | 43 v | 11.1 | 6.2 | 103 | 58 | [119] |
| RTM (including vacuum infusion) | long fibre [f], plain weave biaxial | Thermoset | Flax/VE [0, 90] | 33 v | 7.3 | 4.8 | 81 | 54 | [19] |
| | | | Flax/VE [0, 90] | 35 v | 8.6 | 5.7 | 89 | 59 | [19] |
| | | | Jute/VE [0, 90] | 41 v | 10.0 | 6.7 | 111 | 74 | [19] |
| | | | E-glass/UP [0, 90] | 51 v | 33.0 | 12.8 | 483 | 189 | [19] |

| *Manufacturing technique* | *Reinforcement form* | *Matrix type* | *Composite* | *Fibre content* [a] *[%]* | *Tensile modulus [GPa]* | *Specific tensile modulus* [a] *[GPa/gcm$^{-3}$]* | *Tensile strength [MPa]* | *Specific tensile strength* [a] *[MPa/gcm$^{-3}$]* | *Source* |
|---|---|---|---|---|---|---|---|---|---|
| Prepregging [g] | long fibre [f], 2x2 twill weave biaxial | Thermoset | Flax/epoxy [0, 90] | 45 v | 11.2 | 8.2 | 94 | 69 | [120] |
| | | | Flax/epoxy [0, 90] | 36 v | 10.0 | 7.5 | 104 | 78 | [120] |
| | | | Flax/epoxy [0, 90] | 37 v | 11.2 | 8.5 | 77 | 59 | [121] |
| | | | Flax/epoxy [0, 90] | 54 v | 9.3 | 6.8 | 78 | 57 | [121] |

[a] Fibre content is approximate – note that some sources have presented fibre content in terms of fibre weight fraction $w_f$ and not fibre volume fraction $v_f$. If the specific properties have not been determined in the referenced source, these have been estimated by either using the composite density measured by the authors in their respective studies, or by estimating the composite density (assuming no porosity) using $\rho_c = (\rho_f \rho_m)/(\rho_f - w_f(\rho_f - \rho_m))$ if fibre weight fraction is given, or $\rho_c = \rho_f v_f + \rho_m v_m$ if fibre volume fraction is given.

[b] PP = Polypropylene, MAPP = Maleic Anhydride Polypropylene, UP = Unsaturated Polyester, VE = Vinylester

[c] Injection moulding includes extrusion-injection moulding (*i.e.* pellets/granules obtained from an extruder rather than a melt-blender).

[d] Compression moulding includes press moulding (*i.e.* hand layup or vacuum infusion or filament winding as a pre-cursor to lossy pressing of the mould for compaction of the impregnated preform). Compaction pressures of up to 60 bars, but typically 20-30 bars, are used.

[e] Short fibre = discontinuous reinforcement with fibres less than 30 mm in length. Typically, fibre lengths are less than 1 mm for injection moulding and between 3 to 30 mm for compression moulding.

[f] Long fibre = continuous reinforcement, in the form of slivers, rovings and yarns. Single fibres are typically greater than 30 mm in length.

[g] Prepregging with autoclave consolidation and cure. Autoclave pressures of up to 10 bars, but typically 4-6 bars, are used.

## 2.8 REINFORCEMENT GEOMETRY AND ORIENTATION

### 2.8.1 Length efficiency factors

To ensure that the full reinforcing potential of plant fibres is realised, it is essential that the highest reinforcement efficiency is utilised. As demonstrated by Fig. 2.3, the reinforcement geometry (*i.e.* fibre length and aspect ratio) directly affects the length efficiency factors for stiffness $\eta_{lE}$ and strength $\eta_{lS}$ (Eq. 2.5 and Eq. 2.6). $\eta_{lE}$ and $\eta_{lS}$ can be maximised by using high aspect ratio fibres with fibre lengths significantly longer than the critical fibre length. In fact, fibre aspect ratios of $l_f/d_f > 50$ (*i.e.* fibre lengths of $l_f > 1$ mm) would yield $\eta_{lE} > 0.93$ [44] and provided that the fibre length is about 10 times the critical length ($l_f/l_c > 10$), $\eta_{lS} > 0.95$ can be achieved [50]. This is confirmed by the plots in Fig. 2.3.

Critical fibre lengths for bast fibre reinforced PFRPs have been measured to be in the range of 0.2-3 mm [12, 16, 102-104, 122, 123]. While a majority of bast fibres are typically >30 mm in length [23] and have high aspect ratios (between 100-2000; Table 2.5), depending on the composite manufacturing route, the utilised fibre length and aspect ratio can be much lower. For instance, injection moulding employs fibres with lengths of 1.2-0.1 mm and aspect ratios <20 [103, 110, 124-126]; the resulting length efficiency factors are thus <0.30 [103, 110, 124]. Bos *et al.* [103] have determined the length efficiency factors to be in the range of 0.17-0.20 for injection moulded flax composites. On the other hand, Sawpan *et al.* [122] determine $\eta_{lS}$ to be up to 0.9 for compression moulded hemp/polyester composites based on nonwoven reinforcements (fibre length of $l \approx$ 2-3 mm). Finally, yarns/rovings compose of fibres that are >30 mm in length [16, 27, 127], hence composites utilising textile or unidirectional reinforcements yield length efficiency factors of approximately unity [41, 42]. These results are summarised in Table 2.7.

### 2.8.2 Orientation distribution factors

Due to the anisotropic nature of many fibres, reinforcement orientation has a significant effect on composite properties. The anisotropy of fibre reinforcements may result from the natural structure of the fibre (as is the case of cellulose-based

fibres) [128] and/or from the larger aspect ratio along the axis of the fibre in comparison to the cross-sectional aspect ratio [50].

**Table 2.7. Typical fibre length efficiency factors and fibre orientation distribution factors for various PFRP categories.**

| *PFRP subgroup (see Fig. 2.6)* | *Typical fibre length [mm]* | $\eta_{lE}$ *or* $\eta_{lS}$ | $\eta_o$ | $\eta_l \cdot \eta_o$ |
|---|---|---|---|---|
| Injection moulded (IM) | <1 | <0.3 | ~0.20-0.37 | <0.11 |
| Nonwovens | 3-30 | 0.5-0.9 | ~0.38-0.40 | 0.19-0.36 |
| Multiaxials | >30 | ~1.0 | 0.25-0.50 | ~0.25-0.5 |
| Unidirectionals | >30 | ~1.0 | ~1.00 | ~1.0 |

Once again, the composite manufacturing route can dictate the orientation distribution that is likely in the resulting composite. For a 3D-random orientation of the fibres, it can be shown that $\eta_o$ = 1/5 (= 0.2). In injection moulded PFRPs, fibre orientation is nominally 3D-random, but typically show a preferred orientation [125]. While Garkhail *et al.* [102] and Bos *et al.* [103] have found $\eta_o$ to be 0.21-0.31, Vallejos *et al.* [124] and Serrano *et al.* [125] have determined $\eta_o$ to be in the range of 0.28-0.37, for injection moulded PFRPs. For a 2D-random orientation of the fibres, it can be shown that $\eta_o$ = 3/8 (= 0.375). Conventional nonwoven mat reinforced PFRPs have a nominally 2D-random orientation, but may show a preferred orientation. Bos *et al.* [103] have determined $\eta_o$ to be ~0.40 for nonwoven PFRPs.

Composites reinforced with multiaxial textile fabrics may have a range of orientation distribution factors, depending on the ply orientation. For composites with balanced biaxial reinforcements in a [0,90] and [±45] stacking sequence, it can be shown that $\eta_o$ = 1/2 (= 0.5) and $\eta_o$ = 1/4 (= 0.25), respectively. Finally, to ensure the orientation distribution factor $\eta_o$ is close to unity, unidirectional fibres are required. These results are summarised in Table 2.7.

Table 2.7 presents the typical length efficiency factors $\eta_l$, orientation distribution factors $\eta_o$ and their product (*i.e.* $\eta_l \cdot \eta_o$) for the four PFRP subgroups identified in the Asbhy plot in Fig. 2.6. The product $\eta_l \cdot \eta_o$ is a good estimate of the reinforcing contribution of the fibre to the composite (Eq. 2.1-2.4). The difference in the product

of the efficiency factors between the subgroups (Table 2.7) clearly demonstrates the difference in properties of the materials (Fig. 2.6). Sub-critical length fibre reinforced 3D-random composites have tensile stiffness and strength in the range of 1.0-2.5 GPa and 20-50 MPa, respectively. This is comparable to the tensile properties of the polymer matrix. Short-fibre 2D-random composites have higher tensile stiffness and strength in the range of 2.5-11.0 GPa and 25-80 MPa. Textile reinforcement based PFRPs have tensile stiffness and strength in the range of 5-15 GPa and 75-175 MPa. Barring the performance of aligned hand-layup PFRPs (with inherently low fibre content), which is still better than that of 2D-random composites, unidirectional PFRPs reinforced with slivers/yarns/rovings exhibit 3-5 times better tensile stiffness and strength than 2D-random composites.

## 2.9 SELECTION OF MATRIX AND MANUFACTURING TECHNIQUE

### 2.9.1 Matrix type

A survey on the applications of PFRPs in the EU in 2010, showed that up to 30% of the PFRPs were based on thermoset matrices, while the rest were based on thermoplastic matrices (Fig. 1.1) [15]. There is a general trend, particularly in the automotive industry, of diminishing use of thermoset matrices and increased use of thermoplastic matrices [2, 15, 59]. This is primarily because the latter are faster to process, are fabricated by a cleaner process (dry systems with no toxic by-products), are easier to recycle, and are less expensive (for high volume production). Nonetheless, thermosets may be more suitable for PFRPs in structural applications for three key reasons. Firstly, thermoset matrices have better mechanical properties than thermoplastics, due to the formation of a large cross-linked rigid three-dimensional molecular structure upon curing. Consequently, as highlighted by the literature survey in Table 2.6 and the graphical analysis in Fig. 2.6, thermoset-based PFRPs consistently show better tensile properties (absolute and even specific) than thermoplastic-based PFRPs. Secondly, the low processing temperatures (typically below 100 °C) and viscosity (0.1-10 Pas) of thermoset matrices implies that plant fibre mechanical properties are not degraded due to high temperature exposure during composites manufacture, and resin impregnation and preform wettability are

easier leading to lower void content and better interfacial properties. The low viscosity of thermoset resins also raises the possibility of using liquid composite moulding techniques, such as vacuum infusion and resin transfer moulding (RTM), which are standard manufacturing procedures in the performance-demanding aerospace, marine and wind energy industries. In contrast, the high processing temperatures (up to 200 °C) and viscosity (100-10000 Pas) of thermoplastics are seen as barriers in the development of optimised thermoplastic PFRPs [12]. Thirdly and finally, thermosets have better shear properties than thermoplastics, and they form a better interface with typically polar plant fibres than thermoplastics (which tend to be non-polar).

It should be noted that in terms of end-of-life disposal, the use of thermosetting matrices, rather than thermoplastic matrices, does not necessarily lower the eco-performance of the PFRP produced. This is because the addition of plant fibres can significantly reduce the recyclability and reusability of a thermoplastic system [9, 34, 129]. All PFRPs can be incinerated for energy recovery or re-used as fillers; the additional option with thermoplastic-based PFRPs is that they can also be granulated and re-processed into extrusion/injection moulded components [34]. Notably, thermoplastic-based PFRPs that are recycled by remoulding into new parts exhibit severely deteriorated mechanical properties due to repeated thermal exposure [129]. In fact, the 'recyclability' of PFRPs is an altogether different and unresolved issue.

### 2.9.2 Composite manufacture

Faruk *et al.* [9] and Summerscales *et al.* [34] have discussed the various manufacturing techniques that have been utilised with PFRPs. The literature survey in Table 2.6 and the graphical analysis in Fig. 2.6 eloquently present the mechanical properties of PFRPs achievable when produced through a particular manufacturing route. The analysis reveals that to produce PFRPs with optimum mechanical properties, prepregging technology with autoclave consolidation is most suitable. Compression moulding and infusion processes (RTM and vacuum infusion) produce PFRPs with comparable specific tensile properties. Despite the use of aligned

reinforcements, hand layup produces composites with only moderate mechanical properties. Injection moulded PFRPs have poorest mechanical properties.

The composite manufacturing technique is interrelated with three key composite parameters, each of which has been discussed separately previously: *i)* volumetric composition (maximum achievable fibre volume fraction and porosity), *ii)* reinforcement form, and *iii)* matrix type. Indeed, the interactive effect of all these parameters can, at least qualitatively, explain the variation in mechanical properties of PFRPs produced through different manufacturing processes.

Firstly, the composite manufacturing technique affects the typical achievable fibre volume fraction and porosity. For high composite mechanical properties, high fibre volume fraction and low porosity are desirable. With increasing consolidation pressure, achievable and typical fibre volume fraction tend to increase. As shown in Table 2.8, consolidation pressures and thus typically achievable fibre volume fractions increase in the following order: vacuum infusion/RTM, prepregging (with autoclave consolidation), and compression moulding. This was also discussed in previously in Section 2.6.

**Table 2.8. Manufacturing technique is interrelated with other composite parameters. Here the maximum and typical values of various parameters for PFRPs are quoted. The values are from literatures referenced in Table 2.6.**

| *Manufacturing technique* | *Consolidation pressure [bar]* | *Fibre volume fraction [%]* | *Porosity volume fraction [%]* | *Matrix type useable* |
|---|---|---|---|---|
| Injection moulding (IM) | >1000 bar | Up to 45% (typically 15-30%) | - | Thermoplastic |
| Compression moulding | Up to 40 bar (typically 20-30 bar) | Up to 85% (typically 25-50%) | Up to 25% (typically 2-8%) | Thermoplastic or Thermoset |
| Prepregging (with autoclave) | 0-10 bar (typically 4-6 bar) | Up to 60% (typically 35-50%) | Up to 10% (typically 0-4%) | Thermoset |
| Vacuum infusion/RTM | 0-4 bar (typically 0-2 bar) | Up to 60% (typically 25-50%) | Up to 10% (typically 1-4%) | Thermoset |

Porosity, an almost inevitable phase in a composite material, has significant detrimental effects on composite mechanical performance [50]. As indicated in the modified ROM model (Eq. 2.3 and Eq. 2.4), Madsen *et al.* [44] suggest that the

influence of porosity on PFRP tensile properties can be modelled by including a factor of $(1-v_v)^2$ in the generalised ROM model (Eq. 2.1 and Eq. 2.2). Often, porosity can be managed, if not eliminated, by optimising the manufacturing process [50]. Typically, void contents of <1% are required for aerospace applications, but void contents of up to 5% are acceptable for other less demanding applications (*e.g.* automotive and marine) [130-132]. In literature [43, 44, 133], PFRPs are often quoted to have high void content. Typically, the void volume fraction is up to 5% for PFRPs with a fibre volume fraction below 40% [28, 107, 113, 133-135]. However, when the fibre volume fraction exceeds 40%, void content increases drastically and can even approach 25% [107, 133-136]. Nonetheless, there are some studies [28, 106] which conclude that there is no obvious relationship between fibre volume fraction and void volume fraction for PFRPs. From the literature survey, it is suggested that issues of high porosity in PFRPs are usually related, but not confined, to *i)* sisal fibre composites due to the large lumen size in sisal fibres which remain unfilled after resin infusion [113, 136], *ii)* structural porosity in (particularly, high weight fraction) compression-moulded thermoplastic PFRPs due to insufficient amount of matrix to fill the free space between the yarns [133], and *iii)* randomly-oriented short-fibre PFRPs. It is well known that void content in composites manufactured through different routes is typically in the following order: Hand lay-up > Compression moulding > Infusion processes (vacuum infusion > RTM > vacuum assisted-RTM) > Prepregging (with autoclave consolidation) [50]. This is in agreement with typical literature values observed for PFRPs (Table 2.8). Various studies report that vacuum-infused PFRPs have a low void volume fraction of 0.5-4.0% [113] and prepreg-based PFRPs have a typical void volume fraction of 0.0-4.0% [120, 121], although it may be as high as 10% if low autoclave pressures (< 3 bar) are used [120, 121]. It is of interest to note that Madsen *et al.* [22] show that porosity in hemp yarn reinforced thermoplastics increases linearly ($R^2 = 0.98$) with the logarithm of the matrix processing viscosity. As the viscosity of thermosets is several orders of magnitude lower than that of thermoplastics, the significantly lower void content in thermoset-based PFRPs is comprehendible. In addition, while vacuum-infusion and prepregging techniques employ thermoset matrices,

compression moulding may employ thermoplastics; therefore, the higher void content in the latter is conceivable.

Secondly, the manufacturing technique may affect the reinforcement form (length and orientation). This is particularly the case of injection moulded compounds, where the process implies that at each stage the fibre length reduces. For instance, initially long fibres (of up to 20 mm in length) are first chopped in a blade mill to a nominal length, of say 10 mm, followed by a melt-blending process where the fibre length reduces to 0.3-0.9 mm, followed by the injection moulding process where the fibre length reduces further to <0.3 mm [110]. Furthermore, the melt-blending process and injection/extrusion moulding process results in mixing of the fibres to produce a nominally 3D random fibre orientation. As discussed in Section 2.8, this leads to a small product of length efficiency factor and orientation distribution factor for the PFRPs (Table 2.7).

Thirdly and finally, the manufacturing technique is related to the matrix type that is employed, the effects of which have been analysed previously.

## 2.10 CONCLUSIONS

From the literature review, several recommendations are made in developing PFRPs for structural applications. The recommendations, related to maximising and optimising various composite parameters, are as follows:

- Plant fibre type: Bast fibres are most suitable for reinforcing composites due to their superior mechanical properties which derive from their chemical and structural composition. Typically, fibres with high cellulose content, high cellulose crystallinity, low micro-fibril angles, and high aspect ratios are desirable.
- Plant fibre processing and preparation: Fibres processed specifically for composites applications, rather than textile applications, are desirable to achieve a compromise between *i)* minimal fibre processing, *ii)* employing aligned/continuous reinforcements, and *iii)* limiting the detrimental effects of yarn twist, the order of preference for a reinforcement product is: slivers,

followed by rovings, followed by fine-count yarns. Furthermore, the use of fibre surface modification to improve fibre/matrix adhesion is argued to be unnecessary and possibly detrimental when utilising the previously mentioned long fibre reinforcements.

- Fibre volume fraction: Increasing the fibre content is highly recommended for improving composite properties.
- Reinforcement form: The tensile properties of unidirectional PFRPs are 3-5 times better than short-fibre randomly-oriented composites, due to enhanced reinforcement efficiency. While plant fibres are naturally discontinuous, a continuous product (in the form of slivers, wet-spun rovings and low-count yarns) will ensure that the maximum fibre aspect ratios (or length) and a high degree of alignment are employed. However, aligned plant fibre reinforcements are up to 30 times more expensive than raw and nonwoven plant fibre reinforcements.
- Manufacturing route: Prepregging technology (with autoclave consolidation) is most suitable to produce high quality PFRPs. Compression moulding and RTM/vacuum infusion are follow-up options to produce PFRPs with good mechanical properties.
- Matrix type: Thermosets are more suitable than thermoplastics, due to the formers *i)* capacity in high-performance applications, *ii)* lower viscosity and processing temperatures and, *iii)* better compatibility with plant fibres.

Through the general literature survey a highly useful Ashby plot has been constructed which will help in the material selection stage during product design of a PFRP component. Data for other materials (*e.g.* GFRPs) can also be added to this plot.

## 2.11 REFERENCES

1. Ashby M, Bush SF, Swindells N, Bullough R, Ellison G, Lindblom Y, Cahn RW, Barnes JF. Technology of the 1990s: Advanced materials and predictive design [and discussion]. *Philosophical Transactions of the Royal Society A*, 1987, 322: p. 393-407.

2. Reux F. Worldwide composites market: Main trends of the composites industry, in *5th Innovative Composites Summit - JEC ASIA 2012*. 26-28 June 2012. Singapore.
3. Joshi S, Drzal LT, Mohanty AK, Arora S. Are natural fiber composites environmentally superior to glass fiber reinforced composites? *Composites Part A: Applied Science and Manufacturing*, 2004, 35: p. 371-376.
4. Steger J. Light weight! No matter what the costs? Plant fibres for light weight automotive applications. *Journal of Biobased Materials and Bioenergy*, 2010, 4(2): p. 181-184.
5. Pickering S. Recycling technologies for thermoset composite materials – current status. *Composites Part A: Applied Science and Manufacturing*, 2006, 37: p. 1206-1215.
6. Yang Y, Boom R, Irion B, van Heerden D, Kuiper P, de Wita H. Recycling of composite materials. *Chemical Engineering and Processing: Process Intensification*, 2012, 51: p. 53-68.
7. John M, Thomas S. Biofibres and biocomposites. *Carbohydrate Polymers*, 2008, 71: p. 343-364.
8. Bledzki A, Gassan J. Composites reinforced with cellulose based fibres. *Progress in Polymer Science*, 1999, 24: p. 221-274.
9. Faruk O, Bledzki AK, Fink HP, Sain M. Biocomposites reinforced with natural fibres: 2000-2010. *Progress in Polymer Science*, 2012, 37(11): p. 1552-1596.
10. Mohanty A, Misra M, Drzal LT, ed. *Natural fibers, biopolymers and biocomposites*. 2005. Taylor and Francis.
11. Riedel U. Biocomposites: Long natural fiber-reinforced biopolymers. *Polymer Science: A Comprehensive Reference*, 2012, 10(18): p. 295–315.
12. Pickering K, ed. *Properties and performance of natural-fibre composites*. 2008. CRC Press LLC: Boca Raton.
13. Khot S, Lascala JJ, Can E, Morye SS, Williams GI, Palmese GR, Kusefoglu SH, Wool RP. Development and application of triglyceride-based polymers and composites. *Journal of Applied Polymer Science*, 2000, 82(3): p. 702-723.
14. Wool R, Khot SN. *Bio-based resins and natural fibers*, in *ASM Handbook: Composites*, 2001. p. 184-193.
15. Carus M, Gahle C. Natural fibre reinforced plastics - material with future, 2008. nova-Institut GmbH: Huerth.
16. Bos H. *The potential of flax fibres as reinforcement for composite materials*. PhD, 2004. Technische Universiteit Eindhoven: Eindhoven, Netherlands.
17. Wambua P, Ivens J, Verpoest I. Natural fibres: can they replace glass in fibre reinforced plastics? *Composites Science and Technology*, 2003, 63: p. 1259-1264.
18. Ticoalu A, Aravinthan T, Cardona F. A review of current development in natural fiber composites for structural and infrastructure applications, in *Southern Region Engineering Conference*. 11-12 November 2010. Toowoomba, Australia.
19. Goutianos S, Peijs T, Nystrom B, Skrifvars M. Development of flax fibre based textile reinforcements for composite applications. *Applied Composite Materials*, 2006, 13(4): p. 199-215.
20. Riedel U, Nickel J. Natural fibre-reinforced biopolymers as construction materials – new discoveries. *Die Angewandte Makromolekulare Chemie*, 1999, 272: p. 34-40.
21. Baets J, Plastria D, Ivens J, Verpoest I. Determination of the optimal flax fibre preparation for use in UD-epoxy composites, in *4th International Conference on Sustainable Materials, Polymers and Composites*. 6-7 July 2011. Birmingham, UK.
22. Madsen B. *Properties of plant fibre yarn polymer composites - An experimental study*. PhD, 2004. Technical University of Denmark: Lyngby, Denmark.

23. Dittenber D, Gangarao HVS. Critical review of recent publications on use of natural composites in infrastructure. *Composites Part A: Applied Science and Manufacturing*, 2012, 43: p. 1419-1429.
24. Weyenberg I, Chitruong T, Vangrimde B, Verpoest I. Improving the properties of UD flax fibre reinforced composites by applying an alkaline fibre treatment. *Composites Part A: Applied Science and Manufacturing*, 2006, 37: p. 1368-1376.
25. Miao M, Finn N. Conversion of natural fibres into structural composites. *Journal of Textile Engineering*, 2008, 54(6): p. 165-177.
26. Hanninen T, Thygesen A, Mehmood S, Madsen B, Hughes M. Mechanical processing of bast fibres: The occurrence of damage and its effect on fibre structure. *Industrial Crops and Products*, 2012, 39: p. 7-11.
27. Weyenberg I, Ivens J, Coster A, Kino B, Baetens E, Verpoest I. Influence of processing and chemical treatment of flax fibres on their composites. *Composites Science and Technology*, 2003, 63: p. 1241-1246.
28. Zhang L, Miao M. Commingled natural fibre/polypropylene wrap spun yarns for structured thermoplastic composites. *Composites Science and Technology*, 2010, 70: p. 130-135.
29. Summerscales J, Dissanayake N, Virk AS, Hall W. A review of bast fibres and their composites. Part 1 – Fibres as reinforcements. *Composites Part A: Applied Science and Manufacturing*, 2010, 41(10): p. 1329-1335.
30. Lewin M. *Handbook of fiber chemistry*. Third ed, 2007. Boca Raton: CRC Press LLC.
31. Charlet K, Baley C, Morvan C, Jernot JP, Gomina M, Bréard J. Characteristics of Herme`s flax fibres as a function of their location in the stem and properties of the derived unidirectional composites. *Composites Part A: Applied Science and Manufacturing*, 2007, 28: p. 1912-1921.
32. Hepworth D, Hobson RN, Bruce DM, Farrent JW. The use of unretted hemp fibre in composite manufacture. *Composites Part A: Applied Science and Manufacturing*, 2000, 31: p. 1279-1283.
33. John M, Anandjiwala RD. Recent developments in chemical modification and characterization of natural fiber-reinforced composites. *Polymer Composites*, 2008: p. 187-207.
34. Summerscales J, Dissanayake N, Virk AS, Hall W. A review of bast fibres and their composites. Part 2 – Composites. *Composites Part A: Applied Science and Manufacturing*, 2010, 41(10): p. 1336-1344.
35. Malkapuram R, Kumar V, Negi YS. Recent development in natural fiber reinforced polypropylene composites. *Journal of Reinforced Plastics and Composites*, 2009, 28(10): p. 1169-1189.
36. Rouison D, Sain M, Couturier M. Resin transfer molding of natural fibre reinforced composites: Cure simulation and process optimization. *Composites Science and Technology*, 2003, 64: p. 629-644.
37. Rouison D, Sain M, Couturier M. Resin transfer molding of hemp fiber composites: optimization of the process and mechanical properties of the materials. *Composites Science and Technology*, 2006, 66(7-8): p. 895-906.
38. Ashby M. *Materials selection in mechanical design*, 1992. Oxford, UK: Pergamon Press.
39. Ashby M. The CES EduPack database of natural and man-made materials (MFA, 20/12/2007), 2007. Cambridge University and Granta Design: Cambridge, UK.
40. Shahzad A. Hemp fiber and its composites - A review. *Journal of Composite Materials*, 2012, 46(8): p. 973-986.

41. Summerscales J, Virk AS, Hall W. A review of bast fibres and their composites. Part 3 – Modelling. *Composites Part A: Applied Science and Manufacturing*, 2013, 44: p. 32–139.
42. Virk A, Hall W, Summerscales J. Modulus and strength prediction for natural fibre composites. *Materials Science and Technology*, 2012, 28(7): p. 864-871.
43. Madsen B, Lilholt H. Physical and mechanical properties of unidirectional plant fibre composites - an evaluation of the influence of porosity. *Composites Science and Technology*, 2003, 63: p. 1265-1272.
44. Madsen B, Thygesen, A, Liholt, H. Plant fibre composites - Porosity and stiffness. *Composites Science and Technology*, 2009, 69: p. 1057-1069.
45. Lamy B, Baley C. Stiffness prediction of flax fibers-epoxy composite materials. *Journal of Materials Science Letters*, 2000, 19: p. 979-980.
46. Summerscales J, Hall W, Virk AS. A fibre diameter distribution factor (FDDF) for natural fibre composites. *Journal of Materials Science*, 2011, 46(17): p. 5876-5880.
47. Thomason J, Gentles F, Brennan A. Natural fibre cross sectional area effects on the determination of fibre mechanical properties, in *15th European Conference on Composite Materials (ECCM-15)*. 2012. Venice, Italy.
48. Cox H. The elasticity and strength of paper and other fibrous materials. *British Journal of Applied Physics*, 1952, 3: p. 72-79.
49. Kelly A, Tyson WR. Tensile properties of fibre-reinforced metals: Copper/tungsten and copper/molybdenum. *Journal of the Mechanics and Physics of Solids*, 1965, 13(6): p. 329-350.
50. Harris B. *Engineering composite materials*, 1999. London: The Institute of Materials.
51. Krenchel H. Fibre reinforcement. *Akademisk Forlag*, 1964: p. 16-22.
52. Thomason J, Carruthers J, Kelly J, Johnson G. Fibre cross-section determination and variability in sisal and flax and its effects on fibre performance characterisation. *Composites Science and Technology*, 2011, 71: p. 1008-1015.
53. d'Almeida J, Mauricio MHP, Paciornik S. Evaluation of the cross-section of lignocellulosic fibers using digital microscopy and image analysis. *Journal of Composite Materials*, 2012, 46(24): p. 3057-3065.
54. Virk A. *Numerical models for natural fibre composites with stochastic properties*. PhD, 2010. University of Plymouth: Plymouth, UK.
55. Kadam K, Forrest LH, Jacobson WA. Rice straw as a lignocellulosic resource: Collection, processing, transportation, and environmental aspects. *Biomass and Bioenergy*, 2000, 18: p. 369-389.
56. Putun A, Apaydin E, Putun E. Rice straw as a bio-oil source via pyrolysis and steam pyrolysis. *Energy*, 2004, 29: p. 2171-2180.
57. Steele P, El-Hissewy A, Badawi AEE. Agro-industrial use of rice straw - Exploring opportunities for making better use of rice residues in Egypt, 2009. Food and Agriculture Organization of the United Nations Regional Office for the Near East (Cairo, Egypt) and Ministry of Agriculture and Land Reclamation (Cairo, Egypt): Egypt.
58. *FAOSTAT- Food and Agriculture Organization of the United Nations*. 07 August 2012 [cited 2012; Available from: http://faostat.fao.org/site/567/DesktopDefault.aspx?PageID=567#ancor.
59. Carus M. Bio-composites: Technologies, applications and markets, in *4th International Conference on Sustainable Materials, Polymers and Composites*. 6-7 July 2011. Birmingham, UK.
60. Wolcott M, Englund K. A technology review of wood-plastic composites, in *33rd International Particleboard / Composite Materials Symposium*. 1999. Washington State University, Pullman.

61. Ismail M, Yassen AAM, Afify MS. Mechanical properties of rice straw fiber-reinforced polymer composites. *Fibers and Polymers*, 2011, 12(5): p. 648-656.
62. Buzarovska A, Bogoeva-Gaceva G, Grozdanov A, Avella M, Gentile G, Errico M. Potential use of rice straw as filler in eco-composite materials. *Australian Journal of Crop Science*, 2008, 1(2): p. 37-42.
63. Harish S, Michael DP, Bensely A, Lal DM, Rajadurai A. Mechanical property evaluation of natural fiber coir composite. *Materials Characterization*, 2009, 60: p. 44-49.
64. Venkateshwaran N, Elayaperumal A. Banana fibre reinforced polymer composites - A review. *Journal of Reinforced Plastics and Composites*, 2010, 29: p. 2387-2396.
65. Hassan A, Salema AA, Ani FN, Bakar AA. A review on oil palm empty fruit bunch fiber-reinforced polymer composite materials. *Polymer Composites*, 2010, 31(12): p. 2079-2101.
66. Mishra S, Mohanty AK, Drzal LT, Misra M, Hinrichsen G. A review on pineapple leaf fibers, sisal fibers and their biocomposites. *Macromolecular Materials and Engineering*, 2004, 289: p. 955-974.
67. Li Y, Mai Y, Ye L. Sisal fibre and its composites: A review of recent developments. *Composites Science and Technology*, 2000, 60(11): p. 2037-2055.
68. Kamath M, Bhat GS, Parikh DV, Mueller D. Cotton fiber nonwovens for automotive composites. *International Nonwovens Journal*, 2005, 14(1): p. 34-40.
69. Zini E, Scandola M. Green composites: An overview. *Polymer Composites*, 2011, 32(12): p. 1905-1915.
70. Fu S, Lauke B, Mader E, Yue CY, Hu X. Tensile properties of short-glass-fiber- and short-carbon-fiber-reinforced polypropylene composites. *Composites Part A: Applied Science and Manufacturing*, 2007, 31: p. 1117-1125.
71. van den Oever M, Bos HL, van Kemenade MJJM. Influence of the physical structure of flax fibres on the mechanical properties of flax fibre reinforced polypropylene composites. *Applied Composite Materials*, 2000, 7: p. 387-402.
72. Arib R, Sapuan SM, Ahmad MMHM, Paridah MT, Zaman HMDK. Mechanical properties of pineapple leaf fibre reinforced polypropylene composites. *Materials and Design*, 2006, 27: p. 391-396.
73. Paul S, Joseph K, Mathew GDG, Pothen LA, Thomas S. Influence of polarity parameters on the mechanical properties of composites from polypropylene fiber and short banana fiber. *Composites Part A: Applied Science and Manufacturing*, 2010, 41: p. 1380-1387.
74. Rukmini K, Ramaraj B, Shetty SK, Taraiya A, Bandyopadhyay S, Siddaramaiah. Development of eco-friendly cotton fabric reinforced polypropylene composites: Mechanical, thermal, and morphological properties. *Advances in Polymer Technology*, 2013, 32(1): p. 1-9.
75. Rozman H, Tay GS, Kumar RN, Abusamah A, Ismail H, Ishak ZAM. Polypropylene–oil palm empty fruit bunch–glass fibre hybrid composites: a preliminary study on the flexural and tensile properties. *European Polymer Journal*, 2001, 37(6): p. 1283-1291.
76. Okuba K, Fujii T, Yamamoto Y. Development of bamboo-based polymer composites and their mechanical properties. *Composites Part A: Applied Science and Manufacturing*, 2004, 35: p. 377-383.
77. Lee N, Jang J. The effect of fibre content on the mechanical properties of glass fibre mat/polypropylene composites. *Composites Part A: Applied Science and Manufacturing*, 1999, 30: p. 815-822.
78. Placet V, Trivaudey F, Cisse O, Gucheret-Retel V, Boubakar ML. Diameter dependence of the apparent tensile modulus of hemp fibres: A morphological,

structural or ultrastructural effect? *Composites Part A: Applied Science and Manufacturing*, 2012, 43(2): p. 275-287.
79. Mwaikambo L, Ansell MP. The determination of porosity and cellulose content of plant fibers by density methods. *Journal of Materials Science Letters*, 2001, 20(23): p. 2095-2096.
80. Thygesen A. *Properties of hemp fibre polymer composites - An optimisation of fibre properties using novel defibration methods and fibre characterisation*. PhD, 2006. The Royal Agricultural and Veterinary University of Denmark: Roskilde, Denmark.
81. McLaughlin E, Tait RA. Fracture mechanism of plant fibres. *Journal of Materials Science*, 1980, 15: p. 89-95.
82. Mukherjee P, Satyanarayana KG. An empirical evaluation of structure-property relationships in natural fibres and their fracture behaviour. *Journal of Materials Science*, 1986, 21: p. 4162-4168.
83. Satyanarayana K, Pillai CKS, Sukumaran K, Pillai SGK, Rohatgi PK, Vijayan K. Structure property studies of fibres from various parts of the coconut tree. *Journal of Materials Science*, 1982, 17: p. 2453-2462.
84. Baley C. Analysis of the flax fibres tensile behaviour and analysis of the tensile stiffness increase. *Composites Part A: Applied Science and Manufacturing*, 2002, 33: p. 939-948.
85. Gassan J, Chate A, Bledzki AK. Calculation of elastic properties of natural fibers. *Journal of Materials Science*, 2001, 36: p. 3715-3720.
86. Charlet K, Jernot JP, Moussa G, Baley C, Bizet L, Breard J. Morphology and mechanical behaviour of a natural composite: the flax fiber, in *16th International Conference on Composite Materials (ICCM-16)*. 2007. Kyoto, Japan.
87. Thygesen A, Oddershede J, Liholt H, Thomsen AB, Stahl K. On the determination of crystallinity and cellulose content in plant fibres. *Cellulose*, 2005, 12: p. 563-576.
88. Parikh D, Thibodeaux DP, Condon B. X-ray crystallinity of bleached and crosslinked cottons. *Textile Research Journal*, 2007, 77(8): p. 612-616.
89. Sheng-zuo F, Wen-zhong Y, Xiang-xiang FU. Variation of microfibril angle and its correlation to wood properties in poplars. *Journal of Forestry Research*, 2004, 15(4): p. 261-267.
90. Bodros E, Baley C. Study of the tensile properties of stinging nettle fibres (Urtica dioica). *Materials Letters*, 2008, 62(14): p. 2143-2145.
91. Porter D, Guan J, Vollrath F. Spider silk: Super material or thin fibre? *Advanced Materials*, 2013, 25(9): p. 1275-1279.
92. Hughes M. Defects in natural fibres: their origin, characteristics and implications for natural fibre-reinforced composites. *Journal of Materials Science*, 2012, 47: p. 599-609.
93. Aslan M, Chinga-Carrasco G, Sørensen BF, Madsen B. Strength variability of single flax fibres. *Journal of Materials Science*, 2011, 46: p. 6344-6354.
94. Madsen B, Mehmood S, Aslan M. Variability in properties of natural fibres, in *NATEX Workshop*. 2012. Chesterfield, UK.
95. Goutianos S, Peijs T. The optimisation of flax fibre yarns for the development of high-performance natural fibre composites. *Advanced Composites Letters*, 2003, 12(6): p. 237-241.
96. Dissanayake N. *Life cycle assessment of flax fibres for the reinforcement of polymer matrix composites*. PhD, 2011. University of Plymouth: Plymouth, UK.
97. Dissanayake N, Summerscales J, Grove SM, Singh MM. Life cycle impact assessment of flax fibre for the reinforcement of composites. *Journal of Biobased Materials and Bioenergy*, 2009, 3(3): p. 1-4.

98. Dissanayake N, Summerscales J, Grove SM, Singh MM. Energy use in the production of flax fiber for the reinforcement of composites. *Journal of Natural Fibers*, 2009, 6(4): p. 331-346.
99. Le Duigou A, Davies, P, Baley, C. Environmental impact analysis of the production of flax fibres to be used as composite material reinforcement. *Journal of Biobased Materials and Bioenergy*, 2011, 5(1): p. 153-165.
100. Kalia S, Kaith BS, Kaur I. Pretreatments of natural fibers and their application as reinforcing material in polymer composites - a review. *Polymer Engineering and Science*, 2009, 49(7): p. 1253-1272.
101. Kabir M, Wang H, Lau KT, Cardona F. Chemical treatments on plant-based natural fibre reinforced polymer composites: An overview. *Composites: Part B*, 2012, 43: p. 2883-2892.
102. Garkhail S, Heijenrath RWH, Peijs T. Mechanical properties of natural-fibre-mat-reinforced thermoplastics based on flax fibres and polypropylene. *Applied Composite Materials*, 2000, 7: p. 351-372.
103. Bos H, Mussig J, van den Oever MJA. Mechanical properties of short-flax-fibre reinforced compounds. *Composites Part A: Applied Science and Manufacturing*, 2006, 37: p. 1591-1604.
104. Awal A, Cescutti G, Ghosh SB, Mussig J. Interfacial studies of natural fibre/polypropylene composites using single fibre fragmentation test (SFFT). *Composites Part A: Applied Science and Manufacturing*, 2011, 42: p. 50-56.
105. Oksman K. High quality flax fibre composites manufactured by the resin transfer moulding process. *Journal of Reinforced Plastics and Composites*, 2001, 20(7): p. 621-627.
106. Roe P, Ansell MP. Jute-reinforced polyester composites. *Journal of Materials Science*, 1985, 20: p. 4015-4020.
107. Madsen B, Hoffmeyer P, Lilholt H. Hemp yarn reinforced composites – II. Tensile properties. *Composites Part A: Applied Science and Manufacturing*, 2007, 38: p. 2204-2215.
108. Charlet K, Jernot JP, Gomina M, Bizet L, Bréard J. Mechanical properties of flax fibers and of the derived unidirectional composites. *Journal of Composite Materials*, 2010, 44(24): p. 2887-2896.
109. Arbelaiz A, Fernandez B, Cantero G, Llano-Ponte R, Valea A, Mondragon I. Mechanical properties of flax fibre/polypropylene composites: Influence of fibre/matrix modification and glass fibre hybridization. *Composites Part A: Applied Science and Manufacturing*, 2005, 36: p. 1637-1644.
110. Mutje P, Girones J, Lopez A, Llop MF, Vilaseca F. Hemp strands: PP composites by injection molding: Effect of low cost physico-chemical treatments. *Journal of Reinforced Plastics and Composites*, 2006, 25: p. 313-327.
111. Beckwith S. *Natural fiber reinforcement materials: Lower cost technology for composites applications*, in *Composites Fabrication*, November/December 2003. p. 12-16.
112. Shahzad A. Effects of alkalization on tensile, impact, and fatigue properties of hemp fiber composites. *Polymer Composites*, 2012, 33(7): p. 1129-1140.
113. Rodríguez E, Petrucci R, Puglia D, Kenny JM, Vazquez A. Characterization of composites based on natural and glass fibers obtained by vacuum infusion. *Journal of Composite Materials*, 2005, 39(5): p. 265-282.
114. George J, Ivens J, Verpoest I. Mechanical properties of flax fibre reinforced epoxy composites. *Die Angewandte Makromolekulare Chemie*, 1999, 272(1): p. 41-45.
115. Gil R. *Forming and consolidation of textile composites*. PhD, 2003. The University of Nottingham: Nottingham, UK.

116. Hughes M, Carpenter J, Hill C. Deformation and fracture behaviour of flax fibre reinforced thermosetting polymer matrix composites. *Journal of Materials Science*, 2007, 42: p. 2499-2511.
117. Gassan J, Bledzki AK. Possibilities for improving the mechanical properties of jute/epoxy composites by alkali treatment of fibres. *Composites Science and Technology*, 1999, 59: p. 1303-1309.
118. Daniel M, Ishai O. *Engineering mechanics of composite materials*, 1994. Oxford: Oxford University Press.
119. Liang S, Gning, PB, Guillaumat, L. A comparative study of fatigue behaviour of flax/epoxy and glass/epoxy composites. *Composites Science and Technology*, 2012, 72(5): p. 535-543.
120. Phillips S, Baets J, Lessard L, Hubert P, Verpoest I. Characterization of flax/epoxy prepregs before and after cure. *Journal of Reinforced Plastics and Composites*, 2013, In Press. doi: 10.1177/0731684412473359.
121. Meredith J, Coles SR, Powe R, Collings E, Cozien-Cazuc S, Weager B, Müssig J, Kirwan K. On the static and dynamic properties of flax and Cordenka epoxy composites. *Composites Science and Technology*, 2013, 80: p. 31-38.
122. Sawpan M, Pickering KL, Fernyhough A. Analysis of mechanical properties of hemp fibre reinforced unsaturated polyester composites. *Journal of Composite Materials*, 2012, (In Press). doi:10.1177/0021998312449028.
123. Mwaikambo L, Tucker N, Clark AJ. Mechanical properties of hemp-fibre-reinforced euphorbia composites. *Macromolecular Materials and Engineering*, 2007, 292: p. 993-1000.
124. Vallejos M, Espinach FX, Julián F, Torres LI, Vilaseca F, Mutjé P. Micromechanics of hemp strands in polypropylene composites. *Composites Science and Technology*, 2012, 72: p. 1209-1213.
125. Serrano A, Espinach FX, Julian F, del Rey R, Mendez JA, Mutje P. Estimation of the interfacial shears strength, orientation factor and mean equivalent intrinsic tensile strength in old newspaper fiber/polypropylene composites. *Composites Part B: Engineering*, 2013, 50: p. 232-238.
126. Cabral H, Cisneros M, Kenny JM, Vazquez A, Bernal CR. Structure-properties relationship of short jute fiber-reinforced polypropylene composites. *Journal of Composite Materials*, 2005, 39: p. 51-65.
127. Franck R, ed. *Bast and other plant fibres*. 2005. CRC Press LLC: Boca Raton.
128. Cichocki JF, Thomason JL. Thermoelastic anisotropy of a natural fiber. *Composites Science and Technology*, 2002, 62: p. 669-678.
129. Reussman T, Mieck P, Grützner R, Bayer R. The recycling of polypropylene reinforced with natural fibres. *Kunststoffe Plast Europe*, 1999, 89: p. 80-84.
130. Boey F, Lye SW. Void reduction in autoclave processing of thermoset composites: Part 1: High pressure effects on void reduction. *Composites*, 1992, 23(4): p. 261-265.
131. Anderson J, Altan MC. Properties of composite cylinders fabricated by bladder assisted composite manufacturing. *Journal of Engineering Materials and Technology*, 2012, 134: p. 1-7.
132. Ghiorse S. *Effect of void content on the mechanical properties of carbon/epoxy laminates*, in *SAMPE Quarterly*, 1993. p. 54-59.
133. Madsen B, Thygesen A, Lilholt H. Plant fibre composites - Porosity and volumetric interaction. *Composites Science and Technology*, 2007, 67: p. 1584-1600.
134. Lee B, Kim HJ, Yu WR. Fabrication of long and discontinuous natural fiber reinforced polypropylene biocomposites and their mechanical properties. *Fibers and Polymers*, 2009, 10(1): p. 83-90.

135. Zarate C, Aranguren MI, Reboredo MM. Influence of fiber volume fraction and aspect ratio in resol-sisal composites. *Journal of Applied Polymer Science*, 2003, 89: p. 2714-2722.
136. Oksman K, Wallstrom L, Berglund LA, Filho RDT. Morphology and mechanical properties of unidirectional sisal-epoxy composites. *Journal of Applied Polymer Science*, 2002, 84: p. 2358-2365.

# 3 MECHANICAL PROPERTY CHARACTERISATION OF PLANT YARN REINFORCED THERMOSET MATRIX COMPOSITES

## 3.1 INTRODUCTION

Employing plant fibre yarns as continuous reinforcements for unidirectional composites, this chapter evaluates the mechanical properties of aligned plant fibre composites (PFRPs), against aligned E-glass composites (GFRPs), to appreciate the true potential of biofibres as stiffness-inducing reinforcements. As composite materials are heterogeneous, the reinforcement and matrix type will obviously affect composite properties. Noting the effectiveness of aligned bast fibre reinforcements (*e.g.* flax, hemp and jute) and thermoset matrices (*e.g.* unsaturated polyester and epoxy) for load-bearing composites (as highlighted in *Chapter 2*), this study examines the effect of plant yarn type/quality and thermoset matrix type on composite properties.

## 3.2 EXPERIMENTAL METHODOLOGY

### 3.2.1 Reinforcement materials

Four commercially available plant fibre yarns/rovings were used as composite reinforcements. The material properties of the four yarns are tabulated in Table 3.1, and have been determined by the author of this thesis (*Appendix A*). Notes on fibre/yarn processing are also provided in Table 3.1 Yarns have been named according to the fibre type (denoted by first initial) followed by the twist level in turns per meter (tpm); so, J190 is a jute yarn with a twist level of 190 tpm.

The selected yarns enable studying the effect of fibre/yarn type (jute, hemp and flax) and fibre/yarn quality (F50 and F20) on PFRP mechanical performance. Note that fibre quality is defined 'qualitatively' by the source of the fibre/yarn and the mechanical properties of the resulting composite. Here, F20 is considered as a flax yarn with high-quality fibres, while F50 is a flax yarn with low-quality fibres.

**Table 3.1. List of plant fibre materials and their properties.**

| Yarn ID | Fibre type | Fibre density† $\rho_f$ [gcm$^{-3}$] | Nominal linear density [tex] | True linear density† [tex] | Nominal twist level $T$ [tpm] | Surface twist angle† $\alpha$ [°] | Yarn diameter† $d_y$ [mm] | Packing fraction† $\Phi$ | Price* $C_f$ [£/kg] | Supplier | Notes on yarn processing ψ |
|---|---|---|---|---|---|---|---|---|---|---|---|
| **J190** | Jute | 1.433 ± 0.005 | 250 | 206 ± 21 | 190 | 20.5 ± 5.9 | 0.428 | 0.596 | ~1.1 | Janata and Sadat Jute Ltd (Bangladesh) | Water retted fibres; Z-twist ring spun (dry) yarns; batching oil used as lubricant |
| **H180** | Hemp | 1.531 ± 0.003 | 285 | 278 ± 17 | 180 | 19.5 ± 4.3 | 0.480 | 0.591 | ~7.6 | Safilin (Poland) | Dew retted fibres; Relatively higher shive content; Z-twist ring spun (dry) yarns |
| **F50** | Flax | 1.529 ± 0.003 | 250 | 229 ± 22 | 50 | 4.9 ± 3.8 | 0.437 | 0.421 | ~10.0 | Composites Evolution (UK) | Dew retted fibres; Z-twist core flax yarn with S-twist polyester filament binder (13 wt%) |
| **F20** | Flax | 1.574 ± 0.004 | 400 | 396 ± 16 | 20 | 0.5 ± 0.2 | 0.506 | - | ~13.3 | Safilin (France) | Dew retted fibres; Z-twist ring spun (wet) rovings; fibres boiled in dilute NaOH prior to spinning |

† Characterised and measured in *Appendix A*. Note that the measured fibre density is the absolute density (*i.e.* excluding the lumen) including moisture (typically 10 wt%). Also, the yarn diameter is based on a measured cross-sectional area (using pycnometry), and assuming circular cross-section. However, due to the low-twist and thus low packing fraction of F20, it is a roving with a non-circular cross-section.

* The price of yarn/roving quoted is approximate and based on small quantities. Prices reduce significantly with high quantities (>5 tonnes). For reference, the price of raw flax/hemp fibre ranges between 0.5-1.5 £/kg, while the price of E-glass is $C_f \approx 1.3$ £/kg [1].

ψ Further notes on fibre/yarn processing: During the fibre extraction process, the tropical jute fibres have undergone water retting (a more controlled but water-polluting process), while fibres from the temperate region (flax and hemp) have undergone dew/field retting (a strictly natural process influenced by actual weather conditions). Different batches of fibres were mixed, to ensure consistent yarn quality. All yarn batches consisted of several bobbins of yarn. None of the yarns were dyed or coated with wax to facilitate any subsequent dyeing process. Textile yarns J190 and H180 were obtained in high twist. For the former, 'jute batching oil' was used as a lubricant to increase yarn regularity during the drafting process. F50 is a low-twist flax with a polyester binder yarn, while F20 is a flax roving. F20 is the only yarn produced in a wet-spun process, where the fibres are soaked in a hot dilute solution of NaOH before spinning; this process improves defibration and yarn regularity.

On a side note, Table 3.1 also presents the commercial price of these yarns at the time of writing. Note that significant scales of economy are linked with bulk orders. Nonetheless, it is clear that only jute yarn (produced in developing nations such as Bangladesh) is able to compete against E-glass in terms of cost. Flax and hemp yarns/rovings (often produced in China but processed in Europe [2]), are up to 10 times more expensive than E-glass. Clearly, yarns of temperate fibres (flax and hemp) are not cost-viable substitutes to E-glass for composite reinforcement.

### 3.2.2 Production of unidirectional mats

For use as aligned reinforcements, the yarns were processed in the form of unidirectional mats. The mats were prepared using a drum-winding system (Fig. 3.1). The semi-continuous process involved automatic winding of yarns around a rotating (~60 rpm) and traversing (~0.5 mm/sec) aluminium drum (Ø315 mm, 400 mm long) with periodic manual adjustments of yarns to minimize inter-yarn spacing. Once the drum length was covered, the monolayer winding was uniformly hand painted with 0.6 wt% aqueous hydroxyethylcellulose (HEC) solution and dried at 60 °C for 30 min. HEC was purchased from Dow Chemical (Cellosize HEC QP-52000H). The mat was then recovered upon drying and cut to size (250×250 $mm^2$). The HEC binding agent ensured that the mat held together. Although the binding agent application process is crude with little control over film thickness, the process effectively allowed the production of unidirectional mats with a high degree of alignment and controlled areal density (300-400 ± 32 gsm). The binding agent accounted for 1-3 wt% of the mat. Importantly, the binding agent is cellulose-based (*i.e.* with surface properties similar to plant fibres) and thus has no significant effect on the properties of the resulting composite. This was confirmed (presented in *Appendix B*) through tensile tests on F50/polyester composites manufactured with *i)* mats produced using the technique outlined previously, and *ii)* stitched mats supplied by Formax (UK) Ltd.

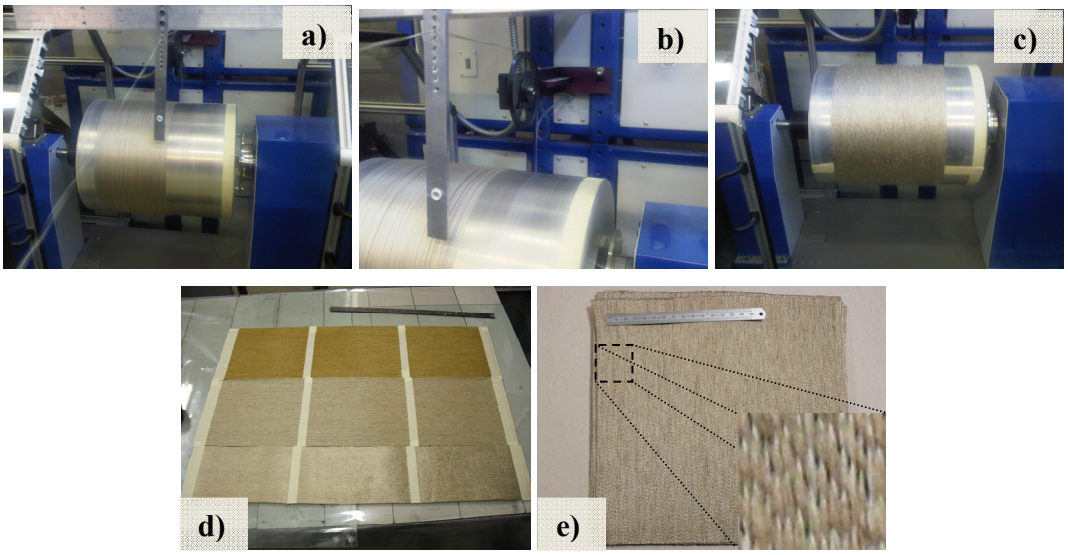


**Fig. 3.1. Developed unidirectional mat fabrication process: *a)* Automatic winding of yarn around a drum; *b)* close-up of yarn guide and roller; *c)* manual shifting of yarn (if required) to produce a completed mono-layer winding; *d)* recovered mat after applying HEC binding agent and drying; *e)* single layer mat (250×250 mm$^2$).**

### 3.2.3 Manufacture of composites

Unidirectional PFRP laminates (250×250 mm$^2$, 3–3.5 mm thick) were fabricated using the vacuum infusion technique (Fig. 3.2). For each plaque, four layers of the reinforcement mat were used as-produced (without any preconditioning, such as drying). The mould tool includes a transparent Perspex top, a steel picture frame (~3 mm thick) and an aluminium base (Fig. 3.2a). Resin infusion was carried out at 70-80% vacuum (200-300 mbar absolute) at ambient temperature. The Perspex top had central and side resin injection/evacuation ports. Preliminary tests illustrated that due to the unidirectional fibre architecture, central injection produced non-isotropic ovular resin flow. On the other hand, line-gate injection perpendicular to the yarn axis generated uniform axial resin flow. Hence, the latter was the preferred method of resin injection (Fig. 3.2b).

Two standard thermoset resins were used as matrices for composite fabrication: *i)* unsaturated polyester (UP) type 420-100 (mixed with 0.25 wt% NL49P accelerator (1% Cobalt solution) and 1 wt% Butanox M50 MEKP initiator), and *ii)* low-viscosity

Epoxy Prime 20LV (mixed with its fast hardener at a 100:26 mass ratio). For both resin systems, post cure was carried out at 55 °C for 6 h after ambient curing for 16 h. Table 3.2 presents datasheet properties of the cured resin systems. Note the similarity in properties of the two thermosetting matrices. The matrix shear modulus $G_m$ is estimated using Eq. 3.1, assuming a matrix Poisson's ratio $v_m$ of 0.38 [3-5].

$$G_m = \frac{E_m}{2(1+v_m)} \qquad \text{Eq. 3.1}$$

Using stitched unidirectional E-glass fabric (1200 ± 32 gsm) obtained from Formax (UK) Ltd, aligned GFRPs were similarly manufactured as reference materials.

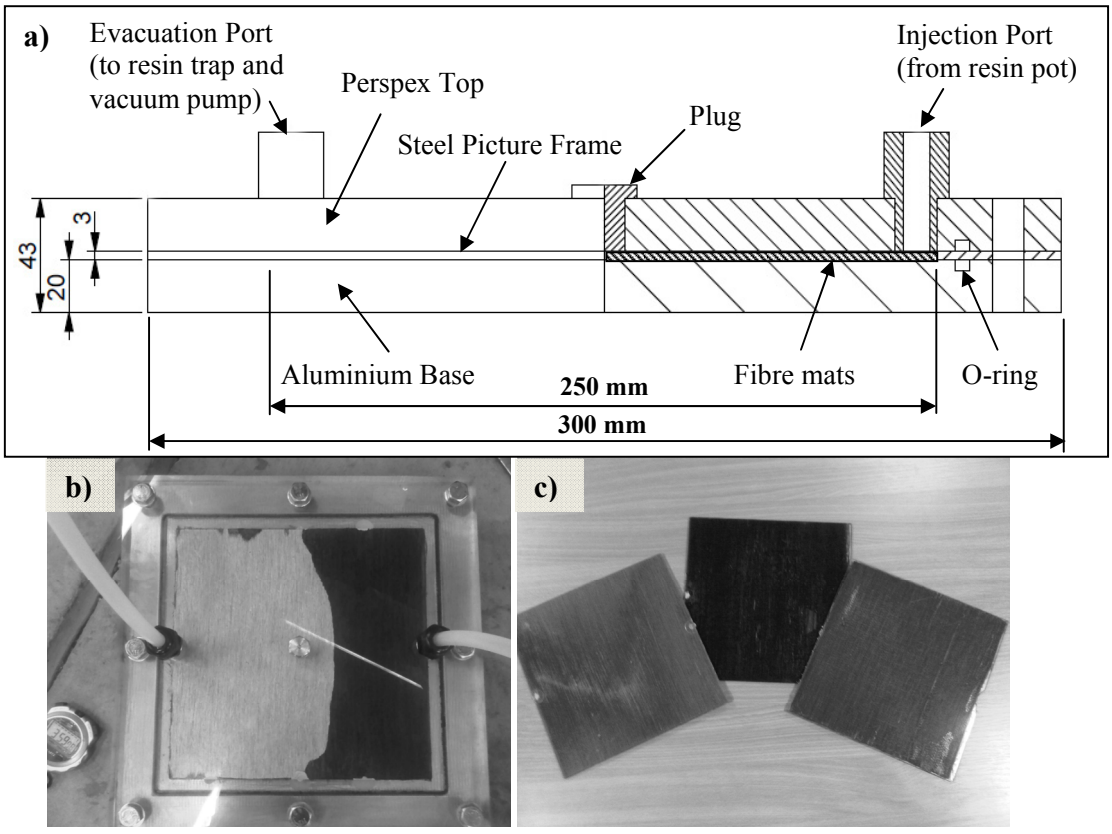


**Fig. 3.2. Composite manufacturing process: *a)* schematic of the mould tool, images of *b)* the infusion process, and *c)* the produced composite laminates.**

**Table 3.2. Resin systems and their datasheet properties.**

| Resin | Supplier | Mixed viscosity [mPas] or [cP] | Geltime at 25 °C [mins] | Cured density $\rho_m$ [gcm$^{-3}$] | Tensile modulus $E_m$ [GPa] | Tensile strength $\sigma_m$ [MPa] | Failure strain $\varepsilon_m$ [%] | Shear modulus $G_m$ [GPa] |
|---|---|---|---|---|---|---|---|---|
| **UP** | Reichhold Norpol | 210 | 30 | 1.202 | 3.7 | 70 | 3.5 | 1.34 |
| **Epoxy** | Gurit UK Ltd | 230 | 30 | 1.153 | 3.2 | 75 | 4.1 | 1.16 |

### 3.2.4 Physical characterisation

The fibre weight fraction $w_f$ of a laminate was calculated using the ratio of the mass of the preform $W_f$ and the resulting laminate $W_c$. The fibre and matrix densities have been presented in Table 3.1 and Table 3.2. The composite density $\rho_c$ was measured using a calibrated Micromeritics AccuPyc 1330 helium pycnometer. A purge fill pressure of 19.0 psig, equilibrium rate of 0.05 psig/min and specimen chamber temperature of 20 ± 1 °C was used. For each laminate a minimum of five samples were tested, where the final density reading for each sample was an average of five systematic readings (from five purges/runs). The fibre volume fraction $v_f$, matrix volume fraction $v_m$ and void volume fraction $v_p$ of the composites were then determined using equation Eq. 3.2, where $w$ and $\rho$ represent weight fraction and density, respectively while the subscripts $f$, $m$ and $c$ denote fibres, matrix and composite, respectively.

$$v_f = \frac{\rho_c}{\rho_f} w_f; \quad v_m = \frac{\rho_c}{\rho_m}(1 - w_f); \quad v_p = 1 - (v_f + v_m) \qquad \text{Eq. 3.2}$$

Optical microscopy was then used to qualitatively image the fibre/yarn packing arrangement and porosity in the composites. For this, three cross-sections from each composite were cast (using casting polyester resin), polished (using 100, 200, 300, 600, 800, 1200 and diamond grit paper) and viewed under a microscope. Images were processed using ImageJ software.

### 3.2.5 Testing of mechanical properties

For all studies in this thesis, all composite samples were stored for at least 48 hours at ambient conditions before any testing. The composite plaques were cut with a high-speed abrasive/diamond cutting machine, without any lubrication fluid (to avoid

moisture intake), to produce specimens for testing. All mechanical testing was conducted under ambient conditions (typically, 15-25 °C and 60-90% relative humidity).

#### 3.2.5.1 Short-beam shear test

Short-beam shear tests were carried out according to ASTM D2344, where un-notched specimens were loaded in a three-point bending configuration at a cross-head speed of 1 mm/min. An Instron 5969 testing machine equipped with a 2 kN load cell was used for these tests. The width $b$ and length $l$ of the test specimen was kept at 2 and 6 times the thickness $t$, respectively. A span-to-thickness ($L_0/t$) ratio of 4:1 was used; the chosen $L_0/t$ ratio encourages failure of specimen through interlaminar shear along the neutral axis, rather than inelastic deformation or flexural failure in compression/tension on the surface. The 'apparent' interlaminar shear strength $\tau$ was calculated using Eq. 3.3, where $P$ is the maximum applied load. Six specimens were tested for each type of composite.

$$\tau = \frac{3}{4}\frac{P}{bt} \qquad \text{Eq. 3.3}$$

#### 3.2.5.2 Tensile test

Longitudinal tensile tests were conducted according to ISO 527-4:1997 using an Instron 5985 testing machine equipped with a 100 kN load cell and a 50 mm extensometer. Six 250 mm long and 15 mm wide specimens were tested for each type of composite at a cross-head speed of 2 mm/min. 'Specimen Protect' was used to ensure that the specimens weren't damaged during gripping. The tensile modulus $E_c$ (in the strain range of 0.025–0.100%), ultimate tensile strength $\sigma_c$, and tensile failure strain $\varepsilon_c$ were measured from the stress-strain curve.

#### 3.2.5.3 Impact test

The impact properties of the composites were determined using an Avery Denison pendulum Charpy testing machine according to ISO 179:1997. The un-notched specimens were loaded flat-wise with weighted hammers at a point perpendicular to the direction of the unidirectional fabric plane. A 2.7 J hammer was used for PFRPs

while a 15 J hammer was used for GFRPs. A striking velocity of 3.46 $ms^{-1}$ was used. Six specimens (100 mm long and 10 mm wide) were tested for each type of composite. The impact strength (or work of fracture) was determined by dividing the measured fracture energy with the specimen cross-sectional area.

## 3.3 RESULTS AND DISCUSSION

### 3.3.1 Manufacturing properties

#### 3.3.1.1 Physical properties

*Density and fibre volume fraction*

Physical properties of the manufactured laminates are presented in Table 3.3. Matrix type has little effect on composite density as the matrices used in this study have very similar densities. As expected, due to the 40-50% lower density of plant fibres compared to E-glass, PFRPs are significantly lighter (30-40%) than GFRPs.

**Table 3.3. Physical properties of manufactured laminates (mean ± stdev).**

| Unidirectional reinforcement | Resin System | Fibre weight fraction $w_f$ [%] | Composite density $\rho_c$ [$gcm^{-3}$] | Fibre volume fraction $v_f$ [%] | Void volume fraction $v_p$ [%] | Cost of composite panel† $C_c$ [£] |
|---|---|---|---|---|---|---|
| **E-glass** | Epoxy | 63.7 | 1.782 ± 0.009 | 42.6 ± 0.2 | 1.3 ± 0.5 | 1.62 |
| **J190** | Epoxy | 40.5 | 1.236 ± 0.006 | 34.9 ± 0.2 | 1.3 ± 0.5 | 1.47 |
| **H180** | Epoxy | 40.6 | 1.259 ± 0.009 | 33.4 ± 0.3 | 1.8 ± 0.7 | 2.22 |
| **F50** | Epoxy | 32.9 | 1.249 ± 0.002 | 26.9 ± 0.1 | 0.5 ± 0.2 | 2.45 |
| **F20** | Epoxy | 36.9 | 1.273 ± 0.004 | 29.9 ± 0.1 | 0.5 ± 0.3 | 2.26 |
| **E-glass** | UP | 63.6 | 1.793 ± 0.035 | 42.8 ± 0.8 | 2.9 ± 1.9 | 0.63 |
| **J190** | UP | 37.1 | 1.226 ± 0.010 | 31.7 ± 0.3 | 4.2 ± 0.8 | 0.46 |
| **H180** | UP | 41.9 | 1.303 ± 0.004 | 35.6 ± 0.2 | 1.3 ± 0.4 | 1.09 |
| **F50** | UP | 33.0 | 1.282 ± 0.004 | 27.7 ± 0.1 | 0.9 ± 0.3 | 1.25 |
| **F20** | UP | 37.3 | 1.304 ± 0.008 | 30.9 ± 0.2 | 1.0 ± 0.6 | 1.64 |

†The materials cost is estimated using $C_c = W_c(C_f w_f + C_m(1-w_f))$, where the cost of the matrix $C_m$ is taken to be 2.50 and 10.00 £/kg for polyester and epoxy, respectively. Note that the cost is 'normalised' for composite volume, where the volume is approximately equal at 3×250×250 $mm^3$.

For the composites produced (Table 3.3), the fibre volume fraction of unidirectional GFRPs (~43%) is higher than that of PFRPs (27–36%). These findings are in agreement with other studies in literature. Producing composites by compression moulding, Madsen *et al.* [6] report that for a constant compaction pressure, unidirectional flax yarn and E-glass composites have a fibre volume fraction of 56% and 71%, while random flax fibre and E-glass composites have a fibre volume fraction of 38% and 52%, respectively. Goutianos *et al.* [7] also find that when employing liquid moulding processes (specifically, hand lay-up and RTM), GFRPs produce higher fibre volume fractions than PFRPs. In essence, random fibre composites produce lower fibre volume fractions than aligned fibre composites, and PFRPs produce lower fibre volume fractions than GFRPs.

Madsen *et al.* [6] argue that fibre alignment and degree of fibre separation affect the compact-ability of a preform. Synthetic fibre assemblies have higher packing-ability than plant fibre assemblies [6, 8]. This is because unidirectional synthetic fibre assemblies are made of rovings with continuous, parallel and uniform (diameter) fibres that are well-separated, while unidirectional plant fibre assemblies are made of yarns with discontinuous, twisted and non-uniform (diameter) fibres that are typically in bundles/clusters. This is confirmed through optical microscopy images (Fig. 3.3a and d).

Typically, the maximum attainable fibre volume fraction for unidirectional GFRPs is of the order of 70-80% [4]. The upper limit for unidirectional PFRPs is in the range of 50–60% [8]. This lower maximum attainable fibre volume fraction is a set-back for PFRPs as composite mechanical properties generally improve with fibre volume fraction.

It is important to note that the manufacturing technique also has a significant effect on achievable fibre volume fractions. For instance, compression moulding or hot-pressing would produce higher fibre volume fractions than vacuum infusion and even RTM (as discussed in *Chapter 2*). This is because in compression moulding the compaction pressure and preform mass can be adjusted to achieve a pre-desired laminate thickness and fibre volume fraction. Commercially, PFRPs are primarily

produced via compression moulding [2]. However, this study employs vacuum infusion as it enables the cost-effective manufacture of large geometrically-intricate components, such as wind turbine blades, in low volumes. As an extension to this study, the possibilities of using vacuum-assisted RTM or prepregging for the manufacture of higher fibre content (and lower void content) PFRPs could be considered. For instance, Weyenberg *et al.* [9] and Baets *et al.* [10] have been able to produce flax/epoxy composites with $v_f \approx 50\%$ using prepreg technology.

Table 3.3 also presents the deviations in the measured readings of density and fibre volume fraction. The standard deviations for PFRPs are low (~1% of the mean values) and comparable to GFRPs, implying that they are producible with consistent and uniform fibre distribution. This is valuable if PFRPs are to be considered for structural applications.

*Reinforcement packing*

Fig. 3.3 shows micrographs of cross-sections in *a)* J190, *b)* H180, and *c)* F20 yarn PFRPs. While it is observed that on a macro-scale yarn bundles in high-twist yarn PFRPs (J190/H180) are distributed relatively uniformly within the matrix and the fibres in the yarn are well impregnated (Fig. 3.3a and b), on a meso-scale the fibre distribution is distinctly heterogeneous. That is, the distribution of fibres within the compact yarn is concentrated/clustered and there are noticeable resin-rich regions. On the other hand, in low twist-low compaction F20 yarn preforms (Fig. 3.3c), inter-yarn spaces are comparable to intra-yarn spaces. In fact, individual rovings are difficult to distinguish. Hence, fibre distribution is more uniform and the fibres are well-separated. This is similar to the distribution of fibres in unidirectional GFRPs (Fig. 3.3d). Such homogeneity in fibre distribution would allow better distribution of stresses/strains upon loading.

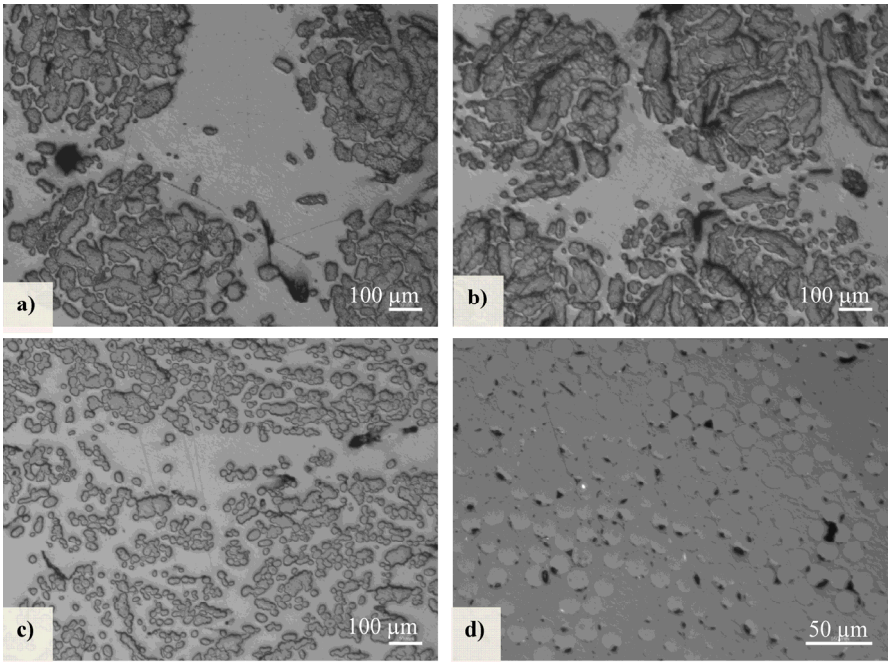


**Fig. 3.3. Microscopy images of *a)* J190 and *b)* H180 epoxy composites showing the large difference in inter-yarn and intra-yarn spacing and inhomogeneous fibre distribution compared to *c)* F20 and *d)* E-glass epoxy composites. Also notice the constant diameter of E-glass, but non-uniform cross-sectional shape and width of plant fibres.**

*Porosity*

The void content of aligned PFRPs is found to be in the range of 0.5-2%, with the exception of J190/polyester, which has a higher void content of 4.2%. Nonetheless, the void content of PFRPs is comparable to that of GFRPs (1-3%). Typically, void contents of <1% are required for aerospace applications, but void contents of up to 5% are acceptable for other less demanding applications (*e.g.* automotive and marine) [11-13].

In literature [8, 14, 15], PFRPs are often quoted to have high void content. Typically, the void volume fraction is up to 5% for PFRPs with a fibre volume fraction below 40% [8, 16-20]. However, when the fibre volume fraction exceeds 40%, void content increases drastically and can even approach 20% [8, 17-19, 21]. Nonetheless, there are some studies [16, 22] which conclude that there is no obvious relationship between PFRP fibre volume fraction and void volume fraction. From the literature

survey, it is suggested that issues of high porosity in PFRPs are usually related, but not confined, to *i)* sisal fibre composites due to the large lumen size in sisal fibres which remain unfilled after resin infusion [20, 21], *ii)* structural porosity in (particularly, high weight fraction) compression-moulded thermoplastic PFRPs due to insufficient amount of matrix to fill the free space between the yarns [8], and *iii)* randomly-oriented short-fibre PFRPs. In this work, comparatively lower void contents have been observed which is in agreement with other studies that use thermoset resins in a vacuum infusion process [20]. Perhaps, the low viscosity of thermoset resins (Table 3.2) allows better impregnation of plant fibre assemblies. In fact, Madsen *et al.* [6] show that porosity in hemp yarn reinforced thermoplastics increases linearly ($R^2 = 0.98$) with the logarithm of the matrix processing viscosity. As the viscosity of thermosets is several orders of magnitude lower than that of thermoplastics, the lower void content in thermoset-based PFRPs is understandable.

This study uses yarns as a form of continuous reinforcement with controlled orientation. It is has been suggested that the twisted nature of such yarns leads to a tightened/compact structure (as observed in Fig. 3.3a), which may cause reduced permeability, hindered impregnation, and thus void formation [16, 23]. Consequently, increasing yarn twist is likely to worsen these issues. However, in their experimental study, Zhang *et al.* [16] found no correlation between composite porosity and yarn structure. Even at different fibre volume fractions, the porosity content in PFRPs composing ring-spun yarns (surface twist angle of 30°) and commingled natural fibre/polypropylene yarns (surface twist angle of 0°) was similar and in the range of 1.4 to 5.2%. Indeed, in this study, the void content of yarn reinforced PFRPs is found to be low as well (0.5-4.2%).

While there may not be an obvious relationship between yarn structure and void content, the yarn structure may dictate the type of voids that form, particularly due to its effects on reinforcement packing and resin-flow dynamics. Madsen *et al.* [8] have described three categories of porosity in PFRPs: *i)* fibre-related porosity, *ii)* matrix-related porosity (characteristic of liquid moulding processes), and *iii)* structural porosity (characteristic of thermoplastic moulding processes). Fibre-related porosity can be broken down into further sub-components: *a)* luminal porosity (in the fibre

lumen), *b)* interface porosity (at the fibre/matrix interface) and *c)* impregnation porosity (between fibre bundles).

In this study, qualitative analysis suggests that fibre porosity related to unfilled luminal cavities in fibres make a larger contribution to the total porosity in jute composites, compared to hemp and flax composites (Fig. 3.4). This observation is in agreement with the literature [1, 8]. Noting that the typical diameter of jute fibres is almost double that of flax/hemp [1, 24, 25], the size of the luminal cavity in flax/hemp and jute fibres is typically 2-11% [1, 6, 8, 26] and 10-14% [1, 8, 27] of their cross-sectional area. However, it is arguable that luminal porosities may not be detrimental to the performance of PFRPs as they do not encourage stress concentration or fibre debonding [8]. In contrast, Baley *et al.* [28] find that the lumen encourages crack initiation, when a unidirectional PFRP is loaded in the transverse direction.

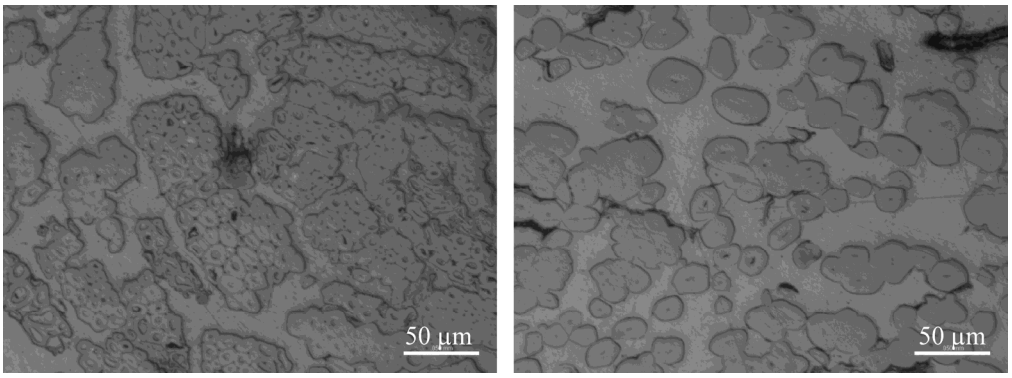


**Fig. 3.4. Luminal spaces in fibres of jute (left) are larger than that in flax (right).**

Microscopy of composite cross-sections also shows that porosity in high-twist yarn J190/H180 composites is primarily associated with impregnation porosity (Fig. 3.5a). Impregnation porosity is due to inadequate or poor matrix impregnation of the yarns [8] and in this case may be a result of high compaction of fibres and low permeability within the yarn. On the other hand, low-twist yarn F50/F20 composites are not susceptible to impregnation porosity due to the low compaction of fibre within the yarn/roving and thus a yarn permeability that is comparable to the preform permeability. Rather, low-twist yarn composites are primarily affected by interface

porosity (Fig. 3.5b). Although this is suggestive of poorer fibre/matrix compatibility in low-twist yarn PFRPs, this is not true because both low- and high-twist yarn PFRPs compose of hydrophilic plant fibres and hydrophobic matrices. A possible explanation is that high-twist yarns, particularly jute, are observed to consist of large fibre sub-assemblies (fibre bundles) within yarns (Fig. 3.3 and Fig. 3.5) while low-twist yarns, particularly flax, are more defibrillated into single fibres due to low compaction (Fig. 3.3 and Fig. 3.5). This means that in low-twist yarn PFRPs, the matrix needs to wet-out a relatively larger surface area of small fibre bundles (if not single fibres) as compared to smaller surface area of large fibre bundles.

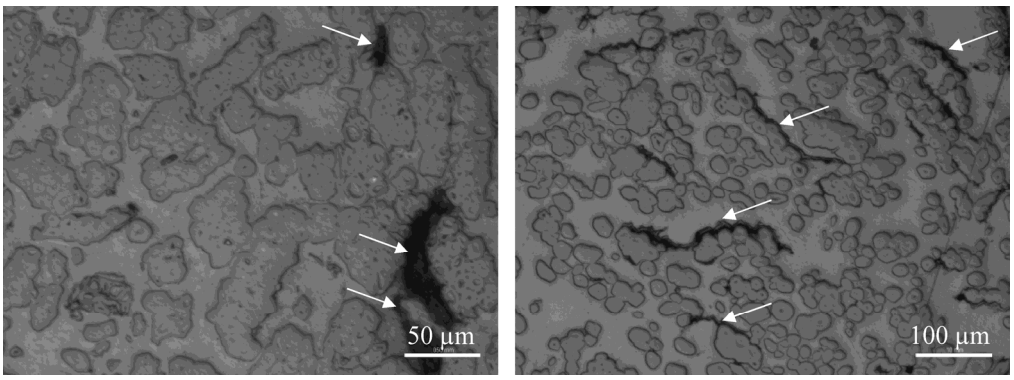


**Fig. 3.5. Microscopy images of J190 (left) and F20 (right) epoxy composites. High-twist yarn J190 composites have impregnation-related porosities while low twist yarn F20 composites have interface-related porosities (indicated by arrows). High-twist yarns (particularly jute) consist of large fibre bundles, while fibres in low-twist yarns (particularly flax) are well-separated.**

#### 3.3.1.2 Materials cost

Table 3.3 presents the materials cost for each type of composite. It is clearly observed that *i)* epoxy composites are more expensive than polyester composites due to the significantly higher cost of epoxy matrix, and *ii)* PFRPs are more expensive than GFRPs. While raw plant fibres are cost-competitive to E-glass, plant fibre yarns/rovings (particularly from temperate fibres) are not cost-viable substitutes to E-glass for composite reinforcement. As cost is often a critical design criterion for industrial applications, employing such yarns for commercial PFRP applications is not foreseeable in the short-term future, unless plant yarn reinforcements become significantly cheaper.

### 3.3.2 Mechanical properties

#### 3.3.2.1 Apparent interlaminar shear strength

Results from short-beam shear tests are presented in Fig. 3.6. Note that the determined results are not absolute values, but purely for relative comparison. The 'apparent' interlaminar shear strength $\tau$ is a measure of the strength of the matrix plus the interface. From Fig. 3.6, it is observed that epoxy composites display higher interlaminar shear strength compared to polyester composites. This is possibly because epoxy has a marginally higher estimated matrix shear strength (using Tresca criteria, $\tau_m = \sigma_m/2$) than polyester. In addition, the better adhesive properties of epoxy may make it more compatible with hydrophilic plant fibres and thus provide a stronger interface. This is in agreement with the results from impact tests and tensile tests (discussed in later sections).

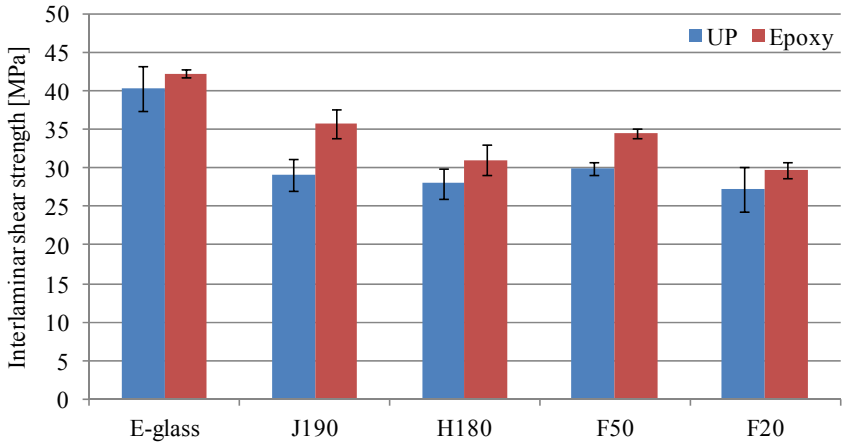


**Fig. 3.6. Interlaminar shear strength of composites. Error bars denote 1 standard deviation.**

It is observed that aligned GFRPs have 20-30% higher interlaminar shear strengths (40-42 MPa) than aligned PFRPs (ranging from 27-36 MPa). The study by Goutianos *et al.* [7] is in agreement with this finding. The higher interlaminar shear strength of GFRPs is a sign of better fibre/matrix adhesion. This is expected as *i)* synthetic fibres are often surface-treated after manufacture in order to improve the interfacial bond, *ii)* plant fibres are highly polar and form a weak interface with typically non-polar

matrices, and *iii)* unlike plant fibres whose surface energy is similar to that of the matrix, the surface energy of E-glass is significantly higher than that of the matrix facilitating good wet-out.

Amongst PFRPs, high-twist J190 yarn composites exhibit best interfacial properties while low-twist F20 composites display lowest properties. This is possibly due to the high content of interface-related porosities in F20 composites (as discussed in Section 3.3.1.1.3). It is also possible that the yarn construction (specifically, twist level) affects the composite interlaminar shear strength. Naik *et al.* [29] show that twisted resin-impregnated yarns show higher shear strength than straight impregnated yarns due to higher transverse pressure in twisted yarns. However, more investigations are necessary to elucidate the differences in the governing mechanisms of (shear) stress development in a single impregnated yarn compared to a yarn reinforced laminate.

*Critical fibre length*

The critical fibre length $l_c$ and fibre aspect ratio $l_f/d_f$ are important parameters that dictate mechanical properties of a composite. In particular, they define the fibre length efficiency factor; that is, the ability of the fibre to transfer strength and stiffness to the composite. Sub-critical length fibres ($l_f < l_c$) will not carry the maximum possible load. To efficiently utilise the fibre properties, either the critical fibre length $l_c$ should be decreased below the fibre length $l_f$ (by improving interfacial properties), or the reinforcing fibre length $l_f$ (and thus aspect ratio) should be increased much above the critical fibre length $l_c$.

The critical fibre length $l_c$ is defined by Eq. 3.4, where $\sigma_f$ is the fibre tensile strength (at the critical fibre length), $d_f$ is the fibre diameter, and $\tau$ is the interfacial strength. The estimated critical fibre length $l_c$ for all the composites produced in this study is presented in Table 3.4. As inputs in Eq. 3.4, typical fibre strength $\sigma_f$ and diameter $d_f$ have been used from various sources.

$$l_c = \frac{\sigma_f d_f}{2\tau} \qquad \text{Eq. 3.4}$$

**Table 3.4. Estimating the critical fibre length and fibre length efficiency factors for composite stiffness and strength.**

| **Unidirectional reinforcement** | **Resin System** | *Fibre stiffness $E_f$ [MPa]* | *Fibre strength $\sigma_f$ [MPa]* | *Fibre diameter $d_f$ [μm]* | *Gauge length $l$ [mm]* | *Source of single fibre properties* | *Typical fibre aspect ratio[†] $l_f/d_f$* | **Critical fibre length $l_c$ [mm]** | **Length efficiency for stiffness $\eta_{lE}$** | **Length efficiency for strength $\eta_{lS}$** |
|---|---|---|---|---|---|---|---|---|---|---|
| **E-glass** | Epoxy | 78.5 | 1956 | 13.8 | 50 | [30] | >3000 | 0.320 | 0.999 | 0.996 |
| **J190** | Epoxy | 32.5 | 558 | 53.9 | 6 | [25] | 100 | 0.421 | 0.976 | 0.961 |
| **H180** | Epoxy | 24.7 | 636 | 27.6 | 8 | [31] | 900 | 0.283 | 0.998 | 0.994 |
| **F50** | Epoxy | 56.0 | 1099 | 17.5 | 10 | [32] | 1750 | 0.278 | 0.998 | 0.995 |
| **F20** | Epoxy | 56.0 | 1099 | 17.5 | 10 | [32] | 1750 | 0.323 | 0.998 | 0.995 |
| **E-glass** | UP | 78.5 | 1956 | 13.8 | 50 | [30] | >3000 | 0.335 | 0.999 | 0.996 |
| **J190** | UP | 32.5 | 558 | 53.9 | 6 | [25] | 100 | 0.515 | 0.977 | 0.952 |
| **H180** | UP | 24.7 | 636 | 27.6 | 8 | [31] | 900 | 0.314 | 0.998 | 0.994 |
| **F50** | UP | 56.0 | 1099 | 17.5 | 10 | [32] | 1750 | 0.321 | 0.998 | 0.995 |
| **F20** | UP | 56.0 | 1099 | 17.5 | 10 | [32] | 1750 | 0.352 | 0.998 | 0.994 |

[†] Typical fibre aspect ratios are from [1, 6].

The critical fibre length $l_c$ for epoxy composites is lower than that for polyester composites. Furthermore, the critical fibre length $l_c$ for PFRPs is found to be in the range of 0.28-0.52 mm, which is comparable to that of GFRPs (0.32-0.34 mm). The estimated $l_c$ for GFRPs is in agreement with values typically quoted in literature [4]. While there are some studies that determine $l_c$ for PFRPs to be >2 mm [33-36], other studies report a smaller critical length $l_c$, similar to values found in this study, of 0.4-0.9 mm [33, 35, 37-39].

While plant fibres are naturally discontinuous, fibres employed in the production of yarns/rovings have lengths >25 mm [35, 40, 41]. Hence, in this study, the plant fibre reinforcements have high aspect ratios and are much longer than the critical length.

*Fibre length efficiency factor*

It is common for scientists working on plant fibre composites to assume that length efficiency factors are unity, when back-calculating fibre properties or predicting composites properties (for instance, [9, 10, 17, 21, 42]). However, it is important to assess if this claim is valid. The calculated critical fibre lengths $l_c$ and typical values of fibre aspect ratio (length/diameter) $l_f/d_f$ can be used to determine the length efficiency of the reinforcements. Cox's shear lag model [43] can be used for the calculation of the fibre length efficiency factor for stiffness $\eta_{lE}$, assuming iso-strain conditions, axial loading of fibres and elastic stress transfer between fibre and matrix. $\eta_{lE}$ is given by Eq. 3.5, where $G_m$ is the shear stiffness of the matrix, $E_f$ is the stiffness of the fibre, and $v_{f,max,FRP}$ is the maximum achievable fibre volume fraction. Assuming square packing arrangement of continuous and parallel fibres, $v_{f,max,FRP}$ of $\pi/4$ (=78.5%) can be used. For the calculation of the fibre length efficiency factor for strength $\eta_{lS}$, Kelly-Tyson's model [44] can be used (Eq. 3.6), with $l_f > l_c$.

$$\eta_{lE} = 1 - \frac{\tanh\left(\frac{\beta l_f}{2}\right)}{\frac{\beta l_f}{2}}, \quad \frac{\beta l_f}{2} = \frac{l_f}{d_f}\sqrt{\frac{2G_m}{E_f \ln\left(\sqrt{v_{f,\max,FRP}/v_f}\right)}} \qquad \text{Eq. 3.5}$$

$$\eta_{lS} = \begin{cases} 1 - l_c/2l_f & for\ l_f \geq l_c \\ l_f/2l_c & for\ l_f \leq l_c \end{cases} \qquad \text{Eq. 3.6}$$

The calculated fibre length efficiency factors for stiffness and strength are found to be very close to unity for all the composites (Table 3.4). This is expected as high aspect ratio fibres ($l_f/d_f$ > 100) are being used and the critical fibre length is very small ($l_f/l_c$ > 50000). Madsen *et al.* [14] show that fibre aspect ratios of $l_f/d_f$ > 50 would yield $\eta_{lE}$ > 0.93 for plant fibre composites, and further increase in aspect ratio would asymptotically increase $\eta_{lE}$ towards unity. Sawpan *et al.* [38] also determine $\eta_{lS}$ to be 0.96 for their short-fibre ($l \approx$ 2-3 mm) hemp/polyester composites. These results confirm that like E-glass, plant fibres, particularly in the form of yarns, can deliver high length efficiency factors and thus, good load-transferring capabilities. Therefore, $\eta_{lE} = \eta_{lS} = 1$ is used for analysis in this thesis.

#### 3.3.2.2 Tensile properties

The measured tensile properties of the composites are presented in Table 3.5. It is encouraging to note that although mechanical properties of single plant fibres are known to have high variability, at a composite scale, the tensile properties of PFRPs are consistent and with a small coefficient of variation of up to 6%, which is similar to that of GFRPs.

From the composite properties, the tensile stiffness $E_f$ and strength $\sigma_f$ of the reinforcing fibres has been 'back-calculated' using the rule of mixtures (Eq. 3.7, Eq. 3.8). The back-calculated fibre properties are useful in evaluating the reinforcing potential of plant fibres and comparing the tensile performance of the various composites at the same fibre volume fraction ($v_f$ = 100%). In light of the results from Section 3.3.2.1, the fibre length efficiency factors ($\eta_{lE}$ and $\eta_{lS}$) have been taken to be unity. As in other studies [9, 10, 17, 42], the fibre orientation efficiency factor $\eta_o$ is assumed to be unity for yarn reinforced unidirectional PFRPs and unidirectional GFRPs. In Eq. 3.8, $\sigma'_m$ is the matrix stress at fibre failure strain $\varepsilon_f$. Assuming iso-strain conditions, the fibre failure strain $\varepsilon_f$ is equal to the composite failure strain $\varepsilon_c$. $\sigma'_m$ is then estimated using Hooke's law to be $\sigma'_m = E_m\varepsilon_c$ [9].

$$E_f = \frac{E_c - v_m E_m}{\eta_{lE}\eta_o v_f} \qquad \text{Eq. 3.7}$$

$$\sigma_f = \frac{\sigma_c - v_m \sigma'_m}{\eta_{ls} \eta_o v_f} \qquad \text{Eq. 3.8}$$

**Table 3.5. Tensile properties of manufactured composite laminates (measured; mean ± stdev) and fibres (back-calculated; mean).**

| Unidirectional reinforcement | Resin System | Fibre volume fraction $v_f$ [%] | Composite tensile modulus $E_c$ [GPa] | Fibre tensile modulus $E_f$ [GPa] | Composite tensile strength $\sigma_c$ [MPa] | Fibre tensile strength $\sigma_f$ [MPa] | Composite failure strain $\varepsilon_c$ [%] |
|---|---|---|---|---|---|---|---|
| **E-glass** | Epoxy | 42.6 ± 0.2 | 34.0 ± 2.1 | 75.6 | 705.7 ± 34.0 | 1603.7 | 1.3 ± 0.4 |
| **J190** | Epoxy | 34.9 ± 0.2 | 15.0 ± 1.4 | 37.0 | 185.8 ± 16.2 | 441.1 | 1.6 ± 0.0 |
| **H180** | Epoxy | 33.4 ± 0.3 | 19.0 ± 1.1 | 50.7 | 195.1 ± 8.9 | 477.3 | 1.7 ± 0.1 |
| **F50** | Epoxy | 26.9 ± 0.1 | 14.2 ± 0.3 | 44.3 | 163.5 ± 3.0 | 449.6 | 1.8 ± 0.1 |
| **F20** | Epoxy | 29.9 ± 0.1 | 24.6 ± 0.4 | 75.1 | 281.4 ± 3.8 | 809.6 | 1.8 ± 0.1 |
| **E-glass** | UP | 42.8 ± 0.8 | 36.9 ± 1.4 | 81.6 | 825.7 ± 49.1 | 1843.0 | 1.9 ± 0.9 |
| **J190** | UP | 31.7 ± 0.3 | 16.1 ± 0.8 | 43.4 | 175.1 ± 10.3 | 442.4 | 1.5 ± 0.2 |
| **H180** | UP | 35.6 ± 0.2 | 17.0 ± 0.5 | 41.2 | 171.3 ± 6.5 | 368.8 | 1.7 ± 0.1 |
| **F50** | UP | 27.7 ± 0.1 | 15.6 ± 0.9 | 47.0 | 143.0 ± 6.8 | 368.2 | 1.6 ± 0.0 |
| **F20** | UP | 30.9 ± 0.2 | 23.4 ± 0.3 | 67.6 | 277.4 ± 8.2 | 760.5 | 1.7 ± 0.3 |

*Effect of matrix type*

There is some disagreement on the effect of matrix type on PFRP tensile performance in literature. Joffe *et al.* [45] find that while the difference in tensile properties of thermoset matrices (polyester, epoxy and vinylester) is large, the resulting randomly-oriented short-fibre flax composites have fairly indistinguishable tensile properties. They suggest that the fibre/matrix interface, and thus load transfer mechanisms and reinforcement efficiency, differ for different fibre/matrix combinations. On the other hand, Madsen *et al.* [17] observe that the noticeable difference in tensile properties of unidirectional hemp yarn reinforced thermoplastics can be correlated to the matrix type (PE, PP, PET). Madsen *et al.* [17] also report that the potential difference in fibre/matrix bonding, due to employing a different matrix, does not result in a visible effect on composite tensile properties or back-calculated fibre properties. Part of the discrepancy can be explained by the fact that compared to random composites, the fibres in unidirectional composites bear a much larger

fraction of the load, and hence interfacial properties would have little effect on longitudinal tensile properties [4].

In this study, there is no clear dependence of composite tensile performance on matrix type (Table 3.5), particularly due to the similar tensile properties of the thermoset matrices (Table 3.2). Comparing the back-calculated fibre tensile properties, it is observed that while E-glass and J190 reinforcements perform up to 15% better in a polyester matrix, H180, F50 and F20 reinforcements perform up to 20% better in an epoxy matrix. This implies that the reinforcing efficiency of the fibres and perhaps the fibre/matrix interfaces differ for the different matrices. It has been previously shown (Fig. 3.6) that all epoxy composites have higher 'apparent' interlaminar shear strength and thus presumably better fibre/matrix adhesion, compared to polyester composites. Hence, epoxy composites should display better longitudinal tensile properties. This, however, is not observed in the presented tensile test results.

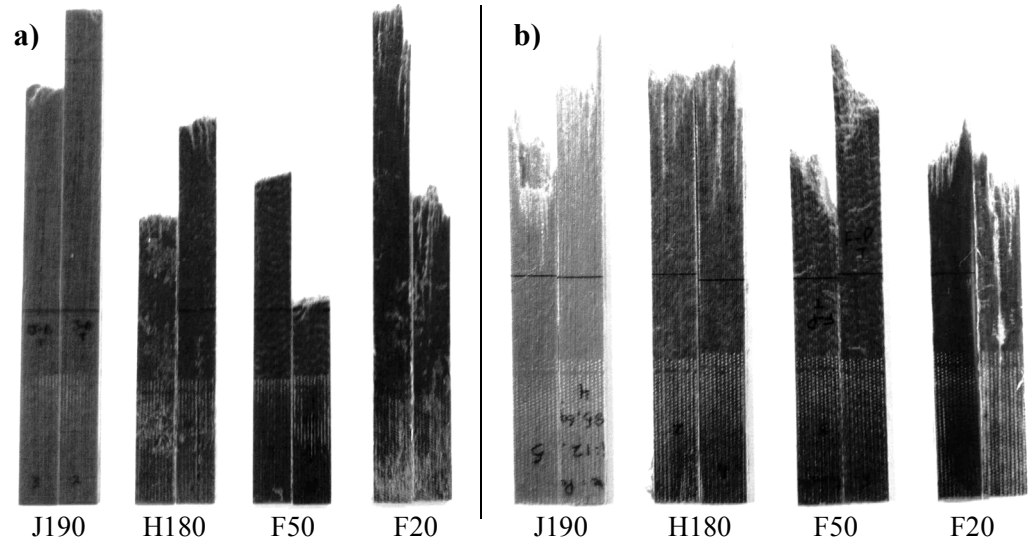


**Fig. 3.7. Tensile fracture surface of *a)* epoxy- and *b)* polyester-based PFRPs.**

Notably, the failure characteristics are different for epoxy- and polyester-based PFRPs (Fig. 3.7), which possibly relate to the difference in fibre/matrix interface properties [6]. It has been previously shown that the 'apparent' interlaminar shear strength of epoxy composites is better than that of polyester composites. Tensile

fracture specimens of epoxy composites display a fairly flat brittle fracture surface with little fibre pull-out resulting from matrix crack growth transverse to the fibre direction. On the other hand, fracture specimens of polyester composites display a more serrated failure surface with extensive fibre pull-out, and even delamination and longitudinal splitting, resulting from shear-induced micro-crack growth along the weaker fibre/matrix interface (that is, along the fibre axis) followed by macro-crack propagation through the micro-voids.

### *Effect of reinforcement type*

*Comparison of PFRPs with GFRPs*

Comparing the effect of reinforcement type on tensile properties (keeping in mind the differences in fibre volume fractions), it is found that unidirectional GFRPs outperform unidirectional PFRPs in terms of tensile strength and stiffness (Table 3.5). E-glass composites are observed to have a tensile strength and stiffness of about 700-825 MPa and 34-37 GPa, respectively. This is considerably higher than the tensile strength and stiffness of PFRPs, which ranges between 140-285 MPa and 14-25 GPa, respectively. Notably, PFRPs and GFRPs have a similar tensile failure strain. It is worth pointing out that the better mechanical properties of unidirectional GFRPs (in comparison to unidirectional PFRPs) is not only due to the superior mechanical properties of the reinforcing E-glass fibres (in comparison to plant fibres), but also due to critical structural differences in the reinforcements. While aligned GFRPs employ continuous fibres that are almost perfectly aligned/parallel, aligned PFRPs employ yarns/rovings that have discontinuous fibres that are twisted.

An advantage of plant fibres over E-glass fibres for reinforcements is their 40-50% lower density. Hence, the specific properties of the composites are of interest; particularly as specific tensile modulus $E_c/\rho_c$ and strength $\sigma_c/\rho_c$ are often used as material selection criteria for components loaded in pure tension [46]. Fig. 3.8 plots the specific tensile properties of epoxy-based PFRPs relative to E-glass/epoxy composites. It is clearly observed that the density of PFRPs is about 40% lower than that of GFRPs. In addition, the specific tensile modulus $E_c/\rho_c$ of J190, H180 and F50 composites is 60-80% that of unidirectional GFRPs, whereas F20 composites have a

specific tensile modulus that is similar to unidirectional GFRPs. Similarly, while the specific tensile strength $\sigma_c/\rho_c$ of J190, H180 and F50 composites is ~40% that of unidirectional GFRPs, F20 composites have a specific tensile strength that is ~60% that of unidirectional GFRPs. Note that increasing the fibre volume fractions of the PFRPs would improve the specific tensile performance of PFRPs further. Nonetheless, the findings suggest that while high-quality unidirectional PFRPs may offer comparable specific stiffness performance to unidirectional GFRPs, the specific strength performance of PFRPs is poor.

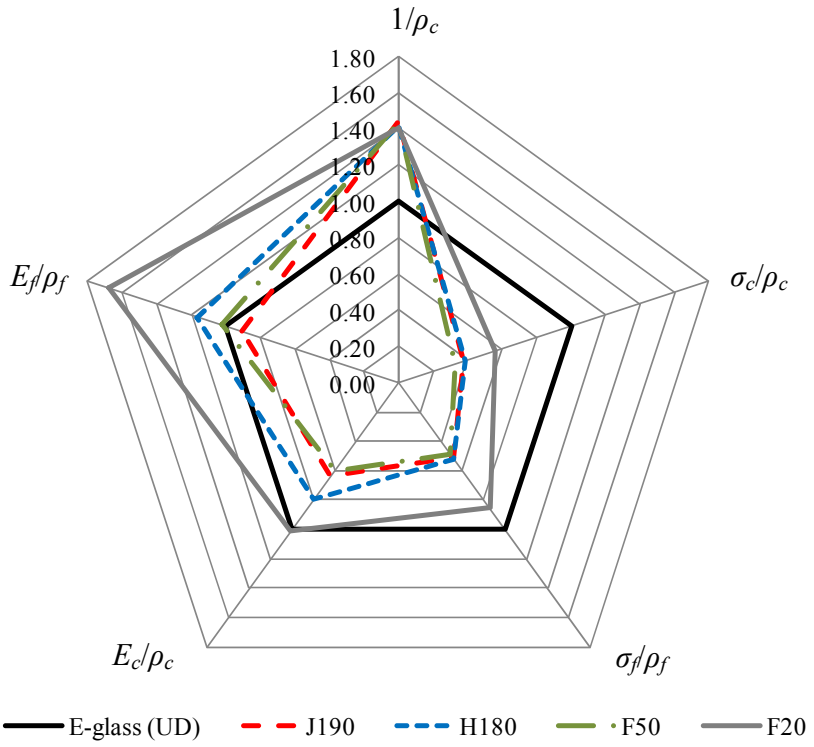


**Fig. 3.8. Specific tensile properties of epoxy composites (measured) and fibres (back-calculated) relative to E-glass composite properties.**

Back-calculated fibre properties have also been determined (Table 3.5). E-glass is estimated to have a tensile stiffness and strength in the range of 76-82 GPa and 1600-1850 MPa, respectively. This in agreement with typically reported literature values [1, 4, 30]. The results show that J190, H180 and F50 reinforcements have a tensile stiffness and strength in the range of 35-50 GPa and 360-480 MPa, respectively. This

is much lower than that of E-glass, but in the range of typically reported literature values [1]. Impressively, F20 flax reinforcements have a tensile stiffness which is comparable to that of E-glass at 67-75 MPa, and a tensile strength half that of E-glass at about 800 MPa. This is indeed a revelation and proof that flax has the reinforcing potential to replace E-glass in stiffness-critical structural applications.

Using the back-calculated fibre properties, specific tensile properties of plant fibres, relative to E-glass, are presented in Fig. 3.8. It is clearly observed that the specific stiffness performance of single plant fibres $E_f/\rho_f$ is comparable to or even significantly outperforms that of E-glass, while the specific strength of plant fibres can range from 50-90% of E-glass. These findings confirm that at the same fibre volume fraction, plant fibres can provide a light and stiff alternative to E-glass reinforcements.

*Effect of plant yarn reinforcement*

All PFRPs have very similar tensile failure strain. In terms of tensile stiffness and strength, F20 composites clearly outperform the other PFRPs (Table 3.5). Comparatively, J190 and H180 composites have similar tensile properties, while F50 composites have the poorest tensile properties. While F20 composites have a tensile stiffness and strength of 23-25 GPa and 275-285 MPa, the other PFRPs have lower tensile stiffness and strength of 14-19 GPa and 140-200 MPa, respectively.

The dissimilarity in mechanical properties of the PFRPs may be a result of several factors. Firstly, the plant fibre type will affect the composite properties. Although plant fibre properties are subject to significant natural variation, typically, flax fibres have better mechanical properties than jute and hemp fibres (Table 3.6). As jute and hemp have better or similar cellulose content, cellulose crystallinity, degree of polymerisation (DP) and microfibril angle (MFA) in comparison to flax (Table 3.6), perhaps the significantly higher fibre aspect ratio of flax results in a higher fibre tensile strength. McLaughlin *et al.* [47] and Mukherjee *et al.* [48] have demonstrated the strong correlation between the structure (cellulose content, MFA and aspect ratio) and tensile properties (strength, modulus and failure strain) of plant fibres. Secondly, fibre/yarn quality will have an inevitable effect on composite properties. For instance,

although both F20 and F50 composites have similar volumetric composition and are made from low-twist flax rovings/yarns, there is a 40% difference in their tensile strength. Madsen *et al.* [49, 50] and Baets *et al.* [10] have shown that an increasing number of defects and an increasing number of processing steps can reduce fibre/yarn quality and thus composite properties. Thirdly, reinforcement construction will have an effect on the properties of the resulting composite. For instance, the hampered performance of F50 composites may be due to the inclusion of polyester as a filament binder in F50 yarn. It is also suggested that increasing yarn twist reduces composite mechanical properties like an off-axis laminate [23]. (This is studied in more detail in *Chapter 5*.) The F20 flax rovings have a significantly lower twist level than J190/H180 yarns, and thus F20 composites would bear minimal effects of reinforcement misorientation. As the yarn construction of J190 and H180 is similar (Table 3.1), and the mechanical properties of jute and hemp fibres are similar (Table 3.6), the comparable mechanical properties of J190 and H180 composites are likely.

**Table 3.6. Structural and mechanical properties of bast fibres [1, 6, 51].**

| *Fibre type* | *Cellulose content [%]* | *Cellulose crystallinity [%]* | *DP** | *MFA†* *[°]* | *Aspect ratio* | *Tensile modulus [GPa]* | *Tensile strength [MPa]* | *Failure strain [%]* |
|---|---|---|---|---|---|---|---|---|
| Flax | 64–71 | 50-70 | 2420 | 5–10 | 1750 | 30–70 | 400–1100 | 2.7–3.2 |
| Hemp | 70–74 | 50-70 | 2300 | 2–6 | 900 | 30–60 | 300–800 | 1.3–2.7 |
| Jute | 61–72 | 50-70 | 1920 | 8 | 100 | 20–55 | 200–600 | 1.4–3.1 |

*DP = degree of polymerization

†MFA = microfibril angle

The estimated fibre properties (Table 3.5) are found to be in the range of literature values (Table 3.6). While fibres from J190, H180 and F50 yarns have a tensile stiffness and strength in the range of 35-50 GPa and 360-480 MPa, respectively, F20 reinforcements have a tensile stiffness of 65-75 MPa and a tensile strength of about 800 MPa. It is noteworthy that such high mechanical properties of the plant fibres, particularly F20 flax fibres, have been transferred to the composites without any active fibre surface treatment.

A literature survey of tensile properties of unidirectional bast fibre reinforced composites is presented in Table 3.7. The measured tensile properties of aligned PFRPs obtained in this study are generally comparable with the results reported in literature. However, some flax composites are observed to have much higher tensile properties than those observed in this study. For instance, Baets *et al.* [10] report a tensile strength and stiffness of 378 MPa and 39.9 GPa for unidirectional flax/epoxy composites ($v_f$ = 42%). They employed minimally-processed (*i.e.* low defect count) hackled flax. Oksman *et al.* [52] also produce flax/epoxy composites ($v_f$ = 42%) with high strength and stiffness of 280 MPa and 35 GPa. They used flax fibres that were extracted in a biotechnical retting process using enzymes and microbial cultures. The extraction process is more environmentally friendly than traditional retting processes and produces fibres that are of uniform quality and more suitable for composites applications. Both studies employed slivers, as a more aligned reinforcement than a roving or a yarn, at high fibre content. In addition, no fibre surface modification techniques, to enhance interfacial properties, were employed in either study.

The back-calculated fibre properties presented in literature (Table 3.7) are also comparable to those obtained in this study (Table 3.5). It is of interest to note that while jute and hemp reinforcements have a tensile stiffness in the range of 30-55 GPa, flax reinforcements consistently deliver higher stiffness; usually in excess of 60 GPa, and up to 90 GPa. Furthermore, flax fibres offer higher reinforcement strength in the composite. Indeed, in this study, F20 flax reinforcements have an impressive back-calculated fibre stiffness and strength of up to 75 GPa and 800 MPa, respectively.

Hence, it is proposed that using minimally-processed flax slivers (or rovings), processed specifically for composites applications rather than textile applications, as reinforcements in an epoxy matrix is a good starting point for producing high-quality PFRPs. Furthermore, employing prepregging technology for composite manufacture would enable the production of high fibre content and thus high-performance PFRPs. In addition, plant fibre surface treatment is not entirely necessary to achieve high PFRP mechanical properties.

**Table 3.7. Tensile properties of unidirectional (long bast fibre reinforced) PFRPs reported in literature.**

| *Unidirectional composite* | *Manufacturing technique* | *Fibre volume fraction* $v_f$ *[%]* | *Tensile modulus* $E_c$ *[GPa]* | *Fibre tensile modulus*[†] $E_f$ *[GPa]* | *Tensile strength* $\sigma_c$ *[MPa]* | *Fibre tensile strength*[†] $\sigma_f$ *[MPa]* | *Source* |
|---|---|---|---|---|---|---|---|
| Jute yarn/epoxy | Filament winding [*] | 40 | 15 | 32 | 155 | - | [53] |
| Jute sliver/polyester | Compression moulding | 32 | 20 | 56 | 170 | 442 | [22] |
| Hemp yarn/PET | Compression moulding | 34 | 18 | 51 | 205 | 538 | [17] |
| Flax yarn/epoxy | Prepregging | 50 | 32 | 61 | 315 | 600 | [10] |
| Flax roving/epoxy | Prepregging | 48 | 37 | 73 | 377 | 751 | [10] |
| Flax sliver/epoxy | Prepregging | 42 | 40 | 90 | 378 | 860 | [10] |
| Flax sliver/epoxy | Prepregging | 48 | 32 | 63 | 268 | 505 | [9] |
| Flax sliver/epoxy | RTM | 42 | 35 | 79 | 280 | 710 | [52] |
| Flax sliver/polyester | Compression moulding | 35 | 14 | 37 | 210 | 496 | [54] |
| Flax yarn/vinylester | RTM | 37 | 24 | 60 | 248 | - | [7] |

[†] The fibre properties have been 'back-calculated' by the authors of the respective articles.

[*] Typically, samples are compression/press moulded after filament winding.

### 3.3.2.3 Impact properties

Impact energy is typically dissipated by fibre and/or matrix fracture, debonding and fibre pull-out. Fibre pull-out dissipates more energy than fibre fracture [55]. Importantly, the former indicates weak interfacial properties, while the latter indicates good fibre/matrix adhesion [55]. The impact strength of the composite laminates is presented in Fig. 3.9. Noticeably, epoxy composites exhibit 10-30% lower impact strength than polyester composites. As improved fibre/matrix adhesion is known to affect impact strength adversely [55], this indicates that plant fibres are more compatible with epoxy than polyester. This is consistent with the fracture surfaces of impact-tested specimens, where epoxy composites exhibit considerably less fibre pull-out than polyester composites, and the fact that the former display higher 'apparent' interlaminar shear strength (Fig. 3.6).

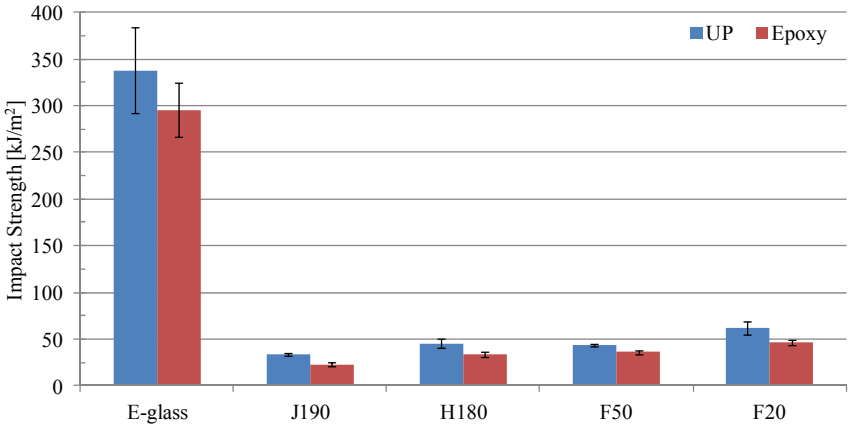


**Fig. 3.9. Impact strength of PFRPs compared to E-glass composites.**

The impact properties of PFRPs compare poorly to GFRPs, even when compared in terms of specific impact strength. Where unidirectional GFRPs have impact strengths of 300-350 kJ/m$^2$, unidirectional PFRPs have 5 to 10 times lower impact strengths of 30-60 kJ/m$^2$. Typically, short random PFRPs have impact strengths in the range of 10-25 kJ/m$^2$ [20, 55].

It is generally accepted that the toughness of a composite is mainly dependent on the fibre stress-strain behaviour, as well as the interfacial bond strength [55, 56]. E-glass

fibres are stronger than bast fibres with similar failure strain, and hence they may impart high work to fracture on the composites. In addition, while E-glass fibres are isotropic due to a 3-dimensional network of $SiO_2$, plant fibres are anisotropic with oriented cellulose microfibrils. Furthermore, synthetic E-glass has uniform properties, while natural fibres have non-uniform properties, particularly due to the presence of various defects (such as kinks). These are the prime reasons for the poorer impact properties of PFRPs [56-58].

Amongst PFRPs, F20 composites have best impact properties. It is interesting to note that impact strength of PFRPs reduces with increasing yarn twist level (Fig. 3.9). It is proposed that yarn construction and composite porosity are key factors in PFRP impact properties. High-twist yarn PFRPs have large intra-yarn voids, which can act as stress-raisers and likely sites for crack propagation. Furthermore, fibres are well-separated ('defibrillated') in low-twist yarn PFRPs, particularly flax F20, while fibre distribution is inhomogeneous in high-twist yarn PFRPs, resulting in resin rich zones (Fig. 3.3). Essentially, the crack path is likely to be more complex in low-twist yarn PFRPs, resulting in a higher work to fracture.

The inferior impact properties of PFRPs can be used as indicators of possible applications. Alternatively, the impact properties can be improved by *i)* using hybrid reinforcements (*e.g.* flax/E-glass or flax/coir) [57, 59], or *ii)* employing alternate textile architectures (*e.g.* mutliaxial non-wovens/wovens) and ply stacking sequence [4, 59]. In a hybrid reinforcement, fibres with good impact resistance (such as, E-glass or plant fibre with high microfibril angles such as coir and sisal) can be combined with bast fibres to produce improved impact properties ([57, 59] and references therein).

## 3.4 CONCLUSIONS

This study on the mechanical properties of aligned plant yarn reinforced thermoset composites has several key conclusions. Plant fibre reinforcements in the forms of yarns/rovings offer high length efficiency factors to the resulting composite due to low critical fibre lengths and high fibre aspect ratios. The manufactured PFRPs are well-impregnated and have low void content and consistent mechanical properties.

Considering the effect of thermoset matrix type, it is found that epoxies form a stronger interface with plant fibres than polyesters do. However, the effects of matrix type on longitudinal tensile properties of yarn reinforced PFRPs are inconclusive.

PFRPs consistently have lower fibre volume fractions than GFRPs, due to the low packing-ability of plant fibre preforms. Apart from the expected (30-40%) lower density of PFRPs, they have 20-30% lower interlaminar shear strength, 5-10 times lower impact strength, 60-80% lower tensile strength and 30-60% lower tensile stiffness than GFRPs. Hence, GFRPs clearly outperform PFRPs in terms of absolute mechanical properties. However, PFRPs have comparable specific stiffness performance to GFRPs.

Amongst the various yarn reinforced PFRPs studied, composites reinforced with flax rovings exhibit exceptional properties, with a back-calculated fibre tensile modulus in the range of 65-75 GPa (comparable to that of E-glass) and fibre tensile strength of about 800 MPa (half that of E-glass). These properties are achieved without using any active fibre surface treatment. Not only the fibre type, but yarn construction (twist level and packing fraction) and fibre/yarn quality are also found to have a significant impact on the mechanical properties of the resulting composite.

It is proposed that using minimally-processed flax rovings/slivers, processed specifically for composites rather than textile applications, as reinforcements in an epoxy matrix is a good starting point for producing high-quality PFRPs. Furthermore, fibre surface modification, for improved fibre/matrix adhesion, is not thought to be compulsory in achieving high mechanical properties.

## 3.5 REFERENCES

1. Lewin M. *Handbook of fiber chemistry*. Third ed, 2007. Boca Raton: CRC Press LLC.
2. Carus M. Bio-composites: Technologies, applications and markets, in *4th International Conference on Sustainable Materials, Polymers and Composites*. 6-7 July 2011. Birmingham, UK.
3. Aly M, Goda IGM, Hassan GA. Experimental investigation of the dynamic characteristics of laminated composite beams. *International Journal of Mechanical & Mechatronics*, 2011, 10(3): p. 59-68.
4. Harris B. *Engineering composite materials*, 1999. London: The Institute of Materials.

5. Cichocki JF, Thomason JL. Thermoelastic anisotropy of a natural fiber. *Composites Science and Technology*, 2002, 62: p. 669-678.
6. Madsen B. *Properties of plant fibre yarn polymer composites - An experimental study*. PhD, 2004. Technical University of Denmark: Lyngby, Denmark.
7. Goutianos S, Peijs T, Nystrom B, Skrifvars M. Development of flax fibre based textile reinforcements for composite applications. *Applied Composite Materials*, 2006, 13(4): p. 199-215.
8. Madsen B, Thygesen A, Lilholt H. Plant fibre composites - Porosity and volumetric interaction. *Composites Science and Technology*, 2007, 67: p. 1584-1600.
9. Weyenberg I, Chitruong T, Vangrimde B, Verpoest I. Improving the properties of UD flax fibre reinforced composites by applying an alkaline fibre treatment. *Composites Part A: Applied Science and Manufacturing*, 2006, 37: p. 1368-1376.
10. Baets J, Plastria D, Ivens J, Verpoest I. Determination of the optimal flax fibre preparation for use in UD-epoxy composites, in *4th International Conference on Sustainable Materials, Polymers and Composites*. 6-7 July 2011. Birmingham, UK.
11. Boey F, Lye SW. Void reduction in autoclave processing of thermoset composites: Part 1: High pressure effects on void reduction. *Composites*, 1992, 23(4): p. 261-265.
12. Anderson J, Altan MC. Properties of composite cylinders fabricated by bladder assisted composite manufacturing. *Journal of Engineering Materials and Technology*, 2012, 134: p. 1-7.
13. Ghiorse S. *Effect of void content on the mechanical properties of carbon/epoxy laminates*, in *SAMPE Quarterly*, 1993. p. 54-59.
14. Madsen B, Thygesen, A, Liholt, H. Plant fibre composites - Porosity and stiffness. *Composites Science and Technology*, 2009, 69: p. 1057-1069.
15. Madsen B, Lilholt H. Physical and mechanical properties of unidirectional plant fibre composites - an evaluation of the influence of porosity. *Composites Science and Technology*, 2003, 63: p. 1265-1272.
16. Zhang L, Miao M. Commingled natural fibre/polypropylene wrap spun yarns for structured thermoplastic composites. *Composites Science and Technology*, 2010, 70: p. 130-135.
17. Madsen B, Hoffmeyer P, Lilholt H. Hemp yarn reinforced composites – II. Tensile properties. *Composites Part A: Applied Science and Manufacturing*, 2007, 38: p. 2204-2215.
18. Lee B, Kim HJ, Yu WR. Fabrication of long and discontinuous natural fiber reinforced polypropylene biocomposites and their mechanical properties. *Fibers and Polymers*, 2009, 10(1): p. 83-90.
19. Zarate C, Aranguren MI, Reboredo MM. Influence of fiber volume fraction and aspect ratio in resol-sisal composites. *Journal of Applied Polymer Science*, 2003, 89: p. 2714-2722.
20. Rodríguez E, Petrucci R, Puglia D, Kenny JM, Vazquez A. Characterization of composites based on natural and glass fibers obtained by vacuum infusion. *Journal of Composite Materials*, 2005, 39(5): p. 265-282.
21. Oksman K, Wallstrom L, Berglund LA, Filho RDT. Morphology and mechanical properties of unidirectional sisal-epoxy composites. *Journal of Applied Polymer Science*, 2002, 84: p. 2358-2365.
22. Roe P, Ansell MP. Jute-reinforced polyester composites. *Journal of Materials Science*, 1985, 20: p. 4015-4020.
23. Goutianos S, Peijs T. The optimisation of flax fibre yarns for the development of high-performance natural fibre composites. *Advanced Composites Letters*, 2003, 12(6): p. 237-241.

24. Baley C. Analysis of the flax fibres tensile behaviour and analysis of the tensile stiffness increase. *Composites Part A: Applied Science and Manufacturing*, 2002, 33: p. 939-948.
25. Virk A, Hall W, Summerscales J. Tensile properties of jute fibres. *Materials Science and Technology*, 2009, 25(10): p. 1289-1295.
26. Thygesen A. *Properties of hemp fibre polymer composites - An optimisation of fibre properties using novel defibration methods and fibre characterisation*. PhD, 2006. The Royal Agricultural and Veterinary University of Denmark: Roskilde, Denmark.
27. Lilholt H, Bjerre AB. Composites based on jute-fibres and polypropylene matrix, their fabrication and characterization, in *18th Risø international symposium on materials science. Polymeric composites – expanding the limits*. 1997. Roskilde, Denmark: Risø National Laboratory.
28. Baley C, Perrot Y, Busnel F, Guezenoc H, Davies P. Transverse tensile behaviour of unidirectional plies reinforced with flax fibres. *Materials Letters*, 2006, 60: p. 2984-2987.
29. Naik N, Singh MN. Twisted Impregnated Yarns: Shear strength. *Journal of the Textile Institute*, 2001, 92(2): p. 164-183.
30. Fu S, Lauke B, Mader E, Yue CY, Hu X. Tensile properties of short-glass-fiber- and short-carbon-fiber-reinforced polypropylene composites. *Composites Part A: Applied Science and Manufacturing*, 2007, 31: p. 1117-1125.
31. Placet V, Trivaudey F, Cisse O, Gucheret-Retel V, Boubakar ML. Diameter dependence of the apparent tensile modulus of hemp fibres: A morphological, structural or ultrastructural effect? *Composites Part A: Applied Science and Manufacturing*, 2012, 43(2): p. 275-287.
32. Charlet K, Jernot JP, Moussa G, Baley C, Bizet L, Breard J. Morphology and mechanical behaviour of a natural composite: the flax fiber, in *16th International Conference on Composite Materials (ICCM-16)*. 2007. Kyoto, Japan.
33. Awal A, Cescutti G, Ghosh SB, Mussig J. Interfacial studies of natural fibre/polypropylene composites using single fibre fragmentation test (SFFT). *Composites Part A: Applied Science and Manufacturing*, 2011, 42: p. 50-56.
34. Garkhail S, Heijenrath RWH, Peijs T. Mechanical properties of natural-fibre-mat-reinforced thermoplastics based on flax fibres and polypropylene. *Applied Composite Materials*, 2000, 7: p. 351-372.
35. Bos H. *The potential of flax fibres as reinforcement for composite materials*. PhD, 2004. Technische Universiteit Eindhoven: Eindhoven, Netherlands.
36. Mwaikambo L, Tucker N, Clark AJ. Mechanical properties of hemp-fibre-reinforced euphorbia composites. *Macromolecular Materials and Engineering*, 2007, 292: p. 993-1000.
37. Bos H, Mussig J, van den Oever MJA. Mechanical properties of short-flax-fibre reinforced compounds. *Composites Part A: Applied Science and Manufacturing*, 2006, 37: p. 1591-1604.
38. Sawpan M, Pickering KL, Fernyhough A. Analysis of mechanical properties of hemp fibre reinforced unsaturated polyester composites. *Journal of Composite Materials*, 2012, (In Press). doi:10.1177/0021998312449028.
39. Vallejos M, Espinach FX, Julián F, Torres LI, Vilaseca F, Mutjé P. Micromechanics of hemp strands in polypropylene composites. *Composites Science and Technology*, 2012, 72: p. 1209-1213.
40. Weyenberg I, Ivens J, Coster A, Kino B, Baetens E, Verpoest I. Influence of processing and chemical treatment of flax fibres on their composites. *Composites Science and Technology*, 2003, 63: p. 1241-1246.
41. Franck R, ed. *Bast and other plant fibres*. 2005. CRC Press LLC: Boca Raton.

42. Virk A, Hall W, Summerscales J. Modulus and strength prediction for natural fibre composites. *Materials Science and Technology*, 2012, 28(7): p. 864-871.
43. Cox H. The elasticity and strength of paper and other fibrous materials. *British Journal of Applied Physics*, 1952, 3: p. 72-79.
44. Kelly A, Tyson WR. Tensile properties of fibre-reinforced metals: Copper/tungsten and copper/molybdenum. *Journal of the Mechanics and Physics of Solids*, 1965, 13(6): p. 329-350.
45. Joffe R, Wallstrom L, Berglund LA. Natural fibre composites based on flax - matrix effects, in *International Scientific Colloquium - Modelling for Saving Resources*. 2001. Riga, Latvia.
46. Ashby M. *Materials selection in mechanical design*, 1992. Oxford, UK: Pergamon Press.
47. McLaughlin E, Tait RA. Fracture mechanism of plant fibres. *Journal of Materials Science*, 1980, 15: p. 89-95.
48. Mukherjee P, Satyanarayana KG. An empirical evaluation of structure-property relationships in natural fibres and their fracture behaviour. *Journal of Materials Science*, 1986, 21: p. 4162-4168.
49. Madsen B, Mehmood S, Aslan M. Variability in properties of natural fibres, in *NATEX Workshop*. 2012. Chesterfield, UK.
50. Hanninen T, Thygesen A, Mehmood S, Madsen B, Hughes M. Mechanical processing of bast fibres: The occurrence of damage and its effect on fibre structure. *Industrial Crops and Products*, 2012, 39: p. 7-11.
51. Pickering K, ed. *Properties and performance of natural-fibre composites*. 2008. CRC Press LLC: Boca Raton.
52. Oksman K. High quality flax fibre composites manufactured by the resin transfer moulding process. *Journal of Reinforced Plastics and Composites*, 2001, 20(7): p. 621-627.
53. Gassan J, Bledzki AK. Possibilities for improving the mechanical properties of jute/epoxy composites by alkali treatment of fibres. *Composites Science and Technology*, 1999, 59: p. 1303-1309.
54. Charlet K, Jernot JP, Gomina M, Bizet L, Bréard J. Mechanical properties of flax fibers and of the derived unidirectional composites. *Journal of Composite Materials*, 2010, 44(24): p. 2887-2896.
55. Wambua P, Ivens J, Verpoest I. Natural fibres: can they replace glass in fibre reinforced plastics? *Composites Science and Technology*, 2003, 63: p. 1259-1264.
56. Pavithran C, Mukherjee PS, Brahmakumar M, Damodaran AD. Impact properties of natural fibre composites. *Journal of Materials Science Letters*, 1987, 6: p. 882-884.
57. Santulli C. Impact properties of glass/plant fibre hybrid laminates. *Journal of Materials Science*, 2007, 42: p. 3699-3707.
58. Yuanjian T, Isaac, DH. Impact and fatigue behaviour of hemp fibre composites. *Composites Science and Technology*, 2007, 67: p. 3300-3307.
59. Nunna S, Chandra PR, Shrivastava S, Jalan AK. A review on mechanical behavior of natural fiber based hybrid composites. *Journal of Reinforced Plastics and Composites*, 2012, 31: p. 759-769.

# 4 EFFECT OF FIBRE VOLUME FRACTION ON THE TENSILE PROPERTIES OF PLANT YARN REINFORCED COMPOSITES*

## 4.1 INTRODUCTION

Fibre reinforced plastics (FRPs) are heterogeneous materials. They consist of reinforcing fibres embedded in a continuous matrix. While the fibres provide strength and stiffness to the composite, the matrix transmits externally applied loads to the fibres and protects the fibres from external damage. As described in *Chapter 2*, the properties of a composite material are generally a weighted linear combination of the properties of the fibre and the matrix; the fibre volume fraction being the critical parameter. In fact, micro-mechanical models, backed by experimental data, show that several composite properties including density, Poisson's ratio, stiffness (tensile, compressive, shear), and strength (tensile, compressive, shear, impact), increase proportionally with fibre volume fraction [1]. However, these composite properties are limited by the minimum, critical and maximum fibre volume fraction. Hence, knowledge of the processing window (in terms of range of fibre volume fractions) which produces composites with useful properties is essential.

Importantly, fibre and matrix volume fractions are not the only volumetric components of a composite. Porosity, defined as air-filled cavities, is often an unavoidable part in all composites. They develop during the mixing and consolidation of the fibre and the matrix, for instance during the injection of resin in a RTM process. Porosity is known to have highly detrimental effects on composite properties [1-4]. To reduce porosity in composites, several innovative techniques have been developed [1, 5]. Nonetheless, knowledge of the void content is essential for the reliable prediction of composite properties using micro-mechanical models.

* This chapter is based on the peer-reviewed journal article:

Shah DU, Schubel PJ, Licence P, Clifford MJ. Determining the minimum, critical and maximum fibre content for twisted yarn reinforced plant fibre composites. *Composites Science and Technology*, 2012, 72(15): p. 1909-1917.

### 4.1.1 Structure-property relationships in PFRPs

Renewable bio-based composite materials provide an exciting opportunity to develop sustainable materials. Plant fibres in particular are an attractive source of reinforcement for FRPs. As a result, they have been subjected to several characterisation and development studies. However, in many studies on plant fibre composite (PFRP) mechanical properties, the volumetric composition of the composites is not well-characterised [6]. While most researchers present the fibre weight fraction, some state the fibre volume fraction assuming no porosity. This is due to issues with the measurement of fibre and void volume fraction in PFRPs. Conventional methods, such as resin burn-off and acid/chemical digestion, prove unsuccessful with PFRPs, as the plant fibres degrade and get consumed alongside the resin upon high temperature exposure and chemical attack [7-9].

There are, however, some well-documented studies on structure-property relationships of PFRPs; be it for randomly-oriented short-fibre reinforcements [10-15], randomly-oriented long-fibre reinforcements [16], uniaxially-oriented long-fibre (slivers) reinforcements [17-20] or aligned staple fibre yarn reinforcements [6, 18, 21-25]. Most of these studies employ density measurement methods (described in [7]) to determine the volumetric composition of the composites. The aims of these studies have been to *i)* characterise the composite properties over a range of fibre volume fractions, *ii)* compare the results with predictive micro-mechanical models (such as the rule of mixtures or Halpin-Tsai equations) and *iii)* compare the performance with E-glass composites.

However, there have been no direct studies on determining the minimum $v_{f,min}$ and critical $v_{f,crit}$ fibre volume fraction for PFRPs. More recently, Sawpan *et al.* [26] did attempt to calculate the minimum fibre volume fraction $v_{f,min}$ for short-fibre hemp/polyester composites, but they could not verify this experimentally as their characterisation study was based on fibre weight fractions (neglecting porosity). The maximum obtainable fibre volume fraction for PFRPs has also not been studied; where a maximum fibre volume fraction has been quoted [6, 17, 21], it has been based on composite processing limitations and tensile test data. For aligned PFRPs, twisted plant fibre staple yarns are the readily available and widely used form of

continuous reinforcement. Such staple fibre yarns themselves have a fibre volume fraction (referred to as the packing fraction ∅ by textile engineers [27]). Hence, the use of such twisted yarn reinforcements has an (unfavourable) effect on the theoretical (geometrically-permissible) maximum fibre volume fraction $v_{f,max,theo}$, which needs to be investigated. Furthermore, the influence of increasing fibre volume fraction on porosity is disputed and needs more insight; while some reports suggest an increase in porosity with fibre content [6, 16, 23], others suggest no correlation [12, 17, 22].

The purpose of this chapter is to analyse the relationship between structure and properties of aligned PFRPs. Specifically, the effect of fibre volume fraction on PFRP physical properties (porosity and fibre packing arrangement) and tensile properties is discussed. Parameters such as minimum, critical and maximum obtainable fibre volume fraction are also determined to identify the range of fibre volume fractions that produce twisted yarn reinforced PFRPs with useful properties.

### 4.1.2 Theory: Minimum and critical fibre volume fraction

In composite theory [1], for brittle-fibres and a ductile-matrix the strength-fibre content relationship is well-understood (Fig. 4.1). If there are very few fibres present ($0 < v_f < v_{f,min}$), the stress on a composite may be high enough to break the fibres. The broken fibres, which carry no load, can be then regarded as an array of aligned holes. The net effect is that the composite tensile strength $\sigma_c$ is even below that of the matrix $\sigma_m$. This defines a minimum fibre volume fraction $v_{f,min}$ below which the fibres weaken the material rather than strengthen it and composite failure is controlled by the matrix. The reinforcing action of the fibres is only observed once the fibre volume fraction exceeds the critical fibre volume fraction ($v_f > v_{f,crit}$). This is mathematically presented in Eq. 4.1 and diagrammatically illustrated in Fig. 4.1. Note that $\sigma'_m$ is the matrix stress at the fibre failure strain $\varepsilon_f$ (schematic in Fig. 4.2). Eq. 4.2 and Eq. 4.3 mathematically define the minimum $v_{f,min}$ and critical $v_{f,crit}$ fibre volume fractions, respectively.

$$\sigma_c = \begin{cases} \sigma_m(1-v_f) & for\ 0 < v_f < v_{f,\min} \\ \sigma_f v_f + \sigma'_m(1-v_f) & for\ v_f > v_{f,\min} \end{cases} \qquad \text{Eq. 4.1}$$

$$v_{f,\min} = \frac{\sigma_m - \sigma'_m}{\sigma_f + (\sigma_m - \sigma'_m)} \qquad \text{Eq. 4.2}$$

$$v_{f,crit} = \frac{\sigma_m - \sigma'_m}{\sigma_f - \sigma'_m} \qquad \text{Eq. 4.3}$$

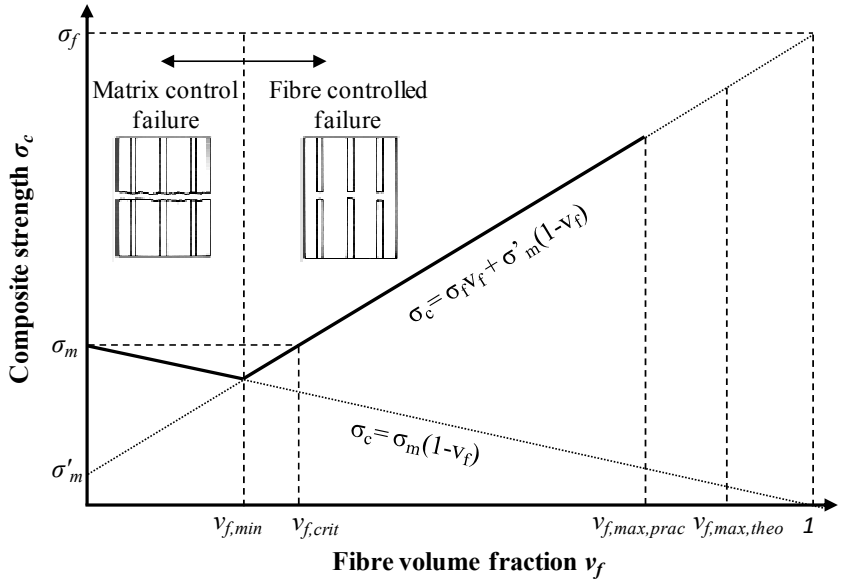


**Fig. 4.1. Schematic illustration of the variation of the strength of a unidirectional (brittle-fibre ductile-matrix) composite with fibre volume fraction.**

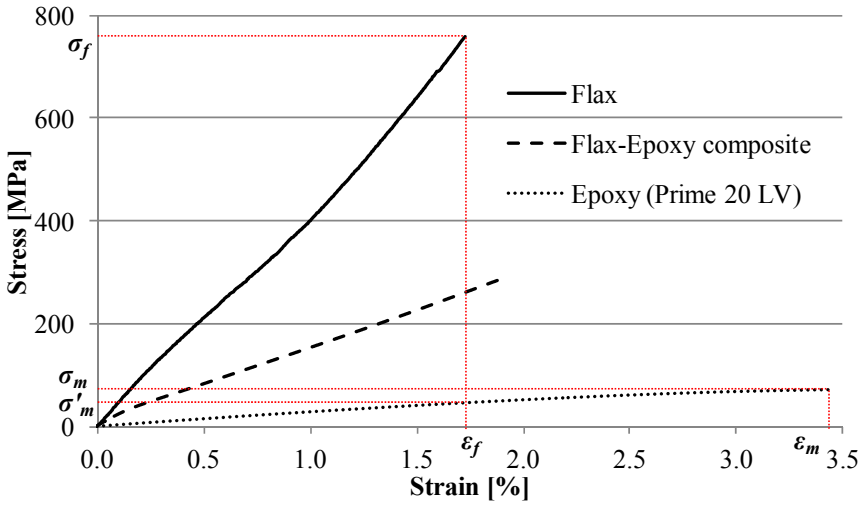


**Fig. 4.2. Plant fibre thermoset composites are a brittle-fibre ductile-matrix system.**

A thermoset bast fibre reinforced composite is also a brittle-fibre ductile-matrix system, where the fibre failure strain $\varepsilon_f$ is lower than the matrix failure strain $\varepsilon_m$ (Fig. 4.2). Hence, if plant fibres are to be used as reinforcements for structural composites, knowing the minimum and critical fibre volume fraction is paramount as the PFRP would be designed for $v_f > v_{f,crit}$. There is only one study (by Ghosh *et al.* [11]) which implicitly illustrates the minimum and critical fibre volume fractions (neglecting porosity) for short banana leaf fibre reinforced vinyl-ester composites to be $v_{f,min} \approx$ 15% and $v_{f,crit} \approx$ 25%. Interpreting the results of Sawpan *et al.* [26], it is found that short fibre hemp/polyester composites have a minimum and critical fibre weight fraction of ~20% and >30% (up to 60%), respectively. While the automotive industry is by far the biggest consumer of PFRPs [28], the plant fibre reinforcements are short, randomly-oriented and employed at fibre volume fractions ranging from 15 to 55% (fibre weight fractions of 20-65%) [28, 29]. This implies that the tensile strength of the matrix is higher than the tensile strength of the composite for many of these PFRP components. In addition, the values of minimum and critical fibre volume fractions for PFRPs, found from Ghosh *et al.* [11], Sawpan *et al.* [26] and this study, are substantially higher than those of conventional FRPs; an aligned carbon/polyester composite would have $v_{f,min}$ = 2.3% and $v_{f,crit}$ = 2.4% [1].

### 4.1.3 Theory: Maximum achievable fibre volume fraction

Several studies (for instance [15, 17, 21, 30, 31]) have concluded that the generalised rule of mixtures (Eq. 2.1 and Eq. 2.2) is valid for PFRPs. As the fibre content exceeds $v_{f,crit}$, the strength of the composite increases proportionally (as in Fig. 4.1). However, there is a 'practical' maximum fibre content $v_{f,max,prac}$ above which composite properties deteriorate [12, 17], often due to a drastic increase in porosity [6, 16, 21] or increased fibre-fibre interactions [32, 33]. Madsen *et al.* [21] found that when aligned hemp/polypropylene laminates were fabricated at a nominal fibre volume content of 61%, the actual measured fibre volume content was only 51% with a larger porosity content of 17%. In essence, impregnation and wettability issues arise close to this maximum fibre volume fraction. Pan [34] has also suggested (according to Cox [35]) that at high fibre volume fractions, fibre-to-fibre spacing becomes so small that the stress transfer between fibre and matrix becomes

inefficient eventually causing premature failure due to increased shear stresses on all planes parallel to the axes of the fibres. The resulting delamination has been observed in jute/polyester composites at high fibre content [17].

The experimentally determined optimal (or practical) maximum fibre volume fractions $v_{f,max,prac}$ for PFRPs range from about 60% for aligned jute roving reinforced polyester [17], 46-54% for aligned hemp yarn reinforced polyethyleneterephthalate (PET) [6, 21], and between 33% and 46% for short random flax and jute reinforced polypropylene [6]. For synthetic fibre composites, $v_{f,max,prac}$ is much higher at 75-80%.

On the other hand, the theoretical maximum fibre volume fraction $v_{f,max,FRP}$ of a fibre reinforced composite is a function of fibre packing geometry. This is higher than the practical maximum fibre volume fraction $v_{f,max,prac}$. Based on ideal fibre packing geometry, quadratic arrangement of the fibres leads to a $v_{f,max,FRP}$ of $\pi/4$ (= 78.5%) while hexagonally-packed fibres generate a higher $v_{f,max,FRP}$ of $\pi/2\sqrt{3}$ (= 90.7%) [34]. Usefully, a more accurate value of the theoretical maximum fibre volume fraction $v_{f,max,FRP}$ can be determined through compaction studies, in which the evolution of fibre volume fraction with compaction pressure is studied. Generally, a power-law function (of the form $v_f = aP^b$, where $P$ is compaction pressure and $a$ and $b$ are material constants) is a suitable fit for the compaction curves [25, 36]. As $P$ increases, after a steep rise in $v_f$, the fibre volume fraction plateaus. The asymptotic value of fibre volume fraction can be regarded as $v_{f,max,FRP}$.

Madsen [25] and Xu *et al.* [36] have conducted such studies on plant and glass fibre preforms. Through such compaction studies, it is found that $v_{f,max,FRP}$ is different for synthetic fibre reinforced plastics and plant fibre reinforced plastics. This is because the packing ability of plant fibre assemblies is lower than that of synthetic fibre assemblies [21, 25, 37, 38]. It is suggested that fibre alignment and the degree of fibre separation affects the compact-ability of a preform. This was discussed previously in *Chapter 3.3.1*.

Importantly, for PFRPs that are reinforced with staple plant fibre yarns, the twist (and packing fraction) of the yarn would also affect preform compaction. The

packing fraction of a high twist yarn is absolute and will not usually change upon compaction (during composite processing) due to the transverse pressure in a yarn induced by the twisting process. However, if the yarn twist level (and thus the packing fraction) is very low, due to negligible transverse pressure in the yarn the yarn may be compacted further. Roe *et al.* [17] were able to produce higher fibre volume fractions in their jute/polyester composites (of up to 60%) as they were using slivers; these are compressible and thus the distance between fibres within the slivers can be reduced.

If the composite manufacturing technique relies on preform consolidation through press-moulding (*i.e.* application of positive pressure), as is typical in compression moulding, $v_{f,max,FRP}$ of preforms produced with higher twist yarns would be lower as the yarns will not spread upon compaction. Lower twist yarns, on the other hand, will spread out (like tows) under the application of pressure and will thus leave less resin rich zones and produce higher $v_{f,max,FRP}$.

The composite manufacturing utilised for studies in this thesis, however, is vacuum infusion in a rigid all-aluminium mould tool. The chosen manufacturing technique does not enable the utilization of a hydraulic press, for instance, to compact the preform. In such a manufacturing technique, the theoretical maximum fibre volume fraction of the plant fibre preform is dependent on the nominal packing fraction of the yarn. In fact, the theoretical maximum fibre content $v_{f,max,theo}$ would be a linear combination of the yarn packing geometry within a composite and fibre packing arrangement within the yarn ∅ (Eq. 4.4).

$$v_{f,\max,theo} = v_{f,\max,FRP} \cdot \phi \qquad \text{Eq. 4.4}$$

The maximum packing fraction of a yarn $\emptyset_{max}$ is 75.0% assuming an open-packed structure [39] or 90.7% assuming hexagonal close-packed fibre arrangement [27, 40]. Hence, the absolute limit of the maximum fibre volume fraction of a PFRP reinforced with twisted yarns ranges from 58.9% to 82.2%, depending on the combination of packing assumed in the composite and the yarn. The lower value of this absolute limit (*i.e.* 58.9%) is comparable to the experimental values of $v_{f,max,prac}$ observed in literature (quoted previously).

Importantly, the yarn packing fraction ∅ is a function of the yarn twist level [41]. Pan [41] derived a semi-empirical relationship (Eq. 4.5) between twist level *T* (turns per meter or tpm) and packing fraction ∅ of such staple fibre yarns. In Eq. 4.5, $\emptyset_{max}$ is the maximum packing fraction of the yarn, and A and B are constants. While Pan [41] used $\emptyset_{max}$, *A* and *B* as 0.7, 0.78 and 0.195, respectively, he suggested that these factors could be modified to suit other particular yarns. Conventional staple fibre ring-spun yarns have a packing fraction ∅ of 50-60% [42].

$$\phi = \phi_{\max}\left(1 - Ae^{-BT}\right) \qquad \text{Eq. 4.5}$$

Substituting Eq. 4.5 into Eq. 4.4 for ∅ results in a mathematical model (Eq. 4.6) for determining the maximum obtainable fibre volume fraction $v_{f,max,theo}$ in PFRPs reinforced with twisted staple plant fibre yarns, produced via vacuum infusion in a rigid mould (without the capacity to compact through application of pressure). The result of Eq. 4.6 is graphically presented in Fig. 4.3 for various combinations of parameter values ($v_{f,max,FRP}$, $\emptyset_{\max}$, *A* and *B*). Experimental data, based on calculated packing fractions ∅ of plant fibre yarns with twist level *T* have also been plotted. The experimental data is for yarns that have been used for PFRP manufacture. The data is from *Chapter 3 and Appendix A*. From Fig. 4.3, it is found that the packing fraction ∅ of staple fibre yarns used for PFRPs (particularly those used for the study described in this thesis), is well described by Eq. 4.5 with the factors $\emptyset_{\max}$, *A* and *B* of 0.6, 0.78 and 0.0195, respectively.

$$v_{f,\max,theo} = v_{f,\max,FRP} \cdot \phi_{\max}\left(1 - Ae^{-BT}\right) \qquad \text{Eq. 4.6}$$

In general, the results in Fig. 4.3 show that increasing yarn twist would lead to a composite with higher fibre volume fractions, before levelling off at a maximum obtainable volume fraction. This is in agreement with the study by Baets *et al.* [18] which reports that epoxy composites reinforced with flax slivers (0 tpm), rovings (41 tpm) and yarns (280 tpm), had fibre volume fractions of 42%, 48% and 50%, respectively. It is important to highlight here again that the above conclusion relates to the use of a manufacturing technique that doesn't enable preform compaction. Using composite manufacturing techniques which enable the application of

consolidation pressure (such as compression moulding and prepregging with autoclave consolidation) can enable the production of high fibre volume fraction composites if lower twist yarns (rovings/slivers) are used, due to their compactability and spread-ability.

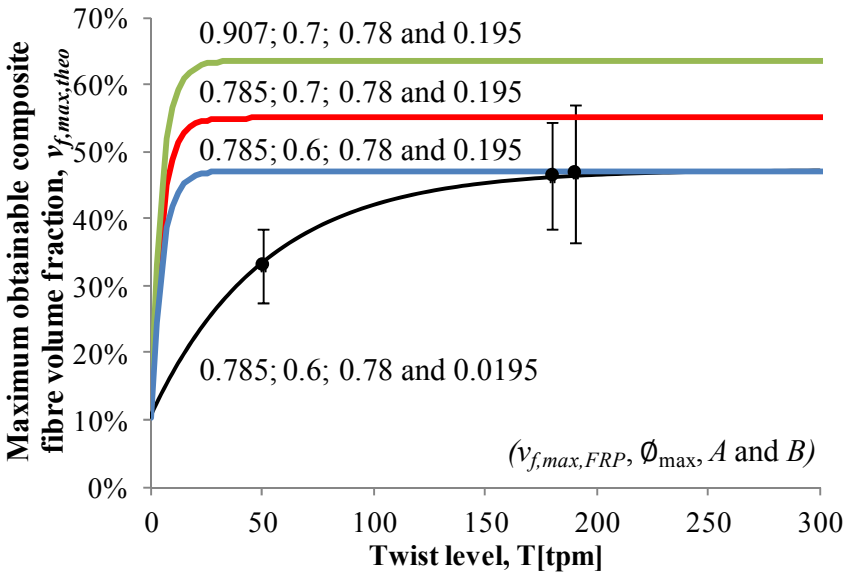


**Fig. 4.3. The effect of yarn twist level on the maximum obtainable fibre volume fraction $v_{f,max,theo}$ for PFRPs reinforced with such twisted yarns. Experimental data is from *Chapter 3 and Appendix A*. Refer to Eq. 4.6 and text for details.**

While the minimum and critical fibre volume fraction set the lower limit of effective reinforcing fibre volume fraction, the maximum fibre volume fraction sets the upper limit. These limits determine the fibre content design envelope for structural PFRPs employing twisted yarn reinforcements.

## 4.2 EXPERIMENTAL METHODOLOGY

### 4.2.1 Materials and composite manufacture

Unidirectional mats were prepared from two commercially available plant fibre yarns: a low twist (50 tpm) flax yarn from Composites Evolution (UK) and a high twist (190 tpm) jute yarn from Janata and Sadat Jute Ltd (Bangladesh). The flax yarn employs polyester as a binder yarn (13 wt% of yarn). These are the same yarns (F50 and J190) used for the study in *Chapter 3*. The aligned mats were prepared using a

drum-winding system and hydroxyethylcellulose binding agent (described in *Chapter 3*).

Unidirectional composite laminates (250 mm square 3-3.5 mm thick) of five different fibre volume fractions were fabricated. To generate different fibre volume fractions, an increasing number of unidirectional mat layers were used (*i.e.* 1, 2, 3, 4 and 5 layers). The reinforcement mats were used as-produced (without any preconditioning). While composite manufacturing processes like hot-pressing and compression moulding can produce much higher fibre content PFRPs, vacuum infusion is the chosen technique in this study as it readily enables the manufacture of large components, such as wind turbine blades. Vacuum infusion was carried out in an all-aluminium mould tool. Resin infusion was carried out at 70-80% vacuum (200-300 mbar absolute pressure). Line-gate resin injection was employed with the flow direction being perpendicular to the yarn axis. The composite manufacturing process has been described in detail in *Chapter 3*.

An unsaturated polyester (Reichhold Norpol type 420-100) matrix was used. The resin was mixed with 0.25 wt% NL49P accelerator (1% Cobalt solution) and 1 wt% Butanox M50 MEKP initiator. Post cure was carried out at 55 °C for 6 h after ambient cure for 16 h. From manufacturer datasheet, the resin has a cured density $\rho_m$ of 1.202 gcm$^{-3}$, tensile modulus $E_m$ of 3.7 GPa, tensile strength $\sigma_m$ of 70 MPa and failure strain $\varepsilon_m$ of 3.5%.

### 4.2.2 Physical characterisation

The fibre weight fraction $w_f$ of a laminate was calculated using the ratio of the mass of the preform and the resulting composite laminate. Composite and fibre density were determined using helium pycnometry (minimum of 5 samples). The fibre volume fraction $v_f$, matrix volume fraction $v_m$ and void volume fraction $v_p$ of the manufactured composites were then determined using equation Eq. 4.7, where $w$ and $\rho$ represent weight fraction and density, respectively while the subscripts $f$, $m$ and $c$ denote fibres, matrix and composite, respectively.

$$v_f = \frac{\rho_c}{\rho_f} w_f; \quad v_m = \frac{\rho_c}{\rho_m}(1 - w_f); \quad v_p = 1 - (v_f + v_m) \qquad \text{Eq. 4.7}$$

Optical microscopy was also used to qualitatively image the fibre/yarn packing arrangement and porosity in the composites. Sample preparation has been previously discussed in *Chapter 3*.

### 4.2.3 Tensile testing

Tensile tests were conducted according to ISO 527-4:1997 using an Instron 5985 testing machine equipped with a 100 kN load cell and an extensometer. At least six 250 mm long and 15 mm wide specimens were tested for each type of composite at a cross-head speed of 2 mm/min. The ultimate tensile strength $\sigma_c$, tensile modulus $E_c$ (in the strain range of 0.025-0.100%) and the strain at failure $\varepsilon_c$ of the specimen were measured from the stress-strain curve. The fracture surfaces were also observed under a Philips XL30 Scanning Electron Microscope (SEM) at an acceleration voltage of 15 kV. The samples were sputter-coated with platinum.

## 4.3 RESULTS AND DISCUSSION

### 4.3.1 Volumetric composition

Flax and jute/polyester unidirectional composites have been produced with 5 different fibre volume fractions, by simply increasing the number of layers of unidirectional mats. The density of the composites is observed to increase with fibre volume fraction; the composite density approaches the density of the flax and jute fibres of 1.529 ± 0.003 $gcm^{-3}$ and 1.433 ± 0.005 $gcm^{-3}$, respectively. However, a drop in density is observed for the jute/polyester composites at $v_f$ = 31.7% due to a relatively higher void content. The volumetric composition of fibre, matrix and void within the composites is tabulated in Table 4.1. Note the consistency in fibre/matrix volume fractions (indicated by the small standard deviations) for the composites; Madsen *et al.* [43] also observed such small variations in fibre volume fraction for their hemp and flax yarn reinforced composites.

Also note the low void content (typically in the range of 0.3-1.4%) of the PFRPs produced. Although the void content seems to be higher for greater fibre content, there is no clear correlation between composite fibre volume fraction and porosity (Fig. 4.4). Very low linear regression $R^2$-values of 0.126 and 0.272 are obtained for

void content as a function of fibre content for flax and jute composites, respectively. This is in agreement with references [12, 17, 22] but disagreement with references [6, 16, 23].

**Table 4.1. Density and volumetric composition (mean ± stdev.) of the fabricated laminates.**

| Fibre (# of layers) | Composite density $\rho_c$ [gcm$^{-3}$] | Fibre volume fraction $v_f$ [%] | Matrix volume fraction $v_p$ [%] | Void volume fraction $v_v$ [%] |
|---|---|---|---|---|
| **Flax (5)** | 1.301 ± 0.009 | 32.5 ± 0.2 | 66.9 ± 0.5 | 0.6 ± 0.7 |
| **Flax (4)** | 1.282 ± 0.002 | 27.3 ± 0.1 | 72.0 ± 0.1 | 0.7 ± 0.2 |
| **Flax (3)** | 1.264 ± 0.001 | 24.0 ± 0.1 | 74.6 ± 0.0 | 1.4 ± 0.1 |
| **Flax (2)** | 1.245 ± 0.001 | 17.8 ± 0.0 | 80.9 ± 0.1 | 1.2 ± 0.1 |
| **Flax (1)** | 1.220 ± 0.001 | 6.1 ± 0.0 | 93.8 ± 0.1 | 0.1 ± 0.1 |
| **Jute (5)** | 1.276 ± 0.002 | 37.8 ± 0.1 | 61.1 ± 0.1 | 1.1 ± 0.2 |
| **Jute (4)** | 1.225 ± 0.002 | 31.7 ± 0.1 | 64.1 ± 0.1 | 4.2 ± 0.1 |
| **Jute (3)** | 1.251 ± 0.004 | 25.2 ± 0.1 | 74.1 ± 0.2 | 0.7 ± 0.3 |
| **Jute (2)** | 1.238 ± 0.003 | 17.1 ± 0.1 | 82.6 ± 0.2 | 0.3 ± 0.2 |
| **Jute (1)** | 1.215 ± 0.002 | 7.6 ± 0.0 | 92.0 ± 0.2 | 0.4 ± 0.2 |

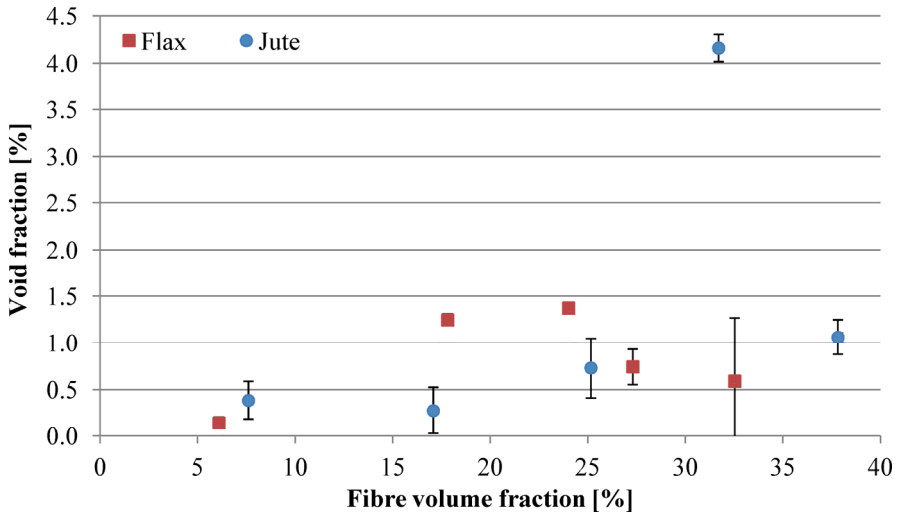


**Fig. 4.4. There is no clear correlation between fibre content and void content.**

The volumetric composition and the presence of voids in composites of different fibre volume fractions can be visually observed from the microscopic images in Fig. 4.5. It is observed that for low fibre volume fractions (up to 2 layers) voids generally form within the yarn bundle (intra-yarn voids). Increasing the fibre volume fraction further results in the formation of voids between adjacent yarns (inter-yarn voids), rather than within the yarn. This is possibly due to the changing resin flow dynamics with fibre content. At low fibre content, impregnation within the yarn is difficult as high overall permeability and low yarn permeability leads to fast infusion elsewhere and slow infusion within the yarn. Essentially, the resin moves faster in the channels than in the yarn; the 'outrun' produces intra-yarn voids (Fig. 4.6a). However, at high fibre content the yarns are much closer to each other and the overall permeability is comparable to the yarn permeability. However, capillary pressure is larger within the yarn. Hence, flow is faster through the yarn so that voids are formed between yarns, *i.e.* inter-yarn voids (Fig. 4.6b). In essence, fibre content does not have an obvious effect on void content, but it does influence the type of voids.

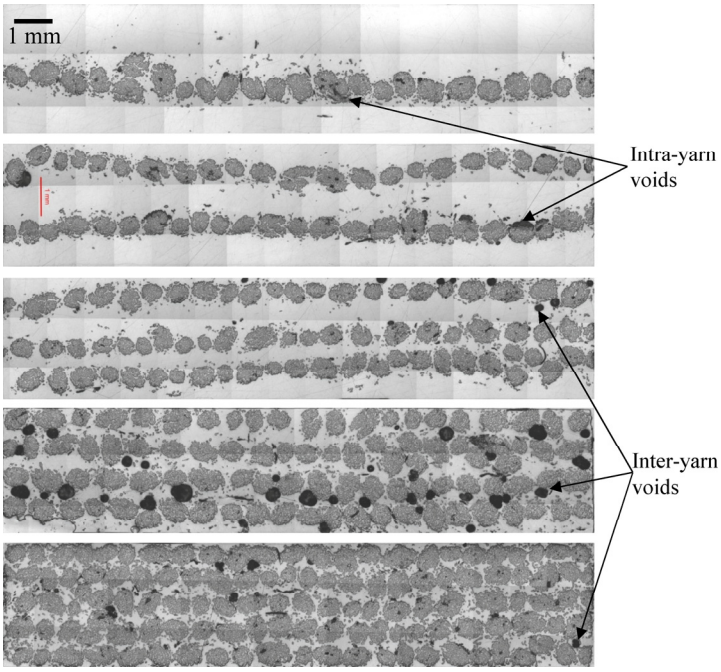


**Fig. 4.5. Microscopic images of the cross-section of jute/polyester composites showing the composition and fibre/yarn packing arrangement for increasing fibre content.**

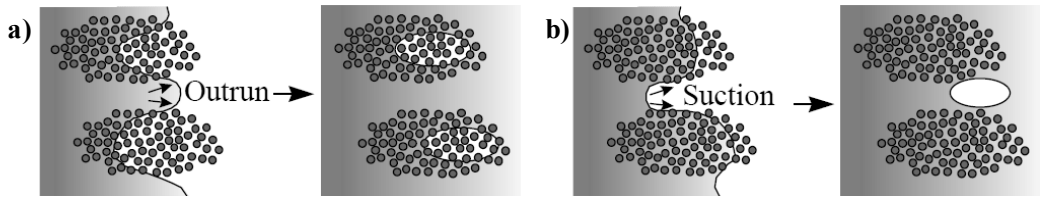


**Fig. 4.6. The packing arrangement and fibre volume fraction affect the type of void formed. *a)* At low fibre content, due to low yarn permeability but high overall permeability, the yarn is not properly impregnated and thus intra-yarn voids are formed. *b)* at high fibre content, although yarn and overall permeability are similar, capillary flow in the yarn dominates and therefore inter-yarn voids are formed.**

### 4.3.2 Maximum fibre volume fraction

The yarns used in this study are flax (50 tpm) and jute (190 tpm). The experimentally known packing fractions ∅ are 0.421 and 0.596 for the flax and jute yarn, respectively (from *Chapter 3*). From Fig. 4.5, it can be seen that the yarns follow a square packing arrangement hence $v_{f,max,FRP}$ is taken to be π/4 (= 78.5%). Using Eq. 4.4, the derived maximum obtainable fibre volume fraction $v_{f,max,theo}$ is 33.1% for the flax composites and 46.8% for jute composites. The bottom-most image in Fig. 4.5 is of jute/polyester with $v_f$ = 37.8% (5 layers). The yarns seem well-packed within the composite cross-section and thus a theoretical maximum fibre content $v_{f,max,theo}$ of 46.8% for the jute composites is realistic. The order of the values of the theoretical maximum fibre content $v_{f,max,theo}$ is similar to the order of values of the practical maximum fibre content $v_{f,max,prac}$ reported in literature (discussed in Section 4.1.3).

### 4.3.3 Tensile properties

The tensile stress-strain curves reveal the general changes in tensile properties of the composite for increasing fibre content. Fig. 4.7 presents stress-strain curves of representative specimens for jute/polyester composites of different fibre volume fractions. The curves are shifted upwards when fibre volume fraction increases, suggesting that the elastic modulus and tensile strength increase. It is also observed that the failure strain increases at first and then becomes fairly constant.

It is interesting to note from the composite stress-strain curves in Fig. 4.7 that for all fibre volume fractions PFRPs show a non-linear response. In fact, increasing fibre

content exaggerates the non-linear response. The stress-strain curve of a single plant fibre is also found to be non-linear (Fig. 4.2). This is different from synthetic fibres and their FRPs (particularly E-glass) whose stress-strain behaviour is entirely linear. The non-linear stress-strain response of plant fibres and their composites is discussed in detail in *Chapter 5*.

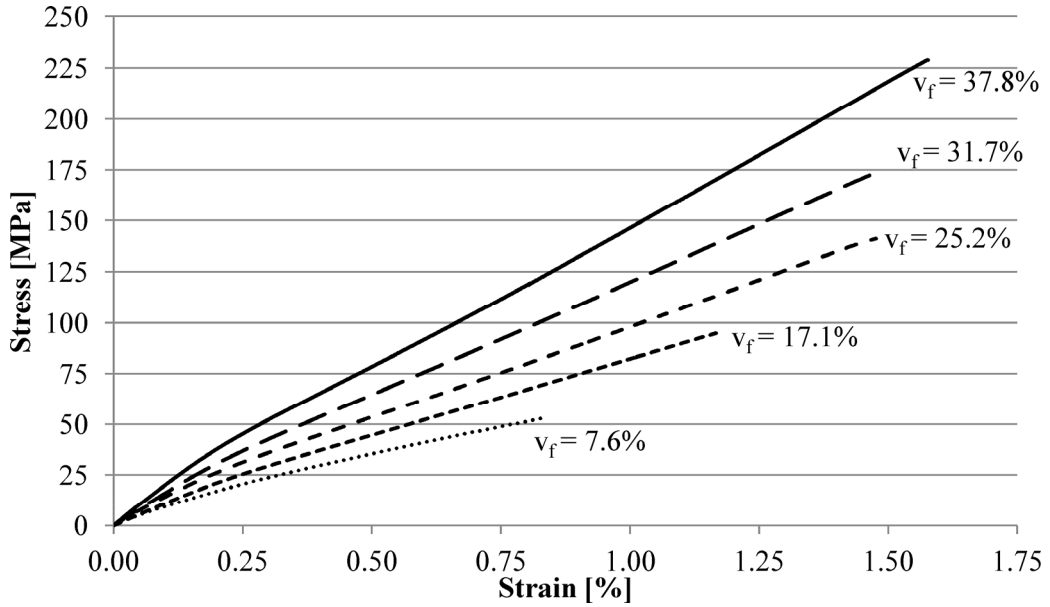


**Fig. 4.7. Typical stress-strain curves of jute/polyester with variable fibre volume fraction.**

The fracture surfaces of the tensile test specimen (Fig. 4.8) also give insight into the reinforcing effect of the plant fibres at different fibre volume fractions. It can be seen in Fig. 4.8 that for the first two specimen (up to $v_f \approx 18\%$), for both flax and jute composites, tensile fracture is macroscopically brittle with a flat fracture surface. The composite failure seems to be matrix-controlled. Little microscopic pull-out of the fibres is noticed in the SEM images (Fig. 4.9). This is also a sign of low impact strength, as fibre pull-out is more energy dissipative than fibre fracture [44].

Increasing the fibre content produces a more serrated and uneven fracture surface, as can be seen in Fig. 4.8. The composite failure is fibre-controlled. SEM images in Fig. 4.9 show that the fibre pull-out length is also increased implying an increase in toughness. For jute/polyester composites in particular, the fracture path becomes

longer and starts running along the length of the fibres/yarns. It can be seen in Fig. 4.8 that at high fibre volume fractions, delamination between adjacent yarns and layers occurs. It is interesting that no sign of delamination is noticed in the flax/polyester composites. This is possibly due to the difference in structure of the yarn (specifically, twist level).

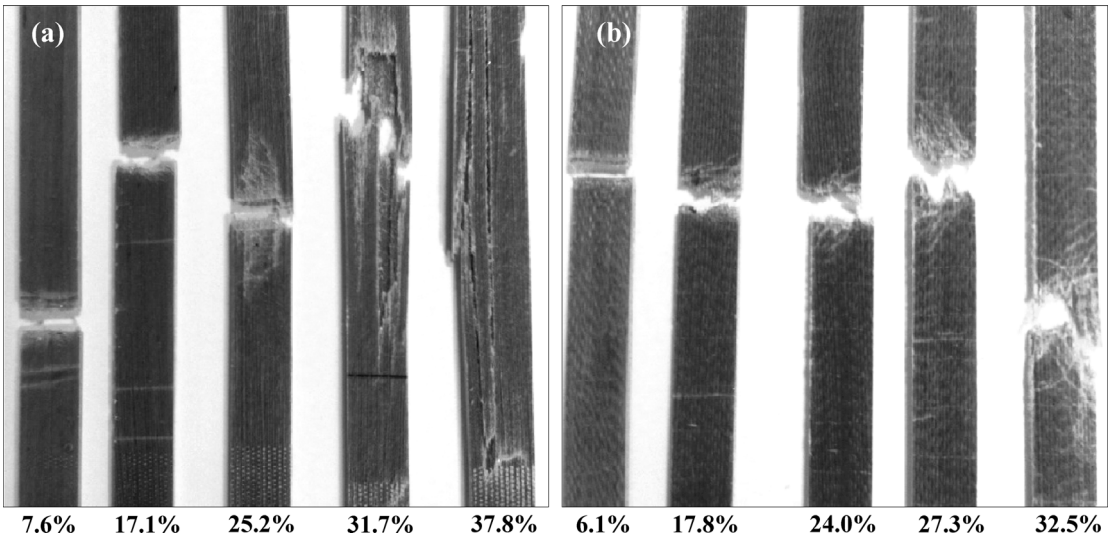


**Fig. 4.8. The effect of fibre volume fraction of *a)* jute and *b)* flax on the fracture of tensile specimen. Increasing fibre content (left to right) produces a more serrated fracture surface and even delamination.**

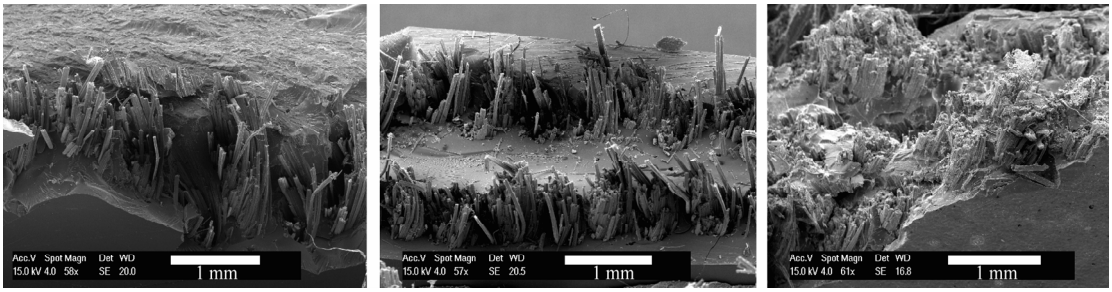


**Fig. 4.9. SEM images of fracture surfaces of jute/polyester composites showing increasing fibre pull-out and serrated surface for increasing fibre content. From left to right: 1 layer, 2 layers and 4 layers of unidirectional reinforcement.**

#### 4.3.3.1 Tensile modulus

The variation of the tensile modulus with fibre volume fraction (Fig. 4.10) of flax ($R^2$ = 0.993) and jute ($R^2$ = 0.992) composites demonstrates that the rule of mixtures (Eq.

4.8) is followed closely. This is in agreement with several other studies (such as [13, 17, 19-21, 30, 31]).

$$E_c = \eta v_f E_f + (1 - v_f) E_m \qquad \text{Eq. 4.8}$$

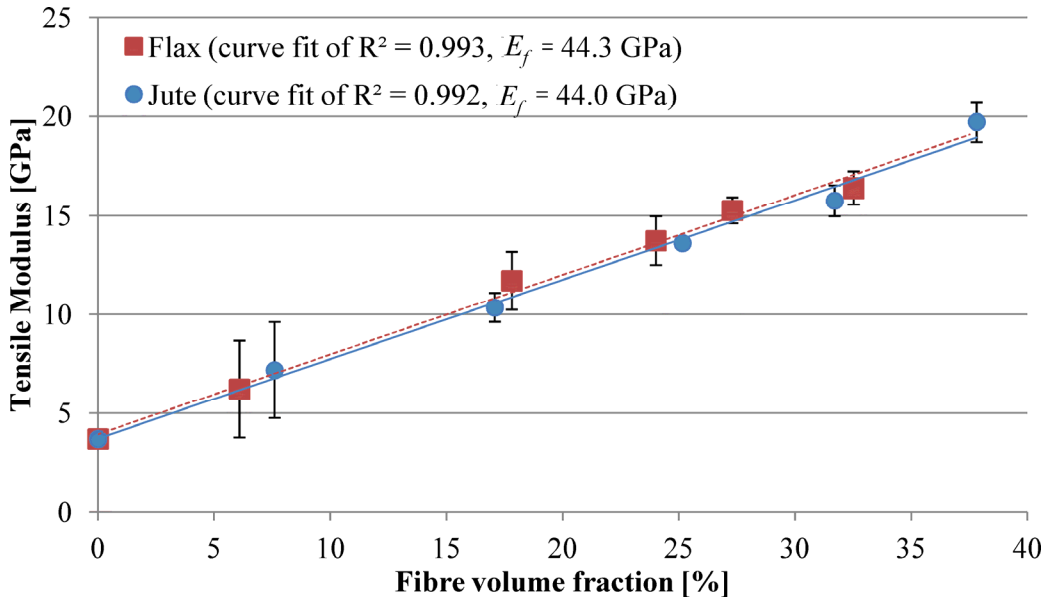


**Fig. 4.10. Variation of tensile modulus with fibre volume fraction.**

The back-calculated effective fibre modulus $\eta E_f$ for flax and jute is thus obtained as 44.3 GPa and 44.0 GPa, respectively. This is in the range of literature values [45, 46] generally quoted for flax and jute, although flax can achieve a much higher tensile modulus (of over 70 GPa), as shown in *Chapter 3*. Note that this effective fibre modulus $\eta E_f$ incorporates any effect of the various efficiency and correction factors in the modified rule of mixtures for PFRPs discussed in detail in *Chapter 2.4* (Eq. 2.3 and Eq. 2.4): *i)* fibre length efficiency, *ii)* fibre orientation distribution, *iii)* fibre diameter distribution, *iv)* fibre cross-sectional area correction factor and *v)* porosity correction factor. Note that it has been shown in *Chapter 3* that the length efficiency factor is almost unity for such yarn reinforced PFRPs.

As the theoretical maximum fibre volume fraction of flax and jute composites is known, the maximum theoretical tensile modulus achievable can be determined. This is found to be 17.3 GPa for flax/polyester (at $v_{f,max,theo}$ = 33.1%) and 22.6 GPa for

jute/polyester (at $v_{f,max,theo}$ = 46.8%). This compares to a tensile modulus of 33.7 GPa for E-glass/polyester (at $v_f$ = 44.0%) (measured in *Chapter 3*). Note that E-glass/polyester has a much higher $v_{f,max,theo}$ (= $v_{f,max,FRP}$), hence it can deliver much higher properties. The low $v_{f,max,theo}$ of PFRPs, in comparison to conventional FRPs, is a therefore a significant disadvantage. However, it should be noted that due to the low density of PFRPs, the high specific stiffness properties of PFRPs still make them attractive materials. Particularly, if high-quality plant fibre reinforcements (like F20) are used.

A note should be made here regarding the effect of porosity on the tensile modulus. The void content for flax and jute composites ranges between 0.1% and 1.4%, with no obvious increase with fibre content. Interestingly, despite the relatively high void content ($v_p$ = 4.2%) of jute/polyester with $v_f$ = 31.7%, no apparent drop in the elastic modulus (or tensile strength) is noticed (considering the standard deviation), despite a drop in density. Madsen *et al.* [6] show that for plant fibre thermoplastic composites, the effect of porosity on material stiffness is approximated by a multiplication factor of $(1 - v_p)^2$. In essence, a void content of 4.2% should reduce the potential composite stiffness (represented by the rule of mixtures) by 8.2%. An extensive study on the effect of void content on mechanical properties of E-glass thermoplastic composites was conducted by Gil [3]; it is observed that a void content of 4% would reduce the composite tensile strength or stiffness by 10-30%. However, Santulli *et al.* [2] suggest that no obvious reduction in mechanical properties is observed for void content below 3-4% for such E-glass thermoplastics. It is proposed that the same may be true for PFRPs. Reviewing the results of Madsen *et al.* [21] it is found that for hemp-PET composites, for up to 3.2% void content (at 40% $v_f$) there is negligible effect (considering the standard deviations) of void content on composite tensile strength and stiffness. Only at 50% fibre content, the void content jumps to 11.6% and is observed to reduce the stiffness and strength significantly. In essence, void content of up to 4% has minimal effect on PFRP properties.

#### 4.3.3.2 Tensile strength

Fig. 4.11 shows the experimental data of tensile strength as a function of fibre content. The characteristic brittle-fibre ductile-matrix variation in composite tensile strength as a function of fibre volume fraction is noticed (as previously illustrated in Fig. 4.1). Again, good agreement with the rule of mixtures (Eq. 4.1) is noticed.

The back-calculated effective fibre tensile strength $\sigma_f$ for flax and jute is obtained as 502.7 MPa and 615.2 MPa, respectively. This is in the range of literature values [45, 46] generally quoted for flax and jute, although flax can achieve a much higher tensile strength (of about 1100 MPa). Again, this effective fibre strength incorporates any effect of length and orientation efficiency factors. No drop in tensile strength is observed for jute/polyester with $v_f$ = 31.7% with a relatively high void content ($v_v$ = 4.2%).

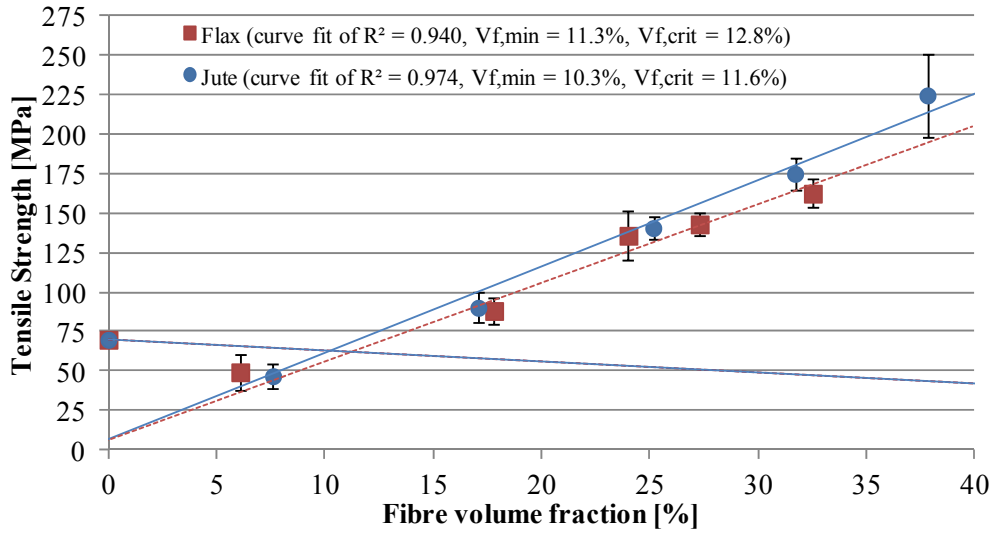


**Fig. 4.11. Variation of tensile strength with fibre volume fraction.**

The minimum and critical fibre volume fractions can also be determined from Fig. 4.11 and using Eq. 4.1-4.3, using $\sigma'_m$ = 6.2 MPa (obtained from the curve fit of data points with $v_f$ > 15%). The minimum and critical fibre volume fractions are found to be $v_{f,min}$ = 11.3% and $v_{f,crit}$ = 12.8% for flax/polyester composites and $v_{f,min}$ = 10.3% and $v_{f,crit}$ = 11.6% for jute/polyester composites. Hence, for the design of useful

aligned PFRPs, where plant fibre twisted yarns are reinforcing the matrix, the fibre volume fraction needs to be in excess of ~10%.

Ghosh *et al.* [11] implicitly illustrate the minimum and critical fibre volume fractions for short banana fibre reinforced vinyl-ester composites to be $v_{f,min} \approx 15\%$ and $v_{f,crit} \approx 25\%$. The significantly higher minimum and critical fibre volume fraction of short fibre PFRPs compared to twisted yarn reinforced PFRPs is the direct result of higher critical load transfer lengths in short fibre PFRPs due to lower interfacial shear strength and lower fibre aspect ratios.

Notably, the minimum and critical fibre volume fractions for PFRPs are substantially larger than those observed in conventional unidirectional FRPs. For an aligned carbon-polyester composite [1], $v_{f,min} = 2.3\%$ and $v_{f,crit} = 2.4\%$. In addition, while the difference in $v_{f,min}$ and $v_{f,crit}$ for a carbon-polyester composite is only 0.1%, it is ~1% for twisted yarn reinforced PFRPs and ~10% for short fibre PFRPs [11]. $\sigma'_m$ (or in fact $(\sigma_m - \sigma'_m)$) relates to the work-hardening efficiency of the matrix for the fibre reinforcement. A low $\sigma'_m$ (and thus a high $(\sigma_m - \sigma'_m)$) correctly implies a higher minimum and critical fibre volume fraction (from Eq. 4.2 and Eq. 4.3). $\sigma'_m$, which defines the matrix stress at fibre failure strain, is about 22 MPa for the carbon-polyester system, but only 6.2 MPa for both the flax/polyester and the jute/polyester systems. From Ghosh *et al.* [11], it is observed that $\sigma'_m$ is even lower at 5 MPa for short banana leaf fibre reinforced vinyl-ester composites. Interestingly, $\sigma'_m$ is often estimated to be about 40-50 MPa (using $\sigma'_m = E_m\varepsilon_f$) for a matrix reinforced with plant fibres [18, 21, 47]; this is clearly a gross over-estimation.

As the theoretical maximum fibre volume fraction of flax and jute composites is known, the maximum theoretical tensile strength can be determined. This is found to be 170.6 MPa for flax/polyester (at $v_{f,max} = 33.1\%$) and 263.1 MPa for jute/polyester (at $v_{f,max} = 46.8\%$). This compares to a tensile strength of 825.7 MPa for an E-glass/polyester (at $v_f = 44.0\%$) (measured in *Chapter 3*). The poor mechanical strength performance of PFRPs, in comparison to E-glass/polyester, is particularly due to *i)* the comparatively poor mechanical strength of plant fibres, and *ii)* the lower (achievable) fibre volume fractions of PFRPs.

It seems that vacuum-infused PFRPs utilising staple fibre twisted yarns have a small window of fibre volume fractions which produce useful composites. A high $v_{f,crit}$ (on the order of 10%), low $v_{f,max,prac}$ (on the order of 45-55%) [6, 21] and low $v_{f,max,theo}$ (on the order of 45-60%) implies that the possible range of employable fibre volume fractions for such PFRPs is only 35-50%. Importantly, short-fibre randomly-oriented PFRPs have a much higher $v_{f,crit}$ (on the order of 25%) and lower $v_{f,max,prac}$ (on the order of 30-45%) [6] implying that the useable range of fibre volume fractions is even lower (5-20%). This significantly limits the maximum exploitation of the mechanical properties of plant fibres in FRPs.

#### 4.3.3.3 Strain at failure

The failure strain is observed to increase with increasing fibre volume fraction before levelling off to a value of about 1.62% for flax composites and 1.47% for jute composites (Fig. 4.12). The strain value corresponds to the effective strain at tensile failure of the fibres. This behaviour is similar to that observed in the literatures [17, 21].

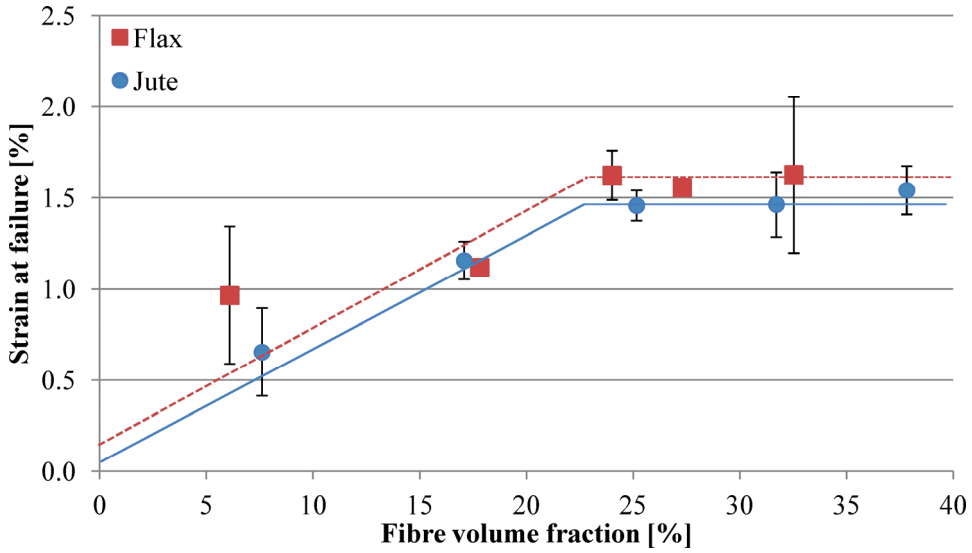


**Fig. 4.12. Variation of tensile failure strain with fibre volume fraction.**

## 4.4 CONCLUSIONS

The effect of fibre volume fraction on the physical and tensile properties of aligned PFRPs has been investigated. Yarn reinforced PFRPs are producible with low local variations in fibre/matrix volume fractions and low void content (typically in the range of 0.3-1.4%). There is no clear correlation between fibre volume fraction and porosity content. However, low fibre content PFRPs are prone to intra-yarn voids, while high fibre content PFRPs are prone to inter-yarn voids. This is possibly due to changing resin flow dynamics with increasing fibre volume fraction. Importantly, a void content of up to 4% is found to have minimal effect on the tensile properties of PFRPs.

The effect of fibre content on PFRP tensile properties is found to closely follow the rule of mixtures, similar to that of conventional FRPs. At low fibre content matrix-dominated brittle fracture occurs; increasing fibre content makes the fracture surface serrated and increases the occurrence and length of fibre pull-out.

A simple model has also been developed to approximate the theoretical maximum obtainable fibre volume fraction $v_{f,max,theo}$ of PFRPs reinforced with staple fibre yarns. The model is a linear combination of the yarn packing arrangement within the composite and the fibre packing arrangement within the yarn. The absolute limit of the theoretical maximum fibre volume fraction of a PFRP reinforced with twisted yarns ranges from 58.9% to 82.2%. The lower value of this absolute limit (*i.e.* 58.9%) is comparable to the experimental values of practical maximum fibre volume fraction $v_{f,max,prac}$ observed in literature. However, $v_{f,max,theo}$ for typical yarn reinforced PFRPs is in the range of 35-50%.

PFRPs utilising staple fibre twisted yarns have a small window of fibre volume fractions which produce composites with useful properties. A high $v_{f,crit}$ (on the order of 10%), low $v_{f,max,prac}$ (on the order of 45-55%) and low $v_{f,max,theo}$ (on the order of 45-60%) implies that the possible range of employable fibre volume fractions for such PFRPs is only 35-50%. Importantly, short-fibre randomly-oriented PFRPs have a much higher $v_{f,crit}$ (on the order of 25%) and lower $v_{f,max,prac}$ (on the order of 30-45%) implying that the useable range of fibre volume fractions is even lower (5-20%). This

significantly limits the maximum exploitation of the mechanical properties of plant fibres in FRPs. In comparison, aligned synthetic fibre reinforced composites have a lower $v_{f,crit}$ (2.4% for carbon/polyester) and much a higher $v_{f,max,prac}$ and $v_{f,max,theo}$ (on the order of 75-80%), implying that the range of fibre volume fractions that produce composites with useful properties is 70-75%.

## 4.5 REFERENCES


1. Harris B. *Engineering composite materials*, 1999. London: The Institute of Materials.
2. Santulli C, Brooks R, Rudd CD, Long AC. Influence of micro-structural voids on the mechanical and impact properties in commingled E-glass/polypropylene thermoplastic composites. *Journal of Materials: Design and Applications Part L*, 2002, 216(2): p. 85-100.
3. Gil R. *Forming and consolidation of textile composites*. PhD, 2003. The University of Nottingham: Nottingham, UK.
4. Ghiorse S. *Effect of void content on the mechanical properties of carbon/epoxy laminates*, in *SAMPE Quarterly*, 1993. p. 54-59.
5. Campbell F. *Manufacturing processes for advanced composites*, 2003. Oxford, UK: Elsevier.
6. Madsen B, Thygesen, A, Liholt, H. Plant fibre composites - Porosity and stiffness. *Composites Science and Technology*, 2009, 69: p. 1057-1069.
7. Truong M, Zhong W, Boyko S, Alcock M. A comparative study on natural fibre density measurement. *The Journal of The Textile Institute*, 2009, 100(6): p. 525-529.
8. Fink H, Bohn A, Pinnow M, Kunze J. Determination of the fiber fraction of cellulose-polypropylene composites, in *5th Global Wood and Natural Fibre Composites Symposium*. 2004. Kassel, Germany.
9. Mahrholz T, Riedel U. Determination of the fibre volume content in natural fibre-reinforced composites by ultimate analysis. *Journal of Materials Science*, 2009, 44: p. 4379–4382.
10. Cabral H, Cisneros M, Kenny JM, Vazquez A, Bernal CR. Structure-properties relationship of short jute fiber-reinforced polypropylene composites. *Journal of Composite Materials*, 2005, 39: p. 51-65.
11. Ghosh R, Reena G, Krishna AR, Raju BHL. Effect of fibre volume fraction on the tensile strength of Banana fibre reinforced vinyl ester resin composites. *International Journal of Advanced Engineering Sciences and Technologies*, 2011, 4(1): p. 89-91.
12. Zarate C, Aranguren MI, Reboredo MM. Influence of fiber volume fraction and aspect ratio in resol-sisal composites. *Journal of Applied Polymer Science*, 2003, 89: p. 2714-2722.
13. Peijs T, Garkhail S, Heijenrath R, van den Oever M, Bos H. Thermoplastic composites based on flax fibers and polypropylene: Influence of fibre length and fibre volume fraction on mechanical properties. *Macromolecular Symposia*, 1998, 127: p. 193-203.
14. Qin C, Soykeabkaew N, Xiuyuan N, Peijs T. The effect of fibre volume fraction and mercerization on the properties of all-cellulose composites. *Carbohydrate Polymers*, 2008, 71: p. 458-467.
15. Bos H. *The potential of flax fibres as reinforcement for composite materials*. PhD, 2004. Technische Universiteit Eindhoven: Eindhoven, Netherlands.

16. Lee B, Kim HJ, Yu WR. Fabrication of long and discontinuous natural fiber reinforced polypropylene biocomposites and their mechanical properties. *Fibers and Polymers*, 2009, 10(1): p. 83-90.
17. Roe P, Ansell MP. Jute-reinforced polyester composites. *Journal of Materials Science*, 1985, 20: p. 4015-4020.
18. Baets J, Plastria D, Ivens J, Verpoest I. Determination of the optimal flax fibre preparation for use in UD-epoxy composites, in *4th International Conference on Sustainable Materials, Polymers and Composites*. 6-7 July 2011. Birmingham, UK.
19. Charlet K, Jernot JP, Gomina M, Bizet L, Bréard J. Mechanical properties of flax fibers and of the derived unidirectional composites. *Journal of Composite Materials*, 2010, 44(24): p. 2887-2896.
20. Oksman K. High quality flax fibre composites manufactured by the resin transfer moulding process. *Journal of Reinforced Plastics and Composites*, 2001, 20(7): p. 621-627.
21. Madsen B, Hoffmeyer P, Lilholt H. Hemp yarn reinforced composites – II. Tensile properties. *Composites Part A: Applied Science and Manufacturing*, 2007, 38: p. 2204-2215.
22. Zhang L, Miao M. Commingled natural fibre/polypropylene wrap spun yarns for structured thermoplastic composites. *Composites Science and Technology*, 2010, 70: p. 130-135.
23. Madsen B, Thygesen A, Lilholt H. Plant fibre composites - Porosity and volumetric interaction. *Composites Science and Technology*, 2007, 67: p. 1584-1600.
24. Gassan J, Bledzki AK. Possibilities for improving the mechanical properties of jute/epoxy composites by alkali treatment of fibres. *Composites Science and Technology*, 1999, 59: p. 1303-1309.
25. Madsen B. *Properties of plant fibre yarn polymer composites - An experimental study*. PhD, 2004. Technical University of Denmark: Lyngby, Denmark.
26. Sawpan M, Pickering KL, Fernyhough A. Analysis of mechanical properties of hemp fibre reinforced unsaturated polyester composites. *Journal of Composite Materials*, 2012, (In Press). doi:10.1177/0021998312449028.
27. Hearle J, Grosberg P, Backer S. Structural mechanics of yarns and fabrics. Vol. 1 p. 180, 1969. New York: Wiley-Interscience.
28. Carus M. Bio-composites: Technologies, applications and markets, in *4th International Conference on Sustainable Materials, Polymers and Composites*. 6-7 July 2011. Birmingham, UK.
29. Bledzki A, Faruk O, Sperber VE. Cars from bio-fibres. *Macromolecular Materials and Engineering*, 2006, 291: p. 449-457.
30. Virk A, Hall W, Summerscales J. Modulus and strength prediction for natural fibre composites. *Materials Science and Technology*, 2012, 28(7): p. 864-871.
31. Summerscales J, Virk AS, Hall W. A review of bast fibres and their composites. Part 3 – Modelling. *Composites Part A: Applied Science and Manufacturing*, 2013, 44: p. 32–139.
32. Williams G, Wool RP. Composites from natural fibers and soy oil resins. *Applied Composite Materials*, 2000, 7: p. 421-432.
33. Devi L, Bhagawan SS, Thomas S. Mechanical properties of pineapple leaf fiber-reinforced polyester composites. *Journal of Applied Polymer Science*, 1997, 64(9): p. 1739-1748.
34. Pan N. Theoretical determination of the optimal fiber volume fraction and fibre-matrix property compatibility of short fiber composites. *Polymer Composites*, 1993, 14(2): p. 85-93.

35. Cox H. The elasticity and strength of paper and other fibrous materials. *British Journal of Applied Physics*, 1952, 3: p. 72-79.
36. Xue D, Miao M, Hu H. Permeability anisotropy of flax nonwoven mats in vacuum assisted resin transfer molding. *Journal of the Textile Institute*, 2011, 102(7): p. 612-620.
37. Goutianos S, Peijs T. The optimisation of flax fibre yarns for the development of high-performance natural fibre composites. *Advanced Composites Letters*, 2003, 12(6): p. 237-241.
38. Goutianos S, Peijs T, Nystrom B, Skrifvars M. Development of flax fibre based textile reinforcements for composite applications. *Applied Composite Materials*, 2006, 13(4): p. 199-215.
39. Petrulis D. Peculiarities of packing fraction of open-packed yarn model. *Materials Science*, 2003, 9: p. 116-119.
40. Petrulis D, Petrulyte S. Properties of close packing of filaments in yarn. *Fibres and Textiles in Eastern Europe*, 2003, 11(1): p. 16-20.
41. Pan N. Development of a constitutive theory for short fiber yarns: Mechanics of staple yarn without slippage effect. *Textile Research Journal*, 1992, 62(12): p. 749-765.
42. Yilmaz D, Göktepe F, Göktepe O, Kremenakova D. Packing density of compact yarns. *Textile Research Journal*, 2007, 77(9): p. 661-667.
43. Madsen B, Lilholt H. Physical and mechanical properties of unidirectional plant fibre composites - an evaluation of the influence of porosity. *Composites Science and Technology*, 2003, 63: p. 1265-1272.
44. Pavithran C, Mukherjee PS, Brahmakumar M, Damodaran AD. Impact properties of natural fibre composites. *Journal of Materials Science Letters*, 1987, 6: p. 882-884.
45. Lewin M. *Handbook of fiber chemistry*. Third ed, 2007. Boca Raton: CRC Press LLC.
46. Pickering K, ed. *Properties and performance of natural-fibre composites*. 2008. CRC Press LLC: Boca Raton.
47. Weyenberg I, Chitruong T, Vangrimde B, Verpoest I. Improving the properties of UD flax fibre reinforced composites by applying an alkaline fibre treatment. *Composites Part A: Applied Science and Manufacturing*, 2006, 37: p. 1368-1376.

# 5 EFFECT OF ORIENTATION ON THE TENSILE PROPERTIES OF PLANT YARN REINFORCED COMPOSITES*

## 5.1 INTRODUCTION

Fibre reinforced plastics (FRPs) typically exhibit anisotropy. That is, some material properties are a function of the geometric axis/plane along which the properties are measured. The anisotropy of FRPs is a direct result of the dependency of composite mechanical properties on the orientation of the fibre reinforcement.

Current applications of plant fibre composites (PFRPs) are primarily based on compression moulded and injection moulded non-structural components for the automotive industry and consumer goods market [1]. The reinforcement is typically in the form of non-woven mats (for compression moulding) or granules/pellets (for injection moulding) [1, 2]. Employing discontinuous fibres in both cases, fibre orientation is 2D-random in the former and 3D-random in the latter. Due to the random orientation of the reinforcement, the resulting PFRP may have quasi-isotropic (for 2D-random) or even isotropic (for 3D-random) properties. However, the random fibre orientation implies that the reinforcement efficiency is severely compromised. According to Krenchel's reinforcement orientation efficiency factor [3], employing randomly oriented fibres in 2D or 3D reduces the reinforcing effect of the fibre (in terms of providing strength and stiffness) to 37.5% and 20.0% of its potential, respectively. For load-bearing applications, the use of reinforcements in the form of continuous aligned fibres is essential as they preserve high efficiency factors

* This chapter is based on the peer-reviewed journal articles:

Shah DU, Schubel PJ, Clifford MJ. Modelling the effect of yarn twist on the tensile strength of unidirectional plant fibre yarn composites. *Journal of Composite Materials*, 2012, 47(4): p. 425-436.

Shah DU, Schubel PJ, Clifford MJ, Licence P. The tensile behavior of off-axis loaded plant fiber composites: an insight on the non-linear stress-strain response. *Polymer Composites*, 2012, 33(9): p. 1494-1504.

(of length and orientation), thus allowing the entire properties of the fibre to be exploited. This was highlighted through the literature survey in *Chapter 2*.

Table 5.1 presents typically reported tensile properties of PFRPs and the unreinforced matrix. In particular, it highlights the difference in magnitude of the tensile properties for PFRPs reinforced with fibres in 3D-random, 2D-random and uniaxial orientation. The results reveal that PFRPs with random fibre orientation posses poor tensile properties with stiffness below 8 GPa and ultimate stress below 70 MPa. In fact, the tensile strength of the PFRPs is of similar order to that of the matrix. If the fibres are aligned, the (longitudinal) tensile properties are considerably improved. In addition, as highlighted in *Chapter 4*, aligned PFRPs have a lower minimum and critical fibre volume fraction and a higher maximum fibre volume fraction, than random fibre PFRPs [4, 5].

**Table 5.1. Typically reported tensile properties of PFRPs with different fibre orientations.**

| *Composite* | *Fibre content [%]* | *Fibre orientation* | *Testing direction* | *Tensile modulus [GPa]* | *Tensile strength [MPa]* | *Source* |
|---|---|---|---|---|---|---|
| Epoxy | - | - | - | 3.2 | 75 | |
| Flax/epoxy | 22 v | 2D-Random | - | 7.9 | 53 | [6] |
| Flax/epoxy | 48 v | Unidirectional | Longitudinal | 32.0 | 268 | [7] |
| Flax/epoxy | 48 v | Unidirectional | Transverse | 4.0 | 18 | [7] |
| PP | - | - | - | 1.7 | 28 | [8] |
| Hemp/PP | 30 wt | 3D-random | - | 1.5 | 30 | [9] |
| Hemp/PP | 40 wt | 2D-Random | - | 3.5 | 40 | [10] |
| Hemp/PET | 30 v | Unidirectional | Longitudinal | 17.6 | 205 | [8] |
| Hemp/PET | 30 v | Unidirectional | Transverse | 3.5 | 19 | [8] |

It should be noted that the transverse tensile properties of unidirectional PFRPs are low due to the anisotropy of the fibre and composite. However, this is often an advantage in structural applications, where the composite anisotropy can be deliberately aligned along a particular direction that is known to be the principally loaded axis/plane. For instance, uniaxial reinforcements are employed along the spar

of a wind turbine blade to resist axial/centrifugal loads. If necessary, multiple plies aligned in different directions (*i.e.* multi-axial reinforcements) can be used to resist off-axis and shear loads. In fact, some plies, in the form of biax [±45°] and triax [0,±45°], are employed in the blade spar and skin/shell, aligned off-axis to the leading edge, to resist shear loads related to torsion.

### 5.1.1 Misorientation in aligned PFRPs

Previously, the effect of orientation (in terms of random and aligned fibre orientation) on PFRP mechanical properties was discussed. However, in aligned PFRPs, (mis)orientation manifests itself in various other forms, at every length scale (Fig. 5.1): *a)* microfibril angle in a single plant fibre, *b)* twist angle in a processed staple fibre yarn, and *c)* off-axis loading angle in a composite laminate. Importantly, these misorientations play a major role in determining the mechanical properties of plant fibres and their composites.

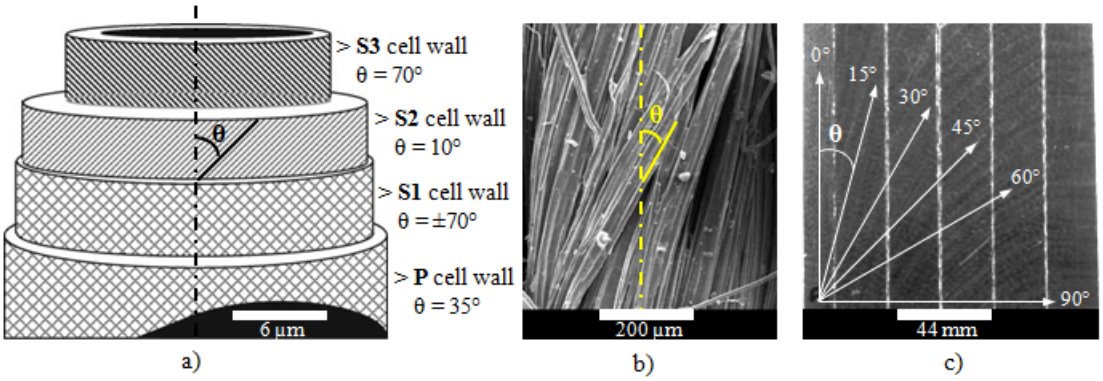


**Fig. 5.1. The forms of misorientation: *a)* in the primary (P) and secondary (S) cell walls of a single flax fibre, cellulose microfibrils are oriented at an angle to the fibre axis [11]; *b)* in a staple fibre flax yarn, twisted fibres are located helically around the yarn axis; *c)* in a composite laminate, plies may be off-axis to the loading direction.**

In this chapter, the effect of (mis)orientation on the mechanical behaviour of aligned PFRPs is investigated. In particular, this chapter aims to *i)* review the effect of the microfibril angle on the tensile properties of plant fibres, *ii)* model the effect of reinforcing yarn twist on PFRP tensile properties, and *iii)* evaluate the effect of off-axis loads on PFRP tensile properties. This will *i)* provide an improved

understanding on the mechanical behaviour and response of PFRPs, *ii)* enable the design and optimisation of PFRPs, and *iii)* enable the development of models to predict the mechanical properties of PFRPs. All of these are key to the employment of PFRPs for load-bearing applications.

## 5.2 THE MICROFIBRIL ANGLE IN PLANT FIBRES

Plant fibres themselves are composites containing cellulose microfibrils which are embedded in a lignin-hemicellulose matrix. Cellulose, the primary constituent of plant fibres, is highly anisotropic in crystalline form. In bast fibres like flax and hemp, cellulose crystallinity can be as high as 70% [12]. While extensive hydrogen bonding leads to a crystalline structure with a theoretical stiffness of 138-250 GPa in the chain direction, the molecular linearity of crystalline cellulose results in a transverse stiffness of only 15-30 GPa [13-19]. Furthermore, the cellulose microfibrils are helically wound around layers of cell walls (Fig. 5.1a) and hence they are not perfectly aligned but are at an angle to the fibre axis. Different layers of cell walls have a different microfibril angle [12, 19]. As the S2 cell wall accounts for more than 80% of the total cell wall thickness [12, 17], it is the microfibril angle (MFA) of the S2 cell wall that is of interest.

The role and effect of MFA on plant fibre tensile properties and stress-strain behaviour has been studied thoroughly by several researchers (for instance, [20] and references therein). The conclusions suggest that alongside the cellulose content of plant fibres, the MFA has a direct contribution to the mechanical properties of plant fibres [19, 21-27]. As Fig. 5.2 depicts, while plant fibre tensile modulus and strength are higher for lower MFA, the failure strain is smaller for lower MFA. In addition, the MFA also dictates the non-linear stress-strain behaviour of plant fibres [21, 23, 26, 28]; while the elastic range is smaller for higher MFA, the plastic range increases with increasing MFA (Fig. 5.2). Suslov *et al.* [29] report that even the mechanical anisotropy of plant seed fibres is dependent on the microfibril orientation.

In fact, the MFA of the S2 cell wall has such a dominating effect on plant fibre tensile properties that it can be used as a parameter to classify plant fibres into different categories. For instance, bast fibres are obtained from the inner bark of

dicotyledonous plants and provide structural strength, stiffness and rigidity to the plant stem. Hence bast fibres, such as flax, hemp and jute, have small MFA (<10°) [13, 30]. Leaf fibres are obtained from the leaves of monocotyledonous plants and provide them with the toughness and ductility required to withstand repetitive flexing motion in windy conditions. Hence leaf fibres, such as sisal, pineapple and banana, have moderate MFA (10–25°) [13, 30]. In seed fibres, like coir, cotton and oil palm, the cellulose microfibrils do not have any structural role and thus seed fibres have a high MFA (>25°) [13, 30]. Although orientation in plant fibres (MFA) cannot be actively controlled [31], it can be used as an indicator for potential applications of PFRPs made from a particular plant fibre.

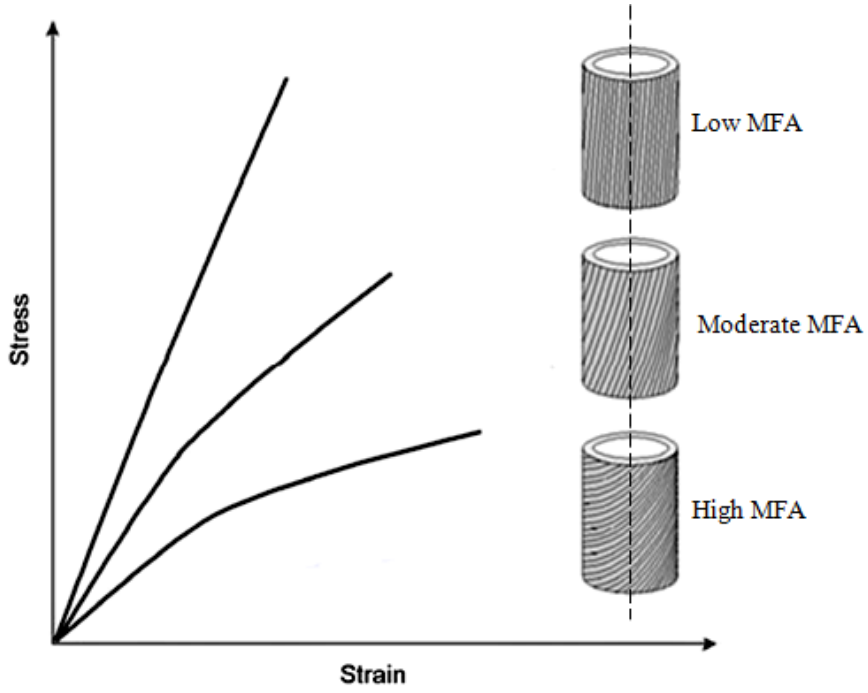


**Fig. 5.2. Schematic tensile stress-strain curves of plant fibres showing the influence of MFA. A higher MFA leads to *i)* reduced elastic range, *ii)* reduced elastic modulus, *iii)* reduced tensile strength, *iv)* increased failure strain and *v)* increased non-linear elastic stress-strain response. Adapted from [26].**

## 5.3 EFFECT OF YARN TWIST ON PFRP TENSILE STRENGTH

### 5.3.1 Twisted yarns as reinforcements

The true structural potential of plant fibres as reinforcing agents can only be realized when the highest reinforcement efficiency is employed. Hence, aligned unidirectional PFRPs are of interest. The manufacture of aligned PFRPs requires the reinforcement to be continuous. Due to the discontinuous length of technical plant fibres, staple fibre yarns – the most readily available 'continuous' plant fibre semi-products – need to be employed. Plant fibre yarns, whose primary application is found in textiles, are conventionally produced through ring-spinning. The spinning process gives the yarn a twisted structure, where twist is the primary binding mechanism. Twist induces inter-fibre friction and thus imparts processability to the yarn. The addition of twist in yarns affects the stress transfer between fibres within the yarn and thus influences both *i)* the strength of the yarn and the *ii)* fracture mechanism of the yarn (Fig. 5.3). In the textile industry, twist is defined by *i)* twist direction (S or Z), *ii)* twist level, $T$ (tpm) and *iii)* twist multiplier, $TM$ ($= T\sqrt{tex}$).

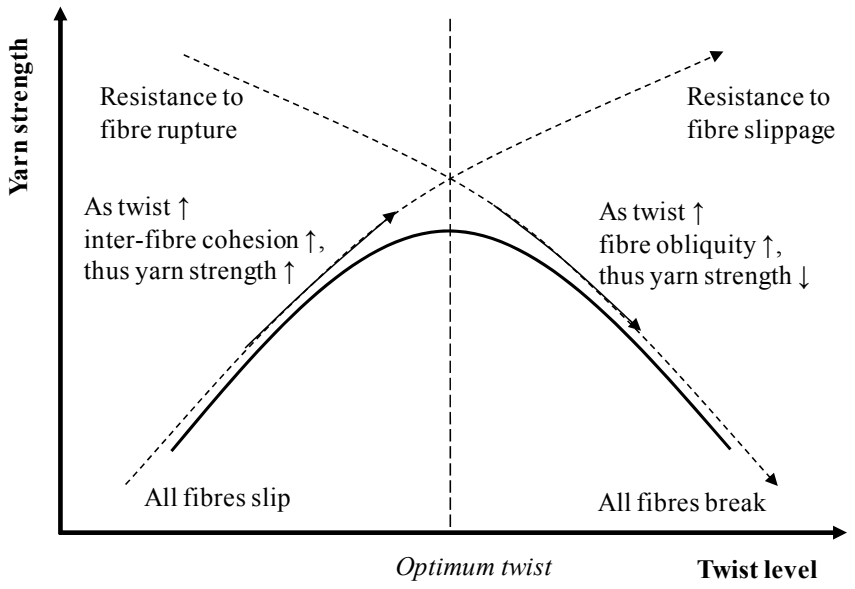


**Fig. 5.3. The effect of twist on yarn tensile strength and failure mechanism. Up to a point, increasing twist level improves inter-fibre friction leading to an increase in yarn strength, after which fibre obliquity effects are significant leading to a drop in yarn strength.**

Although twist is essential in the production of processable staple yarns and thus aligned PFRPs, there are significant detrimental effects on PFRP performance that need to be considered. Firstly, spinning plant fibres to form yarns is a costly and energy intensive process [32]. The price of flax yarns (and rovings) can be as much as 15 €/kg; this is over 10 times higher than the price of short technical flax fibres which cost between 0.5-1.5 €/kg [5, 30]. Finn *et al.* showed that the twist level *T* is inversely proportional to the production rate of a yarn and thus directly proportional to the cost of yarn spinning [33]. Hence, plant fibres would no longer be a low-cost substitute to E-glass. Secondly, when twisted yarns are used to produce woven textile reinforcements they cause 'crimp' which has a detrimental effect on composite properties due to yarn misalignments and resulting stress concentrations [34]. Thirdly, twist tightens the yarn structure which reduces yarn permeability and hinders yarn impregnation [35]. The hindered impregnation has shown to result in impregnation-related voids in PFRPs produced from twisted yarns (*Chapters 3 and 4*). Furthermore, the twisted nature of such textile plant fibre yarns leads to loss in reinforcement orientation efficiency despite laying the yarns as a unidirectional mat. Goutianos *et al.* [36] observed that the tensile strength of epoxy-impregnated twisted flax yarns (the simplest unidirectional PFRP) decreased with twist, similar to an off-axis loaded laminate; high-twist (~200 tpm) impregnated yarns show a drop in tensile strength by up to 70% when compared to low-twist (~50 tpm) impregnated yarns.

There have been efforts to achieve full utilisation of the fibre properties in the final composite by reducing or replacing twist in yarns. Goutianos *et al.* [36] attempted to employ flax yarns with the minimal level of twist (~50 tpm) allowed by yarn processing requirements to produce aligned composites. Some European textile spinning companies are slowly coming to pace with the use of plant fibres for composites and are now producing rovings with insignificant twist levels (20 tpm), although not reduced prices. The author of this thesis has used such rovings (in the form of F20 in *Chapter 3*) for aligned thermoset composites and observed that the back-calculated flax fibre tensile modulus and specific tensile strength were comparable to that of E-glass. Baets *et al.* [37] have looked at the tensile properties of composites produced from flax fibres from different steps in the fibre extraction

and yarn preparation process. They observe that each stage increases the level of twist in the reinforcing fibres and although the dry bundle strength increases, composite properties are highest for minimally-processed hackled flax slivers with no twist. Zhang *et al.* [38] investigated the use of wrap-spinning to produce twist-less reinforcing fibres (wrapped by polypropylene, for instance) for reinforcement purposes. Although they observe a 7-30% higher flexural modulus for wrap-spun flax/PP composites, the flexural strength of wrap-spun flax/PP composites is similar to that of twisted yarn flax/PP composites.

### 5.3.2 Modelling the effect of twist on composite mechanical properties

As ring-spinning is the traditional method of producing yarns, twisted plant fibre yarns will remain the readily available form of textile reinforcements for PFRPs. Hence, modelling the effect of yarn twist on composite mechanical properties is essential for: *i)* appreciating the reduction in properties when twisted yarn reinforcements are used, and *ii)* estimating the potential composite properties if untwisted reinforcements were used.

There are no existing models to accurately predict the effect of yarn twist on composite tensile strength. Although there has been a recent interest in this topic by Ma *et al.* [39], their study considered only three different twist levels (0, 20 and 50 tpm). Twisted ring-spun yarns have a typical twist level of 150-200 tpm. In addition, the model Ma *et al.* [39] developed, doesn't consider structure-property relationships in a twisted staple fibre yarn and its effect on composite tensile strength.

However, some work (for instance, [40-42]) has been done on modelling the effect of yarn twist on the elastic properties (specifically, tensile modulus $E$) of high-performance and high-modulus synthetic impregnated filament yarns. The models of Rao *et al.* [40] and Naik *et al.* [41] to estimate impregnated yarn tensile modulus are comprehensive and take into account the effect of anisotropy, fibre migration, and micro-buckling. However, these models are complex, sophisticated and require the input of several material constants (including $E_x$, $E_y = E_z$, $G_{xy} = G_{xz}$, $G_{yz}$, $\nu_{xy} = \nu_{xz}$ and $\nu_{yz}$) which is cumbersome.

Baets *et al.* [37, 43] conducted a study to observe the evolution of the tensile modulus of unidirectional flax/epoxy composites with changing yarn twist levels. Interestingly, they found good agreement between their experimental data and the predictive models by Rao *et al.* [40] and Naik *et al.* [41]. In another study, Rask *et al.* [44] found no correlation between yarn twist level and uniaxial PFRP tensile modulus. However, it should be noted that Rask *et al.* [44] were employing wrap-spun yarn, as opposed to ring-spun yarn.

There has been no direct study on the effect of yarn twist on composite tensile strength, let alone PFRP tensile strength. This study looks at providing a simple, yet accurate model for the effect of yarn twist on unidirectional tensile strength of PFRPs. The model is validated by extensive experimental data from Goutianos *et al.* [36] showing a near-perfect $R^2$-value (from non-linear regression) of 0.950. Data from Baets *et al.* [37, 43] is also used to further verify the developed model.

### 5.3.3 Structure of a twisted staple yarn

To develop an effective model of unidirectional composite tensile strength of PFRPs reinforced with staple yarns, the structure of a staple yarn needs to be defined.

The effect of twist angle of a continuous filament yarn on the dry yarn tensile modulus was investigated as early as 1907 by Gegauff [45] and then by Platt [46]. The simplest, and widely accepted, structure of a filament yarn was proposed as the ideal coaxial model. Staple fibre yarns are structurally more complex than filament yarns. Filament yarns are more uniform in terms of *i)* fibre distribution (packing fraction ∅), *ii)* fibre configuration within the yarn (small fibre migration) and *iii)* yarn mechanical properties (as the single filaments have uniform properties). In staple yarns, the packing fraction is a function of yarn radius (the centre being more densely packed) and fibre migration is more important due to the short length of the individual fibres. Furthermore, plant fibres have variable physical and mechanical properties, which translate into the staple fibre yarn as well; that is, the fibres do not break at the same time in a staple yarn.

The yarn in this study is assumed to be the so-called idealized staple fibre yarn (as defined by Hearle et al. [47]). In such a yarn, whose cross-section is circular with

radius r (Fig. 5.4), the twist angle $\theta_x$ of an arbitrary fibre at a radial position $x$ ($0 \leq x \leq r$) is given by

$$\tan\theta_x = \frac{2\pi x}{L} \qquad \text{Eq. 5.1}$$

The twist angle at the yarn surface $\alpha$ (at radius $r$, $\alpha = \theta_r$) can be defined in terms of the twist level $T$ (= $1/L$), as in Eq. 5.2, where $L$ is the length of the yarn for one turn.

$$\tan\alpha = \frac{2\pi r}{L} = 2\pi r T \qquad \text{Eq. 5.2}$$

The yarn packing fraction $\emptyset$ is the ratio of the true fibre cross-sectional area $A_f$ to the yarn cross-sectional area $A_y$ and can be written as

$$\phi = \frac{A_f}{A_y} = \frac{\bar{\rho}}{\pi\rho r^2} \qquad \text{Eq. 5.3}$$

where, $\rho$ is the fibre density and $\bar{\rho}$ is the yarn mass per unit length (= $10^{-6}\times tex$).

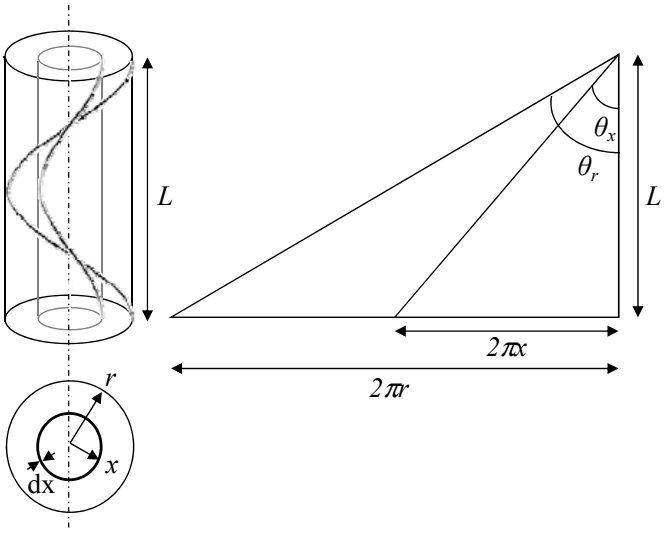


**Fig. 5.4. Idealized structure of a twisted staple fibre yarn.**

As PFRP misalignment or orientation efficiency would be a function of fibre orientation, Eq. 5.2 and Eq. 5.3 are rearranged to calculate the surface twist angle $\alpha$ for known values of twist level $T$, yarn linear density $tex$, fibre density $\rho$ and packing fraction $\emptyset$.

$$\alpha = \tan^{-1}\left(10^{-3} \cdot T\sqrt{4\pi \cdot \frac{tex}{\rho\phi}}\right) \qquad \text{Eq. 5.4}$$

In the above yarn structure model, we adopt all the assumptions made by Hearle *et al.* [47] (*listed in Appendix C*) except that the yarn packing fraction ∅ is no longer neglected (or assumed to be unity), but is allowed to change along with the yarn twist level. Pan [48] derived a semi-empirical equation to describe the relationship between packing fraction ∅ and twist level *T* for staple fibre yarns (Eq. 4.5). In Eq. 4.5, $\emptyset_{max}$ is the maximum packing fraction of the yarn, and A and B are constants.

$$\phi = \phi_{\max}\left(1 - Ae^{-BT}\right) \qquad \text{Eq. 4.5}$$

In *Chapter 4*, it was shown the packing fraction ∅ of staple fibre yarns used for PFRPs is well described by Eq. 4.5 with the factors $\emptyset_{max}$, *A* and *B* of 0.6, 0.78 and 0.0195, respectively. The result of Eq. 4.5 is shown in Fig. 5.5. Fig. 5.5 also presents the effect of packing fraction on the curve of surface twist angle against twist level. It is observed that a constant yarn packing fraction of ∅ = 0.6 approximates Eq. 5.4 well. This is useful as ring-spun yarns typically have a packing fraction of 0.5-0.6 [49].

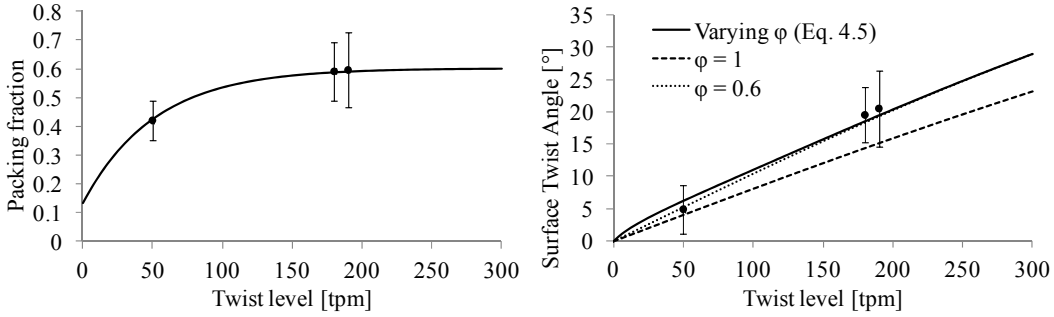


**Fig. 5.5. The effect of twist level on packing fraction and yarn surface twist angle. Experimental data (from *Chapter 3 and Appendix A*) (•) shows good agreement with yarn structure model.**

The effect of yarn linear density on the curves of *i)* packing fraction versus surface twist angle and *ii)* surface twist angle versus twist level have been presented in Fig. 5.6. A fibre density of 1550 $kgm^{-3}$ is assumed. It is observed that a heavier yarn

(higher tex) has a higher surface twist angle and lower packing fraction due to a larger yarn diameter.

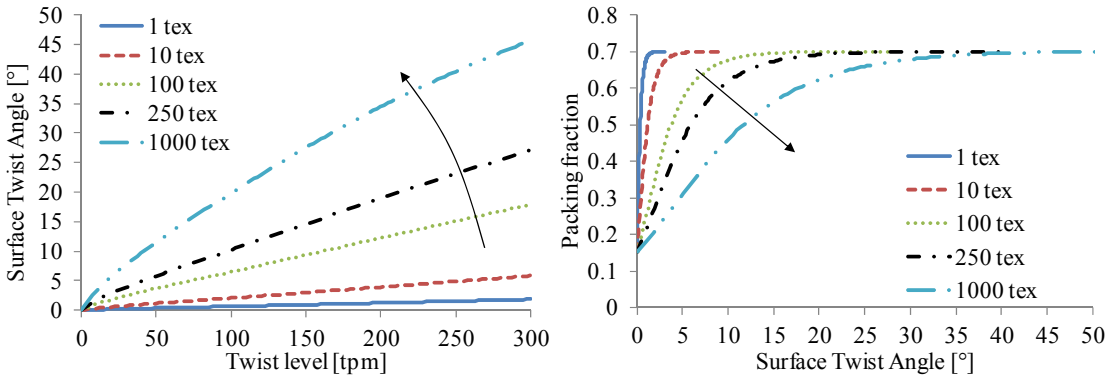


**Fig. 5.6. The effect of increase yarn linear density (tex) on yarn structure.**

Although the packing fraction is allowed to vary with twist level, the packing fraction within a yarn is assumed to be uniform for a given twist level. This structure of the idealized yarn model also assumes no fibre migration and no micro-buckling.

### 5.3.4 Experimental data

To validate the predictive models, experimental data from Goutianos *et al.* [36] has been used. To investigate the effect of twist on tensile strength of aligned composites, they used two different flax yarns: *i)* yarns made from long flax fibres (609 tex) and *ii)* yarns made from short flax fibres (1000 tex). The yarns were first impregnated in epoxy resin and then manually twisted to seven different twist levels (ranging from about 50 tpm to 250 tpm). Twisting of yarn after impregnation ensured that the effect of decreasing permeability with increasing twist was excluded, thus allowing a true study of the effect of twist alone. To examine the tensile strength of the impregnated yarns, they were tested in tension at a cross-head speed of 2 mm/min. They calculated the tensile strength using the yarn cross-sectional area.

As modelling the tensile strength of a twisted yarn composite is more convenient and geometrically sensible when twist is presented in terms of surface twist angle $\alpha$ rather than twist level $T$, the data from Goutianos *et al.* [36] has been translated in terms of surface twist angle (Fig. 5.7). To convert the twist level $T$ to the surface twist angle

$\alpha$, Eq. 5.4 is used where the flax fibre density is taken to be 1550 kgm$^{-3}$, the yarn linear density is taken to be 609 tex for long and 1000 tex for short flax fibre yarns, and the packing fraction ∅ is calculated for different twist levels using Eq. 4.5. The results are graphically presented in Fig. 5.7. It is observed that short flax fibre yarns have a higher surface twist angle than long flax fibre yarns, despite having a lower twist level (tpm). This is because they are heavier (higher tex) and thus have a larger yarn diameter.

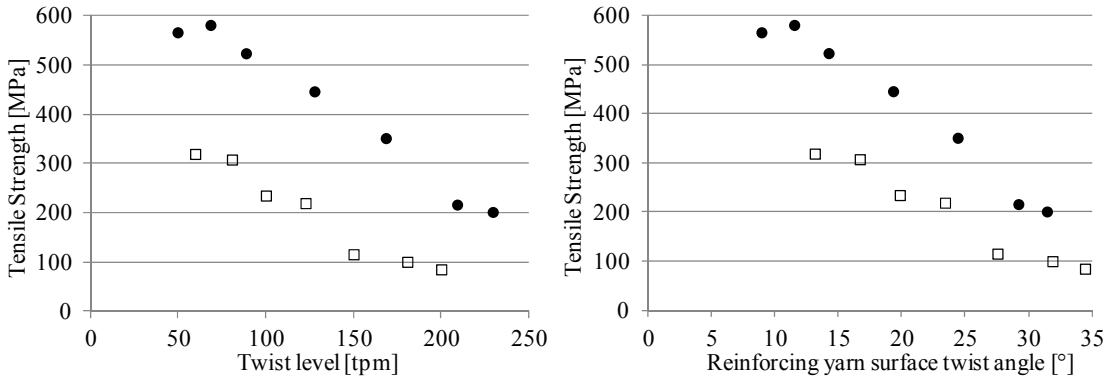


**Fig. 5.7. Tensile strength of (•) long and (□) short flax fibre epoxy impregnated yarns as a function of twist level (left) [36] and surface twist angle (right).**

## 5.3.5 Mathematical models

### 5.3.5.1 Tsai-Hill composite laminate model

An impregnated yarn is fundamentally a composite material. In fact, it seems that a twisted impregnated plant fibre staple yarn is similar to an off-axis unidirectional laminate not only in geometry (as revealed in Fig. 5.8) but also in the way the tensile strength of the impregnated yarn drops with increasing twist (Fig. 5.7).

Hence, the simplest model would be based on an off-axis laminate. The uniaxial failure stress of an off-axis composite $\sigma_\theta$ can be estimated by the empirical Tsai-Hill failure criterion [50], which is defined by equation Eq. 5.5.

$$\sigma_\theta = \left[ \frac{1}{{\sigma_0}^2} \cos^4\theta + \left( \frac{1}{\tau^2} - \frac{1}{{\sigma_0}^2} \right) \cos^2\theta \sin^2\theta + \frac{1}{{\sigma_{90}}^2} \sin^4\theta \right]^{-0.5} \qquad \text{Eq. 5.5}$$

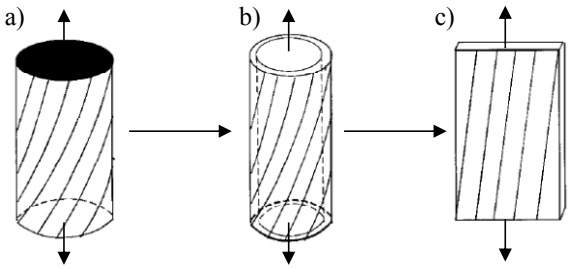


**Fig. 5.8. An impregnated yarn is similar to an off-axis composite. *a)* twisted impregnated yarn with surface twist angle α, *b)* a layer of a twisted impregnated yarn, *c)* the open-up structure of the layer is a laminate with off-axis loading angle *θ*.**

The Tsai-Hill criterion is suitable for idealised twisted staple fibre yarns and their unidirectional composites as they can be considered as transversely isotropic structures under plane stress conditions [40, 48]. From tests on the effect of loading angle on the uniaxial tensile strength of unidirectional flax/polyester composites ($v_f$ = 27%) (*Chapter 3 and Chapter 5.6*), it has been found that the longitudinal tensile strength $\sigma_0$ is 7 times higher than the inter-laminar shear strength $\tau$ and 11 times higher than the transverse tensile strength $\sigma_{90}$ so that

$$\frac{\sigma_0}{\tau} = 7;\ \frac{\sigma_0}{\sigma_{90}} = 11 \qquad \text{Eq. 5.6}$$

Using Eq. 5.6 and trigonometric identities (specifically, $\cos^4\theta + 2\sin^2\theta\cos^2\theta + \sin^4\theta = 1$ and $\cos^2\theta = 1 - \sin^2\theta$) the Tsai-Hill criterion in Eq. 5.5 can be generalized as given in Eq. 5.7 to predict the composite tensile strength as a function of misorientation $\theta$.

$$\sigma_\theta = \sigma_0\left[1 + 46\sin^2\theta + 74\sin^4\theta\right]^{-0.5} \qquad \text{Eq. 5.7}$$

As the idealised yarn structure depicts (Section 5.3.3), the twist angle $\theta_x$ is a function of the yarn radius. The twist angle increases from 0 at the yarn centre to a maximum of $\alpha$ at the yarn surface. To incorporate the structure of the staple fibre yarn into the Tsai-Hill model, it is possible to define a mean twist angle $\theta_{mean}$ which can be then substituted into Eq. 5.7. Madsen *et al.* [51] have derived an expression for this mean twist angle $\theta_{mean}$ by integrating the proportional contribution of $\theta_x$ over $0 \le x \le r$ (Eq.

5.8). They find that $\theta_{mean}$ is conveniently a function of the surface twist angle $\alpha$ (Eq. 5.9).

$$\theta_{mean} = \int_0^r \frac{2\pi x}{\pi r^2} \tan^{-1}\left(\frac{2\pi x}{L}\right) dx \qquad \text{Eq. 5.8}$$

$$\theta_{mean} = \alpha + \frac{\alpha}{\tan^2 \alpha} - \frac{1}{\tan \alpha} \qquad \text{Eq. 5.9}$$

The Tsai-Hill criterion in Eq. 5.7 can be re-written for $\theta_{mean}$ (Eq. 5.10).

$$\sigma_{\theta=\theta_{mean}} = \sigma_0 \left[1 + 46 \sin^2 \theta_{mean} + 74 \sin^4 \theta_{mean}\right]^{-0.5} \qquad \text{Eq. 5.10}$$

Eq. 5.10 can be then used to apply the Tsai-Hill model onto the experimental data. This is presented graphically in Fig. 5.9 and Fig. 5.10. The best fit is given for a $\sigma_0$ of 670 MPa for long flax fibre impregnated yarns and 400 MPa for short flax fibre impregnated yarns. It is expected that the longitudinal tensile strength $\sigma_0$ will be smaller for short fibre composites.

An $R^2$-value (non-linear regression) of 0.893 for long flax fibre impregnated yarns and 0.913 for short flax fibre impregnated yarns is observed. The high $R^2$-values suggest that the Tsai-Hill model (accounting for yarn structure and geometry) is a reasonable fit to the experimental data. However, it can be graphically seen (Fig. 5.9 and Fig. 5.10) that the model does not accurately depict the variation of composite tensile strength with increasing yarn twist angle. None of the experimental data-points lie on the curve. The Tsai-Hill model under-estimates the tensile strength of impregnated yarns for $\alpha < 27°$ (or $\theta_{mean} < 18.5°$) and over-predicts the tensile strength for $\alpha > 27°$ (or $\theta_{mean} > 18.5°$).

Although the Tsai-Hill criterion in Eq. 5.10 accounts for the yarn structure, it does not model the experimental data accurately possibly because incorrect stress ratios, $\sigma_0/\sigma_{90}$ and $\sigma_0/\tau$, may have been used. As the experimental data is based on impregnated yarns rather than true aligned composite laminates, the stress ratios that should be used should be based on the former rather than the latter. The Tsai-Hill criterion in Eq. 5.11 uses stress ratios that best fit the experimental data, giving an $R^2$-value > 0.940. The stress ratios that have been used in Eq. 5.11 are $\sigma_0/\tau = 3.6$ and

$\sigma_0/\sigma_{90}$ = 22.6. The physical implication of the best-fit stress ratios used in Eq. 5.11 is that best-fit interlaminar shear strength and best-fit transverse strength are double and half the values that were used in Eq. 5.6 and Eq. 5.10 (based on testing of aligned PFRP laminates). While the difference in stress ratios between impregnated yarns and composite laminates of plant fibres is large, it is not the case for synthetic fibre impregnated yarns and composite laminates. While $\sigma_0/\tau$ and $\sigma_0/\sigma_{90}$ for epoxy impregnated T300/5208 carbon yarn ($v_f$ = 0.7) is 16.2 and 33.2, respectively, $\sigma_0/\tau$ and $\sigma_0/\sigma_{90}$ for a unidirectional T300/5208 carbon/epoxy composite laminate ($v_f$ = 0.7) is 22.1 and 37.5, respectively [52]. In fact, it is surprising that while the estimated best-fit interlaminar shear strength of the flax/epoxy impregnated yarn ranges between $\tau$ = 111-186 MPa (depending on long or short flax fibres), the interlaminar shear strength of the T300/5208 carbon/epoxy impregnated yarn is much lower at 100-108 MPa. The reliability of the best-fit stress ratios and the applicability of Eq. 5.11 are thus questionable.

$$\sigma_{\theta=\theta_{mean}} = \sigma_0\left[1+10\sin^2\theta_{mean}+500\sin^4\theta_{mean}\right]^{-0.5} \qquad \text{Eq. 5.11}$$

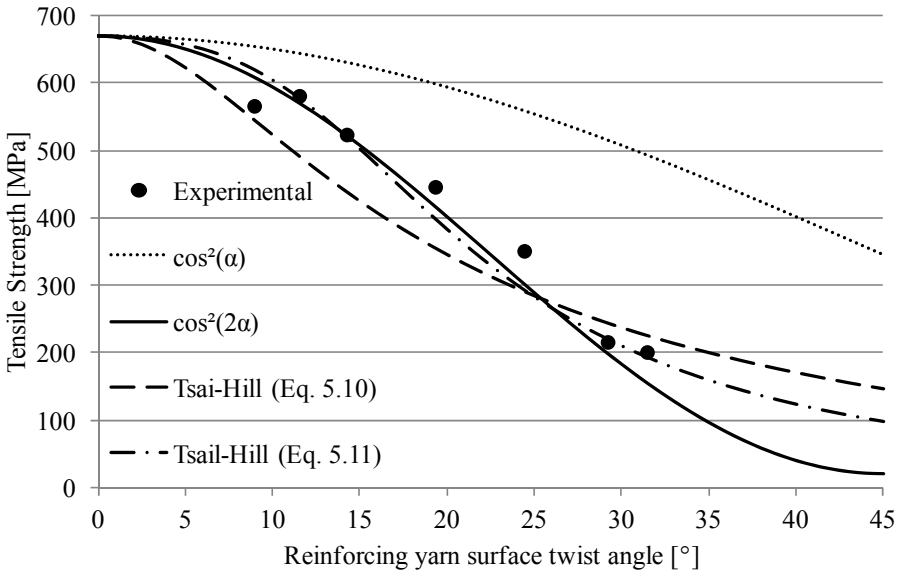


**Fig. 5.9. Modelling the effect of yarn twist on long flax fibre impregnated yarn (unidirectional PFRP). The derived $\cos^2(2\alpha)$ model (based on Eq. 5.24) in this study provides best agreement with the experimental data with an $R^2$-value of 0.950.**

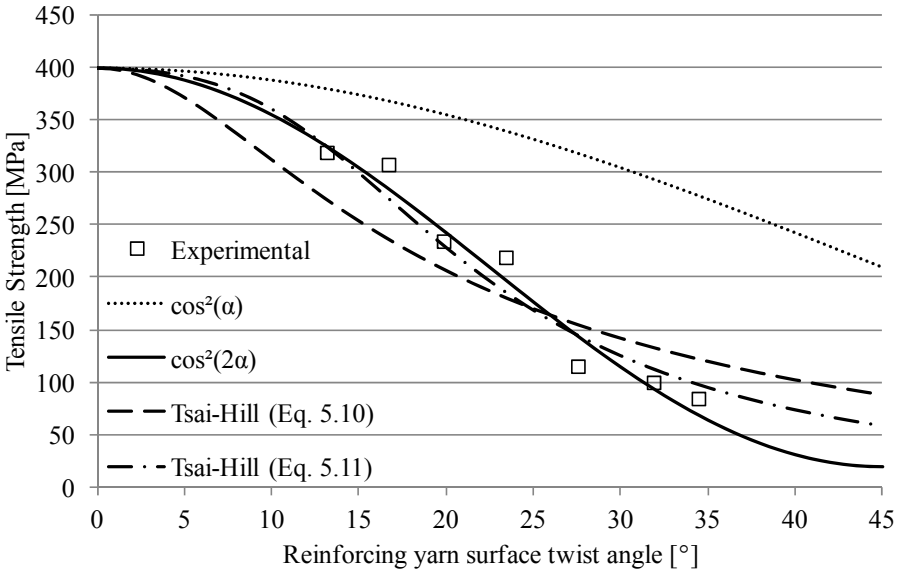


**Fig. 5.10. Modelling the effect of yarn twist on short flax fibre impregnated yarn (unidirectional PFRP). The derived $\cos^2(2\alpha)$ model (based on Eq. 5.25) in this study provides best agreement with the experimental data with an $R^2$-value of 0.961.**

A limitation of the Tsai-Hill criterion is that it does not account for the non-uniform radial stress and strain distribution within an axially loaded impregnated yarn [53], and is solely dependent on the stress ratios. An alternate model is of interest.

#### 5.3.5.2 Derived model: Krenchel efficiency factor for twisted yarns

The approach used here to model how the tensile strength of aligned PFRPs is influenced by the degree of twist is straightforward. This involves integrating the ideal twisted structure of a staple yarn into the Krenchel orientation efficiency factor and substituting the result into the rule of mixtures for composites to produce a mathematical model.

*The rule of mixtures for PFRPs*

The rule of mixtures for composites is the simplest and widely used model to describe variables that affect composite properties and parameters that account for the efficiency of the reinforcing fibres. As discussed in detail in *Chapter 2.4*, Summerscales *et al.* [54] have suggested a modified rule of mixtures for PFRPs with

efficiency terms that account for *i)* porosity $v_p$, *ii)* fibre length and interface $\eta_{lS}$, *iii)* fibre orientation distribution $\eta_o$, and *iv)* fibre diameter distribution $\eta_d$.

$$\sigma_c = \left(\eta_{lS}\eta_o\eta_d v_f \sigma_f + v_m \sigma'_m\right)\left(1 - v_p\right)^2 \qquad \text{Eq. 5.12}$$

where $\sigma'_m$ is defined as the matrix stress at fibre failure strain. To allow for the effect of fibre orientation distribution $\eta_o$ on composite mechanical performance, typically the Krenchel orientation efficiency factor (Eq. 5.13) [3] can be calculated

$$\eta_o = \sum\nolimits_n a_n \cos^4 \theta_n \qquad \text{Eq. 5.13}$$

where $a_n$ is the fraction of fibre with orientation angle $\theta_n$ with respect to the axis of loading. These models assume iso-strain conditions, perfect fibre/matrix interface, elastic response of fibre and matrix, and no transverse deformations (ignore Poisson's effects).

*Integrating the staple yarn structure into the Krenchel efficiency factor*

A twisted staple fibre yarn, whose structure has been depicted in an earlier section (Fig. 5.4), is basically an induced misalignment of the fibres. The misalignment can be described in terms of the twist angle of the individual fibres $\theta_x$ within the yarn as a function of fibre radial position $x$ ($0 \le x \le r$) using Eq. 5.1. This can then be integrated into the orientation efficiency factor of Eq. 5.13. The analysis is presented hence-forth.

As the spatial fibre distribution (packing fraction) in the yarn cross-section (of a given twist level) is assumed uniform and the radial location of a given fibre is fixed (that is, no fibre migration), $a_n$ is given by Eq. 5.14. The values of $a_n$ sum to unity.

$$a_n = \frac{2\pi x dx}{\pi r^2}; \quad \int_0^r a_n = 1 \qquad \text{Eq. 5.14}$$

From Eq. 5.1, Eq. 5.13 and Eq. 5.14, the Krenchel orientation efficiency factor $\eta_o$ is then given by the integral

$$\eta_o = \int_0^r \frac{2\pi x}{\pi r^2} \cos^4\left(\tan^{-1}\frac{2\pi x}{L}\right) dx \qquad \text{Eq. 5.15}$$

Using the trigonometric identity $\cos^4(\tan^{-1}(u)) = 1/(1+u^2)^2$ to solve the integral in Eq. 5.15, results in an expression for the orientation efficiency factor $\eta_o$ which is given in Eq. 5.16.

$$\eta_o = \frac{L^2}{L^2 + 4\pi^2 r^2} \quad \text{Eq. 5.16}$$

Eq. 5.16 can be simplified using Eq. 5.2 to give Eq. 5.17. An expression for $\eta_o$ (Eq. 5.17) is then found to be simply a function of the twist angle at the yarn surface $\alpha$.

$$\eta_o = \frac{L^2}{L^2 + L^2 \tan^2 \alpha} \quad \text{Eq. 5.17}$$

$$\eta_o = \cos^2 \alpha \quad \text{Eq. 5.18}$$

When modelling the effect of fibre obliquity (yarn twist) on dry yarn tensile modulus, Pan [55] observed that a better agreement with experimental data was found when $\alpha$ is replaced with $2\alpha$. Pan [55] suggested that this is because the actual effect of the fibre helix angle is represented by $2\alpha$ due to the structural difference between filament and staple yarns. However, the actual physical implication of the $2\alpha$ in terms of the limiting twist angle for a staple yarn is not fully understood [55]. Filament yarns have a maximum permissible twist angle of 70.5°; staple yarns will have a smaller limiting twist angle [47]. A factor of $2\alpha$ restricts this limiting twist angle to 45°. Nonetheless, as Pan [55] observed better agreement with their experimental data, here the chosen model is based on $2\alpha$ (Eq. 5.19) to predict the effect of twist on the tensile strength of aligned PFRPs.

$$\eta_o = \cos^2 2\alpha \quad \text{Eq. 5.19}$$

*Model for tensile strength prediction of twisted yarn PFRPs*

The derived orientation efficiency factor (Eq. 5.19) needs to be substituted into the rule of mixtures for PFRPs (Eq. 5.12). The modified rule of mixtures which takes into account the effect of fibre obliquity in twisted yarn reinforcements is given by Eq. 5.20.

$$\sigma_c = \left(\cos^2 2\alpha \cdot \eta_{ls} \eta_d v_f \sigma_f + v_m \sigma'_m\right)\left(1 - v_p\right)^2 \quad \text{Eq. 5.20}$$

To compare the generalized model in Eq. 5.20 with the experimental data, some simplification is necessary. It is assumed that $\eta_d$ is unity and that the composite contains no voids ($v_p = 0$ and $v_m = 1 - v_f$). The simplified model can be written as in Eq. 5.21

$$\sigma_\alpha = \cos^2 2\alpha \cdot \eta_{lS} v_f \sigma_f + (1 - v_f)\sigma'_m \qquad \text{Eq. 5.21}$$

As a side note, it is interesting that Eq. 5.21 is of similar form to that presented by McLaughlin *et al.* [21] to describe the effect of microfibril angle in single plant fibres on their elastic modulus (described in *Chapter 2*). A single plant fibre can be thought to be a twisted yarn composite; single plant fibres are a lignin-hemicellulose matrix reinforced by cellulose fibrils, where the microfibrils are helically wound around layers of the cell wall (previously described in Section 5.2).

Goutianos *et al.* [36] determined the tensile strength of the impregnated yarns using the cross-sectional area of the yarn. The cross-sectional area of a yarn is directly related to the yarn packing fraction (Eq. 5.3; $\emptyset = A_f/A_y$). Ring-spun yarns typically have a packing fraction of 0.5-0.6 [49]. As also discussed previously in Section 5.3.3, a constant packing fraction of $\emptyset = 0.6$ is a good match to Eq. 4.5. For an impregnated yarn, the yarn packing fraction $\emptyset$ also represents the fibre volume fraction $v_f$. Hence, to compare the simplified model in Eq. 5.21 with the experimental data, the composite fibre volume fraction is taken to be $v_f = 0.6$. Other researchers, when modelling the elastic properties of impregnated twisted yarns, have also used a constant $v_f = 0.6$ [41]. Weyenberg *et al.* [7] calculated the matrix stress at fibre failure strain $\sigma'_m$ (based on composite tensile strain of approximately 1.5%) of an epoxy matrix as $\sigma'_m = 50$ MPa.

The simplified model in Eq. 5.21 (with $v_f = 0.6$ and $\sigma'_m = 50$ MPa) can then be fitted to the experimental data for an adjusted effective fibre strength $\eta_{lS}\cdot\sigma_f$. The effective fibre strength $\eta_{lS}\cdot\sigma_f$ represents the potential reinforcing ability the fibres (of a given length) can provide to the composite. Typically, shorter fibres produce poorer composites due to smaller length efficiency factor $\eta_{lS}$ and thus smaller effective fibre strength $\eta_{lS}\cdot\sigma_f$. The effective fibre strength is taken to be $\eta_{lS}\cdot\sigma_f = 1083$ MPa for long

flax fibres and $\eta_{lS} \cdot \sigma_f$ = 633 MPa for short flax fibres. These values are in the range of typical tensile strength of technical flax fibres [30].

On a side note, if $\eta_{lS}$ is assumed to be unity for long flax fibres (that is, $\sigma_f$ = 1083 MPa), then $\eta_{lS}$ = 0.58 for short flax fibres. The length efficiency factor $\eta_{lS}$ is related to the critical (or ineffective) fibre length $l_c$ (Eq. 5.22) [56], and $l_c$ itself is defined by the composite interfacial shear strength $\tau$, fibre strength $\sigma_f$ and fibre diameter $d_f$ (Eq. 5.23) [13, 56]. Hence, a value of $\eta_{lS} \approx 1$ implies that the reinforcing fibre length is significantly higher than the critical fibre length ($l_f >> l_c$), while $\eta_{lS}$ = 0.58 implies that the reinforcing fibre length is approximately equal to the critical fibre length ($l \approx l_c$).

$$\eta_{lS} = \begin{cases} 1 - l_c / 2l_f & for\ l_f \geq l_c \\ l_f / 2l_c & for\ l_f \leq l_c \end{cases} \quad \text{Eq. 5.22}$$

$$l_c = \frac{\sigma_f d_f}{2\tau} \quad \text{Eq. 5.23}$$

In short, the derived mathematical models for the experimental data are given in Eq. 5.24 for long flax fibre impregnated yarn strength and Eq. 5.25 for short flax fibre impregnated yarn strength (where $v_f$ = 0.6, $\sigma'_m$ = 50 MPa and $\eta_{lS} \cdot \sigma_f$ = 1083 MPa for long flax fibres and $\eta_{lS} \cdot \sigma_f$ = 633 MPa for short flax fibres).

$$\sigma_\alpha = \cos^2 2\alpha \cdot 650 + 20 \quad \text{Eq. 5.24}$$

$$\sigma_\alpha = \cos^2 2\alpha \cdot 380 + 20 \quad \text{Eq. 5.25}$$

The $\cos^2(2\alpha)$ models have been compared with experimental data for long and short flax fibre yarns in Fig. 5.9 and Fig. 5.10. The $\cos^2(2\alpha)$ model is a near-perfect fit for the experimental data, where almost all the points lie on the curve. The non-linear regression $R^2$-value is found to be 0.950 and 0.961 for long and short flax fibre impregnated yarns, respectively. A $\chi^2$-goodness of fit test suggests that the $\cos^2(2\alpha)$ is a suitable model for the experimental data at a p-value of 0.23% for the long flax impregnated yarns and at a p-value of 4.72% for the short flax impregnated yarns.

It is thus proposed that the simplified model in Eq. 5.21 is a good model to predict the influence of yarn twist on aligned PFRP tensile strength. If required, the other

efficiency factors and the effect of porosity can be reintroduced by using the generalized model in Eq. 5.20. An interesting inference of the model is that employing yarns with $\alpha > 26°$ or $\alpha > 32°$ as composite reinforcements will reduce the reinforcement orientation efficiency factor as in a 2D-random and 3D-random composite, respectively.

*Applying the derived model to other studies*

Although the derived model is in strong agreement with experimental data from Goutianos *et al.* [36], to validate the model further it is necessary to compare it with experimental results of real composites (rather than just impregnated yarns), from other studies.

Apart from Goutianos *et al.* [36], Baets *et al.* [37, 43] and Rask *et al.* [44] have investigated the effect of yarn twist on PFRP mechanical properties. As mentioned earlier, both Baets *et al.* [37, 43] and Rask *et al.* [44] focussed on the evolution of the tensile modulus of unidirectional composites for increasing yarn twist levels. Rask *et al.* [44] haven't presented data on composite tensile strength. Hence, the experimental data for Baets *et al.* [37, 43] has been used here.

Baets *et al.* [37, 43] manufactured unidirectional flax/epoxy composites from three different forms of flax: hackled, roving and yarn. Starting from the same source, the three different forms of flax were obtained from different steps in the fibre extraction and yarn preparation process. The key difference in them is their level of twist: 0 tpm, 41 tpm and 280 tpm, respectively. The corresponding surface twist angles were determined by Baets *et al.* [37, 43] and are presented in Table 5.2.

Baets *et al.* [37, 43] measured the tensile strength of the three UD composites. The experimental data is presented in Table 5.2. They determined the fibre tensile strength $\sigma_f$ through back-calculation from the rule of mixtures – using Eq. 5.21, with the corresponding $v_f$ and assuming $\eta_{IS} = 1$ and $\sigma'_m = 40$ MPa. They also assumed $\eta_o = 1$ and consequently didn't consider the effect of (mis)orientation from increasing twist angle. What they observed is that the back-calculated single fibre tensile strength decreased with increasing twist level (Table 5.2). For instance, flax fibres from the yarn ($\alpha = 14.8°$) have a mean tensile strength of 590 MPa, which is 30%

lower than the mean tensile strength of flax fibres from a hackled bundle ($\alpha$ = 0°). The difference in mean tensile strength of the three flax fibres is accountable to the level of twist in the reinforcement type.

**Table 5.2. Verification of the developed model with experimental data from Baets *et al.* [37, 43] (with column titles in italics).**

| | **Fibre properties** | **Composite properties** | | | **Fibre tensile strength $\sigma_f$ [MPa]*** | |
|---|---|---|---|---|---|---|
| **Flax type** | *Surface twist angle $\alpha$ [°]* | *Fibre content $v_f$* | *Tensile Strength $\sigma$ [MPa]* | $\cos^2(2\alpha)$ | *For $\eta_o = 1$†* | For $\eta_o = \cos^2(2\alpha)$ ‡ |
| **Hackled** | 0 | 42 ± 2 | 378 ± 38 | 1.000 | 845 ± 90 | 845 ± 90 |
| **Roving** | 7.8 | 48 ± 1 | 377 ± 24 | 0.928 | 742 ± 50 | 800 ± 54 |
| **Yarn** | 14.8 | 50 ± 1 | 315 ± 46 | 0.607 | 590 ± 92 | 780 ± 151 |

* The fibre tensile strength is back-calculated using the rule of mixtures in Eq. 5.21, assuming $\eta_{lS}$ = 1 and $\sigma'_m$ = 40 MPa [11, 21].

† Baets *et al.* [11, 21] determined the fibre tensile strength assuming no effect of (mis)orientation from yarn twist (that is, $\eta_o$ = 1). The back-calculated fibre strengths are hence very dissimilar.

‡ Using $\eta_o = \cos^2(2\alpha)$ in Eq. 5.21 accounts for the effect of yarn twist. The back-calculated fibre strengths are now similar to each other.

Hence, to assess the validity of the model derived in the previous section, rather than assuming $\eta_o$ to be unity, $\eta_o = \cos^2(2\alpha)$ is used in Eq. 5.21. The back-calculated fibre tensile strength will now account for misorientation from yarn twist. As can be seen in Table 5.2, the fibre tensile strengths are now very similar and in the range of 780–845 MPa; a difference of means t-test suggests an insignificant difference in the mean fibre tensile strengths ($p>0.35$). This shows that both the derived model and the $\cos^2(2\alpha)$ orientation efficiency factor are able to capture the effect of yarn twist on composite tensile strength.

### 5.3.6 Conclusions

The true structural potential of plant fibres as reinforcing agents can only be realized when the highest reinforcement efficiency is employed. Hence, aligned unidirectional PFRPs are of interest. However, due to the short length of technical plant fibres, the manufacture of aligned PFRPs requires the reinforcement to be in the

form of staple fibre yarns. Staple fibre yarns have a twisted structure. Although twist facilitates yarn processability, it has several detrimental effects on the composites produced from such twisted yarn reinforcements. One of these detrimental effects is fibre obliquity and misalignment (to the composite loading axis) which results in a drastic drop in mechanical properties of the composite.

Prior to this investigation, no analytical model was available to accurately predict the effect of yarn twist on aligned PFRP tensile strength. In this study, a novel mathematical model based on *i)* the modified rule of mixtures for PFRPs, *ii)* idealised twisted structure of a staple fibre yarn, and *iii)* Krenchel orientation efficiency factor is used to predict the influence of yarn twist on composite strength. The simple model is based on the yarn surface twist angle $\alpha$. Through a discussion of the idealized staple yarn structure, relationships between structure and properties have been identified. A rule of mixtures model with a modified orientation efficiency factor of $\cos^2(2\alpha)$ is validated with extensive experimental data from Goutinos *et al.* [36] and shows strong agreement. The derived model is a near-perfect fit for the experimental data (with $R^2 = 0.950$). The model is verified further using experimental data from another study on aligned PFRPs by Baets *et al.* [37, 43]. An interesting inference of the model is that employing yarns with $\alpha > 26°$ or $\alpha > 32°$ as composite reinforcements will reduce the reinforcement orientation efficiency factor as in a 2D-random and 3D-random composite, respectively.

## 5.4 EFFECT OF OFF-AXIS LOADS ON PFRP TENSILE PROPERTIES

### 5.4.1 Off-axis loading of composites

Composites in load-bearing applications are often exposed to off-axis loads, which are loads at an angle to the primary fibre orientation (Fig. 5.1c). As mentioned in Section 5.1, the anisotropic nature of composites implies that off-axis loads have a significant detrimental effect on their effective mechanical properties. In fact, as the loading direction is varied from parallel to the principal fibre direction to normal to the principal fibre direction, the mechanical behaviour of the composite changes from fibre-dominated to matrix-dominated [57]. Testing the effect of off-axis loads is not only useful but also critical in understanding and assessing the manner in which

composite mechanical properties degrade as the loading direction is changed from the optimum fibre direction.

Although there are several researchers who have looked at longitudinal and transverse tensile properties of aligned PFRPs (for instance [7, 58]), there are limited articles that have evaluated tensile properties for a range of loading angles. Kumar [59] tested jute-polyester composites only in three directions – 0, 45 and 90°. Although Ntenga *et al.* [60] and Cichocki *et al.* [61] considered the effect of at least five off-axis angles other than 0 and 90°, to investigate the (thermo-)elastic anisotropy of aligned PFRPs they only measured elastic properties. Their studies focussed on the application of micro-mechanical models. The only complete results are by Madsen *et al.* [8] who measured tensile properties (modulus, strength and failure strain) of unidirectional hemp/PET in the directions 0, 10, 20, 30, 45, 60 and 90°. They found that the tensile modulus and strength drop drastically with increasing loading angle, as traditional composite laminate models predict. Nonetheless, more experimental data is required for further validation.

This section aims to *i)* characterise the stress-strain response, *ii)* investigate the tensile properties, and *iii)* analyse the fracture modes, of vacuum-infused unidirectional flax/polyester composites subjected to off-axis tensile loading. This study also looks to determine whether conventional composite micro-mechanical models can be used with confidence to quantitatively describe the off-axis tensile behaviour of PFRPs.

### 5.4.2 Experimental methodology

#### 5.4.2.1 Reinforcement material

Flax yarn (Fig. 5.11) was obtained from Composites Evolution (UK). This is the same yarn (F50) used for the study in *Chapters 3 and 4*. The flax yarn (250 tex) employs a S-twist polyester filament binder (32 tex, ~13 wt% of yarn). This binder enables the core flax fibres to be of low twist (50 tpm, mean twist angle of 3.3°). The density of the flax yarn $\rho_f$ (inclusive of the polyester binder) was measured, by

helium pycnometry, to be 1.529 ± 0.003 gcm$^{-3}$. Formax (UK) Ltd produced 300 gsm stitched unidirectional (0°) and biaxial (±45°) fabrics from this yarn.

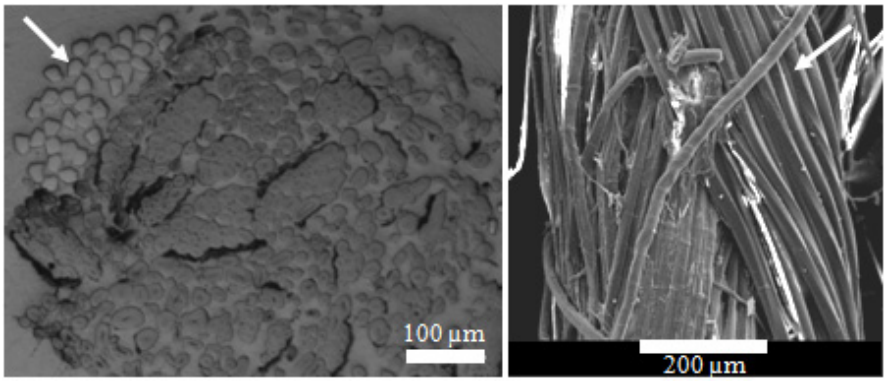


**Fig. 5.11. Low twist flax yarn: optimal microscope image of cross-section (left) and SEM image of surface (right), showing the core flax fibres and polyester binder (indicated by arrow).**

#### 5.4.2.2 Composite manufacture

To study off-axis properties of the composites, the unidirectional fabric was laid-up in an aluminium mould tool at different inclination angles (0, 15, 30, 45, 60 and 90°). Unidirectional composite laminates (250 mm square, 3-3.5 mm thick) were manufactured from four layers of the as-received fabric using the vacuum infusion technique. Resin infusion was carried out at 70-80% vacuum (200-300 mbar absolute pressure).

An unsaturated polyester (Reichhold Norpol type 420-100) matrix was used. The resin was mixed with 0.25 wt% NL49P accelerator (Cobalt(II) 2-ethyl hexanoate, 1% Co in di-isobutyl phthalate) and 1 wt% Butanox M50 MEKP initiator. Post cure was carried out at 55 °C for 6 h after ambient cure for 16 h. From the manufacturer's datasheet, the polyester resin has a cured density $\rho_m$ of 1.202 g·cm$^{-3}$, tensile modulus $E_m$ of 3.7 GPa, tensile strength $\sigma_m$ of 70 MPa and failure strain $\varepsilon_m$ of 3.5%. Taking the matrix Poisson's ratio $\nu_m$ as 0.38 for cured polyester [52, 61, 62] and assuming isotropic properties, the matrix shear modulus $G_m$ is estimated to be 1.34 GPa (Eq. 5.26).

$$G_m = \frac{E_m}{2(1+\nu_m)} \quad \text{Eq. 5.26}$$

Noting the mass of the fabric preform and the resulting composite plaque, the fibre weight fraction $w_f$ of the laminates was determined. The composite density $\rho_c$ was measured using helium pycnometry. The composite fibre volume fraction $v_f$ was then determined using Eq. 5.27, allowing for porosity $v_p$.

$$v_f = \frac{\rho_c}{\rho_f} w_f; \quad v_m = \frac{\rho_c}{\rho_m}(1-w_f); \quad v_p = 1-(v_f+v_m) \quad \text{Eq. 5.27}$$

The laminates have almost identical fibre volume fraction $v_f$ of 26.9 ± 0.6 %, while the void content $v_p$ ranges from 0.7–1.3%. Fig. 5.13 presents images of example test specimens; the off-axis angles are clearly visible from the sample surface. For comparative purposes, a laminate was also manufactured using the biaxial flax fabric ($v_f$ = 28.6%). Although ~13 wt% (~11 v%) of the flax yarn is polyester filament, it is assumed that flax fibre accounts for the total fibre volume fraction. The polyester filament has a density and tensile strength (~1.39 gcm$^{-3}$, 539-1181 MPa) similar to flax fibre (1.40-1.55 gcm$^{-3}$, 343-1035 MPa) [30].

#### 5.4.2.3 Tensile testing

After the manufacture of composite laminates, tensile tests were conducted according to ISO 527-4:1997 (BS 2782-3:1997) [63] using an Instron 5985 testing machine equipped with a 100 kN load cell and an extensometer. Samples from the unidirectional laminates were loaded with the fibres at the defined inclination angles (0, 15, 30, 45, 60 and 90°) to the testing direction, while the biaxial samples were loaded in bias extension with fibres at ±45° to the testing direction. At least six 250 mm long and 25 mm wide specimens were tested for each type of composite at a cross-head speed of 2 mm/min. The elastic Young's modulus $E_c$, ultimate tensile strength $\sigma_c$, and failure strain $\varepsilon_c$ were determined from the stress-strain data (Fig. 5.12). As Fig. 5.12b illustrates, the tensile modulus $E_c$ is determined using the initial tangent modulus in the strain range of 0.025–0.100%. Note that the tensile modulus is not the same as the 'apparent stiffness'. Finally, the fracture surfaces of the failed

specimen were sputter coated with platinum and observed under a Philips XL30 SEM (acceleration voltage of 15 kV).

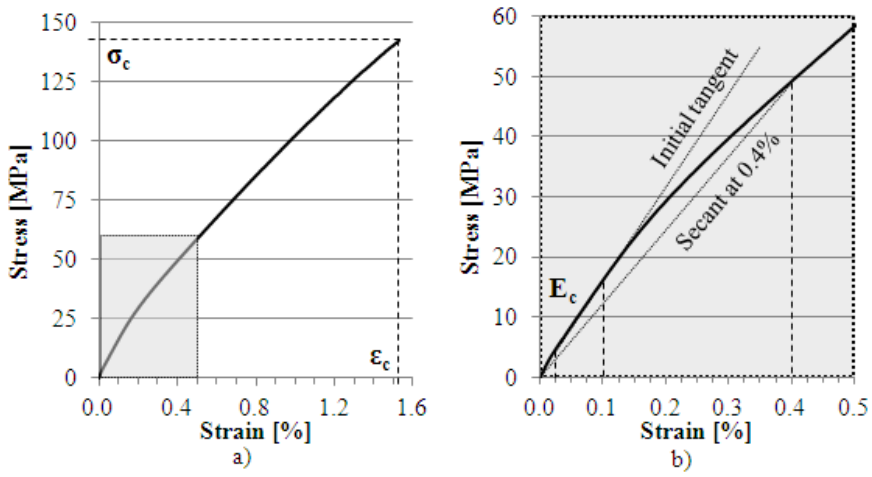


**Fig. 5.12. Tensile mechanical properties extracted from the material stress-strain curve. The elastic Young's modulus $E_c$ is determined using the initial tangent modulus in the strain range of 0.025-0.100%. The 'apparent stiffness' at ε% strain can be determined using the slope of the secant at ε% strain.**

### 5.4.3 Results and Discussion

#### 5.4.3.1 Tensile stress-strain behaviour

The typical stress-strain curves in Fig. 5.13 reveal the general changes in tensile properties of flax/polyester composites loaded at various off-axis angles. As the curves shift downwards for increasing loading angles, deterioration in composite tensile properties is observed. Essentially, the tensile modulus, strength and failure strain decrease with increasing misorientation.

As Fig. 5.13 illustrates, it is interesting that biaxial flax/polyester composites have a significantly higher failure strain of 3.76 ± 0.68 % compared to the other off-axis loaded unidirectional composites. With a tensile modulus and strength of 5.7 ± 0.1 GPa and 51.4 ± 2.8 MPa respectively, biaxial flax/polyester composites perform better than uniaxial flax/polyester composites loaded at 30° (Fig. 5.13). Thus, it can be said that biaxial composites are a better option than uniaxial composites for applications where loads are at an off-axis angle larger than 30°. Chamis [64]

concluded the same in their investigation of the off-axis tensile properties of unidirectional and bidirectional graphite-epoxy composites ($v_f \approx 50\%$).

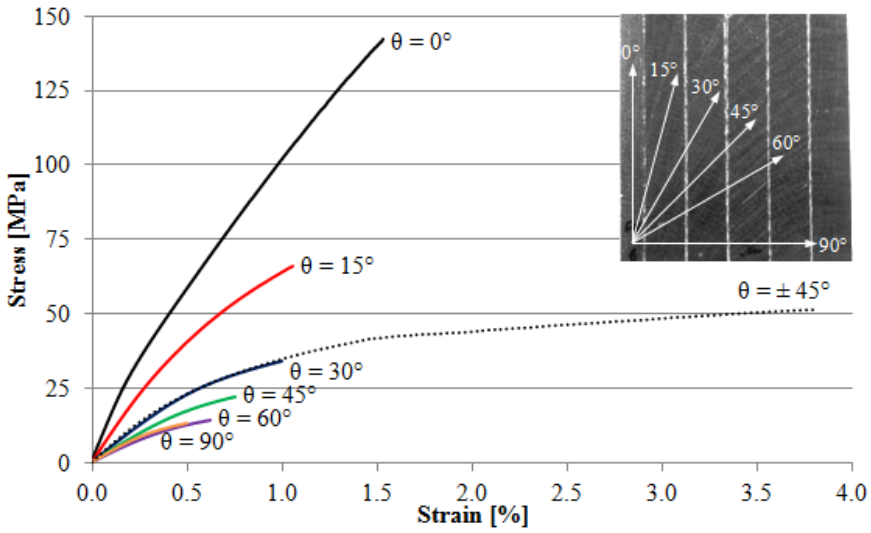


**Fig. 5.13. Typical stress-strain curves of off-axis loaded unidirectional flax/polyester composites. Example test specimens are shown on the top right-hand corner. The typical stress-strain curve of a biaxial flax–polyester composite (loaded at ±45°) is also shown.**

Fig. 5.12 and Fig. 5.13 also show that even at low strains (< 0.5%) the stress-strain response of PFRPs, like single plant fibres [17, 23, 26, 65, 66], is non-linear. This is better observed in a plot of 'apparent stiffness' against strain (Fig. 5.14). Here, the apparent stiffness at ε% strain is defined as the secant modulus at ε% strain (shown in Fig. 5.12b).

The elastic Young's modulus is typically measured in the strain range of 0.05–0.25% (ISO 527-4:1997/BS 2782-3:1997 [63]). As Fig. 5.14 illustrates, while the apparent stiffness is fairly constant in this strain range for unidirectional E-glass–polyester composites due to their linear stress-strain curve ($v_f \approx 43\%$; material data from *Chapter 3*), there is significant variation in the apparent stiffness for PFRPs due to their non-linear stress-strain curve. In fact, the apparent stiffness of all the flax/polyester laminates reduces by ~30% in the strain range of 0.05–0.25%. Baets *et al.* [37] have also noticed this evolution in apparent stiffness for flax/epoxy composites. This observation has major implications on the strain range to be used

for the determination of the elastic Young's modulus. To overcome this issue, Baets *et al.* [37] measured the tensile modulus in the strain range of 0.05–0.10%. In this study (*and in fact, all studies in this thesis*), the tensile modulus is measured in the strain range of 0.025–0.100%. Both approaches are acceptable as ISO 527-4:1997 [63] recommends determining the secant modulus at 0.1% strain as the tensile modulus, if the tangent modulus in the strain range of 0.05–0.25% cannot be measured.

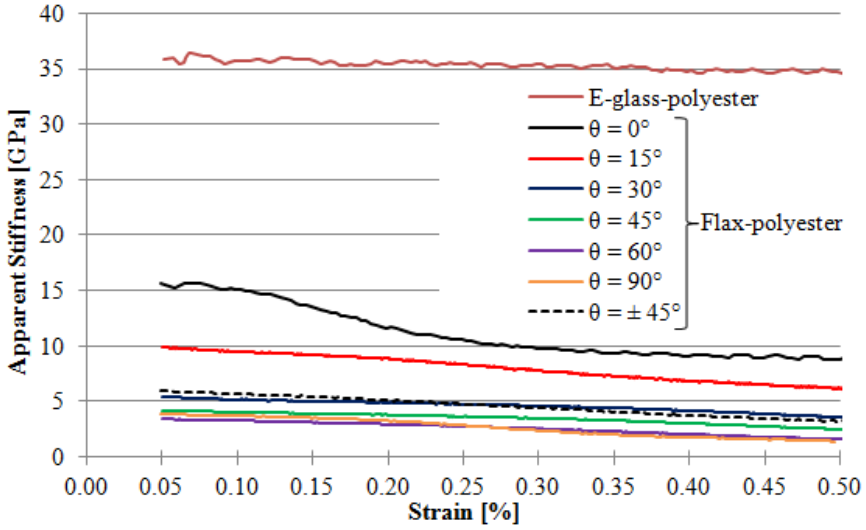


**Fig. 5.14. Evolution of the apparent stiffness (secant modulus) with strain, for off-axis loaded flax/polyester composites. In the region of <0.25% strain, the apparent stiffness drops significantly for flax/polyester, but remains fairly constant for E-glass-polyester.**

*Cyclic stress-strain behaviour*

The proposal to measure the elastic Young's modulus for PFRPs in the strain range of 0.025–0.100% becomes more attractive when the cyclic stress-strain behaviour of the material is studied. Elastic deformation is reversible and non-permanent; hence, there exists an elastic limit beyond which non-reversible permanent deformation occurs. To determine the elastic strain limit for PFRPs, six tensile specimens of unidirectional (0°) flax/polyester were subjected to successively larger loading-unloading cycles (load-unload rate of 7000 N/min). The applied load regime and the typical stress-strain response of the material are presented in Fig. 5.15a and b,

respectively. From the stress-strain response, the hysteresis and the effective plastic strain at the end of every cycle can be determined. The results are tabulated in Table 5.3.

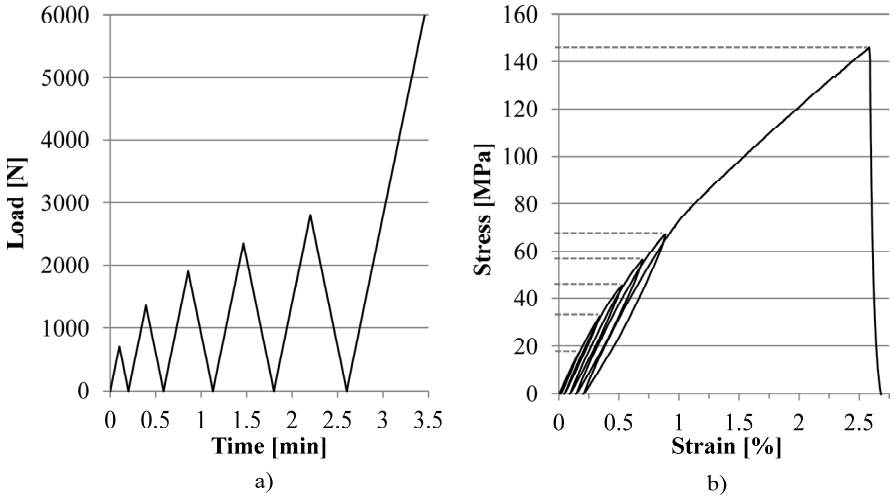


**Fig. 5.15.** ***a)*** **Unidirectional (0°) flax/polyester composites were subjected to successively larger loading-unloading cycles with load increasing in every cycle.** ***b)*** **From the stress-strain response of the material, the plastic strain upon unloading after every cycle can be recorded.**

**Table 5.3. Strain upon loading and plastic strain upon unloading for unidirectional flax/polyester composites subjected to the load regime in Fig. 5.15a.**

| Cycle | Maximum Load [N] | Strain upon loading [%] | Plastic strain upon unloading [%] |
|---|---|---|---|
| **1** | 700 | 0.165 ± 0.005 | 0.016 ± 0.002 |
| **2** | 1350 | 0.343 ± 0.011 | 0.046 ± 0.006 |
| **3** | 1900 | 0.528 ± 0.017 | 0.094 ± 0.010 |
| **4** | 2350 | 0.703 ± 0.026 | 0.146 ± 0.010 |
| **5** | 2800 | 0.895 ± 0.033 | 0.205 ± 0.006 |
| **6** | Up to failure | 2.476 ± 0.182 | - - |

If the material has been loaded in the elastic range, the plastic strain upon unloading will be zero. From the distinctive growing hysteresis loops in Fig. 5.15b and the analysed data in Table 5.3, it is seen that the plastic strain upon unloading increases

with applied load. Hence, there is certainly a degree of irreversibility in the deformation process of the microstructure. In addition, a non-zero plastic strain (of 0.016%) is observed even when the composite is loaded up to only 0.165% tensile strain. Using the results in Table 5.3, a linear regression analysis between strain upon loading and plastic strain upon unloading ($R^2 = 0.989$), suggests that the plastic strain is zero for tensile loading up to 0.146%. Consequently, the elastic Young's modulus for PFRPs can only be determined below this elastic strain limit of ~0.15%. Hughes *et al.* [67] conducted a similar study on flax/polyester composites and also found that this 'yield point' occurred at an average strain of 0.12%. In essence, measuring the tensile modulus for PFRPs in the strain range of 0.025–0.100% is sensible. Again, note that the composite tensile modulus has been measured in this strain range for all studies in this thesis.

Although the causes of the non-linear stress-strain response of the PFRPs (and the resulting stiffness reduction at low strains) are not yet clear [37, 67], they are possibly a result of 'non-reversible reorientation' on two length scales: *i)* untwisting/stretching of the reinforcing twisted staple fibre yarns [8, 37, 68], and *ii)* rigid body rotation and subsequent stretching and aligning of the cellulose microfibrils in a single plant fibre [12, 37, 65, 67]. The latter is believed to have a dominant role; particularly as plant single fibres themselves have a non-linear response to tensile loading (described in Section 5.2).

Several studies (for instance, [17, 23, 26, 28, 65, 66]) suggest that the non-linear stress-strain response of plant single fibres is a result of the initial misorientation of the cellulose microfibrils (represented by the MFA) and the 'non-reversible' uncoiling/aligning of the microfibrils upon loading. Burgert *et al.* [26] and Spatz *et al.* [28] have attempted to explain this phenomenon in more detail by comparing the tensile stress-strain response of low and high MFA single fibres. Spatz *et al.* [28] show that the yield point (or elastic limit) for single plant fibres, like PFRPs, is also very low. They argue that irreversible permanent plastic deformation above the yield point causes the non-linear stress-strain curve. They propose, with some critical backing from experimental evidence, that the irreversible visco-elasto-plastic deformation is driven by *i)* various complex micro-damage mechanisms, and *ii)*

structural changes (reorientation of microfibrils). Discussing the former, Burgert *et al.* [26] and Spatz *et al.* [28] suggest that the possible order of micro-damage progression is: *a)* the shear deformation and consequent viscous flow of the lignin-hemicellulose matrix, *b)* the sliding of cellulose microfibrils past each other, *c)* the consequential breakage and reformation of hydrogen bonds between fibril-fibril and fibril-matrix, and *d)* the continuous stripping of cellulose bridging hemicellulose chains. Hughes *et al.* [67] have also suggested that microstructural defects in the fibre (in the form of kink bands), may directly contribute to the non-linear strain behaviour of plant fibres and thus their composites. At least, the fact that the stress-strain response is linear for E-glass and its composites, and non-linear for plant fibres and their composites PFRPs, highlights *i)* the fundamental differences in the fibres, and *ii)* the varying stress-strain and damage accumulation mechanisms in the fibres and composites.

#### 5.4.3.2 Theory and comparison with experiments

The tensile properties of a composite at a given off-axis loading angle can be estimated by well-known micro-mechanical models, such as the Tsai-Hill criterion [50]. These models are valid for transversely isotropic laminates under plane stress conditions. Unidirectional PFRPs are composed of transversely isotropic fibres/yarns embedded in an isotropic matrix, and hence they satisfy this requirement [8, 48, 60]. Here, comparisons are made between experimental data and predicted results from micro-mechanical models to *i)* show the validity of conventional composite models for PFRPs and *ii)* determine, otherwise difficult to measure, material properties (for instance, fibre shear modulus $G_f$ and transverse tensile modulus $E_{f,90}$) through numerical methods. Note that in this study, the contribution of yarn twist to effective ply orientation $\theta$ has been neglected, as low-twist flax yarns have been used.

##### *Elastic properties*

The influence of ply orientation $\theta$ on the tensile modulus $E_c$ of the composites is graphically presented in Fig. 5.16. Unidirectional flax/polyester composites loaded in the fibre direction (0°) have a stiffness $E_{c,0}$ of 15.3 ± 0.6 GPa. This is 4 times higher than the composite transverse tensile modulus $E_{c,90}$ of 3.8 ± 0.2 GPa. Madsen *et al.*

[8] noted a similar anisotropy ratio between longitudinal (17.6 ± 0.7 GPa) and transverse tensile modulus (3.5 ± 0.1 GPa) from tests on hemp/PET composites ($v_f \approx$ 33.5%).

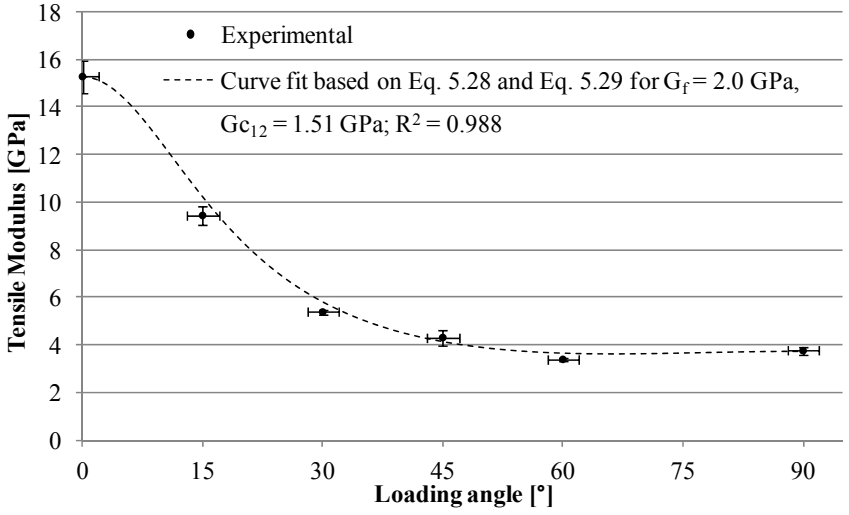


**Fig. 5.16. Variation in tensile modulus of unidirectional flax/polyester composites for increasing off-axis loading angle. Experimental data (•) is presented with error bars (1 stdev). The dotted line is a theoretical prediction based on Eq. 5.28 and Eq. 5.29 for $G_f$ = 2.0 GPa (and $G_{c12}$ = 1.51 GPa).**

It is observed from Fig. 5.16 that the composite tensile modulus drops significantly for increasing loading angle between $0° < \theta < 30°$. While it is of interest to note that composites loaded at $\theta = 60°$ have the lowest tensile modulus, there is little variation in composite stiffness for $30° < \theta < 90°$. Assuming that the unidirectional laminates are transverse isotropic structures under plane stress conditions, Eq. 5.28 can be used to predict the change in composite tensile modulus for increasing off-axis loading angle, given that four composite properties are known: longitudinal and transverse tensile modulus ($E_{c,0}$, $E_{c,90}$), shear modulus $G_{c12}$ and Poisson's ratio $v_{c12}$.

$$E_{c,\theta} = \left[ \frac{1}{E_{c,0}} \cos^4\theta + \left( \frac{1}{G_{c12}} - \frac{2\nu_{c12}}{E_{c,0}} \right) \cos^2\theta \sin^2\theta + \frac{1}{E_{c,90}} \sin^4\theta \right]^{-1} \qquad \text{Eq. 5.28}$$

The composite longitudinal and transverse stiffness ($E_{c,0}$, $E_{c,90}$) have been experimentally determined. The Poisson's ratio $v_{c12}$ of the composite is taken to be

0.31 [61]. The composite shear modulus $G_{c12}$ can be estimated using the semi-empirical Halpin-Tsai equation [69] (Eq. 5.29). The Halpin-Tsai equation expresses the composite shear modulus $G_{c12}$ as a function of the fibre shear modulus $G_f$. Hence, the fibre shear modulus $G_f$ can be adjusted to determine a composite shear modulus $G_{c12}$ (using Eq. 5.29) that best fits the experimental data. Here, best fit is determined using least squares (non-linear) regression $R^2$ values.

$$G_{c12} = \frac{G_m\left(1+\xi\eta v_f\right)}{\left(1-\eta v_f\right)}, \text{ where } \eta = \frac{\frac{G_f}{G_m}-1}{\frac{G_f}{G_m}+\xi} \qquad \text{Eq. 5.29}$$

In Eq. 5.29, a fibre shape factor $\xi$ needs to be entered. $\xi$ correlates to the geometry (aspect ratio) of the reinforcement, but also packing arrangement and loading conditions [70]. Typically, assuming circular cross-section fibres [69, 70] and using $\xi$ = 1 produces satisfactory results for PFRPs [8, 17]. However, it is well known that the cross-section of plant fibres is variable, irregular and non-circular. Only recently have researchers quantitatively estimated the deviation of the fibre cross-section shape from circularity [71-73]. The studies suggest that calculating the cross-section area $A_C$, assuming a circular cross-section with an average fibre diameter '*d*', overestimates the true cross-section area $A_T$ by a factor $\kappa$ of 1.42–2.55 [71-73]. Therefore, in this study, an attempt is made to use a value of $\xi$ representative of the non-circular cross-section of plant fibres. Some studies, for instance [18, 74], show that an ellipse is a much better model of a natural fibre cross section than a circle. If the true fibre cross-section $A_T$ is assumed to be elliptical with major axis '*a*' and minor axis '*b*', the factor κ is equal to the ratio *a*/*b* (shown in Eq. 5.30). As $\xi$ depends on cross-sectional aspect ratio [70], assuming an elliptical fibre cross-section should suffice in estimating the resulting anisotropy. Halpin and Kardos [70] have semi-empirically derived Eq. 5.31 to determine the fibre shape factor $\xi$ for composites with elliptical/rectangular cross-section fibres to calculate $G_{c12}$. As a quick check of Eq. 5.31, in the limiting case for circular cross-section fibres, $\xi$ = 1 since *a* = *b*. For elliptical cross-section plant fibres with *a*/*b* = 1.42–2.55, $\xi$ = 1.84–5.06 should be

used to determine $G_{c12}$. The effect of $\xi$ on $G_{c12}$ is found to be negligible; for $G_f$ = 2.0 GPa, $G_{c12}$ ranges from 1.49–1.51 for $\xi$ ranging from 1.00–5.06.

$$\kappa = \frac{A_C}{A_T} = \frac{\pi \frac{d^2}{4}}{\pi \frac{ab}{4}} = \frac{d^2}{ab} = \frac{a}{b} \quad (\text{for } \kappa > 1 \text{ and assuming } d = a) \qquad \text{Eq. 5.30}$$

$$\xi = \left(\frac{a}{b}\right)^{\sqrt{3}} \quad (\text{for } G_{c12}) \qquad \text{Eq. 5.31}$$

Fig. 5.16 shows that using $G_{c12}$ = 1.51 GPa (taking $G_f$ = 2.0 GPa in Eq. 5.29) gives the best fit Eq. 5.28 for the experimental data of flax/polyester. Using the shear modulus of native cellulose as 4.4 GPa [18], Baley [17] estimated the shear modulus of flax fibre to be in the range of $G_f$ = 2.4–3.4 GPa. For jute/epoxy composites, Cichocki *et al.* [61] measured $G_f$ and $G_{c12}$ to be 3.5 GPa and 1.4 GPa, respectively. In a study by Ntenga *et al.* [60] $G_{c12}$ was measured to be 1.68–2.04 GPa for sisal–epoxy composites. Hence, the shear modulus of flax and its composite determined in this study are in agreement with other studies in literature.

The macroscopic response of the composite, in the form of longitudinal and transverse stiffness, can be incorporated in other micro-mechanics equations to determine fibre properties. The longitudinal tensile modulus $E_{f,0}$ of the flax fibres can be back-calculated using the rule of mixtures (Eq. 5.32) to be $E_{f,0}$ = 46.3 GPa. This is in the range of literature values [13, 30] generally quoted for flax.

$$E_{f,0} = \frac{1}{v_f}\left[E_{c,0} - v_m E_m\right] \qquad \text{Eq. 5.32}$$

The transverse tensile modulus $E_{f,90}$ of the flax fibres can be estimated by re-arranging the semi-empirical Halpin-Tsai equation [69] from Eq. 5.33 to Eq. 5.34. Typically, assuming circular cross-section flax fibres [69, 70] and using $\xi$ = 2 produces satisfactory results for PFRPs [8, 17]. Halpin and Kardos [70] have semi-empirically derived Eq. 5.35 to determine the fibre shape factor $\xi$ for composites with elliptical/rectangular cross-section fibres to calculate $E_{f,90}$. As a quick check of Eq. 5.35, in the limiting case for circular cross-section fibres, $\xi$ = 2 since $a$ = $b$. For

elliptical plant fibres with $a/b$ = 1.42–2.55, $\xi$ = 2.84–5.10 should be used to determine $E_{f,90}$. Again, it should be noted that the effect of $\xi$ on $E_{f,90}$ is found to be negligible. Substituting the relevant material data ($E_m$, $E_{c,90}$, $v_f$) into Eq. 5.34 gives the transverse tensile modulus of flax to be $E_{f,90}$ = 3.9 GPa for $\xi$ = 2.84–5.10. Nonetheless, this estimate of fibre transverse tensile modulus $E_{f,90}$ is in the range of values found by other researchers: 5–9 GPa for flax fibres [58], 5.5 GPa for jute fibres [61] and 1.4 GPa for sisal fibres [60]. The ratio of longitudinal to transverse fibre stiffness is 11.7 and hence the fibres are highly anisotropic. This is also in agreement with findings from other studies, where fibre anisotropy ratios of 8.4 for flax [58], 7.2 for jute [61], 7.7 for hemp [8] and 8.1 for sisal [60] have been reported.

$$E_{c,90} = \frac{E_m\left(1+\xi\eta v_f\right)}{\left(1-\eta v_f\right)}, \text{ where } \eta = \frac{\frac{E_{f,90}}{E_m}-1}{\frac{E_{f,90}}{E_m}+\xi} \qquad \text{Eq. 5.33}$$

$$E_{f,90} = \frac{E_m\xi\left(1-v_f\right)-E_{c,90}\left(\xi+v_f\right)}{\frac{E_{c,90}}{E_m}\left(1-v_f\right)-\left(1+\xi v_f\right)} \qquad \text{Eq. 5.34}$$

$$\xi = 2\left(\frac{a}{b}\right) \text{ (for } E_{c,90}\text{)} \qquad \text{Eq. 5.35}$$

*Fracture stress*

The influence of ply orientation $\theta$ on the tensile strength $\sigma_c$ of the composites is graphically presented in Fig. 5.17. Unidirectional flax/polyester composites loaded in the fibre direction (i.e. 0°) have a tensile strength $\sigma_0$ of 143.0 ± 6.8 MPa. This is 10.8 times higher than the composite transverse tensile strength $\sigma_{90}$ of 13.2 ± 0.4 MPa. Madsen *et al.* [8] noted a similar ratio between longitudinal (205 ± 5 GPa) and transverse tensile strength (19 ± 0 GPa) from tests on hemp/PET composites ($v_f \approx$ 33.5%).

Again, it is observed from Fig. 5.17 that the composite tensile strength drops significantly for increasing loading angle between $0° < \theta < 30°$. For $30° < \theta < 90°$, there is little variation in composite strength. The composite off-axis fracture stress

$\sigma_\theta$ can be predicted using either the maximum stress (Stowell-Liu) criterion [52] or the maximum strain energy (Tsai-Hill) criterion [50]. The maximum stress criterion is defined by three equations (Eq. 5.36), each of which characterises three failure regimes. The Tsai-Hill criterion is defined by Eq. 5.37. Both failure criteria require three known composite properties: longitudinal and transverse tensile strength ($\sigma_0$, $\sigma_{90}$) and inter-laminar shear strength $\tau$. As $\sigma_0$ and $\sigma_{90}$ have been measured, it is possible to adjust the value of $\tau$, so that the micro-mechanical criteria can be used to fit the experimental data using least squares non-linear regression.

$$\sigma_\theta = \begin{cases} \dfrac{\sigma_0}{\cos^2\theta} & \text{(longitudnal tensile failure of fibres, } \theta < 5°) \\ \dfrac{\tau}{\sin\theta\cos\theta} & \text{(shear failure at fibre/matrix interface, } 5° < \theta < 45°) \\ \dfrac{\sigma_{90}}{\sin^2\theta} & \text{(transverse tensile failure of fibres, } 45° < \theta < 90°) \end{cases} \qquad \text{Eq. 5.36}$$

$$\sigma_\theta = \left[ \frac{1}{\sigma_0^{\,2}}\cos^4\theta + \left( \frac{1}{\tau^2} - \frac{1}{\sigma_0^{\,2}} \right)\cos^2\theta\sin^2\theta + \frac{1}{\sigma_{90}^{\,2}}\sin^4\theta \right]^{-0.5} \qquad \text{Eq. 5.37}$$

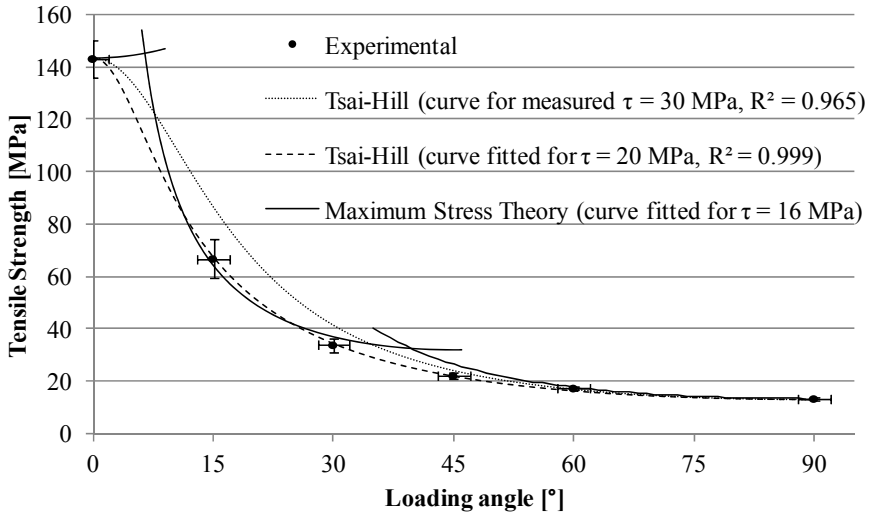


**Fig. 5.17. Variation in tensile strength of unidirectional flax/polyester composites for increasing off-axis loading angle. Experimental data (•) is presented with error bars (1 stdev). Lines are theoretical predictions using Tsai-Hill criterion (dotted) and maximum stress theory (solid) for different composite shear strength $\tau$.**

From Fig. 5.17, it is observed that the maximum stress criterion and the Tsai-Hill criterion are in good agreement with the experimental data, for $\tau$ = 16 MPa and 20 MPa, respectively. Chamis and Sinclair [75, 76] have reported that the inter-laminar shear strength can be extracted from the 10° off-axis tensile test of a unidirectional specimen. Although the tensile strength of a unidirectional flax/polyester specimen loaded at an off-axis angle of 10° has not been tested in this study, data from the 15° off-axis test can be used to estimate the inter-laminar shear strength to be $\tau$ = 16.7 MPa. This is in good agreement with the estimated inter-laminar shear strength of 16-20 MPa (Fig. 5.17).

*Incorporating the effect of yarn twist*

Curve fitting methods and micro-mechanical criteria (Eq. 5.28, Eq. 5.36 and Eq. 5.37) have enabled accurate prediction of the dependence of PFRP tensile properties (stiffness and strength) on ply orientation. As an extension, it is possible to rearrange Eq. 5.28 and Eq. 5.37 in the form of Eq. 5.38 and Eq. 5.39 respectively. This is useful for two reasons. Firstly, Eq. 5.38 and Eq. 5.39 require stiffness ratios ($E_{c,0}/G_{c12}$, $E_{c,0}/E_{c,90}$) and strength ratios ($\sigma_0/\sigma_{90}$, $\sigma_0/\tau$) as inputs. Typical values of these ratios are presented in Table 5.4. These values can be used in conjunction with Eq. 5.38 and Eq. 5.39 for preliminary design of structural composites from PFRPs.

$$\frac{E_{c,\theta}}{E_{c,0}} = \left[ \cos^4\theta + \left( \frac{E_{c,0}}{G_{c12}} - 2\nu_{c12} \right) \cos^2\theta \sin^2\theta + \frac{E_{c,0}}{E_{c,90}} \sin^4\theta \right]^{-1} \qquad \text{Eq. 5.38}$$

$$\frac{\sigma_\theta}{\sigma_0} = \left[ \cos^4\theta + \left( \left( \frac{\sigma_0}{\tau} \right)^2 - 1 \right) \cos^2\theta \sin^2\theta + \left( \frac{\sigma_0}{\sigma_{90}} \right)^2 \sin^4\theta \right]^{-0.5} \qquad \text{Eq. 5.39}$$

Secondly, while the contribution of yarn twist on ply orientation has been neglected in this study, Eq. 5.38 and Eq. 5.39 can be modified to accommodate for the effect of yarn twist on the off-axis tensile properties of PFRPs. In Section 5.3, we developed a mathematical model that accurately predicts the effect of reinforcing yarn surface twist angle $\alpha$ on PFRP tensile strength $\sigma_0$. Baets *et al.* [37] have also applied existing models which relate yarn surface twist angle $\alpha$ to PFRP tensile modulus $E_{c,0}$. These models can be substituted for $E_{c,0}$ and $\sigma_0$ in Eq. 5.38 and Eq. 5.39.

**Table 5.4. Typical values of strength and stiffness ratios for unidirectional PFRPs found from literature.**

| *Composite* | $v_f$ [%] | $E_{c,0}$ [GPa] | $E_{c,0}/E_{c,90}$ | $E_{c,0}/G_{c12}$ | $\sigma_0$ [MPa] | $\sigma_0/\sigma_{90}$ | $\sigma_0/\tau$ | $v_{c12}$ | *Source* |
|---|---|---|---|---|---|---|---|---|---|
| Flax/polyester | 26.9 | 15.3 | 4.1 | 10.1 | 143 | 10.8 | 7.2 | - | |
| Hemp/PET | 33.5 | 17.6 | 5.0 | 9.3 | 205 | 10.8 | 7.9 | - | [8] |
| Jute/epoxy | 30.0 | 13.8 | 3.7 | 9.9 | - | - | - | 0.31 | [61] |
| Flax/epoxy | 40.0 | 26.0 | 6.5 | - | 190 | 19.0 | - | - | [7] |
| Flax/epoxy | 48.0 | 32.0 | 8.0 | - | 268 | 14.9 | - | - | [7] |
| Sisal/epoxy | 39.0 | 6.9 | 2.6 | 3.7 | - | - | - | 0.42 | [60] |

While the resulting equations can then be used to obtain indicative off-axis properties inclusive of the contribution from yarn twist, the equations should be used with caution. This is because, unlike 2D ply orientation, yarn twist is a complex 3D phenomenon. Firstly, the twist angle of an arbitrary fibre in the yarn is a function of *i)* its radial position in the yarn, *ii)* yarn twist level, *iii)* yarn packing fraction and *iv)* yarn density. Secondly, the twist level of the reinforcing yarn will not only affect $E_{c,0}$ and $\sigma_0$, but will also affect the stiffness and strength ratios, which are additional inputs to Eq. 5.38 and Eq. 5.39. In fact, the effect of yarn twist on *i)* in-plane ($E_{c,90}$, $\sigma_{90}$, $G_{c12}$, $\tau$), *ii)* out-of-plane and *iii)* off-axis properties of PFRPs warrants specific investigation.

#### 5.4.3.3 Fracture strain and fracture modes

The failure strain of unidirectional flax/polyester composites decreases with increasing off-axis loading angle (Fig. 5.18). While composites loaded in the fibre direction (*i.e.* 0°) have a failure strain of 1.56 ± 0.04 %, composites loaded in the transverse direction (*i.e.* 90°) have a failure strain of only 0.49 ± 0.03 %.

A more insightful observation is that while the transverse failure strain of unidirectional flax/polyester decreases linearly with increasing fibre content [58], the longitudinal failure strain of unidirectional flax/polyester increases with increasing fibre content, before levelling off. This is graphically presented in Fig. 5.19.

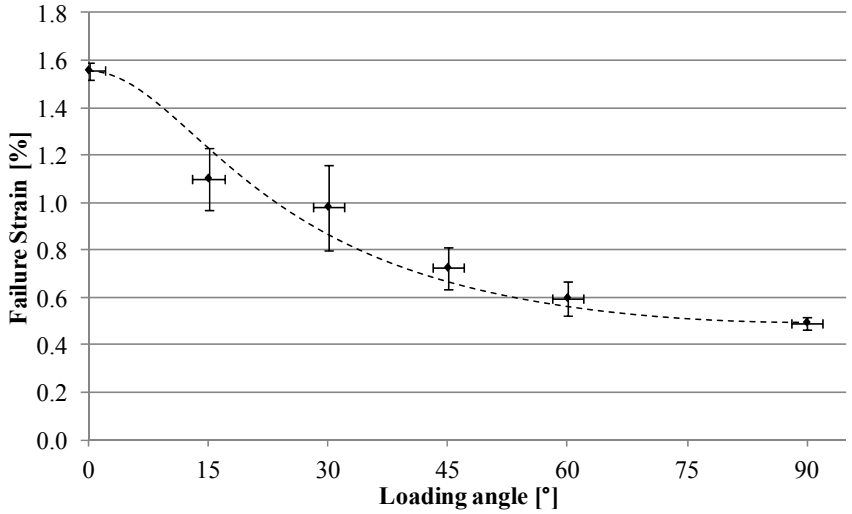


**Fig. 5.18. Variation in failure strain of unidirectional flax/polyester composites for increasing off-axis loading angle.**

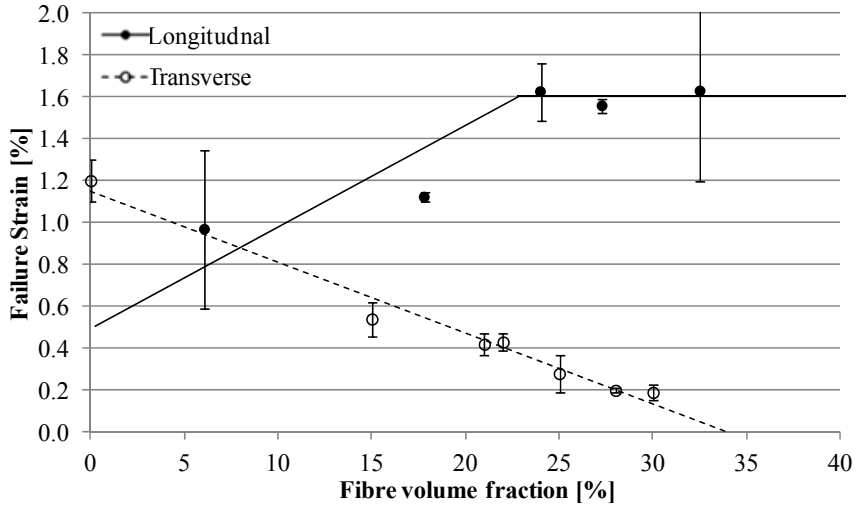


**Fig. 5.19. Variation in (•) longitudinal and (o) transverse failure strain of unidirectional flax/polyester composites for increasing fibre volume fraction. Results are from *Chapter 4* (for longitudinal) and [58] (for transverse).**

These observations are indicative of changes in failure mode with increasing off-axis loading angle. For low off-axis angles ($\theta < 5°$), the composite failure strain of 1.56% is close to the tensile failure strain of a single flax fibre. The SEM micrograph in Fig. 5.20a) confirms that the composite fracture surface is serrated and irregular due to

fibre-dominated failure. Extensive fibre pull-out is also observed and the lateral surfaces of these pulled out fibres are clear from matrix residue; this is indicative of poor adhesion between fibre and matrix. While some matrix laceration is observed, matrix cleavage and irregular fibre fracture surfaces are attributable to longitudinal tensile fracture of the composite [76]. As the fibres are failing in pure tension, the corollary is that increasing the fibre content would lead to an increase in the longitudinal failure strain of the composite, before levelling off at the fibre failure strain. This is observed in Fig. 5.19.

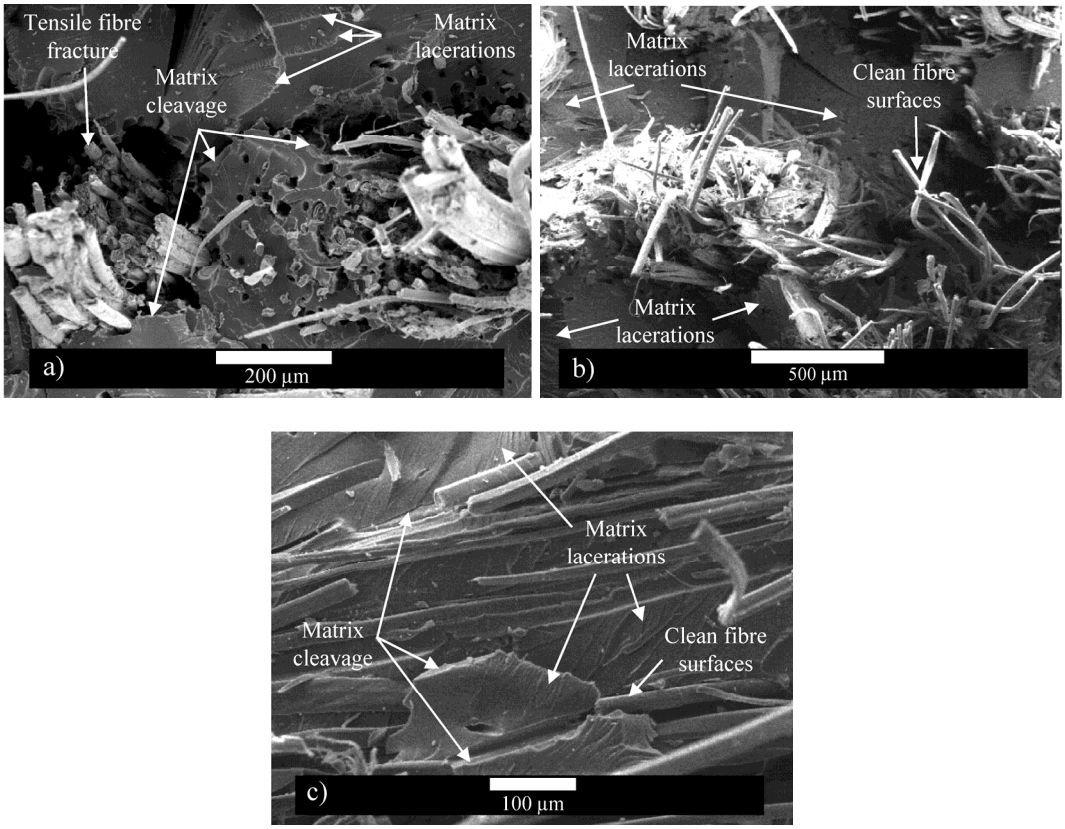


**Fig. 5.20. Fracture surfaces of flax/polyester at different off-axis load angles present different fracture modes: *a)* $\theta$ = 0°, longitudinal tensile fracture, fibre-dominated failure; *b)* $\theta$ = 15°, inter-laminar shear; *c)* $\theta$ = 90°, transverse fracture, matrix-dominated failure.**

In the range of 5° < θ < 45°, the fracture strain reduces drastically from 1.5% to 0.5%. As misorientation increases, inter-laminar shear stresses and then transverse tensile stresses become more dominant [75]. The SEM micrograph in Fig. 5.20b)

shows that the fracture surface is dominated by matrix lacerations, indicating some inter-laminar shear stress fracture [76]. Some matrix cleavage (with irregular boundary) is also observed due to transverse tensile fracture of the matrix [76]. Again the fibre surfaces are free from matrix residue due to poor interfacial bonding.

For off-axis angles in the range of $45° < \theta < 90°$, the failure strain is very low (0.5–0.7%). This is because flax fibres and their composites are highly anisotropic and transverse tensile stress is the predominant fracture mode in this range [75]. The SEM micrograph in Fig. 5.20c) confirms that the fracture surface is dominated by extensive matrix cleavage. However, some matrix laceration is observed in resin rich zones, indicating shear fracture. Baley *et al.* [58] have reported that during transverse failure of unidirectional flax/polyester composites, cracks propagate along the fibre-matrix interface. These observations are consistent with the fracture surface in Fig. 5.20c), as the fibre surfaces are free from matrix residue suggesting poor fibre-matrix adhesion. An increase in the fibre content would lead to more fibre-matrix interfaces. Hence, crack propagation would be easier and the failure strain would be smaller for high fibre content PFRPs loaded in the transverse direction [58]. This is observed in Fig. 5.19.

### 5.4.4 Conclusions

The highly anisotropic nature of plant fibres and their aligned composites implies that misorientation influences their tensile behaviour significantly. For PFRPs to be readily considered for structural applications, an experimental assessment of their off-axis mechanical behaviour is essential.

A key finding of this study is that due to the non-linear stress-strain response of PFRPs, the apparent stiffness of the composite reduces by ~30% in the strain range of 0.05–0.25%. In addition, through cyclic tests on the composites, the elastic strain limit is found to be only ~0.15%. This has major implications on the strain range to be used for the determination of the composite elastic Young's modulus. Consequently, it is proposed that the tensile modulus for PFRPs should be measured in the strain range of 0.025–0.100%. It is argued that the non-linear stress-strain

response (decreasing 'apparent' stiffness with increasing strain) of single plant fibres has been transferred to the PFRPs.

The PFRP elastic modulus, tensile strength and failure strain reduce drastically with increasing off-axis loading angle. In fact, biaxial (±45°) composites have better mechanical properties than uniaxial composites loaded at off-axes angles larger than 30°. Conventional composite micro-mechanical models are found to be in good agreement with the experimental data, suggesting that reliable prediction of PFRP off-axis properties is possible. The application of such models has enabled the determination of, otherwise difficult to measure, material properties through numerical methods. For instance, the shear modulus and transverse modulus of flax fibre is determined to be 2.0 GPa and 3.9 GPa, respectively. Through qualitative analysis of the fracture surfaces of off-axis loaded PFRPs, three distinct fracture modes are determined in three different off-axis ranges.

## 5.5 REFERENCES


1. Carus M. Bio-composites: Technologies, applications and markets, in *4th International Conference on Sustainable Materials, Polymers and Composites*. 6-7 July 2011. Birmingham, UK.
2. Faruk O, Bledzki AK, Fink HP, Sain M. Biocomposites reinforced with natural fibres: 2000-2010. *Progress in Polymer Science*, 2012, 37(11): p. 1552-1596.
3. Krenchel H. Fibre reinforcement. *Akademisk Forlag*, 1964: p. 16-22.
4. Lu Y. *Mechanical properties of random discontinuous fiber composites manufactured from wet-lay process*. MSc, 2002. Virginia Polytechnic Institute and State University: Blacksburg, Virginia.
5. Madsen B. *Properties of plant fibre yarn polymer composites - An experimental study*. PhD, 2004. Technical University of Denmark: Lyngby, Denmark.
6. George J, Ivens J, Verpoest I. Mechanical properties of flax fibre reinforced epoxy composites. *Die Angewandte Makromolekulare Chemie*, 1999, 272(1): p. 41-45.
7. Weyenberg I, Chitruong T, Vangrimde B, Verpoest I. Improving the properties of UD flax fibre reinforced composites by applying an alkaline fibre treatment. *Composites Part A: Applied Science and Manufacturing*, 2006, 37: p. 1368-1376.
8. Madsen B, Hoffmeyer P, Lilholt H. Hemp yarn reinforced composites – II. Tensile properties. *Composites Part A: Applied Science and Manufacturing*, 2007, 38: p. 2204-2215.
9. Mutje P, Girones J, Lopez A, Llop MF, Vilaseca F. Hemp strands: PP composites by injection molding: Effect of low cost physico-chemical treatments. *Journal of Reinforced Plastics and Composites*, 2006, 25: p. 313-327.
10. Shahzad A. Hemp fiber and its composites - A review. *Journal of Composite Materials*, 2012, 46(8): p. 973-986.
11. Summerscales J, Hall W, Virk AS. A fibre diameter distribution factor (FDDF) for natural fibre composites. *Journal of Materials Science*, 2011, 46(17): p. 5876-5880.

12. Placet V, Trivaudey F, Cisse O, Gucheret-Retel V, Boubakar ML. Diameter dependence of the apparent tensile modulus of hemp fibres: A morphological, structural or ultrastructural effect? *Composites Part A: Applied Science and Manufacturing*, 2012, 43(2): p. 275-287.
13. Pickering K, ed. *Properties and performance of natural-fibre composites*. 2008. CRC Press LLC: Boca Raton.
14. Diddens I, Murphy B, Krisch M, Muller M. Anisotropic elastic properties of cellulose measured using inelastic x-ray scattering. *Macromolecules*, 2008, 41(24): p. 9755–9759.
15. Mark R. *Cell wall mechanics of tracheids*, 1967. New Haven: Yale University Press.
16. Nishino T, Takano K, Nakamae K. Elastic modulus of the crystalline regions of cellulose polymorphs. *Journal of Polymer Science B*, 1995, 33: p. 1647-1651.
17. Baley C. Analysis of the flax fibres tensile behaviour and analysis of the tensile stiffness increase. *Composites Part A: Applied Science and Manufacturing*, 2002, 33: p. 939-948.
18. Gassan J, Chate A, Bledzki AK. Calculation of elastic properties of natural fibers. *Journal of Materials Science*, 2001, 36: p. 3715-3720.
19. Bergander A, Salmen L. Cell wall properties and their effects on the mechanical properties of fibers. *Journal of Materials Science*, 2002, 37: p. 151-156.
20. Bledzki A, Gassan J. Composites reinforced with cellulose based fibres. *Progress in Polymer Science*, 1999, 24: p. 221-274.
21. McLaughlin E, Tait RA. Fracture mechanism of plant fibres. *Journal of Materials Science*, 1980, 15: p. 89-95.
22. Mukherjee P, Satyanarayana KG. An empirical evaluation of structure-property relationships in natural fibres and their fracture behaviour. *Journal of Materials Science*, 1986, 21: p. 4162-4168.
23. Reiterer A, Lichtenegger H, Tschegg S, Fratzl P. Experimental evidence for a mechanical function of the cellulose microfibril angle in wood cell walls. *Philosophical Magazine A*, 1999, 79(9): p. 2173-2184.
24. Sheng-zuo F, Wen-zhong Y, Xiang-xiang FU. Variation of microfibril angle and its correlation to wood properties in poplars. *Journal of Forestry Research*, 2004, 15(4): p. 261-267.
25. Via B, So CL, Shupe TF, Groom LH, Wikaira J. Mechanical response of longleaf pine to variation in microfibril angle, chemistry associated wavelengths, density, and radial position. *Composites Part A: Applied Science and Manufacturing*, 2009, 40: p. 60-66.
26. Burgert I, Fratzl P. Plants control the properties and actuation of their organs through the orientation of cellulose fibrils in their cell walls. *Integrative and Comparative Biology*, 2009, 49(1): p. 69-79.
27. Satyanarayana K, Pillai CKS, Sukumaran K, Pillai SGK, Rohatgi PK, Vijayan K. Structure property studies of fibres from various parts of the coconut tree. *Journal of Materials Science*, 1982, 17: p. 2453-2462.
28. Spatz H, Kohler L, Niklas KJ. Mechanical behaviour of plant tissues: composite materials or structures? *The Journal of Experimental Biology*, 1999, 202: p. 3269–3272.
29. Suslov D, Verbelen JP. Cellulose orientation determines mechanical anisotropy in onion epidermis cell walls. *Journal of Experimental Botany*, 2006, 57(10): p. 2183-2192.
30. Lewin M. *Handbook of fiber chemistry*. Third ed, 2007. Boca Raton: CRC Press LLC.

31. Barnett J, Bonham VA. Cellulose microfibril angle in the cell wall of wood fibres. *Biological Reviews*, 2004, 79: p. 461-472.
32. Dissanayake N, Summerscales J, Grove SM, Singh MM. Life cycle impact assessment of flax fibre for the reinforcement of composites. *Journal of Biobased Materials and Bioenergy*, 2009, 3(3): p. 1-4.
33. Finn N, Miao M. Low cost composite preforms from natural fibres, in *Composites Australia 2008: Conference & Exhibition*. 13-14 March 2008. Melbourne, Australia.
34. Arnold E, Weager, BM, Hoydonckx HE, Madsen B. Next generation sustainable composites: Development and processing of furan-flax biocomposites, in *17th International Conference on Composite Materials*. 27-31 July 2009. Edinburgh, UK.
35. Goutianos S, Peijs T, Nystrom B, Skrifvars M. Development of flax fibre based textile reinforcements for composite applications. *Applied Composite Materials*, 2006, 13(4): p. 199-215.
36. Goutianos S, Peijs T. The optimisation of flax fibre yarns for the development of high-performance natural fibre composites. *Advanced Composites Letters*, 2003, 12(6): p. 237-241.
37. Baets J, Plastria D, Ivens J, Verpoest I. Determination of the optimal flax fibre preparation for use in UD-epoxy composites, in *4th International Conference on Sustainable Materials, Polymers and Composites*. 6-7 July 2011. Birmingham, UK.
38. Zhang L, Miao M. Commingled natural fibre/polypropylene wrap spun yarns for structured thermoplastic composites. *Composites Science and Technology*, 2010, 70: p. 130-135.
39. Ma H, Li Y, Luo Y. The effect of fiber twist on the mechanical properties natural fiber reinforced composites, in *18th International Conference on Composite Materials*. 2011. Jeju, South Korea.
40. Rao Y, Farris, RJ. A modeling and experimental study of the influence of twist on the mechanical properties of high-performance fiber yarns. *Journal of Applied Polymer Science*, 2000, 77: p. 1938-1949.
41. Naik N, Madhavan V. Twisted impregnated yarns: Elastic properties. *Journal of Strain Analysis*, 2000, 35(2): p. 83-91.
42. Shioya M, Itoh T, Kunugi T, Takaku A. Variation of longitudinal modulus with twist for yarns composed of high modulus fibers. *Textile Research Journal*, 2001, 71: p. 928-936.
43. Baets J, Plastria D, Ivens J, Verpoest I. Determination of the optimal flax fibre preparation for use in UD-epoxy composites, in *18th International Conference on Composite Materials (ICCM-18)*. 2011. Jeju, South Korea.
44. Rask M, Madsen B. Twisting of fibres in yarns for natural fibre composites, in *18th International Conference on Composite Materials (ICCM-18)*. 2011. Jeju, South Korea.
45. Gegauff G. Force et elasticite des files en cotton. *Bulletin De La Societe Industrielle De Mulhouse*, 1907, 77: p. 153.
46. Platt M. Mechanics of elastic performance of textile materials, Part III: Some aspects of stress analysis of textile structures - Continuous filament yarns. *Textile Research Journal*, 1950, 20: p. 1.
47. Hearle J, Grosberg P, Backer S. Structural mechanics of yarns and fabrics. Vol. 1 p. 180, 1969. New York: Wiley-Interscience.
48. Pan N. Development of a constitutive theory for short fiber yarns: Mechanics of staple yarn without slippage effect. *Textile Research Journal*, 1992, 62(12): p. 749-765.
49. Yilmaz D, Göktepe F, Göktepe O, Kremenakova D. Packing density of compact yarns. *Textile Research Journal*, 2007, 77(9): p. 661-667.

50. Azzi V, Tsai SW. Anisotropic strength of composites. *Experimental Mechanics*, 1965, 5: p. 283-288.
51. Madsen B, Hoffmeyer P, Thomsen AB, Lilholt H. Hemp yarn reinforced composites – I. Yarn characteristics. *Composites Part A: Applied Science and Manufacturing*, 2007, 38: p. 2194–2203.
52. Harris B. *Engineering composite materials*, 1999. London: The Institute of Materials.
53. Naik N, Singh MN. Twisted impregnated yarns: Transverse tensile strength. *Journal of Strain Analysis for Engineering Design*, 2001, 36(4): p. 347-358.
54. Summerscales J, Dissanayake N, Virk AS, Hall W. A review of bast fibres and their composites. Part 2 – Composites. *Composites Part A: Applied Science and Manufacturing*, 2010, 41(10): p. 1336-1344.
55. Pan N. Development of a constitutive theory for short fiber yarns: Part III: Effects of fiber orientation and bending deformation. *Textile Research Journal*, 1993, 63(7): p. 565-572.
56. Kelly A, Tyson WR. Tensile properties of fibre-reinforced metals: Copper/tungsten and copper/molybdenum. *Journal of the Mechanics and Physics of Solids*, 1965, 13(6): p. 329-350.
57. Aghdam M, Pavier MJ, Smith DJ. Micro-mechanics of off-axis loading of metal matrix composites using finite element analysis. *International Journal of Solids and Structures*, 2001, 38: p. 3905-3925.
58. Baley C, Perrot Y, Busnel F, Guezenoc H, Davies P. Transverse tensile behaviour of unidirectional plies reinforced with flax fibres. *Materials Letters*, 2006, 60: p. 2984-2987.
59. Kumar P. Mechanical behaviour of jute fibre and their composites. *Indian Journal of Technology*, 1986, 24: p. 29-32.
60. Ntenga R, Béakou A, Atéba JA, Ohandja LA. Estimation of the elastic anisotropy of sisal fibres by an inverse method. *Journal of Materials Science*, 2008, 43: p. 6206-6213.
61. Cichocki JF, Thomason JL. Thermoelastic anisotropy of a natural fiber. *Composites Science and Technology*, 2002, 62: p. 669-678.
62. Aly M, Goda IGM, Hassan GA. Experimental investigation of the dynamic characteristics of laminated composite beams. *International Journal of Mechanical & Mechatronics*, 2011, 10(3): p. 59-68.
63. *BS EN ISO 527-4:1997 (BS 2782-3)*, *Plastics - Determination of tensile properties - Part 4: Test conditions for isotropic and orthotropic fibre-reinforced plastic composites*, 1997. British Standards Instituition: London.
64. Chamis C. *NASA TN-D6696*, Design properties of randomly reinforced fibre composites, 1972. Nationaol Aeronautics and Space Administration: Washington DC.
65. Herrera-Franco P, Valadez-Gonzalez A. Mechanical properties of continuous natural fibre-reinforced polymer composites. *Composites Part A: Applied Science and Manufacturing*, 2004, 35(3): p. 339-345.
66. Charlet K, Jernot JP, Moussa G, Baley C, Bizet L, Breard J. Morphology and mechanical behaviour of a natural composite: the flax fiber, in *16th International Conference on Composite Materials (ICCM-16)*. 2007. Kyoto, Japan.
67. Hughes M, Carpenter J, Hill C. Deformation and fracture behaviour of flax fibre reinforced thermosetting polymer matrix composites. *Journal of Materials Science*, 2007, 42: p. 2499-2511.
68. Carpenter J, Miao M, Brorens P. Deformation behaviour of composites reinforced with four different linen flax yarn structures. *Advanced Materials Research*, 2007, 29-30: p. 263-266.

69. Halpin J, Tsai SW. *AFML-TR-67-423*, Environmental factors in composite design, 1967. Wright Aeronautical Laboratories: Dayton.
70. Halpin J, Kardos JL. The Halpin-Tsai equations: A review. *Polymer Engineering and Science*, 1976, 16(5): p. 344-352.
71. Thomason J, Carruthers J, Kelly J, Johnson G. Fibre cross-section determination and variability in sisal and flax and its effects on fibre performance characterisation. *Composites Science and Technology*, 2011, 71: p. 1008-1015.
72. Virk A. *Numerical models for natural fibre composites with stochastic properties*. PhD, 2010. University of Plymouth: Plymouth, UK.
73. d'Almeida J, Mauricio MHP, Paciornik S. Evaluation of the cross-section of lignocellulosic fibers using digital microscopy and image analysis. *Journal of Composite Materials*, 2012, 46(24): p. 3057-3065.
74. Thomason J, Gentles F, Brennan A. Natural fibre cross sectional area effects on the determination of fibre mechanical properties, in *15th European Conference on Composite Materials (ECCM-15)*. 2012. Venice, Italy.
75. Sinclair J, Chamis CC. Fracture modes in off-axis fiber composites. *Polymer Composites*, 1981, 2(1): p. 45-52.
76. Sinclair J, Chamis CC. *NASA TP-1081*, Mechanical behavior and fracture characteristics of off-axis fiber composites: I - Experimental Investigation, 1977. NASA: Cleveland.

# 6 FATIGUE LIFE EVALUATION OF PLANT YARN REINFORCED COMPOSITES*

## 6.1 INTRODUCTION

Fatigue loads are often 'normal operation' loads for many structural applications, including wind turbine blades, buildings, bridges, helicopters and aeroplanes (Fig. 6.1) [1]. In general, fatigue occurs when a material is subjected to repeated, variable/constant amplitude loading-unloading-reloading cycles, over a period of time. The fatigue life of a material, defined as the number of cycles to failure, is dependent on several factors including stress level, stress state, mode of cycling, process history, material composition, dimension and geometry, load history, environmental conditions, and lastly, by the mutual influence of all these parameters [2]. Importantly, the fatigue strength of a material (or the nominal maximum stress $S_{max}$ a material can endure under cyclic loads) is less than the ultimate stress limit $S_0$ (under static loads). Moreover, $S_{max}/S_0$ reduces with increasing number of load cycles. Hence, if a material is to be employed in a fatigue critical component, it is imperative that its response to cyclic loads is well-characterised.

Natural fibres for composite applications have become a topic of growing interest. Although the usage of plant fibre composites (PFRPs) is on the rise, certain aspects of their behaviour are still inadequately understood or investigated. To date, there exists neither an adequate database of PFRPs subjected to cyclic loads (in the form of stress-life diagrams and lifetime data), nor an adequate fatigue lifetime prediction methodology (in the form of constant-life diagrams) for structures built from PFRPs. On the other hand, the fatigue behaviour of E-glass composites (GFRPs) is well-

* This chapter is based on the peer-reviewed journal article:

Shah DU, Schubel PJ, Licence P, Clifford MJ, Fatigue life evaluation of aligned plant fibre composites through S-N curves and constant-life diagrams. *Composites Science and Technology*, 2013, 74: p. 139-149.

documented. This seriously limits the prospective use of PFRPs, and the potential replacement of GFRPs, in fatigue critical structural components.

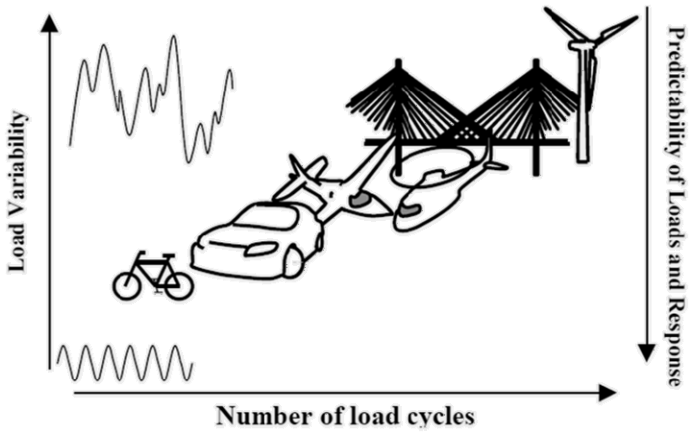


**Fig. 6.1. The severity of fatigue in structural components depends on *i)* load variability, *ii)* number of load cycles, and *iii)* predictability of loads and component response [1].**

## 6.2 LITERATURE REVIEW

A few researchers have attempted to uncover the fatigue behaviour of plant fibres and their composites. Investigating the cyclic loading behaviour of single plant leaf fibres, Spatz *et al.* [3] observed that the fibre elastic modulus increased with subsequent loading cycles due to the progressive reorientation of the cellulose microfibrils towards the loading direction. Baley [4] and Silva *et al.* [5] also reported this strain hardening behaviour for flax and sisal fibres, the majority of which occurs during the early stages of cyclic deformation. For instance, the flax fibre elastic modulus can increase by 60-80% between the 1$^{st}$ and the 200$^{th}$ cycle (from 40 GPa to 72 GPa) [4]. With an average ultimate tensile strength (UTS) of 400 MPa, sisal fibres can survive at least $10^6$ cycles when subjected to a ratio of maximum applied fatigue stress to ultimate tensile strength $S_{max}/UTS$ of 0.5 [5]. The slope of the S-N curve for a single sisal fibre is approximately 9% of the UTS per decade of cycles [5]. In comparison, E-glass fibres with average UTS of 2130 MPa survive at least $10^6$ cycles when subjected to a higher ratio $S_{max}/UTS$ of 0.8 with their fatigue strength degrading at a slower rate of 3% per decade of cycles [6].

The fatigue fracture surface of plant fibres shows formation of micro-cracks in the secondary cell wall (perpendicular to the load), followed by subsequent propagation to the middle lamellae and delamination between adjacent fibres [5, 7]. In addition, a characteristic peeling-off of the primary/secondary cell wall layers is also observed, due to degradation of the cellulosic fibrillar structure and the weakening of the cellulose/lignin-hemicellulose interface, with increasing number of load cycles [5, 7].

The fatigue deformation mechanism of a fibre reinforced composite is more complex and largely dependent on strain development and damage accumulation at the fibre/matrix interface [8]. Unlike metals, composite materials are inhomogeneous and anisotropic. While fatigue in metals is a localised process involving the nucleation and growth of a dominant crack to unstable failure, fatigue in composites occurs in a general fashion due to the gradual accumulation and interaction of dispersed damage [8].

Recently, Liang *et al.* [9] compared the tension-tension (stress ratio of $R = 0.1$) fatigue behaviour of biaxial flax/epoxy and glass/epoxy composites. The authors found that while glass/epoxy composites exhibit a higher resistance to fatigue loading due to their higher static strength, the stress-life (S-N) curve of glass/epoxy is much steeper implying a more significant decrease in fatigue strength with respect to cycles to failure. In fact, the fatigue stress level drops by 57 and 21 MPa every decade of cycles for [0,90] and [±45] glass/epoxy composites, but by only 25 and 7 MPa every decade for [0,90] and [±45] flax/epoxy composites. In composite materials, fatigue damage does not always immediately reduce the strength of the composite, although it often reduces the stiffness [8]. Liang *et al.* [9] reported that while the stiffness of glass/epoxy composites reduced by 7-25% and 50-70% for [0,90] and [±45] samples, flax/epoxy composites offered a more stable fatigue performance during their fatigue life with a stiffness increase of 2% or decrease of only 15-20% for [0,90] and [±45] samples, respectively.

In an extensive study on fibre and interface parameters affecting the tension-tension fatigue behaviour of PFRPs, Gassan [10, 11] recorded the dynamic stress-strain curve and calculated the specific damping capacity SDC (ratio of energy dissipated

every cycle to the initial maximum strain energy [11]) as a value indicative of progressive material damage. However, a material SDC-load curve is not useful when designing against fatigue. Nonetheless, the author found that PFRPs manufactured with *i)* fibres of higher strength and modulus, *ii)* improved fibre/matrix interface through fibre surface treatment, *iii)* unidirectional plies rather than woven biaxial architecture, or *iv)* higher fibre volume fractions, possess *a)* higher damage initiation loads, *b)* comparable or lower damage propagation rates, and *c)* higher failure loads.

Towo and Ansell [12, 13] conducted a more classic study on the fatigue properties of unidirectional sisal fibre thermoset matrix composites, presenting data in the more convenient format of S-N diagrams and constant life diagrams, albeit for only two stress ratios. Studying the effect of fibre alkali treatment, they observed that treated fibre composites exhibit better load carrying capacities in tension-tension ($R$ = 0.1) and tension-compression ($R$ = -1) fatigue, for up to ~$10^8$ cycles. This is due to improved adhesion between the fibre and the matrix upon fibre treatment, which is confirmed by the smaller damping capacity (area of the stress-strain hysteresis loop) for treated fibre composites. However, Towo and Ansell [12, 13] do declare that treated fibre composites exhibit a steeper slope in their S-N curve compared to untreated fibre composites.

Finally, Isaac and co-workers [14-16] have looked into the fatigue properties of non-woven random mat hemp/polyester composites subjected to *i)* fibre alkali treatment, *ii)* low-velocity impact damage, and *iii)* water immersion. They observed that while composites made from 1% and 5% NaOH treated hemp fibres showed an improvement in the fatigue performance compared to untreated hemp fibre composites, the fatigue properties of composites made from 10% NaOH treated hemp fibres was comparable to that of untreated hemp fibre composites. In addition, while it was expected that the fatigue performance of impact damaged hemp composites would be extremely poor, it was surprising to discover that water immersion had negligible effect on the S-N curve of the hemp/polyester composite.

At present, there are limited papers that enable the preliminary design of PFRPs against fatigue. The objective of this study is to provide a complete set of fatigue data on aligned PFRPs to enable the design of a PFRP component against fatigue. A primary aim of the study described in this chapter is to thoroughly characterise the fatigue performance of aligned PFRPs through S-N lifetime diagrams, and specifically investigate the effect of *i)* plant fibre type, *ii)* fibre volume fraction, *iii)* textile architecture, and *iv)* stress ratio, on PFRP cyclic loading behaviour. At each stage, the fatigue performance of PFRPs is compared to that of E-glass/polyester composites (material data from [17]). In addition, to facilitate fatigue life prediction of a PFRP component, a comprehensive constant-life diagram is generated. Recently, the author of this thesis has applied the data for the fatigue design and life prediction of a 3.5-meter hemp/polyester rotor blade [18, 19].

## 6.3 EXPERIMENTAL METHODOLOGY

### 6.3.1 Reinforcement materials

Four commercially available plant fibre yarns/rovings were used as composite reinforcements. The yarns employed in this study are the same as those used in the study described in *Chapter 3*. The material properties of the four yarns are tabulated in Table 6.1. The yarns are denoted according to their fibre type and twist level; so, J190 is a jute yarn with a twist level of 190 tpm. The selected yarns enabled studying the effect of fibre type (jute, hemp and flax) and fibre quality (F50 and F20) on PFRP fatigue performance. Note that fibre quality is defined 'qualitatively' by the source of the fibre/yarn and the mechanical properties of the resulting composite. F50 and F20 yarns/rovings are obtained from different sources (Table 6.1) and the static strength of composites made from the yarns are very different (Table 6.2). Here, F20 is considered as a yarn with high-quality fibres, while F50 is a yarn with low-quality fibres.

For use as aligned reinforcements, the yarns were processed in the form of unidirectional mat and stitched biaxial fabric. Unidirectional (0°) mats were prepared from all the four yarns using a simplified drum winding facility and hydroxyethylcellulose binding agent (Cellosize HEC QP-52000H supplied by Dow

Chemical), as described in *Chapter 3*. Formax (UK) Ltd also produced 300 gsm stitched biaxial (±45°) fabric from the F50 yarn. This enabled studying the effect of textile architecture on the fatigue behaviour of F50 flax fibre composites.

**Table 6.1. List of plant fibre material and their properties (means ± stdev).**

| Yarn ID | Fibre Type | Supplier | Density† [gcm$^{-3}$] | Linear density† [tex] | Twist level† [tpm] |
|---|---|---|---|---|---|
| **J190** | Jute | Janata and Sadat Jute Ltd (Bangladesh) | 1.433 ± 0.005 | 206 ± 21 | 190 |
| **H180** | Hemp | Safilin (Poland) | 1.531 ± 0.003 | 278 ± 17 | 180 |
| **F50** | Flax | Composites Evolution (UK) | 1.529 ± 0.003 | 229 ± 22 | 50 |
| **F20** | Flax | Safilin (France) | 1.574 ± 0.004 | 396 ± 16 | 20 |

†Measured in *Chapter 3 and Appendix A*.

### 6.3.2 Composite manufacture

Aligned composite laminates (250 mm square, 3-3.5 mm thick) were fabricated using the vacuum infusion technique in an aluminium mould tool. The reinforcement mats/fabrics were used as-received (without any preconditioning). Resin infusion was carried out at 70-80% vacuum (200-300 mbar absolute) under ambient temperature. The manufacturing process has been described in detail in *Chapter 3*. All composites were made with unsaturated polyester (Reichhold Norpol type 420-100) as the matrix. The resin was mixed with 0.25 wt% NL49P accelerator (1% Cobalt solution) and 1 wt% Butanox M50 MEKP initiator. Post cure was carried out at 55 °C for 6 h after ambient cure for 16 h. From the manufacturer's datasheet, the resin has a cured density $\rho_m$ of 1.202 gcm$^{-3}$.

As tabulated in Table 6.2, composites with different *i)* yarn/fibre types (J190, H180, F50 and F20 in $[0]_4$ layup), *ii)* fibre volume fractions ($[0]_{2\text{-}5}$ layup of J190 generating four different fibre volume fractions in the range of 17-38%), and *iii)* textile architectures (F50 in $[0]_4$, $[\pm45]_4$, and $[90]_4$ layups), were fabricated by the above-mentioned procedure.

The fibre weight fraction $w_f$ of a laminate was calculated using the ratio of the mass of the preform and the resulting composite laminate. The composite density $\rho_c$ was measured using helium pycnometry (minimum of 5 samples). The composite fibre volume fraction $v_f$ was then determined using Eq. 6.1, allowing for porosity $v_p$. Note the consistency in fibre/matrix volume fractions and the low void content (with the exception of J190 $[0]_4$) of the PFRPs produced (Table 6.2).

$$v_f = \frac{\rho_c}{\rho_f} w_f; \quad v_m = \frac{\rho_c}{\rho_m}(1 - w_f); \quad v_p = 1 - (v_f + v_m) \qquad \text{Eq. 6.1}$$

For all studies in this thesis, all composite samples were stored for at least 48 hours at ambient conditions before any testing. In addition, all testing was conducted under ambient conditions (typically, 10-20 °C and 60-90% relative humidity).

### 6.3.3 Mechanical testing

#### 6.3.3.1 Static tests

In order to determine the stress levels for fatigue testing, the static ultimate strengths of the different composites needed to be measured. The ultimate tensile strength UTS was measured for all the composites through static tensile tests, conducted according to ISO 527-4:1997, on an Instron 5985 testing machine equipped with a 100 kN load cell. Six specimens were tested for each type of composite at a cross-head speed of 2 mm/min. While all specimens were 250 mm long, specimens from unidirectional and biaxial composites had a different width of 15 mm and 25 mm, respectively. The physical and tensile properties of the composites are presented in Table 6.2.

The ultimate compressive strength UCS of H180/polyester was measured through static compression tests, conducted according to ASTM D3410, on an Instron 5581 testing machine equipped with a 50 kN load cell and a compression test fixture. Six specimens (140 mm long, 15 mm wide) were tested at a cross-head speed of 1 mm/min. The test fixture and selected gauge length of 12.7 mm prevent the specimen from buckling. The test specimens were speckle-coated prior to testing, enabling longitudinal/transverse strain measurement using a camera. The UCS of H180/polyester composite was measured to be 95.1 ± 6.9 MPa.

**Table 6.2. Physical and mechanical (static and fatigue) properties (means ± stdev) of the fabricated composite laminates.**

| Test Variable | Fibre type | Layup | Fibre volume fraction $v_f$ [%] | Composite density $\rho$ [gcm$^{-3}$] | Void volume fraction $v_p$ [%] | Experimental ultimate Strength UTS/(UCS) [MPa] | Fatigue stress ratio $R$ tested under | Theoretical single cycle ultimate strength $S_0$ [MPa]$^{\Psi}$ | Fatigue strength coefficient $b^{\Psi}$ |
|---|---|---|---|---|---|---|---|---|---|
| Fibre type | J190 | $[0]_4$ | 31.7 ± 0.1 | 1.225 ± 0.002 | 4.2 ± 0.8 | 175.1 ± 10.3 | 0.1* | 211.3 | -0.0657 |
| | H180 | $[0]_4$ | 35.6 ± 0.8 | 1.303 ± 0.006 | 1.3 ± 0.4 | 171.3 ± 6.5 | 0.1* | 196.4 | -0.0623 |
| | F50 | $[0]_4$ | 27.7 ± 0.3 | 1.282 ± 0.004 | 0.9 ± 0.3 | 143.0 ± 6.8 | 0.1* | 164.3 | -0.0739 |
| | F20 | $[0]_4$ | 26.9 ± 0.1 | 1.291 ± 0.006 | 0.9 ± 0.4 | 236.3 ± 12 | 0.1* | 297.4 | -0.0690 |
| Fibre volume fraction | J190 | $[0]_2$ | 17.1 ± 0.1 | 1.238 ± 0.003 | 0.3 ± 0.2 | 90.2 ± 9.9 | 0.1* | 99.8 | -0.0585 |
| | J190 | $[0]_3$ | 25.2 ± 0.1 | 1.251 ± 0.004 | 0.7 ± 0.3 | 140.7 ± 7.7 | 0.1* | 173.5 | -0.0656 |
| | J190 | $[0]_4$ | 31.7 ± 0.1 | 1.225 ± 0.002 | 4.2 ± 0.8 | 175.1 ± 10.3 | 0.1* | 211.3 | -0.0657 |
| | J190 | $[0]_5$ | 37.8 ± 0.1 | 1.276 ± 0.002 | 1.1 ± 0.2 | 224.7 ± 26.5 | 0.1* | 262.6 | -0.0669 |
| Textile architecture | F50 | $[0]_4$ | 27.7 ± 0.3 | 1.282 ± 0.004 | 0.9 ± 0.3 | 143 ± 6.8 | 0.1* | 164.3 | -0.0739 |
| | F50 | $[\pm45]_4$ | 28.9 ± 0.1 | 1.293 ± 0.005 | 0.3 ± 0.2 | 51.4 ± 2.8 | 0.1* | 73.7 | -0.0872 |
| | F50 | $[90]_4$ | 25.8 ± 0.3 | 1.278 ± 0.004 | 0.7 ± 0.2 | 13.2 ± 0.4 | 0.1* | 19.8 | -0.0698 |
| Stress ratio | H180 | $[0]_4$ | 35.6 ± 0.8 | 1.303 ± 0.006 | 1.3 ± 0.4 | 171.3 ± 6.5 | 0.1* | 196.4 | -0.0623 |
| | H180 | $[0]_4$ | 35.6 ± 0.8 | 1.303 ± 0.006 | 1.3 ± 0.4 | 171.3 ± 6.5 | 0.3* | 234.8 | -0.0548 |
| | H180 | $[0]_4$ | 35.6 ± 0.8 | 1.303 ± 0.006 | 1.3 ± 0.4 | 171.3 ± 6.5 | 0.5* | 255.4 | -0.0526 |
| | H180 | $[0]_4$ | 35.6 ± 0.8 | 1.303 ± 0.006 | 1.3 ± 0.4 | (95.1 ± 6.9) | -1† | (161.7/50.5) | -0.1567/-0.03 |
| | H180 | $[0]_4$ | 35.6 ± 0.8 | 1.303 ± 0.006 | 1.3 ± 0.4 | (95.1 ± 6.9) | 2.5‡ | (124.4) | -0.0373 |

*Tension-Tension (TT) mode; †Tension-Compression (TC) mode; ‡Compression-Compression (CC) mode

$^{\Psi}$ $S_0$ and $b$ are material fatigue parameters described in Section 6.3.3.2.3 and Eq. 6.2. They are obtained by fitting Eq. 6.2 on the fatigue data obtained for each material tested under the different fatigue stress ratios $R$.

#### 6.3.3.2 Fatigue tests

*Specimen preparation*

Rectangular test specimens were obtained by cutting the composite laminates with a high-speed abrasive/diamond cutting machine. To avoid moisture intake, lubrication fluid was not used during cutting of the PFRP specimens. Upon cutting, all edges and ends were polished and roughened, respectively, with 600 grit sand paper. Aluminium end-tabs (50 mm long, 1 mm thick) were then glued to the specimens using Araldite Rapid adhesive, to protect the specimen surface from damage from the jaws of the test machine.

Table 6.2 states which composites were tested in tension-tension (TT) mode, tension-compression (TC) mode and compression-compression (CC) mode. For tests in TT mode, test specimens were 250 mm long and 15 mm wide with a gauge length of 150 mm. For tests in TC and CC modes, test specimens were 120 mm long and 15 mm wide with a gauge length of 11.5 mm. The smaller gauge length of specimens tested in TC/CC modes ensured that the specimens didn't buckle under compressive loads.

*Test parameters*

Fatigue tests were performed on an Instron 8801 servo-hydraulic testing machine under load-control mode. The calibrated load cell had a force rating of ±100 kN and accuracy of 0.047 kN. Constant amplitude loads were applied in a sinusoidal waveform at a frequency of 10 Hz. BS ISO 13003:2003 [20] advices that while high testing frequencies (of up to 25 Hz) are desirable, to avoid self-generated heating in the specimen, for rate-dependent materials the rise in specimen surface temperature should normally be limited to 10 °C during the test. BS ISO 13003:2003 [20] does highlight that the limit of 10 °C does not apply to rapid temperature rises associated with final failure. Gassan *et al.* [10, 11, 21] observed that for woven and unidirectional flax/jute composites with a fibre content of 22-40% (similar to this study), a test frequency of 10 Hz led to a temperature rise of less than 7 °C. As is common practise in fatigue testing [12, 22, 23], all tests in this study were conducted in ambient laboratory air (typically, 15-20 °C and 60-90% relative humidity).

Preliminary tests were conducted to determine an optimised jaw pressure (of 20 bar) to grip the specimens. This enabled minimising the number of specimens that failed at the jaw. TT mode ($R$ = 0.1) fatigue tests were carried out on all composite samples (Table 6.2). To study the effect of stress ratio $R$ on fatigue performance and to then generate a complete constant-life diagram for H180 composites, only they were studied under five different stress ratios: $R$ = 0.1, 0.3, 0.5 in TT mode, $R$ = -1 in TC mode, and $R$ = 2.5 in CC mode (Table 6.2). Fig. 6.2 presents example load waveforms used for fatigue testing, showing definition of terms and illustration of $R$-values. Anti-buckling guides were not used during TC/CC loading as they could cause extra heating of the specimen [24].

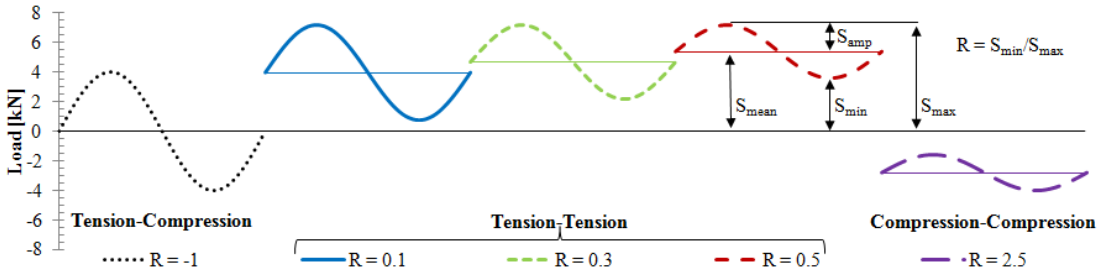


**Fig. 6.2. Example sinusoidal constant amplitude load waveforms showing definition of terms and illustration of *R*-values (for a constant $S_{max}$ of 90% of the UTS or UCS).**

In accordance with BS ISO 13003:2003 [20], at least five specimens were tested to failure at a minimum of five levels of maximum (absolute) stress $S_{max}$ (*eg.* 90%, 80%, 70%, 60%, 50% and 45% of UTS or UCS), up to at least $10^6$ cycles, for the determination of the material S-N lifetime diagram. Specimens with failures initiated in the tab area were not included in the data. While the number of specimens tested do not allow a statistical analysis, they are sufficient for such exploratory investigations [20].

*Data analysis*

As illustrated in Fig. 6.3, after plotting Wohler stress-life (S-N) diagrams, power-law regression equations (Eq. 6.2) were determined for each material, where $S_{max}$ is the maximum (absolute) stress applied, $N$ is the number of cycles to failure, $S_0$ is the

single cycle (static) ultimate strength of the material, and $b$ is the material fatigue strength coefficient. Eq. 6.2 yields a linear S-N curve on a log-log plot.

Table 6.2 presents material fatigue parameters ($S_0$ and $b$) based on Eq. 6.2, for each material tested under the different fatigue stress ratios $R$. The material fatigue strength coefficient $b$ is a very useful parameter; a smaller value of $b$ implies a steeper slope of the logS-logN curve and thus faster fatigue strength degradation every decade of cycles. For reference, Eq. 6.2 derives from the integration of the Paris fatigue crack growth rate law (Eq. 6.3) through the substitution of Eq. 6.4, where $a$ is the crack length, $K$ is the (maximum) stress intensity factor, and $A$ and $Y$ are constants. Note that $b$ is the same in Eq. 6.2 and Eq. 6.3.

The trend in S-N lifetime data can also be described by Eq. 6.5, where $c$ (like $b$) is a material constant. Generally, S-N data for composites may follow either Eq. 6.2 or Eq. 6.5 or both, depending on the material system [22]. As the power-law regression curve of Eq. 6.2 is found to be a better fit to the experimental results, it is used here.

$$S_{\max} = S_0 N^b \qquad \text{Eq. 6.2}$$

$$\frac{da}{dN} = AK^{-(1/b)} \qquad \text{Eq. 6.3}$$

$$K = SY\sqrt{\pi a} \qquad \text{Eq. 6.4}$$

$$S_{\max} = S_0(1 - c\log N) \qquad \text{Eq. 6.5}$$

While static strength was plotted on the S-N diagram at N = 1 (Fig. 6.3), it was ignored when obtaining the power-law regressions representing the trend in S-N data for three prime reasons. Firstly, the static data was obtained at a strain rate an order of magnitude below the fatigue strain rate. Secondly, the failure mechanism of a static failure is fundamentally different to a fatigue failure [1]. Thirdly, as including the static strength data weakened the strength of the regression (indicated by the $R^2$-value), its omission is reasonable, particularly as low-cycle fatigue ($N < 10^3$) is usually of little interest.

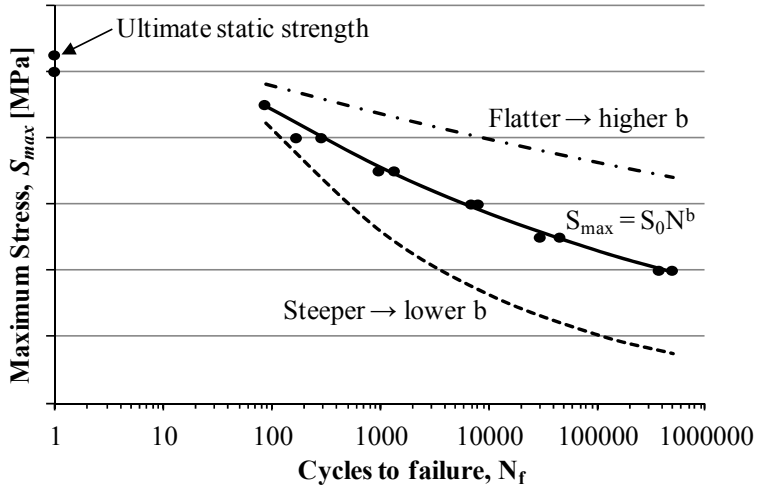


**Fig. 6.3. Typical S-N lifetime diagram with example data following a power-law regression curve, where b is the material fatigue strength coefficient.**

A complete Haigh constant-life diagram was then constructed using data obtained from the power-law regression lines, of the S-N diagrams, for H180/polyester composite specimens tested under the five different stress ratios. A constant-life diagram plots the mean stress $S_{mean}$ along the x-axis and stress amplitude $S_{amp}$ along the y-axis. The combination of amplitude stress $S_{amp}$ and mean stress $S_{mean}$ were determined for each decade of fatigue cycles (*eg.* $10^2$, $10^3$, $10^4$ and so on), for the five stress ratios. Lines of constant life were drawn through the corresponding data points; no curve fitting was used. The static failure conditions, *i.e.* the end points on the x-axis, were defined by the UCS and the UTS.

## 6.4 RESULTS AND DISCUSSION

### 6.4.1 Effect of fibre type

#### 6.4.1.1 Static tests

The static tensile test results in Table 6.2 show the effect of yarn/fibre type on composite tensile strength. This has been previously discussed in *Chapter 3*. While J190 and H180 composites have similar UTS of 170-175 MPa, F20 composites exhibit significantly higher UTS of 236.3 ± 12 MPa despite having lower fibre content. This is probably a result of three possibilities. Firstly, flax fibres have better

mechanical properties than jute and hemp fibres (Table 6.3). As jute and hemp have a better or similar cellulose content, cellulose crystallinity, degree of polymerisation (DP) and microfibril angle (MFA) in comparison to flax (Table 6.3), perhaps the significantly higher fibre aspect ratio of flax results in a higher fibre tensile strength [25-27]. McLaughlin *et al.* [28] and Mukherjee *et al.* [29] have statistically established the strong correlation between plant fibre structural parameters (cellulose content, MFA and aspect ratio) and their tensile properties (strength, modulus and elongation). Secondly, the F20 flax rovings used in this study have a significantly lower twist level than the J190 and H180 yarns. In *Chapter 5*, it has been shown that increasing reinforcement yarn twist has a quantifiable detrimental effect on composite tensile strength. For instance, composites made from J190 yarns (with yarn surface twist angle α of 20.5 ± 5.9) only receive 57% (= $\cos^2(2\alpha)$) of the fibre strength, while composites made from F20 rovings (with α = 0.5 ± 0.1) receive the entire fibre strength, due to no losses through reinforcement misorientation. Thirdly, plant fibre/yarn quality will affect the fibre and composite mechanical properties. Although both F20 and F50 composites have similar fibre content and are made from low-twist flax rovings/yarns, there is a 40% difference in their UTS. Madsen *et al.* [30, 31] and Baets *et al.* [32] have shown that an increasing number of defects and an increasing number of processing steps can reduce fibre/yarn quality and thus composite properties. It is encouraging to note that although mechanical properties of single plant fibres have high variability (Table 6.3), at a composite scale, the UTS of all the PFRPs have a small coefficient of variation between 4-6 %, which is similar to that of GFRPs (as confirmed in *Chapter 3*).

**Table 6.3. Structural and mechanical properties of plant fibres [25-27].**

| *Fibre type* | *Cellulose content [%]* | *Cellulose crystallinity [%]* | *DP** | *MFA†* *[°]* | *Aspect ratio* | *Tensile modulus [GPa]* | *Tensile strength [MPa]* | *Failure strain [%]* |
|---|---|---|---|---|---|---|---|---|
| Flax | 64–71 | 53-70 | 2420 | 5–10 | 1750 | 30–70 | 400–1100 | 2.7–3.2 |
| Hemp | 70–74 | 53-70 | 2300 | 2–6 | 900 | 30–60 | 300–800 | 1.3–2.7 |
| Jute | 61–72 | 53-70 | 1920 | 8 | 100 | 20–55 | 200–600 | 1.4–3.1 |

*DP = degree of polymerization

†MFA = microfibril angle

#### 6.4.1.2 Fatigue tests

Based on static tensile test results, the four different PFRPs were subjected to tension-tension ($R$ = 0.1) fatigue tests at different stress levels (% of respective UTS). Fig. 6.4 presents S-N fatigue data for these PFRPs. The arrowhead at 1.4 x $10^7$ cycles indicates a 'run-out' test which did not fail. A gradual decline in fatigue strength with increasing number of fatigue cycles is observed. It is observed that the power-law model of Eq. 6.2 is a good fit to the experimental fatigue data; in fact all regressions have an $R^2$-value > 0.95. This is generally characteristic of composites whose lifetime is dominated with matrix crack growth and inter-laminar cracking [22, 23]. Indeed, matrix cracks normal to the stress direction often occurred on the specimen surface early in the lifetime. The type of final failure observed in specimens tested in static tensile tests and tension-tension fatigue tests was similar; specimens failed in a catastrophic brittle manner with a jagged fracture surface and often showing delamination and longitudinal splits (sometimes reaching the tab area) that terminate and arrest at matrix surface crack(s). Unidirectional GFRPs and unidirectional carbon fibre composites are known to fail in a similar manner [22, 23, 33]. Fracture modes and surfaces are further discussed in Section 6.4.4.

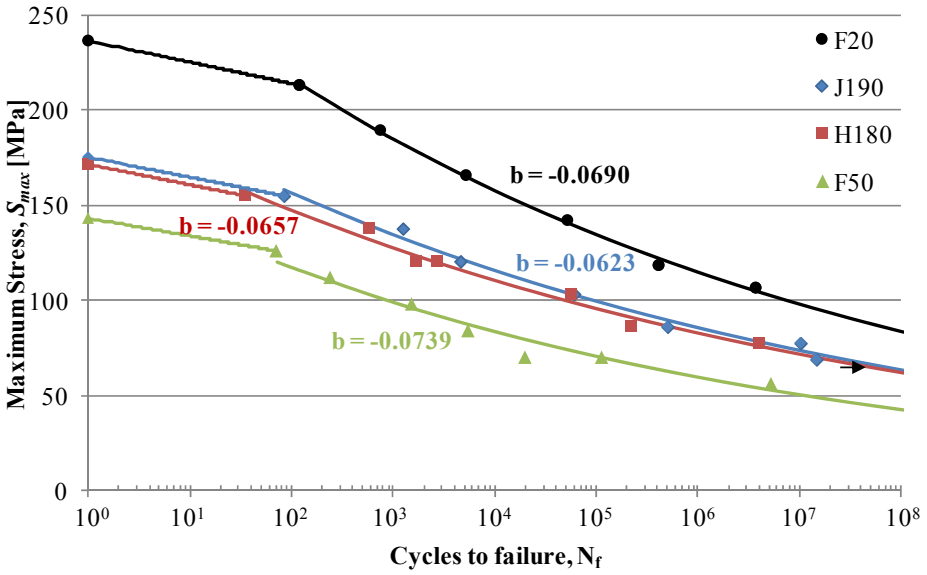


**Fig. 6.4. Lifetime S-N diagram for polyester composites reinforced with different plant fibres/yarns. Power-law regression lines and the material fatigue strength coefficient (b-values) are also presented.**

From the S-N diagram in Fig. 6.4 and Fig. 6.5, it is observed that although the static UTS of the PFRPs ranges from 140 to 240 MPa, the material fatigue strength coefficients *b* are very similar, ranging from -0.0739 to -0.0623. In fact, F20 composites have 40% higher static UTS than F50 composites, but similar rates of fatigue strength degradation (Fig. 6.5). This indicates that the fatigue failure mechanism in PFRPs, and the resulting gradual fatigue strength degradation, is independent of plant fibre/yarn type. This is possibly because jute, hemp and flax bast fibres are structurally very similar (Table 6.3) and the interfaces that form in thermoset composites reinforced with such fibres are also very similar. Hence, micro-crack growth rates at *i)* the fibre/matrix interface in the composite and *ii)* the cellulose/hemicellulose-lignin interface in the viscoelastic fibre (or fibre bundles) [5, 7] are similar. In his study on the fatigue behaviour of unidirectional flax and jute epoxy composites, Gassan [10] also noticed that the composites had very similar progressive damage propagation (indicated by SDC-load curves). These observations not only confirm that failure mechanisms in static and fatigue loading are dissimilar, but indeed that the static UTS can be used as an indicator of the lifetime fatigue performance of PFRPs. In essence, a PFRP with higher UTS usually has a higher load carrying capacity throughout its fatigue life, due to no detrimental effects to the strength degradation rate.

#### 6.4.1.3 Comparison with GFRPs

Commonly, material S-N data is presented in normalised form on a plot of $S_{max}/UTS$ against N (Fig. 6.5). Importantly, the material fatigue strength coefficient *b* remains the same. The normalised S-N diagram readily enables the comparison of the rate of fatigue strength degradation (*b*-values) of several materials. Fig. 6.5 not only presents normalised S-N data for the various unidirectional PFRPs, it also presents normalised S-N data for unidirectional GFRPs and carbon/epoxy. Data on the GFRPs material ($v_f$ = 30% in $[0]_5$ lay-up, UTS = 570 MPa) is from extensive tests done by Prof. Mandell's group [17, 22, 23], while data on typical carbon/epoxy composites is from [34].

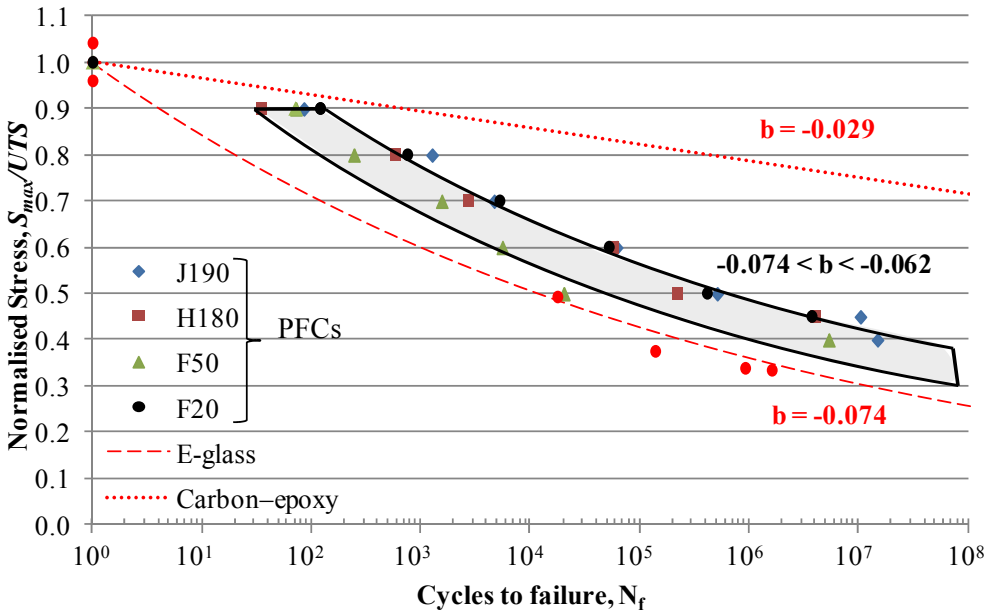


**Fig. 6.5. Normalised S-N diagram comparing the tension-tension ($R$ = 0.1) fatigue performance of unidirectional thermoset matrix composites reinforced with plant (shaded), E-glass [22] and carbon [34] fibres.**

From Fig. 6.5, it is immediately clear that unidirectional carbon/epoxy composites outperform both GFRPs and PFRPs in terms of fatigue properties. While carbon/epoxy composites have a value of $b \approx -0.029$, GFRPs and PFRPs have a much lower value of $b$. It is of great interest to observe that material fatigue strength coefficient of PFRPs ($b \approx -0.074$ to $-0.062$) is higher than or comparable to GFRPs ($b \approx -0.074$). This implies that damage development and fatigue strength degradation are relatively slower in PFRPs. Liang *et al.* [9] also find that in comparison to bidirectional flax composites, bidirectional GFRPs had a much steeper S-N curve, implying a more significant decrease in fatigue strength with respect to cycles to failure. Shahzad *et al.* [15] also confirm that randomly-oriented short-fibre hemp/polyester composites and chopped-strand GFRPs have a similar fatigue strength coefficient. However, it should be noted that aligned GFRPs have a much higher UTS than aligned PFRPs, and in terms of absolute stress, the fatigue and static properties of GFRPs is significantly better than that of PFRPs. This is clearly depicted in Fig. 6.6.

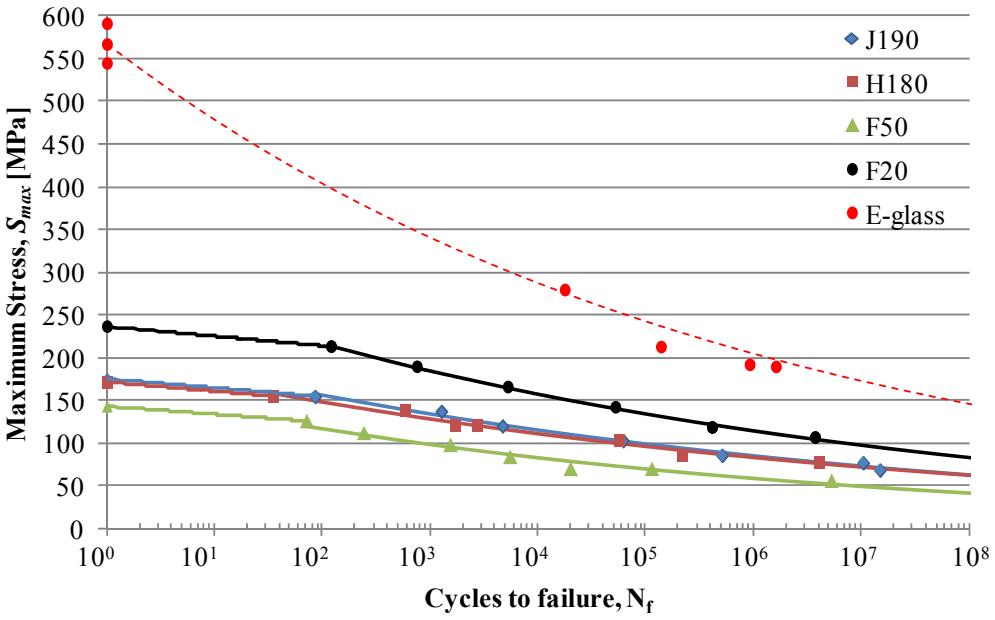


**Fig. 6.6. S-N diagram comparing the tension-tension fatigue performance of UD PFRPs and UD GFRPs ($v_f$ = 30% in $[0]_5$ lay-up, UTS = 570 MPa; material data from [22]).**

While it is widely quoted that the fibre/matrix interface in PFRPs is weak due to poor adhesion between hydrophilic plant fibres and hydrophobic matrix [35-37], the interface in GFRPs has been optimised through sizing of glass fibres (specific to a resin system). Hence, it is surprising that damage accumulation rates in PFRPs are slower than in GFRPs. The causes of this behaviour are still unclear, however, there are three possible explanations. Firstly, several studies [4, 5, 9, 15] have shown that not only do plant fibres and their composites exhibit strain hardening when subjected to cyclic loads, but PFRPs also show much lower (if any at all) stiffness degradation over their fatigue life in comparison to GFRPs. As mentioned in Section 6.2, Liang *et al.* [9] observe that the loss of modulus of biaxial glass/epoxy composites is three times higher than that of flax/epoxy composites. It is known that the progressive reorientation of cellulose microfibrils in plant fibres towards the loading direction is the most plausible explanation for this observation [3, 4, 9]. In constant amplitude load-controlled fatigue tests, a gradual loss of modulus implies a gradual increase in strain amplitudes and thus faster damage accumulation. Perhaps, it is this ability of PFRPs to maintain stiffness over their fatigue life which imparts them with slow

damage accumulation rates. Secondly, the complex composite structure of visco-elastic plant fibres may provide them with crack absorbing and deflecting mechanisms [5, 7, 38]. This includes the ability of plant fibres to *i)* 'shed' layers of damaged structural cell walls [5, 7], *ii)* continually transfer loads onto adjacent layers and fibres [5, 7], *iii)* directly resist against delamination crack growth through interactions of the cellulose microfibrils and the hemicellulose-lignin matrix by imperfect microfibrillar alignment and subsequent microfibrillar bridging (relative to the crack plane) [7], and *iv)* reshape fibre cells into an ovular rather than circular cross-section [5], effectively increasing fibre aspect ratio and load-transferring ability [26]. Finally, plant fibres may be more capable of transferring stresses and strains to the matrix due to their rough surfaces. While glass fibres have a constant diameter across their length and have smooth surfaces, the diameter of plant fibres varies across their length and their surface is very rough. Sretenovic *et al.* [39] measured the development and distribution of strain in a single wood fibre-low density polyethylene composite by means of electronic laser speckle interferometry (ESPI). While it is typically expected that due to the different elastic modulus of the fibre and the matrix axial strain distribution is discontinuous across the fibre ends, they found that due to the roughness of wood fibre ends and the resulting larger effective surface area, the transition of strain from the fibre to the matrix was continuous. However, Sretenovic *et al.* [39] do acknowledge that pixel averaging effects in the ESPI method may cause the continuous strain distribution.

### 6.4.2 Effect of fibre volume fraction

Composite mechanical properties can often be tailored by changing, for instance, the fibre volume fraction. J190/polyester composites were manufactured at four different fibre volume fractions, ranging from 17 to 38%. The static tests results in Table 6.2 show that the UTS of J190/polyester increases linearly with fibre volume fraction ($R^2$ = 0.974), as per the rule of mixtures (*Chapter 4*). This shows that although different batches/types/quality of plant fibres may have variable properties, at a composite scale, PFRPs made from a single batch of fibre do follow conventional composite micro-mechanical models.

S-N data from tension-tension ($R$ = 0.1) fatigue tests on these composites is presented in Fig. 6.7. Again, the power-law regressions are in good agreement with the experimental data ($R^2 > 0.95$). PFRPs with higher fibre content not only exhibit improved static (single cycle) properties, they also maintain higher fatigue load carrying capacities over their fatigue life. None of the S-N curves seem to be converging into each other before at least $10^{10}$ cycles, which is significantly higher than the number of stress cycles even wind turbine blades would face. In fact, the material fatigue strength coefficient $b$ is fairly constant at $b \approx -0.0646$ for all the fibre volume fractions (Fig. 6.8), despite a small dip at $v_f$ = 25%. This implies that the slope of the S-N curves and the fatigue strength degradation rates are very similar. Hence, it can be concluded that increasing the fibre content of a PFRP is useful for improving both static and fatigue performance.

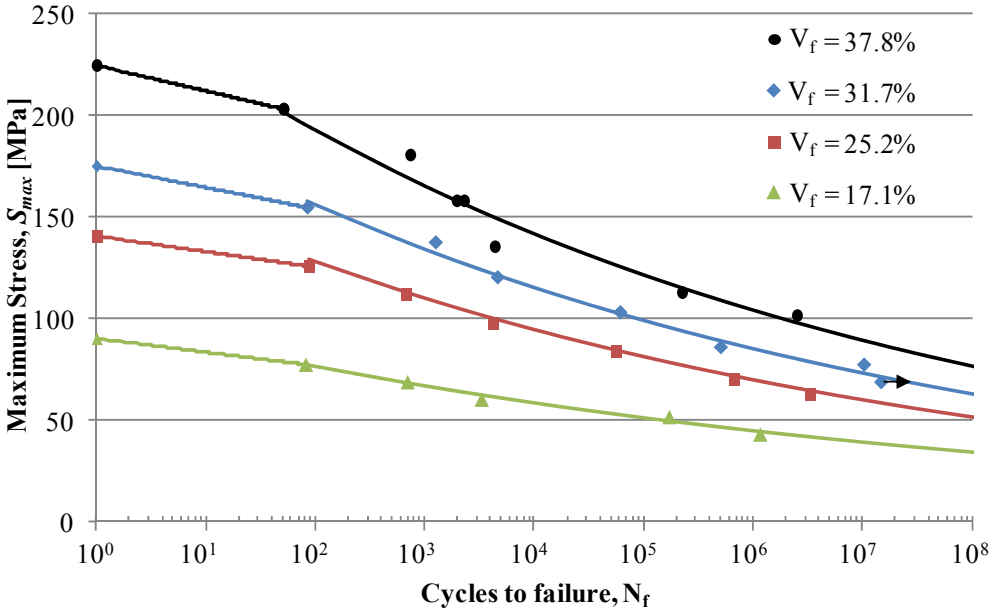


**Fig. 6.7. S-N diagram showing fatigue life data for J190/polyester composites composing of different fibre volume fractions.**

However, note that the fatigue behaviour up to only $v_f \approx$ 40% has been investigated in this study. Several authors [1, 17, 40, 41] have shown that fatigue performance tends to degrade with increasing fibre content. This is because increased fibre content leads to *i)* more fibre/matrix interfaces, *ii)* more fibre-fibre interactions/contacts (as seen in

Fig. 6.9) and *iii)* more regions of high local volume fractions due to increased yarn/strand compaction [42]. Although the interface enables stress transfer between the fibre and the matrix, it is also the region where the largest stress/strain gradients lie. Hence, the interface is the region where micro-cracks are most likely to grow and propagate. Increasing fibre content implies that fibres are now closer to each other and hence stress/strain gradients at the interface are even higher, leading to accelerated crack growth. In addition, touching fibres are likely sites for crack growth. Samborsky and Mandell [17, 41] have shown that increasing fibre content beyond 40-45% typically results in a drop in the fatigue strength coefficient *b* and thus poorer fatigue performance. Fig. 6.8 plots the variation in the fatigue strength coefficient *b* with increasing fibre content for triaxial GFRPs ([0,±45,0] lay-up with 72%-0's; material data from [17]). Mandell *et al.* [42] have also demonstrated that while increasing the localised fibre volume fraction in a composite sample can improve static properties, it has a detrimental effect on the fatigue performance.

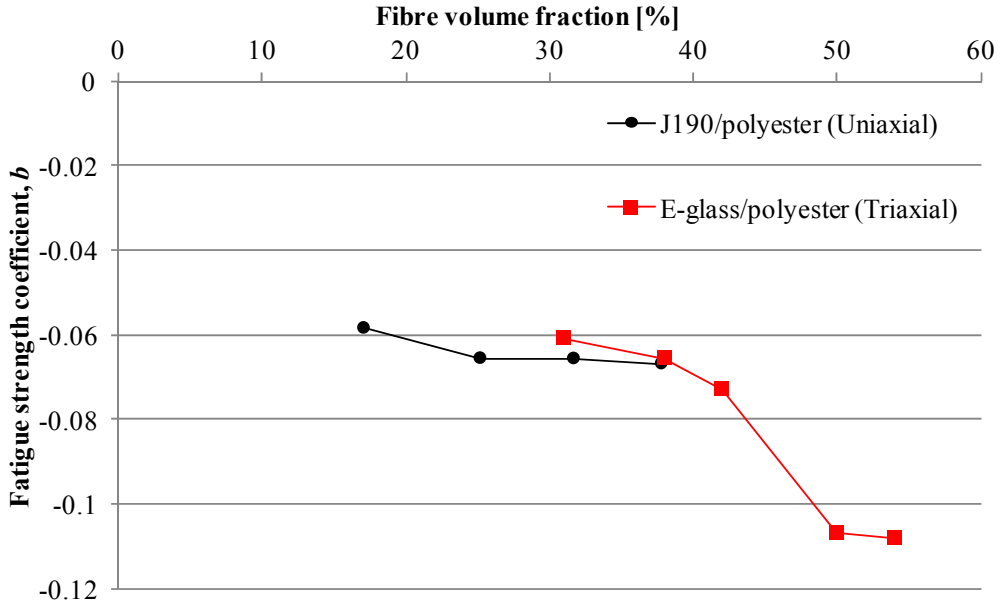


**Fig. 6.8. Variation in the material fatigue strength coefficient b with fibre volume fraction, for J190/polyester and E-glass/polyester (material data from [17]).**

As illustrated in Fig. 6.9, increasing the fibre content of J190/polyester composites affected the failure mechanism in tension-tension fatigue. At low fibre content, more matrix cracks formed at the specimen surface normal to the loading direction very early on in the fatigue life (Fig. 6.9a). Specimen failure was brittle, matrix dominated, with no longitudinal splitting and the fracture surface was flat with no delamination. At higher fibre volume fractions (Fig. 6.9b), fewer surface matrix cracks formed and specimen failure was brittle, catastrophic and with extensive fibre failure. The fracture surface was more jagged with extensive delamination and longitudinal splitting (even extending into the end tabs). Often, longitudinal splits extended into and arrested at a matrix surface crack normal to the loading direction. Interestingly, the fracture surfaces of specimen failed under static and fatigue loading were similar, which is typical in fatigue failure of composites [1, 17].

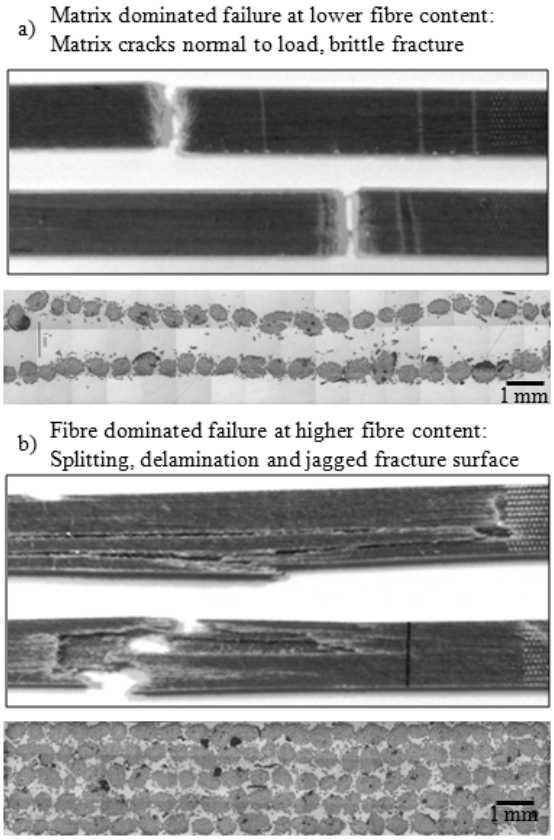


**Fig. 6.9. Typical cross-section micrograph and failure modes of J190/polyester composites with *a)* low ($v_f$ = 17%) and *b)* high ($v_f$ = 38%) fibre content subjected to tension-tension fatigue loading. See text for details.**

### 6.4.3 Effect of textile architecture

To characterise the influence of textile architecture on the fatigue performance of PFRPs, unidirectional ($[0]_4$ and $[90]_4$) and biaxial ($[\pm45]_4$) F50/polyester composites were manufactured and tested. Static tensile results in Table 6.2 show that although the three composites have a similar fibre content, the UTS of $[0]_4$ composites is 11 and 3 times the UTS of $[90]_4$ and $[\pm45]_4$ composites, respectively. Plant fibres are highly anisotropic due to their structure and composition. It follows that uniaxial composites reinforced with these plant fibres are also highly anisotropic. In fact, as has been revealed in *Chapter 5*, biaxial ($[\pm45]_4$) PFRPs are a better option than uniaxial ($[0]_4$) PFRPs, for applications where loads are at an off-axis angle larger than 30°.

Fig. 6.10 illustrates the effect of textile architecture on the fatigue performance of F50/polyester composites. The power-law regressions are in good agreement with the experimental data ($R^2 > 0.95$). Increasing off-axis loading angle seems to improve the fatigue life at 90% of the UTS. While $[\pm45]_4$ F50/polyester has a steeper S-N curve (lower value of *b*) in comparison to $[0]_4$ samples, $[90]_4$ has a flatter S-N curve. Fig. 6.10 clearly shows that under tension-tension load regime, textile architectures with fibre orientations off-axis to the loading direction result in a significant drop in composite static UTS which results in lower fatigue loading capacities throughout their fatigue life; that is, slight improvement in the fatigue strength coefficient does little to offset the reduction in UTS.

From Fig. 6.11, it is encouraging to see that fatigue strength degradation rate of $[\pm45]_4$ F50/polyester is better than that of uniaxial ($[0]_5$ lay-up, $v_f$ = 30%, UTS = 570 MPa), biaxial ([±45] lay-up, $v_f$ = 28%, UTS = 139 MPa) and triaxial ([0,±45] lay-up with 48%-0's, $v_f$ = 36%, UTS = 361 MPa) GFRPs (material data from [17, 22]) for up to at least $10^8$ cycles. This is due to *i)* the higher fatigue strength coefficient *b* and *ii)* the significantly better low-cycle fatigue properties, of PFRPs in comparison to GFRPs. Note that the ratio of the UTS of unidirectional and biaxial GFRPs is 4.1 (= 570/139), which is higher than that of unidirectional and biaxial F50/polyester (2.8 = 143/51).

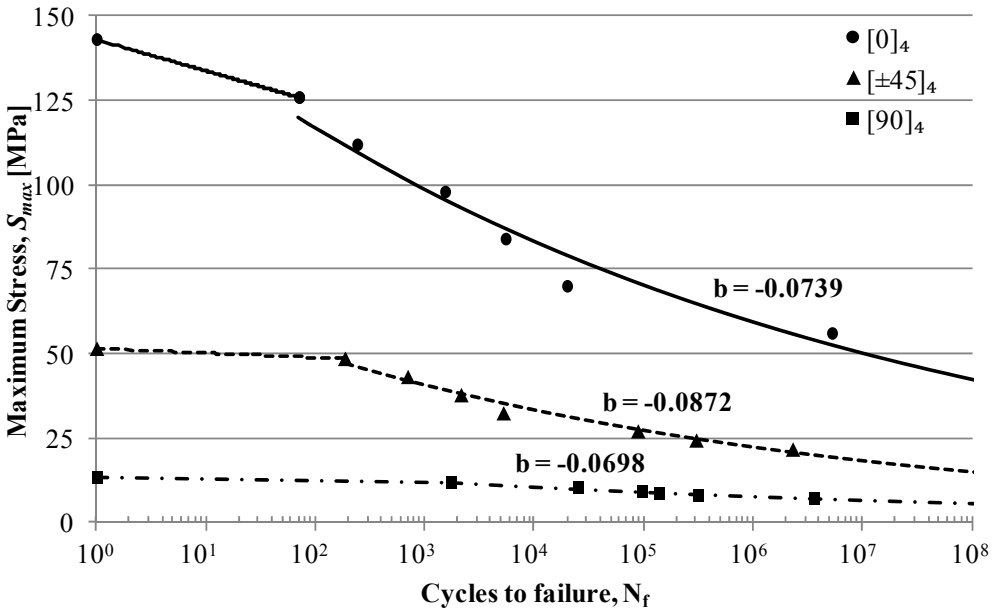


**Fig. 6.10. S-N diagram showing fatigue life data for F50/polyester composites composing of different textile architectures.**

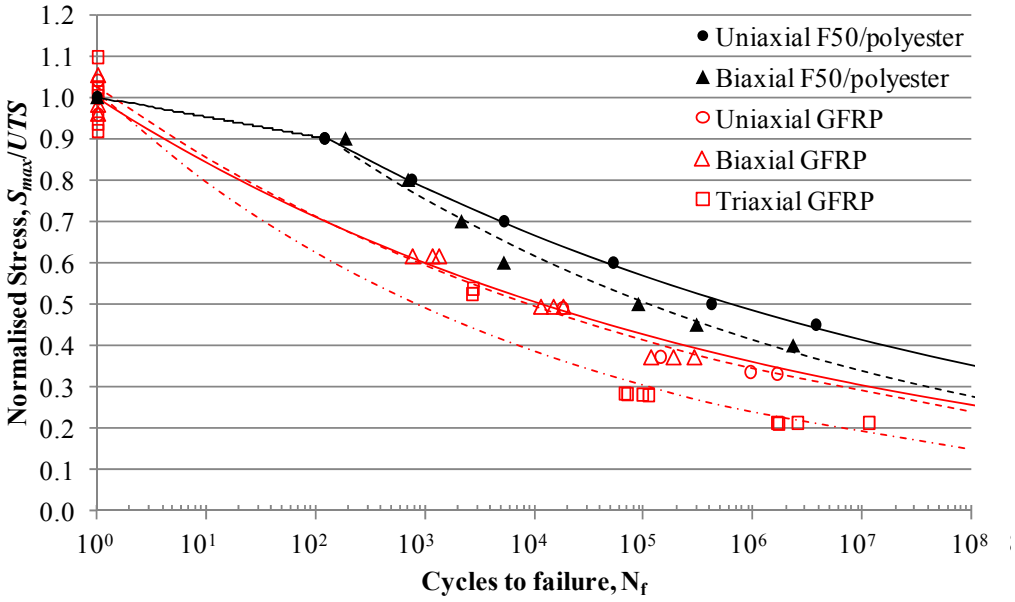


**Fig. 6.11. Normalised S-N diagram comparing the tension-tension ($R$ = 0.1) fatigue performance of multi-axial composites reinforced with F50 and E-glass fibres.**

In general, Fig. 6.11 shows that biaxial composites have a steeper S-N curve than unidirectional composites. Interestingly, traixial GFRPs has a higher fatigue strength degradation rate in comparison to both uniaxial and biaxial GFRPs. This is because the failure mechanism in triaxial composites is different to the failure mechanisms in uniaxial and biaxial composites. In triaxial composites, matrix cracking causes the ±45° layers to fail separately and then delaminate from the 0° material [22, 23]. This would also be expected from triaxial PFRPs.

Several researchers have studied the effect of off-axis loads and textile architecture on composite fatigue performance, including [10, 17, 22, 33, 43]. The most widely discussed topic is the difference in macroscopic failure morphology of (on-axis and off-axis) unidirectional and multi-axial composites, subjected to fatigue loads. Unidirectional composites subjected to on-axis (0°) loads fail due to fibre/matrix interfacial debonding and splitting along the fibre direction. Unidirectional composites subjected to off-axis loads (say 90°) fail at a single well-defined cross-section parallel to the fibre and thickness directions [33], typically due to cracks coalescing along interfaces [10]. On the other hand, biaxial composites typically fail due to matrix cracks forming and growing parallel to the fibres of each ply, followed by inter-laminar separation of the plies [17].

### 6.4.4 Effect of stress ratio

To generate a complete constant-life diagram for H180/polyester composites, they were systematically tested over five different stress ratios. From static tests, it is found that the UTS (170 MPa) is almost double the UCS (95 MPa). Fig. 6.12 plots the normalised stress-life data of the composites loaded at different stress ratios. While all power-law regression lines show strong fit to the experimental data ($R^2 >$ 0.97), for tests in TC load range ($R$ = -1) a piece-wise power-law regression is required as the composite hits a 'fatigue endurance limit' at about $10^4$ cycles. Beyond this limit, cyclic stresses applied to the material (at $R$ = -1) cause less fatigue damage. Although the fatigue strength drops drastically up to $10^4$ cycles, it is encouraging to observe an endurance limit so early on in the fatigue life of H180 composites

subjected to fully-reversed ($R$= -1) cyclic loads as this is the most severe fatigue load regime.

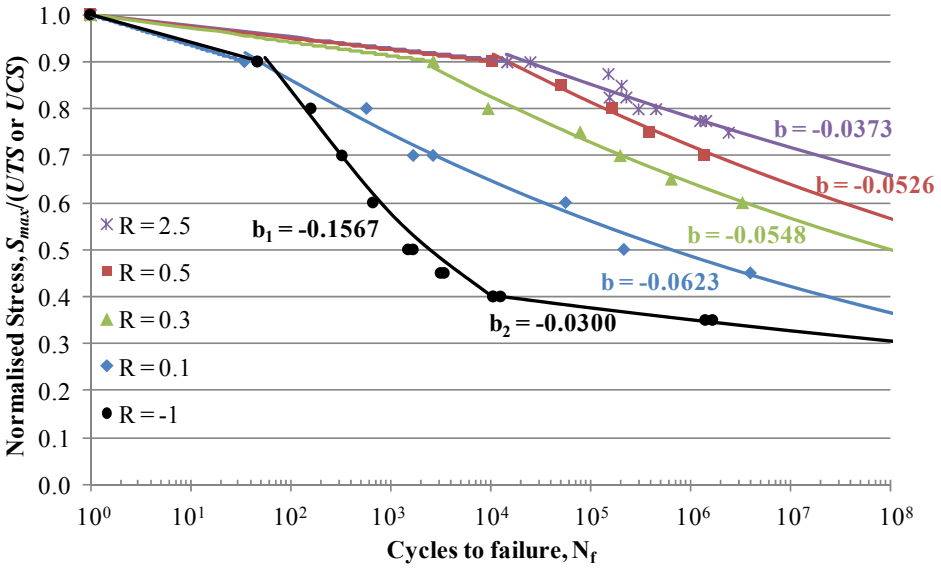


**Fig. 6.12. Normalised S-N diagram showing the effect of stress ratio on fatigue life of H180/polyester composites. Data for TT mode is normalised by the UTS, while data for TC and CC mode is normalised by the UCS.**

Fig. 6.12 shows that increasing the stress ratio $R$ substantially increases the fatigue life at high stresses. For instance, when constant amplitude cyclic loads are applied at stress ratios $R$ of -1, 0.1, 0.3, 0.5 and 2.5 at $S_{max}$/(UTS or UCS) of 70%, according to the regression equations based on the experimental data, H180 composites would survive $2.8\times10^2$, $2.7\times10^3$, $2.1\times10^5$, $1.8\times10^6$, and $1.9\times10^7$ cycles. That is, the fatigue life increases by at least a decade of cycles for every stress ratio. In addition, increasing the stress ratio $R$ increases the material fatigue strength coefficient $b$. A similar trend is also observed for GFRPs materials [17, 41, 44]. This implies that increasing the stress ratio $R$ leads to a flatter S-N curve on a logS-logN plot and essentially, slower fatigue degradation and damage accumulation rates. A possible explanation for this is that increasing the stress ratio $R$, reduces the stress amplitude $S_{amp}$ (for a constant maximum (absolute) stress $S_{max}$)) of the load regime. The load spectrum in Fig. 6.2 shows this graphically. At higher stress ratios, the material is being subjected to lower stress amplitudes, and hence it will have to endure lower

stress/strain gradients in the fibre, matrix and at the fibre/matrix interface. This would in turn lead to reduced crack growth rates and less significant fatigue strength degradation with increasing number of cycles.

The stress ratio also has an effect on the failure mode of the composites. Example failure surfaces from tests in the different load ranges are shown in Fig. 6.13. Composites tested under TT mode ($R$ = 0.1, 0.3 and 0.5) fail in a brittle manner including extensive fibre fracture, matrix cracking, delamination and longitudinal splitting (Fig. 6.13a). Crack growth, in this case, is a result of Mode 1 (opening mode) and Mode 2 (in-plane shear mode) crack loading [22]. Importantly, single plant fibres subjected to TT fatigue loads also experience mode mixities (Mode 1 and Mode 2), although Mode 1 prevails due to lower fracture resistance [7]. Composites tested under TC ($R$ = -1) and CC ($R$ = 2.5) load range display the typical single-kink failure and wedge-shaped failure, respectively. Mode 2 (in-plane shear mode) should be the dominant crack loading mechanism for TC and CC load ranges [22]. In TC load range, the specimen fails when a kink develops at a plane 45° to the loading direction (Fig. 6.13b) due to pure in-plane shear resulting from each half sliding over the other half. Specimen failure in CC load range occurs in the form of a symmetrical double-kink (Fig. 6.13c) resulting from both halves forcing into each other and folding on the same side.

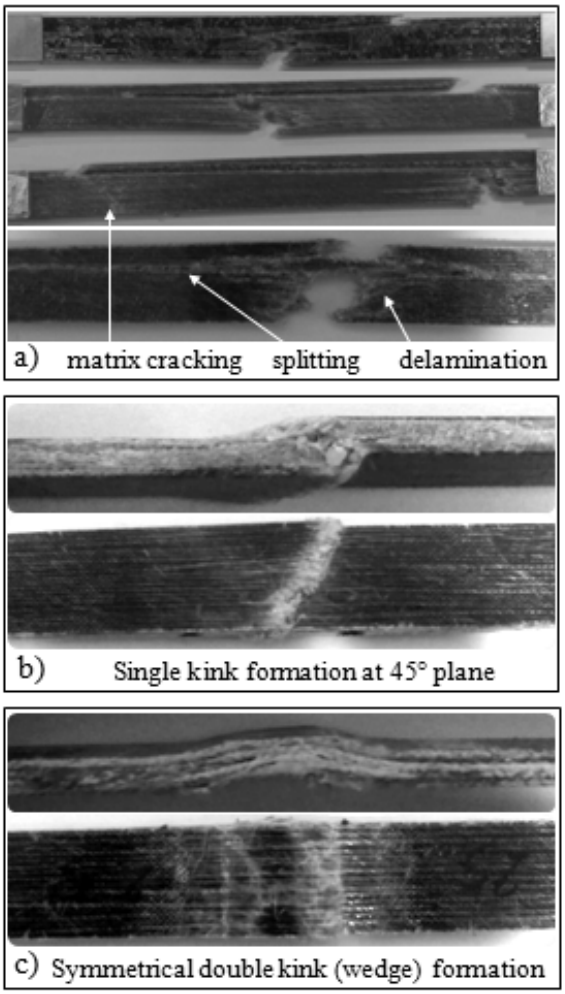


**Fig. 6.13. Typical failure modes of PFRPs loaded in *a)* tension-tension load range, *b)* tension-compression load range and *c)* compression-compression load range. See text for details.**

### 6.4.5 Constant-life diagram

The power-law regression equations describing the trend in the fatigue lifetime data over different stress ratios can be used to plot a constant-life diagram. This is typically a graph of stress amplitude $S_{amp}$ against mean stress $S_{mean}$. Each curve on the graph is a 'line of constant life'. Fig. 6.14 shows a complete Haigh constant-life diagram that has been constructed for H180/polyester composites. The power-law regression curves have been extrapolated to $10^9$ cycles to failure. Obviously, the accuracy of this diagram can be improved by testing more samples at more stress ratios. Although the UCS of H180/polyester is half the UTS, the CC fatigue

behaviour is impressive due to the high fatigue strength coefficient *b* (flatter logS-logN curve). In fact, except the low-cycle (N < $10^3$) fully-reversed (*R* = -1) TC fatigue performance, PFRPs offer very stable and useful fatigue properties.

The constant-life diagram in Fig. 6.14 can be used for the life prediction of a component made from H180/polyester, given that the loads the component is subjected to are known. For instance, if a component made from unidirectional H180/polyester has to sustain ($S_{mean}$, $S_{amp}$) of (90, 20), the component will survive ~$10^8$ cycles. Recently, the author of this thesis has applied this constant-life diagram for the fatigue design and life prediction of a 3.5-meter hemp/polyester small wind turbine blade [18, 19].

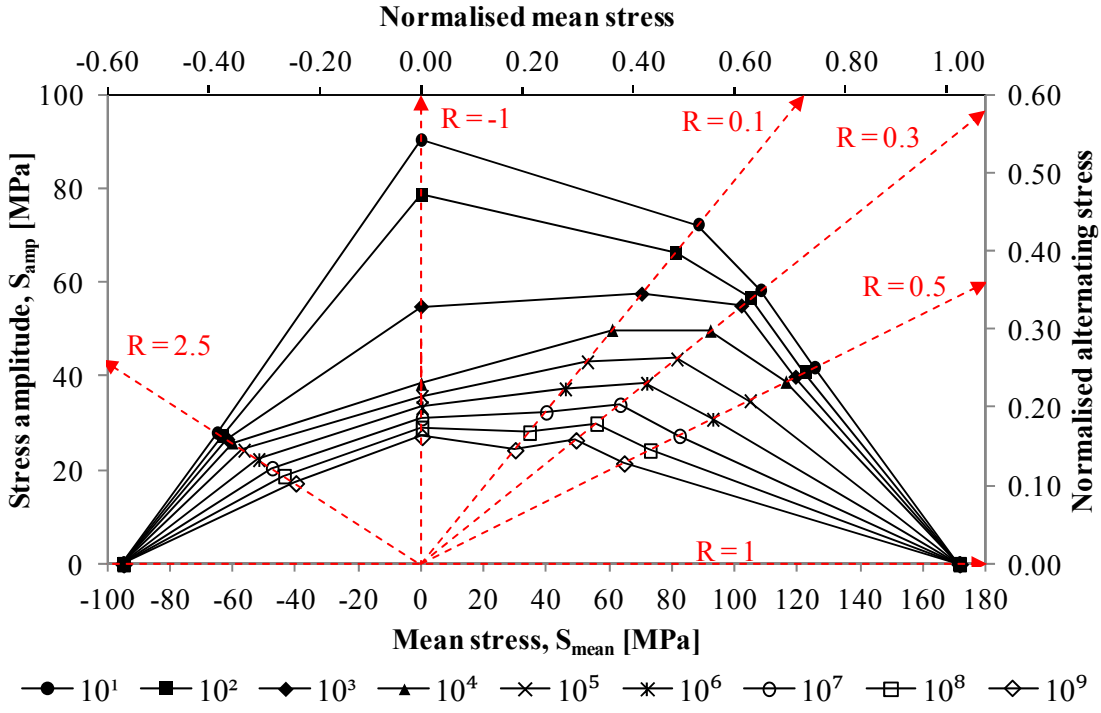


**Fig. 6.14. Constant-life diagram for H180/polyester composites. The secondary axes have been normalised to the UTS (171.3 MPa).**

Often constant-life diagrams are presented in normalised form (Fig. 6.14), where both axes are normalised to the bigger of the static tensile or compressive strength. This allows the use of the constant-life diagram for life prediction of components made from another material whose fatigue behaviour (depicted by S-N curves) is

similar [44, 45]. In Section 6.4.1.2 it was concluded that the fatigue performance of PFRPs is independent of fibre type, due to the several chemical, structural and mechanical similarities in bast fibres. Hence, using the normalised axes scales, Fig. 6.14 could be used for the fatigue life prediction of a component made from flax/polyester, for example.

Mandell *et al.* [41, 44] have produced constant-life diagrams for an E-glass/epoxy laminate ($[\pm 45/0_2]$ lay-up with 64%-0°, $v_f$ = 53%), up to $10^7$ cycles to failure. The UTS and UCS of this laminate are 843 MPa and -687 MPa, respectively. Due to the significantly higher static properties of GFRPs compared to PFRPs, the fatigue properties of GFRPs is far superior to PFRPs. In fact, the constant-life diagram of GFRPs is almost 4-fold that of H180/polyester.

## 6.5 CONCLUSIONS

There is a noticeable lack of fatigue data on plant fibre composites (PFRPs) which seriously limits their prospective use in fatigue critical components. The objective of this chapter was to provide a complete set of fatigue data on vacuum-infused aligned PFRPs. S-N lifetime diagrams have been constructed to specifically investigate the effect of *i)* plant fibre type/quality, *ii)* fibre volume fraction, *iii)* textile architecture, and *iv)* stress ratio, on PFRP cyclic loading behaviour. At each stage, the fatigue performance of PFRPs has been compared to that of GFRPs (material data from [17]). To facilitate fatigue design and life prediction of a PFRP component, a complete constant-life diagram has been generated.

It has been demonstrated that power-law regression lines are a good fit to S-N fatigue data for PFRPs ($R^2 > 0.95$), and thus useful in predicting the fatigue life of PFRPs. While plant fibre type, plant fibre quality, textile architecture and composite fibre content have a significant impact on the static (tensile) properties of the PFRP, they have little impact on the material fatigue strength coefficient $b$ (which dictates the slope of the S-N curve). In essence, higher static properties are a sign of superior fatigue loading capacities throughout the lifetime of PFRPs. Increasing stress ratios lead to improved fatigue performance (increasing $b$) in PFRPs. Fatigue fracture mechanisms and modes are the same for all plant fibre types, but depend on fibre

content, textile architecture and load regimes (stress ratios). Although the absolute fatigue performance of GFRPs is far superior to PFRPs, it is a revelation to find that fatigue strength degradation rates are lower in PFRPs than in GFRPs.

## 6.6 REFERENCES


1. Nijssen R. *Fatigue life prediction and strength degradation of wind turbine rotor blade composites*. PhD, 2006. Delft University: Delft, Netherlands.
2. Shahzad A. *Impact and fatigue properties of natural fibre composites*. PhD, 2009. Swansea University: Swansea, UK.
3. Spatz H, Kohler L, Niklas KJ. Mechanical behaviour of plant tissues: composite materials or structures? *The Journal of Experimental Biology*, 1999, 202: p. 3269–3272.
4. Baley C. Analysis of the flax fibres tensile behaviour and analysis of the tensile stiffness increase. *Composites Part A: Applied Science and Manufacturing*, 2002, 33: p. 939-948.
5. Silva F, Chawla N, Filho RDDT. An experimental investigation of the fatigue behaviour of sisal fibers. *Materials Science and Engineering A*, 2009, 516: p. 90-95.
6. Mandell J, McGarry FJ, Hsieh AJY, Li CG. Tensile fatigue of glass fibers and composites with conventional and surface compressed fibers. *Polymer Composites*, 1985, 6(3): p. 168-174.
7. Hamad W. On the mechanisms of cumulative damage and fracture in native cellulose fibres. *Journal of Materials Science Letters*, 1998, 17: p. 433-436.
8. Harris B. *Engineering composite materials*, 1999. London: The Institute of Materials.
9. Liang S, Gning, PB, Guillaumat, L. A comparative study of fatigue behaviour of flax/epoxy and glass/epoxy composites. *Composites Science and Technology*, 2012, 72(5): p. 535-543.
10. Gassan J. A study of fibre and interface parameters affecting the fatigue behaviour of natural fibre composites. *Composites Part A: Applied Science and Manufacturing*, 2002, 33: p. 369-374.
11. Gassan J, Bledzki AK. Possibilities for improving the mechanical properties of jute/epoxy composites by alkali treatment of fibres. *Composites Science and Technology*, 1999, 59: p. 1303-1309.
12. Towo A, Ansell MP. Fatigue of sisal fibre reinforced composites: Constant-life diagrams and hysteresis loop capture. *Composites Science and Technology*, 2008, 68: p. 915-924.
13. Towo A, Ansell MP. Fatigue evaluation and dynamic mecahnical thermal analysis of sisal fibre-thermosetting resin composites. *Composites Science and Technology*, 2008, 68: p. 925-932.
14. Yuanjian T, Isaac, DH. Impact and fatigue behaviour of hemp fibre composites. *Composites Science and Technology*, 2007, 67: p. 3300-3307.
15. Shahzad A, Isaac DH. Fatigue properties of hemp fibre composites, in *17th International Conference on Composite Materials (ICCM-17)*. 2009. Edinburgh, UK.
16. Shahzad A. Effects of alkalization on tensile, impact, and fatigue properties of hemp fiber composites. *Polymer Composites*, 2012, 33(7): p. 1129-1140.
17. Samborsky D. *Fatigue of E-glass fiber reinforced composite materials and substructures*. MSc, 1999. Montana State University: Bozeman.

18. Shah D, Schubel PJ, Clifford MJ, Licence P. Fatigue characterisation of plant fibre composites for small-scale wind turbine blade applications, in *5th Innovative Composites Summit - JEC Asia 2012*. 26-28 June 2012. Singapore.
19. Shah D, Schubel PJ, Clifford MJ, Licence P. *Fatigue characterisation of plant fibre composites for rotor blade applications*, in *JEC Composites Magazine, No. 73: Special JEC Asia*, June 2012. JEC Composites: Paris. p. 51-54.
20. *BS ISO 13003:2003*, *Fibre-reinforced plastics - Determination of fatigue properties under cyclic loading conditions*, 2003. British Standards Institution: London.
21. Gassan J, Bledzki AK. The influence of fiber-surface treatment on the mechanical properties of jute-polypropylene composites. *Composites Part A: Applied Science and Manufacturing*, 1997, 28A: p. 1001-1005.
22. Mandell J, Reed RM, Samborsky, DD. *SAND92-7005*, Fatigue of fiberglass wind turbine blade materials, 1992. Sandia National Laboratories.
23. Mandell J, Reed RM, Samborsky DD, Pan Q. Fatigue performance of wind turbine blade composite materials. *Wind Energy*, 1993, 14: p. 191-198.
24. Bach P. *ECN-C-92-072*, Fatigue properties of glass and glass/carbon-polyester composites for wind turbines, 1992. Netherlands Energy Research Foundation ECN: Petten.
25. Lewin M. *Handbook of fiber chemistry*. Third ed, 2007. Boca Raton: CRC Press LLC.
26. Pickering K, ed. *Properties and performance of natural-fibre composites*. 2008. CRC Press LLC: Boca Raton.
27. Madsen B. *Properties of plant fibre yarn polymer composites - An experimental study*. PhD, 2004. Technical University of Denmark: Lyngby, Denmark.
28. McLaughlin E, Tait RA. Fracture mechanism of plant fibres. *Journal of Materials Science*, 1980, 15: p. 89-95.
29. Mukherjee P, Satyanarayana KG. An empirical evaluation of structure-property relationships in natural fibres and their fracture behaviour. *Journal of Materials Science*, 1986, 21: p. 4162-4168.
30. Madsen B, Mehmood S, Aslan M. Variability in properties of natural fibres, in *NATEX Workshop*. 2012. Chesterfield, UK.
31. Hanninen T, Thygesen A, Mehmood S, Madsen B, Hughes M. Mechanical processing of bast fibres: The occurrence of damage and its effect on fibre structure. *Industrial Crops and Products*, 2012, 39: p. 7-11.
32. Baets J, Plastria D, Ivens J, Verpoest I. Determination of the optimal flax fibre preparation for use in UD-epoxy composites, in *4th International Conference on Sustainable Materials, Polymers and Composites*. 6-7 July 2011. Birmingham, UK.
33. Kawai M, Yajima S, Hachinohe A, Takano Y. Off-axis fatigue behaviour of unidirectional carbon fiber-reinforced composites at room and high temperatures. *Journal of Composite Materials*, 2001, 35: p. 545-575.
34. Manwell J, McGowan J, Rogers A. *Wind energy explained: Theory, design and application, Second edition*, 2009. Chichester: John Wiley and Sons, Ltd.
35. Kalia S, Kaith BS, Kaur I. Pretreatments of natural fibers and their application as reinforcing material in polymer composites - a review. *Polymer Engineering and Science*, 2009, 49(7): p. 1253-1272.
36. Mwaikambo L, Ansell MP. Chemical modification of hemp, sisal, jute and kapok fibers by alkalization. *Journal of Applied Polymer Science*, 2002, 84: p. 2222-2234.
37. John M, Anandjiwala RD. Recent developments in chemical modification and characterization of natural fiber-reinforced composites. *Polymer Composites*, 2008: p. 187-207.

38. Nosti J. Performance analysis and life prediction for small wind turbine blades: A wood laminate case study, 2009. California Polytechnic State University: San Luis Obispo.
39. Sretenovic A, Muller U, Gindl W. Mechanism of stress transfer in a single wood fibre-LDPE composite by means of electronic laser speckle interferometry. *Composites Part A: Applied Science and Manufacturing*, 2006, 37: p. 1406-1412.
40. Boller K. *ML-TDR-64-86*, Effect of tensile mean stresses on fatigue properties of plastic laminates reinforced with unwoven glass fibers, 1964. Air Force Materials Laboratory: Dayton.
41. Mandell J, Samborsky DD, Agastra P. Composite materials fatigue issues in wind turbine blade construction, in *SAMPE 2008*. 2008. Long Beach.
42. Mandell J, Samborsky DD, Sutherland HJ. Effects of materials parameters and design details on the fatigue of composite materials for wind turbine blades, in *European Wind Energy Conference*. 1999. Nice, France.
43. van Den Oever M, Peijs T. Continuous-glass-fibre-reinforced polypropylene composites- II. Influence of maleic-anhydride modified polypropylene on fatigue behaviour. *Composites Part A: Applied Science and Manufacturing*, 1998, 29A: p. 227-239.
44. Samborsky D, Wilson TJ, Mandell JF. Comparison of tensile fatigue resistance and constant life diagrams for several potential wind turbine blade laminates, 2006. American Institute of Aeronautics and Astronautics: Reston.
45. Mandell J, Samborsky DD, Wahl NK, Sutherland HJ. Testing and analysis of low cost composite materials under spectrum loading and high cycle fatigue conditions, in *14th International Conference on Composite Materials (ICCM-14)*. 2003. San Diego.

# 7 CAN FLAX REPLACE E-GLASS IN STRUCTURAL COMPOSITES? A SMALL WIND TURBINE BLADE CASE STUDY*

## 7.1 INTRODUCTION

Plant fibre reinforcements, particularly if used in combination with a degradable polymer matrix, are perceived to serve as inexpensive and highly renewable alternatives to traditional synthetic fibres. As E-glass fibres dominate today's FRP market (Fig. 1.1) [1] and as plant fibres offer several technical advantages over E-glass (Table 1.1), the former have been marketed as potential substitutes to the latter. Indeed, the composites industry has seen a growing usage of plant fibre reinforced composites in recent years; albeit for predominantly non-structural automotive applications [2, 3] and replacing primarily wood fibre reinforced composites [4]. The current applications of plant fibre composites (PFRPs) have been listed in *Chapter 1*. Despite the historic use of PFRPs in structural components, such as the exterior body of automotives [5, 6] and the fuselage of military aircrafts [5, 7], and the promising mechanical properties of cellulose [2], the uptake of PFRPs by industry in structural applications has been limited [5]. This is attributable to the fact that the impressive theoretical properties of plant fibres have been difficult to exploit in practice. The major issues impeding the wide-spread use of PFRPs, in both non-structural and structural application, have been discussed in *Chapter 2*.

Nonetheless, an interest, at least in the scientific community, has lingered on the development and potential use of PFRPs for performance-demanding applications. For the certification of a structural component, both small-scale specimen tests and full-scale tests are acceptable as proof of component structural integrity (Fig. 7.1).

* This chapter is based on the peer-reviewed journal article:

Shah DU, Schubel PJ, Clifford MJ. Can flax replace E-glass in structural composites? A small wind turbine blade case study. *Composites Part B: Engineering,* 2013, 52: p. 172-181.

However, the safety factors associated with the former are significantly greater than the later. For instance, small wind turbine (SWT) blades designed only through limit state (ultimate strength) analysis based on small-scale specimen tests require a safety factor of 9.0, while blades designed and subsequently tested in a full-scale (ultimate strength) test require a safety factor of 3.3 [8]. Although there has been serious headway in developing PFRPs for structural applications (*e.g.* [9-11]), investigations are at lab-scale coupon tests. To date, there are only limited, if any, scientific studies that conclusively show the suitability of PFRPs over E-glass reinforced composites (GFRPs) for structural applications at a full-scale level [5]. Using the findings of this thesis thus far, this study aims to demonstrate whether PFRPs are potential structural replacements for GFRPs, through full-scale testing of a composite structure.

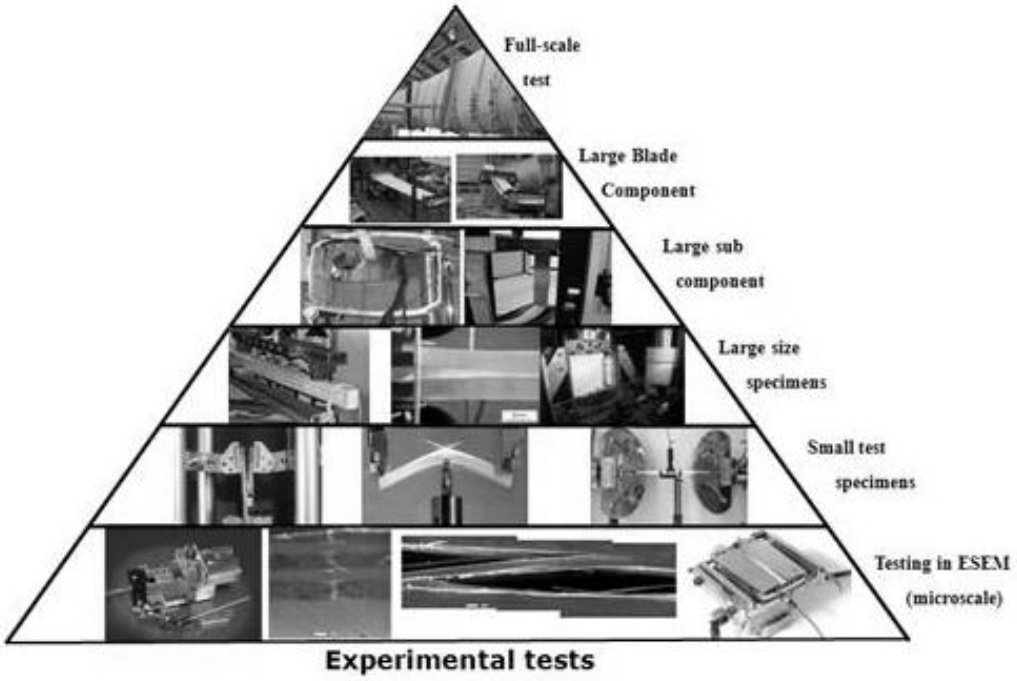


**Fig. 7.1. Certifying agencies accept both small-scale tests and full-scale tests as proof of component structural integrity [12].**

### 7.1.1 Reinforcements for rotor blades: plant fibres or E-glass?

GFRPs are by far the most widely used material for rotor blade manufacture. In recent years, carbon fibre has become of increasing interest due to the structural demands of ever-larger blades and the decreasing price of carbon fibres. Nonetheless,

natural or bio-based materials are of potential interest as rotor blade materials, due to their moderate mechanical performance and attractive environmental profile [13]. While wood was one of the first materials for rotor blades, today wood epoxy laminates are a less frequent but not an uncommon material for rotor blades; indeed a large material database exists, accredited by certification standards [8], to support their utilisation. However, the design limitations with using wood, its low stiffness and high variability in quality, alongside the higher performance capacity of GFRPs, give wood-based materials a tough run.

PFRPs may be more suitable to compete against GFRPs. Over the past five years, some researchers have attempted to evaluate the potential of PFRPs specifically for wind turbine blade applications. Brondsted *et al.* and their group [14, 15] extensively studied the mechanical properties of bamboo/epoxy laminates, aiming to develop bamboo composites for large (>1 MW) turbine blades. They concluded that bamboo composites had higher strength, stiffness, fatigue life and fracture toughness than wood [14]. They also compared the sustainability of a bamboo blade against a GFRP blade through qualitative life cycle analysis and suggested that bamboo composites are a more environmentally-friendly option than GFRPs [15]. However, Brondsted *et al.* did not manufacture or test a full-scale biocomposite blade. Frohnapfel *et al.* [16] produced small vertical axis wind turbine blades using woven flax reinforcements. Note that rotor blades for vertical axis turbines observe much lower loads than those faced by rotor blades for horizontal axis turbines. This is because the load-bearing members in vertical axis turbines are the cross-members holding the blade. Nonetheless, Frohnapfel *et al.* [16] demonstrated that a 1.2 m flax blade, manufactured via press-moulding, successfully met the static test requirement (with a 2.5 times safety factor). However, their attempt at manufacturing a larger 3 m flax blade, via vacuum infusion, was unsuccessful. More recently, aiming to produce a wind turbine car, Mikkelsen *et al.* [17, 18] investigated the possibility of manufacturing 0.6 m long flax and flax/carbon hybrid blades. Through mechanical tests, they found that although an optimised hybrid blade with a dominating amount of flax fibres performed as well as the pure carbon blade, the pure flax blade performed poorly. The masses of the manufacture carbon, carbon/flax and flax

blades were 0.26 kg, 0.31 kg and 0.56 kg. Mikkelsen *et al.* [17] estimated that the embodied energy of the flax blade was 40% lower than that of the carbon blade.

The Wind Energy Materials Group (within the Polymer Composites Research Group) at The University of Nottingham has been involved with the design and manufacture of wind turbine blades. The Group is currently working on an 11 kW horizontal axis 3-bladed turbine with a rotor diameter of 7 m. In particular, through this NIMRC funded research project, the Group has been investigating the potential of sustainable plant fibre reinforcements as a replacement to conventional E-glass reinforcements in small wind turbine (SWT) blades. A small wind turbine is classified as one with a rotor diameter < 16 m or rated capacity < 100 kW [8]. This investigation has large implications owing to the unprecedented growth of the global SWT industry (Fig. 7.2). It is estimated that by 2020, the total UK small wind capacity will exceed 1300 MW, through the installation of more than ~400,000 SWTs [19]. Assuming these are 3-bladed systems, more than 1 million blades will need to be manufactured [19].

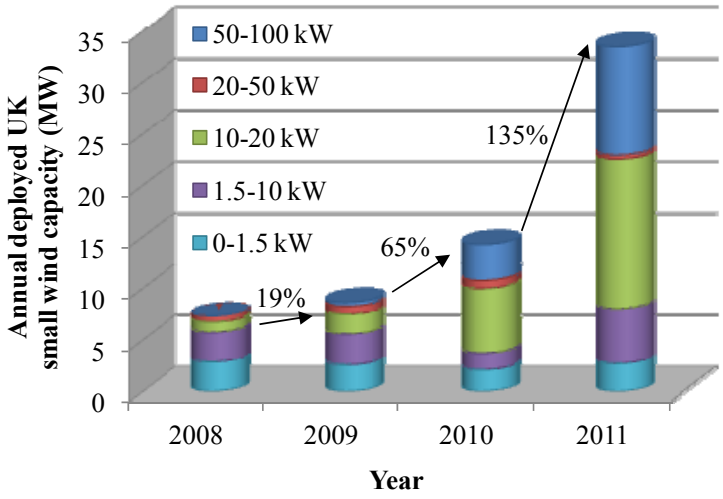


**Fig. 7.2. Annual deployed UK small wind system capacity (MW). Data for 2011 is based on manufacturing forecasts. Adapted from [19].**

The blades of a wind turbine are a critical and costly component of a wind turbine system. Having a service life of 20–30 years and cycling in excess of 200 rpm, small rotor blades are designed against several major structural conditions including strength, stiffness and tip deflection during operational loading (design wind speeds

of 11.9 $ms^{-1}$) and severe loading (extreme wind speeds of 59.5 $ms^{-1}$), as well as very high numbers of fatigue cycles (> $10^9$ cycles) during service.

The loads on a rotor blade can be categorised as aerodynamic loads (such as drag, lift and shear), inertial loads (such as gravitational, gyroscopic, centrifugal) and operational loads (resulting from turbine control such as yawing, pitching). These are depicted in Fig. 7.3. Typically, gravitational loads are insignificant for small blades. As shown in Fig. 7.3, the loads can be divided into three directions: flap-wise (bending the blade downwind), edge-wise (bending the blade in the rotational direction) and axial (along the blade length) directions. For small blade, the flap-wise loads are significantly larger than the axial loads and edge-wise loads.

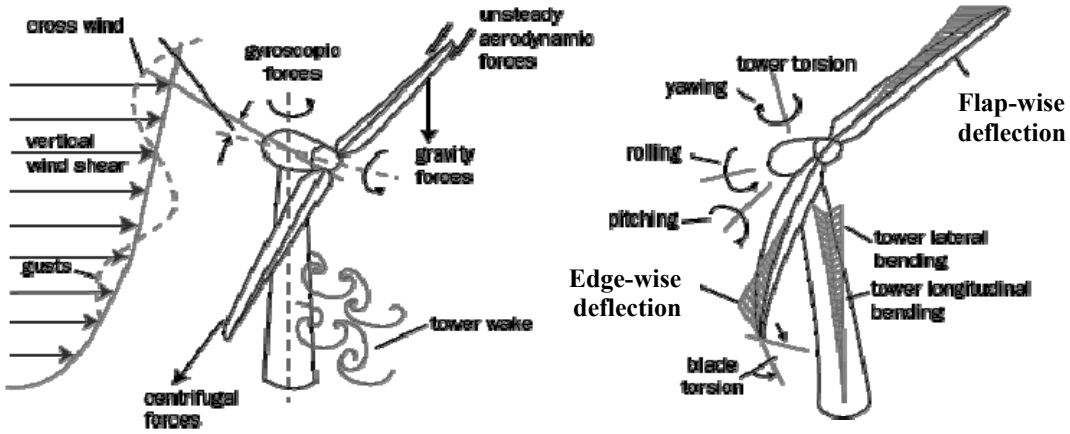


**Fig. 7.3. The blades of a wind turbine system experience various loads [20].**

Naturally, for certification of the SWT blades, the structural integrity of the blade needs to be demonstrated by analysis and full-scale mechanical tests, as per BS-EN 61400-2:2006 [8] and BS-EN 61400-23:2002 [21]. Recently, the author of this thesis has shown [22, 23], using fatigue data based on lab-scale coupon tests (*Chapter 6*) and combining the flap-wise, edge-wise and axial design blade loads into pure tensile/compressive loads (see Fig. 7.4), that a PFRP (hemp/polyester) SWT blade can survive the design fatigue loads (inclusive of a 1.50 safety factor) for the required 20-year design life.

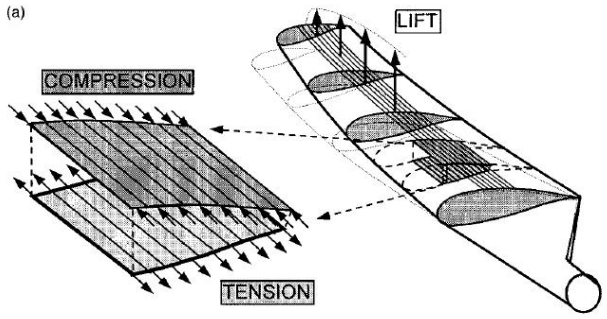


**Fig. 7.4. For simplified fatigue analysis, the axial, flap-wise and edge-wise loads can be translated into tension/compression loads along the blade length [24].**

This chapter details a comparative case study looking at the manufacture, analysis and mechanical testing of 3.5 m composite rotor blades (suitable for an 11 kW SWT) built from flax/polyester and E-glass/polyester. Firstly, this chapter compares the manufacturing properties, weight, cost, and sustainability of the two blades. Secondly, through static flap-wise testing of the blades (in accordance to certification standards [8, 21]), their mechanical properties are compared. It is eventually confirmed that like the E-glass/polyester blade, the flax/polyester blade satisfies the design and structural integrity requirements for an 11 kW turbine. Hence, flax can potentially replace E-glass in this structural application.

## 7.2 DESIGN AND MANUFACTURE OF BLADES

### 7.2.1 Blade design summary

The study blade is 3.50 m in length, with an average chord length of 0.29 m. For improved blade efficiency, an aerodynamically optimised blade shape, generated through an in-house developed design software (*BladeShaper v2.0*) considering *i)* blade element momentum theory including wake rotation, *ii)* turbine performance, and *iii)* part manufacturability, was employed.

To achieve the desired structural performance, based on past experience, a conventional blade construction is used (Fig. 7.5). The blade consists of a CNC machined core and fibre reinforced composite structural blister caps and constant-thickness outer shell. The core provides resistance against buckling, the

unidirectional fibre reinforced blister caps provide maximum axial (tensile) and bending (flexural) stiffness and strength, and the multiaxial fibre reinforced outer skin provides resistance against torsion-related shear loads. The composite material has a nominal fibre volume fraction of 32-38%. The ratio of multiaxial reinforcement (in the shell) to unidirectional reinforcement (in the blister caps) is ~180-250 wt%.

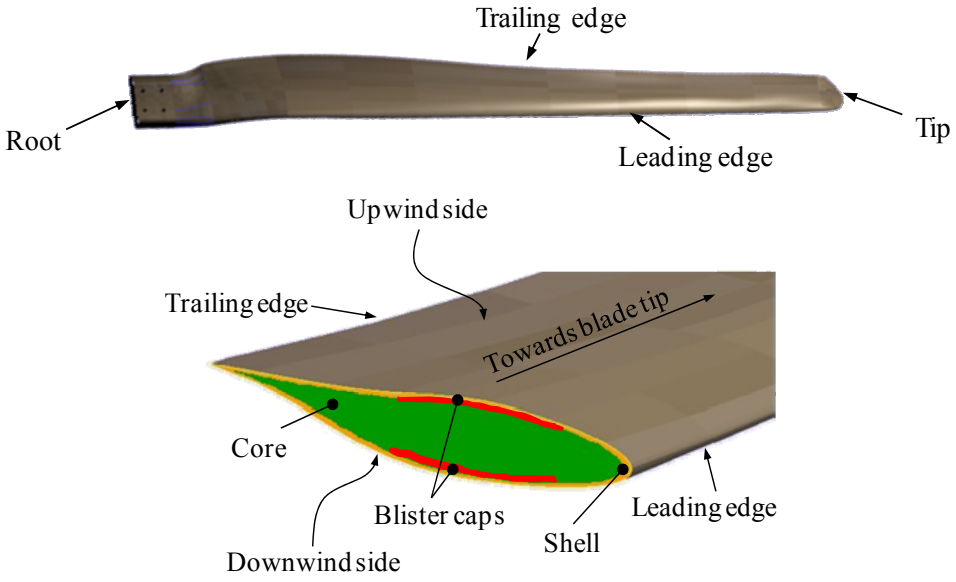


**Fig. 7.5. Profile and lay-up of the composite blades.**

## 7.2.2 Blade manufacture

### 7.2.2.1 Reinforcement materials and their properties

Two identical blades were manufactured using flax and E-glass as reinforcements, employing the same stacking sequence. Low-twist (20 tpm, 400 tex) flax rovings (referred to as F20 in *Chapters 3 and 6*) were sourced from Safilin (France) and produced into aligned (unidirectional (300 gsm) and multi-axial (600-900 gsm)) stitched mats by Formax (UK) Ltd. Aligned E-glass stitched fabrics (300-900 gsm) were also sourced from Formax (UK) Ltd.

The justification behind selecting the plant fibre reinforcement F20 is as follows. In *Chapters 3 and 6*, it was shown that F20 composites exhibit best mechanical properties (static and fatigue) amongst all the PFRPs studied. For the manufacture of

the plant fibre blade and to realise the true structural potential of plant fibres, an optimised reinforcement form (*i.e.* aligned fabrics from F20 low-twist flax rovings) has been selected. Bast fibres in the form of flax are employed, as they are characteristically useful as composite reinforcements. The flax fibres have undergone (field/dew) retting, which is necessary for high fibre quality, and are at least 25 mm in length, ensuring high fibre aspect ratios and length efficiency factors. During roving production, the flax fibres have also undergone caustic soda treatment, implying possibly improved fibre/matrix adhesion and thus load transferring capabilities. Furthermore, low-twist rovings are used so that a continuous reinforcement product could be utilised for preform manufacture, with negligible detrimental effects of yarn twist on composite properties. In addition, the use of aligned fabrics (unidirectional and multi-axial) ensures that the fibre properties are being transferred and utilised where necessary. The nominal fibre volume fractions employed (32-38%) are also much above the estimated critical fibre content (~10%).

To illustrate the difference in mechanical performance of the F20 flax reinforcement and the E-glass reinforcement, Table 7.1 presents the tensile, compressive and fatigue properties of polyester composites made from the unidirectional and biaxial reinforcements (evaluated in *Chapter 3-6*). To assess the comparative performance of the two materials, material performance indices (from *Chapter 2*) are reintroduced here as a form of design criteria. The blade has a sandwich construction (Fig. 7.5) such that it can be assumed that the fibre reinforced plastic material in the shell and blister caps experience pure tension and pure compression (Fig. 7.4). The useful material performance indices are shaded in Table 7.1.

Comparing the tensile properties, it is evident that the relative performance of unidirectional flax composites to unidirectional E-glass composites is similar to the relative performance of biaxial flax composites to biaxial E-glass composites. For instance, the specific tensile stiffness of both unidirectional and biaxial flax composites is ~65% that of unidirectional and biaxial E-glass composites, respectively. The tensile material performance indices for the blade are specific stiffness ($E/\rho$) and specific strength ($\sigma/\rho$). Notably, F20 composites have a comparable (up to 87%) specific stiffness to GFRP; this is also reflected by the back-

calculated fibre modulus, where flax exhibits a stiffness of 68 MPa. On the other hand, the specific strength of both unidirectional and biaxial flax composites is only ~45% that of unidirectional and biaxial GFRP. Again, the effective fibre strength reinforces this assertion. It is expected, therefore, that for the same mass of material, a flax composite would elongate as much as an E-glass composite, but the flax composite would fail at a significantly lower tensile stress.

From Table 7.1 it is clear that in terms of absolute properties flax composites do not perform as well as they do in tension. E-glass on the other hand, performs only marginally worse in compression; this is one of its well-known advantages [25]. While the compression modulus of unidirectional F20/polyester is 54% that of unidirectional E-glass/polyester, the compression strength of the former is only 32% of the latter. However, the material performance indices reveal a different story. The compressive material performance indices for the blade are specific stiffness ($E^{1/3}/\rho$) and specific strength ($\sigma^{1/2}/\rho$). The specific modulus of F20/polyester is marginally (3%) larger than that of E-glass/polyester, and the specific strength of the former is 70% of the latter. In terms of the material performance indices, flax composites perform better in compression than in tension, and flax composites are more competitive with GFRP in compression. Some researchers [26] have revealed that the compressive properties of elementary flax fibres is approximately 80% of their tensile properties, and this ratio is very high compared to other anisotropic fibres.

Finally, comparing the fatigue performance of unidirectional and biaxial F20 composites with GFRPs (Table 7.1), it is found that the fatigue strength at $10^6$ cycles (the fatigue material performance index for a blade) for flax composites is 40-55% that of GFRP.

The comparison in material properties of the flax and E-glass composites show that GFRPs, on the whole, outperform PFRPs, although the specific stiffness performance of PFRPs may be comparable to GFRPs. In addition, PFRPs compete better with GFRPs in specific compressive properties than in specific tensile properties.

**Table 7.1. Tensile, compressive and fatigue properties of unidirectional [0] and biaxial [±45] F20/polyester and E-glass/polyester composites. Material performance indices are shaded.**

| | | | Unidirectional | | | Biaxial | | |
|---|---|---|---|---|---|---|---|---|
| | Property | | Flax | E-glass | Flax/E-glass | Flax | E-glass | Flax/E-glass |
| Tensile | Fibre volume fraction | % | 30.9 | 42.8 | | 29.2 | 28.0 | |
| | Density | $gcm^{-3}$ | 1.31 | 1.79 | 0.732 | 1.30 | 1.61 | 0.807 |
| | Composite stiffness | GPa | 23.4 | 36.9 | 0.634 | 5.70 | 8.77 | 0.650 |
| | Composite specific stiffness | $GPa/gcm^{-3}$ | 17.9 | 20.6 | 0.869 | 4.38 | 5.45 | 0.804 |
| | Effective fibre stiffness† | GPa | 67.6 | 81.6 | 0.828 | - | - | |
| | Composite strength | MPa | 277 | 826 | 0.335 | 51.4 | 139 | 0.370 |
| | Composite specific strength | $MPa/gcm^{-3}$ | 213 | 461 | 0.462 | 39.5 | 86.3 | 0.458 |
| | Effective fibre strength† | MPa | 883 | 1920 | 0.460 | - | - | |
| | Composite failure strain | % | 1.70 | 1.90 | 0.895 | 3.76 | 4.12 | 0.913 |
| Compressive | Fibre volume fraction | % | 32.5 | 30.0 | | N/A‡ | N/A‡ | N/A‡ |
| | Density | $gcm^{-3}$ | 1.30 | 1.64 | 0.793 | N/A‡ | N/A‡ | N/A‡ |
| | Composite stiffness | GPa | 11.3 | 21.0 | 0.538 | N/A‡ | N/A‡ | N/A‡ |
| | Composite specific stiffness | $GPa^{1/3}/gcm^{-3}$ | 1.73 | 1.68 | 1.03 | N/A‡ | N/A‡ | N/A‡ |
| | Composite strength | MPa | 101 | 313 | 0.323 | N/A‡ | N/A‡ | N/A‡ |
| | Composite specific strength | $MPa^{1/2}/gcm^{-3}$ | 7.73 | 10.8 | 0.717 | N/A‡ | N/A‡ | N/A‡ |
| | Composite failure strain | % | 3.44 | 3.70 | 0.930 | N/A‡ | N/A‡ | N/A‡ |
| Fatigue ($R$=0.1) | Fibre volume fraction | % | 26.9 | 30.0 | | 29.2 | 28.0 | |
| | Density | $gcm^{-3}$ | 1.29 | 1.64 | 0.787 | 1.30 | 1.61 | 0.807 |
| | Single cycle strength | MPa | 236 | 567 | 0.416 | 51.4 | 139 | 0.370 |
| | Fatigue strength at $10^6$ cycles | MPa | 115 | 204 | 0.564 | 22.1 | 57.3 | 0.386 |

† The effective fibre properties are 'back-calculated' using the rule of mixtures.

‡ N/A = not measured

#### 7.2.2.2 Fabrication of the blade

The blades were manufactured using an unsaturated polyester resin in a light resin transfer moulding (LRTM) process. Both blades took ~1.5 hrs to infuse showing that using plant fibre reinforcements does not significantly alter infusion times. Post cure was conducted at 40 °C for 2 hr. The manufactured flax/polyester and E-glass/polyester blades are shown in Fig. 7.6. An insightful manufacturing advantage of using flax over E-glass is that the former doesn't cause itching during handling and is non-hazardous if inhaled.

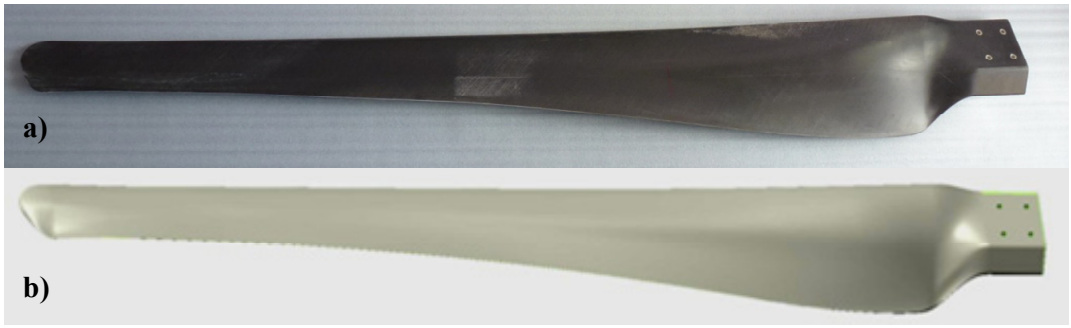


**Fig. 7.6. Images of the *a)* flax/polyester and *b)* E-glass/polyester blades.**

Note that as the flax reinforcements were in the form of rovings (rather than twisted yarns), they were loose (rather than compact). The bulkiness of the fabric layers implied that closing the tool after placing the fabric was difficult, particularly at the maximum chord length where there is also a large variation in cross-sectional thickness. Nonetheless, as increasing yarn twist has several detrimental effects on PFRP performance (as discussed in *Chapter 5*) including lowered permeability, hindered impregnation, formation of impregnation related voids and significant loss in orientation efficiency; rovings are preferred for PFRP components.

### 7.2.3 Comparison of mass properties

Fig. 7.7a) shows the difference in mass of the flax and E-glass blades. Weighing at 23.3 ± 0.1 kg, the flax blade is 10% lighter than the E-glass blade (25.8 ± 0.1 kg). Interestingly, the density of the flax reinforcement was measured to be 1.57 $gcm^{-3}$, which is 60% that of E-glass (2.66 $gcm^{-3}$). The reason why the flax blade is only 10%

lighter than the E-glass blade is that the fibre accounts for only 18% and 30% of the flax and E-glass blade masses. Directly comparing the fibre masses allows to appreciate the weight savings that flax provides; while the E-glass blade has 7.7 kg of fibre, the flax blade has only 4.2 kg of fibre. That is, using flax, rather than E-glass, reduces the fibre mass by 45%.

As Fig. 7.7a) illustrates, the mass of the core is identical in both blades and accounts for 32–36% of the blade mass. Interestingly, the resin accounts for 38% of the E-glass blade mass but 46% of the flax blade mass. The intake of 1 kg more resin in the flax blade is possibly due to *i)* the slightly lower volume of fibre (accounting for ~0.3kg of extra resin), and *ii)* a cavity forming over certain regions of the blade (specifically, at the maximum chord length) resulting from the deflection of the mould tool.

Note that the volume of fibre reinforcement used in both blades is similar at 0.0027–0.0029 $m^3$. The fibre volume fraction in the composite part of the blades is calculated to be 23-26% (Table 7.2). The lower fibre weight fraction of the flax composite, compared to the E-glass composite (Table 7.2), is solely due to the difference in densities of the flax and E-glass fibres. Therefore, the difference in fibre weight fraction cannot be avoided (if the composites have the same fibre volume fraction).

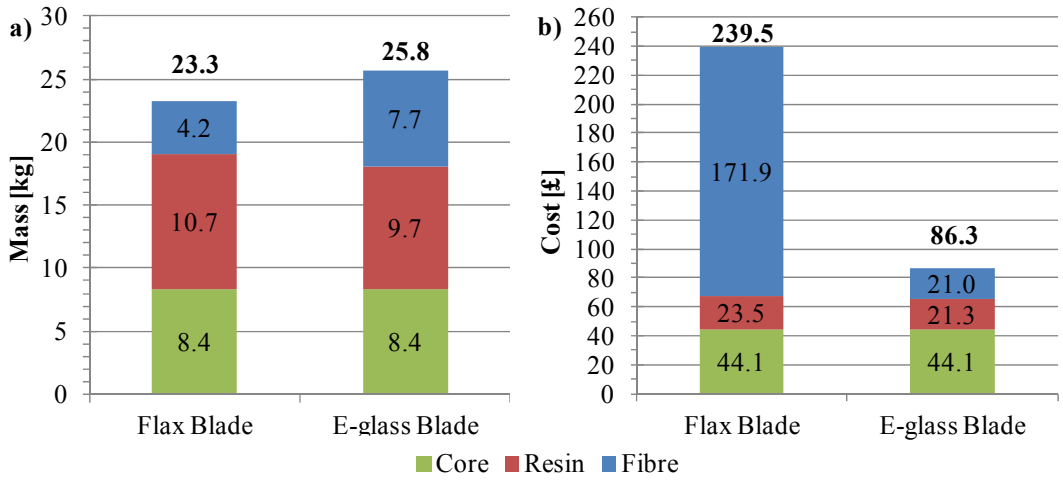


**Fig. 7.7. Comparison of the *a)* mass and *b)* materials cost of the flax and E-glass blades.**

The centre of gravity $C_g$ from the blade root is 1.26 ± 0.01 m for the flax blade and 1.29 ± 0.01 m for the E-glass blade. The $C_g$ is fairly similar for both blades, as the blade construction and fabric stacking sequence is identical.

**Table 7.2. Calculated overall fibre weight and volume fractions in the composite part of the blades (excluding the core).**

| | Flax blade | E-glass blade |
|---|---|---|
| Density [gcm$^{-3}$] | 1.28 | 1.59 |
| Fibre weight fraction [%] | 28.2 | 44.3 |
| Fibre volume fraction [%] | 22.9 | 26.4 |

### 7.2.4 Comparison of materials cost

Fig. 7.7b) presents the difference in materials cost of making the flax and E-glass blades. The materials cost for the flax blade amounts to £239.48, making it approximately 3 times more expensive than the E-glass blade (£86.34). The material cost of the foam core (5.28 £/kg) and the polyester resin (2.20 £/kg) are almost identical for the two blades, amounting to ~£65. Fig. 7.7 shows that despite requiring less fibre in a flax blade, the fibre cost of the flax blade is 8 times that of the E-glass blade. Hence, it is the cost of the fibre reinforcement which is causing the cost disparity between the flax and E-glass blades.

Unlike E-glass, costs of flax reinforcements increase tremendously with processing steps. This is because *i)* E-glass reinforcements are an established mature market, and *ii)* the processing (and incurred costs) of flax and E-glass reinforcements is different. As Table 7.3 highlights, under current market conditions, aligned flax reinforcements are more expensive than aligned E-glass reinforcements at every stage: raw fibre, yarn/roving and aligned fabric. Raw flax itself is barely cost-competitive against raw E-glass [27, 28]. Interestingly, the cost of non-woven mats of flax fibres is comparable to (or even lower than) that of E-glass (Table 7.3). This is possibly a result of the fact that naturally discontinuous plant fibres are readily (without much processing) useable in the production of non-wovens. It is thus not surprising that current industrial applications of PFRPs are principally based on non-woven precursors [3]. However, to make aligned fabric reinforcements, staple plant fibres like flax need to be first processed into yarns/rovings, unlike E-glass which is a

synthetic filament. Flax rovings/yarns are up to 10 times more expensive than E-glass. Madsen *et al.* [29] have also commented on the high market price of such plant fibre yarns. In addition, the actual cost associated with aligned fabric manufacture needs to be accounted. The flax reinforcements were specially produced for this study; the costs for the multi-axial fabrics (300–600 gsm) ranged from 13.8 £/m$^2$ to 22.0 £/m$^2$. E-glass fabrics (300–600 gsm) were off-the-shelf items, which typically cost 1.80 £/m$^2$. By weight, the cost of aligned flax fabric is 6–15 times greater than that of aligned E-glass fabric. In essence, the development of low-cost aligned plant fibre semi-products is a critical and potentially limiting factor in encouraging the future industrial use of PFRPs, as an alternative to GFRPs.

**Table 7.3. Flax is costlier than E-glass at every stage. Costs for raw fibre, yarn/roving and aligned fabrics are obtained from materials suppliers (and assumed indicative of the market prices) as of Dec 2012. Costs for non-woven mats are from [29].**

| Cost of reinforcement | Flax‡ | E-glass | Flax/E-glass |
|---|---|---|---|
| Raw fibre [£/kg] | 1.5 | 1.3 | 1.2 |
| Yarn/roving [£/kg] | 10.0–13.0 | 1.3 | 7.7–10.0 |
| Aligned fabric [£/kg] | 36.7–45.9 | 3.0-6.0 | 6.1-15.3 |
| Non-woven mat [£/kg] | 1.5 | 2.2 | 0.7 |

‡ Note that the prices of the flax reinforcements quoted here are based on small quantities and should only be used as guidelines. Prices reduce significantly with higher quantities (> 5 tonnes), but also depend on other factors such as market conditions and fibre quality.

### 7.2.5 Comparison of eco-impact

In composites manufacture, the embodied energies of the various materials (fibre reinforcement, matrix and core) typically account for over 80% of the total environmental impact of the composite component [30]. The manufacturing process and operations, on the other hand, typically account for less than 15% of the total eco-impact [30]. As the flax and E-glass blade have been manufactured in an identical manner, the eco-impact of replacing E-glass with flax can be gauged by estimating the cumulative embodied energies of the materials in the two blades.

As discussed in *Chapter 2*, based on life cycle assessment studies on plant fibre reinforcements, while the energy required in the cultivation of plant fibres is low (4-

15 MJ/kg [31-35]), further processing steps (*e.g.* retting and spinning) can significantly increase the cumulative energy demand to 54-118 MJ/kg for flax sliver and 81-146 MJ/kg for flax yarn [32-34, 36]. Conversion from slivers/yarns to fabrics would require further energy inputs. The aligned flax fibre fabrics used in this study employ flax rovings; here, it is assumed that the embodied energy of the flax fabrics will be in the range of 54-118 MJ/kg (similar to the flax sliver). On the other hand, the embodied energy of E-glass yarns and fabrics is in the range of 30-55 MJ/kg [34, 35]. Pre-empting the conclusions, it is clear that aligned plant fibre preforms have a larger eco-impact than E-glass preforms. Note however that the eco-impact of component end-of-life disposal is not considered here; while GFRPs are generally landfilled or incinerated (for energy recovery from the resin alone), PFRPs would be incinerated (for energy recovery from both the plant fibres and the resin). Unsaturated polyester resin and foam core have embodied energies of approximately 63-78 MJ/kg [37] and 80-120 MJ/kg [30], respectively.

Using these estimates of embodied energies of the various constituent materials and the quantity of material used in each blade (Fig. 7.7), the cumulative materials embodied energy of the flax and E-glass blade is estimated to be in the ranges of 1573-2338 MJ (or 68-100 MJ/kg) and 1514-2188 MJ (or 59-85 MJ/kg), respectively. In essence, despite requiring 45% less fibre mass, the flax blade has an up to 15% larger eco-impact than the E-glass blade. Certainly, increasing the fibre content in the flax blade (to enhance structural integrity) would result in a much larger eco-impact.

It can also be commented here that perhaps the cost of a product may be a useful indicator of the embodied energy of a product; while raw flax fibres and non-woven mats are low-cost and require low energy for production, aligned plant fibre semi-products are high-cost and require high energy inputs for production. These findings highlight that for structural PFRPs to be projected as environmentally benign alternatives to GFRPs, the development of sustainable processes for the manufacture of aligned plant fibre semi-products is a critical step ahead. Furthermore, it is suggested that as the matrix and core are the other constituents of the blade, which notably make up a larger weight fraction of the blade than the fibre constituent, to truly reduce the eco-impact of the final product, it is essential that not only the fibre

reinforcement but also the matrix and core are bio-based or at least bio-sourced. Indeed, the development of high-performance bio-resins and bio-cores is another critical factor in the wide acceptance of PFRPs as sustainable materials.

## 7.3 MECHANICAL TESTING OF BLADES

Upon the design and manufacture of the two blades, their structural integrity was assessed through design load analysis and full-scale mechanical tests, as per BS-EN 61400-2:2006 [8] and BS-EN 61400-23:2002 [21]. This section details the flap-wise static testing of the two blades.

### 7.3.1 Description and derivation of test loads

#### 7.3.1.1 Design loads

The SWT, for which the blades are to be used, is an 11 kW Class-II horizontal axis 3-bladed upwind stall regulated turbine, with a rigid hub, cantilever blades, active yaw mechanism and fixed pitch. Hence, design loads for the blades can be determined using simplified conservative load equations in [8]. For the flap-wise static testing of the blade, as per [21] it is the blade root bending moment $M_{yB}$ (acting to bend the blade tip downwind) that is of interest. [21] acknowledges that stresses caused by radial loads ($F_{zB}$) are relatively low. This is confirmed through a simple stress analysis at the blade root. At the design wind speed (11.9 $ms^{-1}$) and design rotor speed (170 rpm) under normal operating conditions (*Load Case A* in [8]), the flax and E-glass blade experience a radial load of 23.6 kN and 26.2 kN, respectively (due to difference in masses). The resultant mean stress at the blade root is only 1.22–1.35 MPa.

Typically, the blade is tested against the calculated blade root bending moment $M_{yB}$ under normal operating conditions (*Load Case A* in [8]) and worst case loading. Note that this turbine has an active yaw mechanism which ensures that when subjected to extreme gusts (*Load Case H* in [8] at extreme wind speed of 59.5 $ms^{-1}$), the turbine is parked at 90° yaw angle, leading to minimal exposure. Using known values for constants, blade/turbine parameters and wind condition parameters, the design loads on the blade have been determined for the several load cases [38]. For this particular

turbine setup, the worst case loading was found to occur when there is a yaw error of 30° (*Load Case C* in [8] at design wind speed of 11.9 $ms^{-1}$). Conveniently, blade root bending moment $M_{yB}$ at *Load Case A* and *Load Case C* are not a function of blade mass, and hence are the same for both the blades.

#### 7.3.1.2 Target test loads

To determine the target test loads, partial safety factors have to be incorporated with the design loads. In particular, BS-EN 61400-2:2006 [8] and BS-EN 61400-23:2002 [21] require the inclusion of the product of the following partial safety factors: load $\gamma_f$, consequence of failure $\gamma_n$ and blade to blade manufacturing variations $\gamma_s$. It appears that the recommended combined safety factor is similar in various certification standards [39].

As is later revealed, a single-point test method is employed, where a single concentrated point load is applied at $l$ m from the blade root. The target point load $F$ ($F = M_{yB}/l$), associated with the target blade root bending moment $M_{yB}$, at the normal operation and worst case loads is 1.48 kN and 3.99 kN, respectively.

### 7.3.2 Experimental set-up

#### 7.3.2.1 Test equipment

For the static flap-bending test, a single point test method was employed. The blade root was fixed to a specially designed rigid steel test rig (Fig. 7.8a)) via a simple bolted connection. No inserts or studs are used; rather, the bolts go through holes in the composite sandwich (skin/cap/core/cap/skin). The test rig mimics the real blade root to hub connection, with the same bolt pattern, plate thickness and plate local geometry. The test rig was attached to two structural poles. The blade was fixed horizontal (flap-wise up) and was loaded by an overhead crane. A composite saddle was specially built to enclose the blade's cross-section at the desired load point ($l$ m from the blade root). This is presented in Fig. 7.8b). A rubber lining was placed between the saddle and the blade, to provide grip and to protect the blade from local damage due to a concentrated pressure at the load application point.

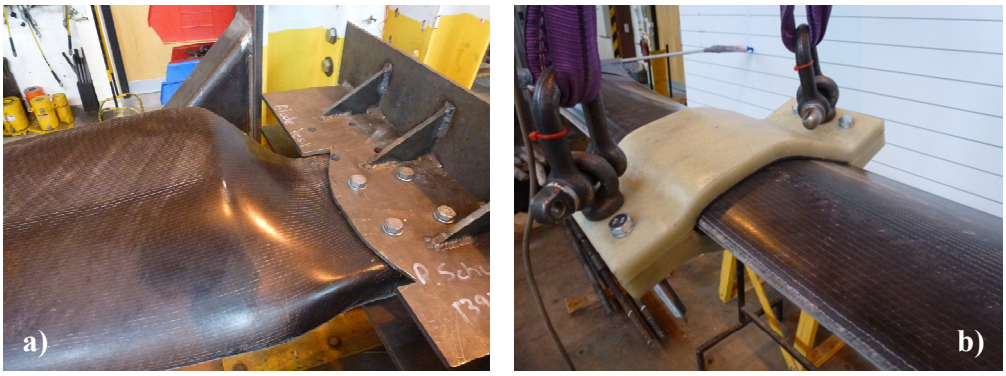


**Fig. 7.8. Image showing the *a)* test rig and *b)* composite saddle.**

The overall loading arrangement is presented in Fig. 7.9. The external sleeves of the saddle have eyebolts which are used to connect to a 12 kN calibrated load cell. The load cell rests on a spreader beam and is attached to a 5 tonne overhead crane. As the blade deflects, the load direction relative to the blade orientation can change. To ensure that the load is perpendicular to the load application point on the blade, the overhead crane is periodically moved towards the blade root after releasing some load. A spring-loaded marker, attached at the blade tip, provides in-situ tip displacement monitoring.

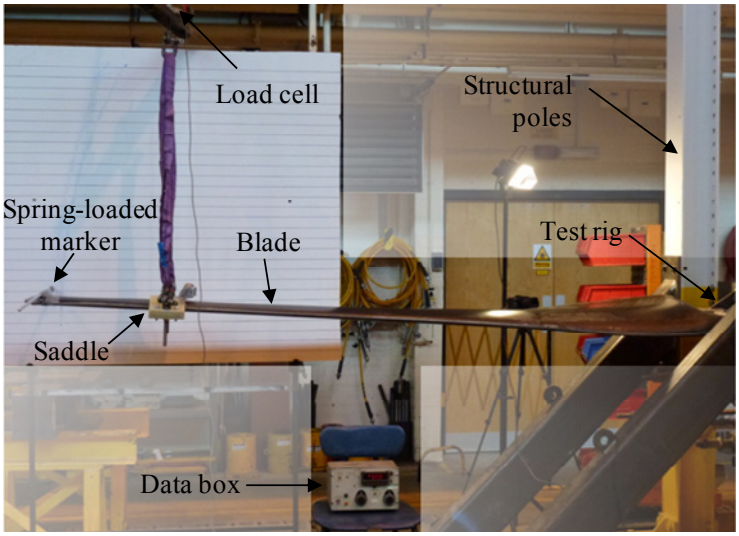


**Fig. 7.9. Blade flap-wise test loading arrangement.**

#### 7.3.2.2 Test regime

To systematically achieve the target point test loads $F$, a loading sequence was developed (Fig. 7.10). The test has three stages: *i)* loading up to the 100% normal operation load ($F$ = 1.48 kN), *ii)* loading up to the worst case load ($F$ = 3.99 kN, *i.e.* 270% (= 3.99/1.48) of normal operation load), and *iii)* loading to failure. To ensure steady loading, small steps of 0.01–0.03 kN are used. Regular load dwells are incorporated to allow the blade to settle.

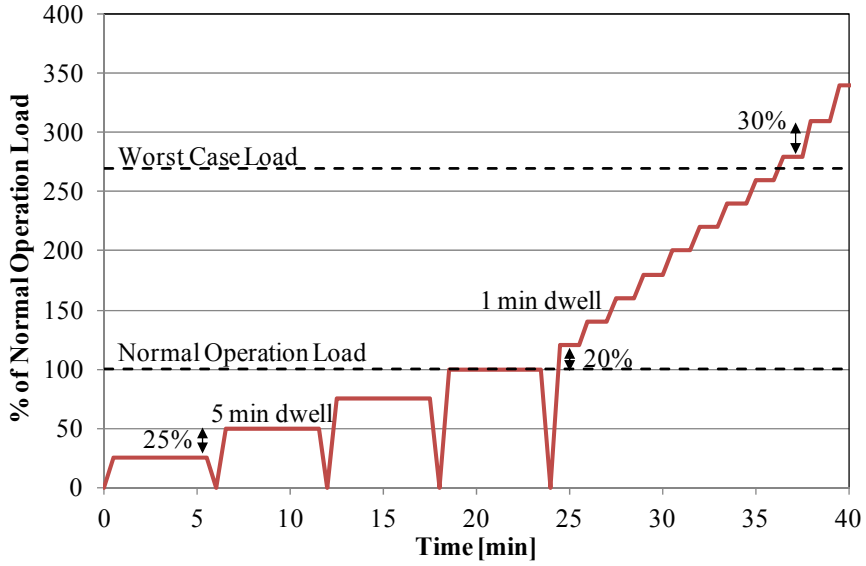


**Fig. 7.10. Blade flap-wise test loading regime. Load values (y-axis) are normalised by the normal operation load (of 1.48 kN).**

#### 7.3.2.3 Description of failure criteria

To satisfy BS-EN 61400-23:2002 [21], no superficial failure (small cracks, buckling or delamination) should occur below the normal operation load. In addition, no functional failure (substantial loss in functionality through permanent deformation) or catastrophic failure (complete disintegration or collapse) should occur below the worst case load.

### 7.3.3 Results and discussion

The flax and E-glass blades were subjected to flap-bending tests according to the experimental set-up and loading regime described in Section 7.3.2. Fig. 7.11 presents

graphs of test load and tip displacement as a function of test duration, for both the blades. It is observed that both the blades survive the normal operation load without any superficial failure and survive the worst case load without any functional/catastrophic failure. As both the blades satisfy the ultimate strength requirements of BS-EN 61400-23:2002 [21], the flax blade can be viewed as a potential replacement to the E-glass blade. The failure load and corresponding tip displacement of the flax blade is 4.14 kN and 2300 mm, respectively. The failure data of the E-glass blade is not disclosed. BS-EN 61400-23:2002 [21] does not formally require measuring the failure load and tip deflection.

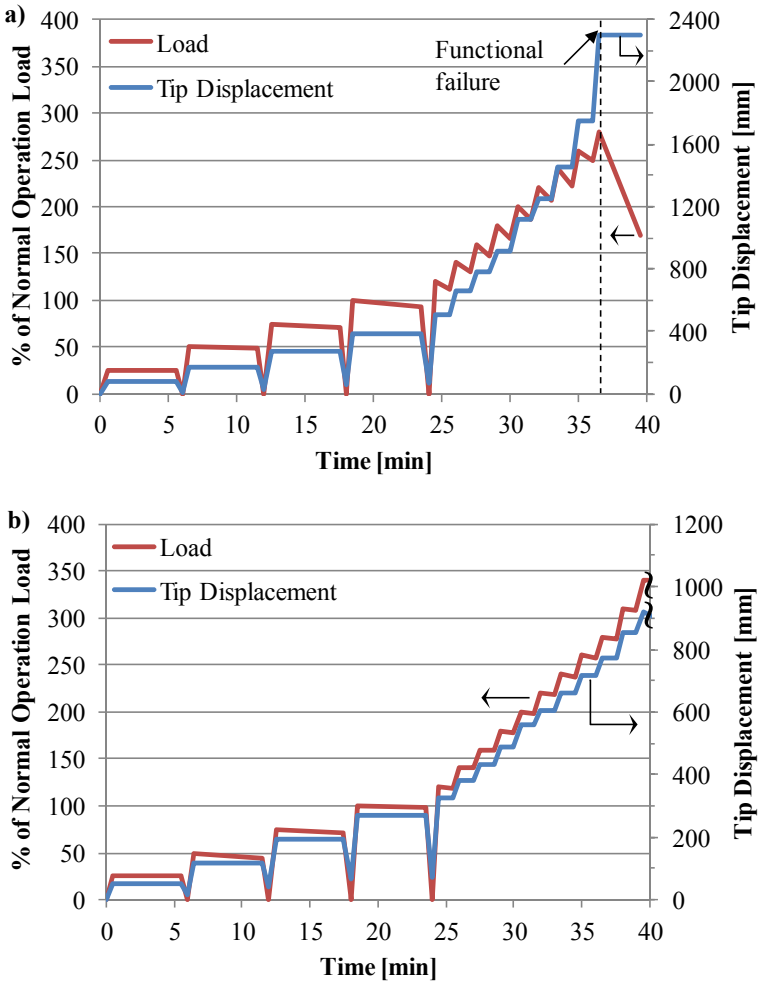


**Fig. 7.11. Test load and tip displacement as a function of time, for the *a)* flax and *b)* E-glass blades. The point of functional failure has been indicated. Load values (y-axis) are normalised by the normal operation load (of 1.48 kN).**

Table 7.4 presents useful information from the graphs in Fig. 7.11, enabling direct comparison of the performance of the E-glass and flax blades. At normal operation loads, the E-glass blade has a tip deflection of 270 mm while the flax blade has a 40% higher tip deflection of 388 mm. The tip deflections are 8–11% of the blade length. While the flax blade survives the worst case loading like the E-glass blade, the flax blade is significantly more flexible than the E-glass blade. The E-glass and flax blades have a tip displacement of 743 mm and 2025 mm under worst case loading, which is 22% and 60% of the blade length, respectively. To avoid tower strike, BS-EN 61400-23:2002 [21] requires that the tip displacement should be less than the clearance provided between the blade tip and the tower, even at worst case loading. As the traditional practise in designing a turbine is to accommodate the requirements of the blade (*i.e.* blade-centered design), a turbine can be designed so that a generous clearance is available to accommodate the large tip deflection of the flax blade. A possible design solution is to increase the distance between the rotor centre and tower axis, and use a yaw drive mechanism (or thicker flanges) to balance the increased overturning moment of the rotor. In addition, a modified flax blade design incorporating a spar (with shear webs/caps) will enable major reductions in tip deflection by increasing the flexural rigidity of the blade.

**Table 7.4. Loads and corresponding tip displacements of the flax and E-glass blades, at the end of test stages 1, 2 and 3.**

| Stage of test loading | Flax blade | | | | E-glass blade | | | |
|---|---|---|---|---|---|---|---|---|
| | Load | | Tip displacement | | Load | | Tip displacement | |
| | kN | % of NO† load | mm | % of blade length | kN | % of NO† load | mm | % of blade length |
| Normal operation | 1.48 | 100 | 388 | 11 | 1.48 | 100 | 270 | 8 |
| Worst case | 3.99 | 270 | 2025 | 60 | 3.99 | 270 | 743 | 22 |
| Failure | 4.14 | 280 | 2300 | 68 | N/A‡ | N/A‡ | N/A‡ | N/A‡ |

† NO load is 'normal operation' load.

‡ Non-disclosable data.

The load curves in Fig. 7.11 show relaxation in loads during dwells. It is observed that load relaxation is much higher in the flax blade than the E-glass blade. In fact, in

stage 2, the magnitude of load relaxation averages 0.03 kN for the E-glass blade but 0.18 kN for the flax blade. Interestingly, during periods of load relaxation, the blade tip displacement remains fairly constant. The greater load relaxation in the flax blade implies reducing blade stiffness. This could possibly be due to a poorer fibre/matrix interface resulting in gradual plastic deformation through progressive micro-mechanical damage mechanisms such as fibre/matrix debonding and pull-out. This is common in PFRPs [40, 41] (shown in *Chapters 3 and 4*). In addition, it has been shown in *Chapter 5* that plant fibre composites have a non-linear stress-strain curve, resulting from a very small elastic strain limit of ~0.15%, implying that plastic deformation from micro-damage occurs very early in the load curve [42].

#### 7.3.3.1 Displacement- load curves

Fig. 7.12 presents tip displacement versus load curves for the flax and E-glass blades. Interestingly, while the tip displacement increases at a constant rate with load (linear growth, $R^2$ = 0.996) for the E-glass blade, the tip displacement increases at an increasing rate with load (quadratic growth, $R^2$ = 0.989) for the flax blade. This is in agreement with the load-displacement curve of the different materials. E-glass composites have a linear load-displacement curve, while plant fibre composites have a non-linear load-displacement curve [10, 42, 43] (*Chapter 5*). In particular, plant fibre composites exhibit softening (*i.e.* decreasing stiffness with increasing strain/load) [10]. As demonstrated in *Chapter 5*, the stiffness of flax/polyester composites reduces by up to 30% in the 0-0.25% strain range, while the stiffness of E-glass composites is fairly constant. These observations highlight the differing stress-strain accumulation and damage-growth mechanisms in E-glass reinforced composites and plant fibre reinforced composites, particularly due to the differing fibre structure and morphology and fibre/matrix interactions. It is thought that the non-linear stress-strain curve of the plant fibres, resulting from progressive reorientation of cellulose microfibrils and visco-elasto-plastic deformation of the hierarchal cell wall structure, is translated into the PFRP component [10, 42, 43] (as discussed in *Chapter 5*).

Fig. 7.12 clearly demonstrates the significantly higher deflection of the flax blade in comparison to the E-glass blade. Fig. 7.12 also presents images of the flax blade under *i)* no load, *ii)* normal operation load, *iii)* worst case load, and *iv)* failure load.

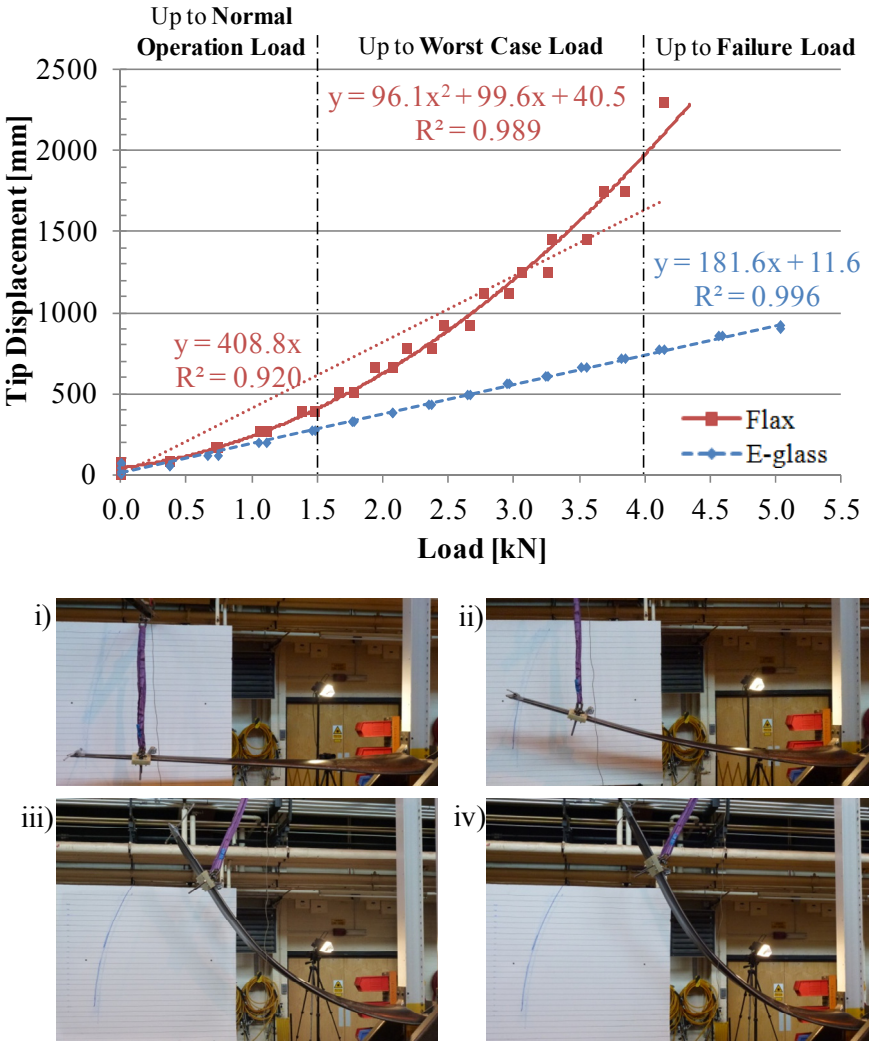


**Fig. 7.12. Tip displacement versus load curves for the flax and E-glass blades. Images of the flax blade under *i)* no load, *ii)* normal operation load, *iii)* worst case load, and *iv)* failure load, are also presented.**

#### 7.3.3.2 Flexural rigidity of blades in the flap-wise direction

Two strategies are available to estimate the flexural rigidity (*EI*) of a blade. The first technique involves assuming that the blade can be considered as a uniform cross-section cantilever beam subjected to a single concentrated load at *l* m from the blade

root. Assuming small deflections and applying appropriate boundary conditions at the ends of the cantilever beam, a simple static analysis using Macaulay's method (Eq. 7.1) can be conducted to estimate the mean flexural stiffness $EI_{mean}$ of the blade (In Eq. 7.2). In Eq. 7.2, $y_{tip}/F$ is the slope of the tip displacement–load curve, $z_{tip}$ (= 3.395 m) is the length of the blade and $l$ is the distance between the point of load application along the blade from the blade root. This simple analysis conveniently shows that the blade flexural stiffness is inversely proportional to the slope of the tip displacement to load curve.

$$EI_{mean}\frac{d^2y}{dz^2} = M;\ M = F\left([z-l]-[z]+l\right) \qquad \text{Eq. 7.1}$$

$$EI_{mean} = \frac{K}{y_{tip}/F},\quad K = \frac{[z_{tip}-l]^3}{6} - \frac{z_{tip}^{\ 3}}{6} + \frac{lz_{tip}^{\ 2}}{2} \qquad \text{Eq. 7.2}$$

Using the slope ($y_{tip}/F$) of the linear tip displacement–load curve for the E-glass blade (181.6 mm/kN) and the flax blade (408.8 mm/kN) from Fig. 7.12, and substituting the relevant constants in Eq. 7.2, the mean flexural stiffness $EI_{mean}$ of the E-glass and flax blades is found to be 53.1 kNm$^2$ and 23.6 kNm$^2$, respectively. That is, the flax blade is 2.25 times more flexible than the E-glass blade. As the displacement-load curve for flax is non-linear and follows a quadratic equation better, a better approximation of $EI_{mean}$ can be obtained if the differential of the quadratic best-fit equation (in Fig. 7.12) is taken as $y_{tip}/F$. The mean flexural stiffness $EI_{mean}$ of the flax blade is then a function of load, and is found to reduce with increasing load. For instance, $EI_{mean}$ at loads of 0 kN, 1.48 kN (normal operation load) and 3.99 kN (worst case load) is 96.9 kNm$^2$, 25.1 kNm$^2$ and 11.1 kNm$^2$, respectively.

An alternate, and more rigorous, method to estimate the flexural rigidity of the blade involves measuring the vertical deflection (using the video footage) of a blade $y_i$, subjected to say normal operation loads ($F$ = 1.48 kN, $M$ = 4.15 kNm), at various points along the blade length $z_i$. 18 points along the leading and trailing edges are used for deflection measurement. From the vertical deflections, the bending angle $\theta$

= $\tan^{-1}(dy/dz)$, and bending rate per unit length $d\theta/dz$ can be calculated using finite difference methods. Eq. 7.3 and Eq. 7.4 present the central difference for $\theta$ and $d\theta/dz$, respectively. The flexural rigidity at different points along the blade can then be determined by using Eq. 7.5 [44]. The results for the E-glass and flax blades are presented in Fig. 7.13. The curves observed for the 3.5 m flax and E-glass blades of this study, have a similar profile to those found in literature for a larger 7.5 m GFRP wind turbine blade [44].

$$\theta_i = \tan^{-1}\left(\left(\frac{dy}{dz}\right)_i\right) = \tan^{-1}\left(\frac{y_{i+1} - y_{i-1}}{z_{i+1} - z_{i-1}}\right) \quad \text{Eq. 7.3}$$

$$\left(\frac{d\theta}{dz}\right)_i = \frac{\theta_{i+1} - \theta_{i-1}}{z_{i+1} - z_{i-1}} \quad \text{Eq. 7.4}$$

$$EI = \frac{M}{d\theta/dz} \quad \text{Eq. 7.5}$$

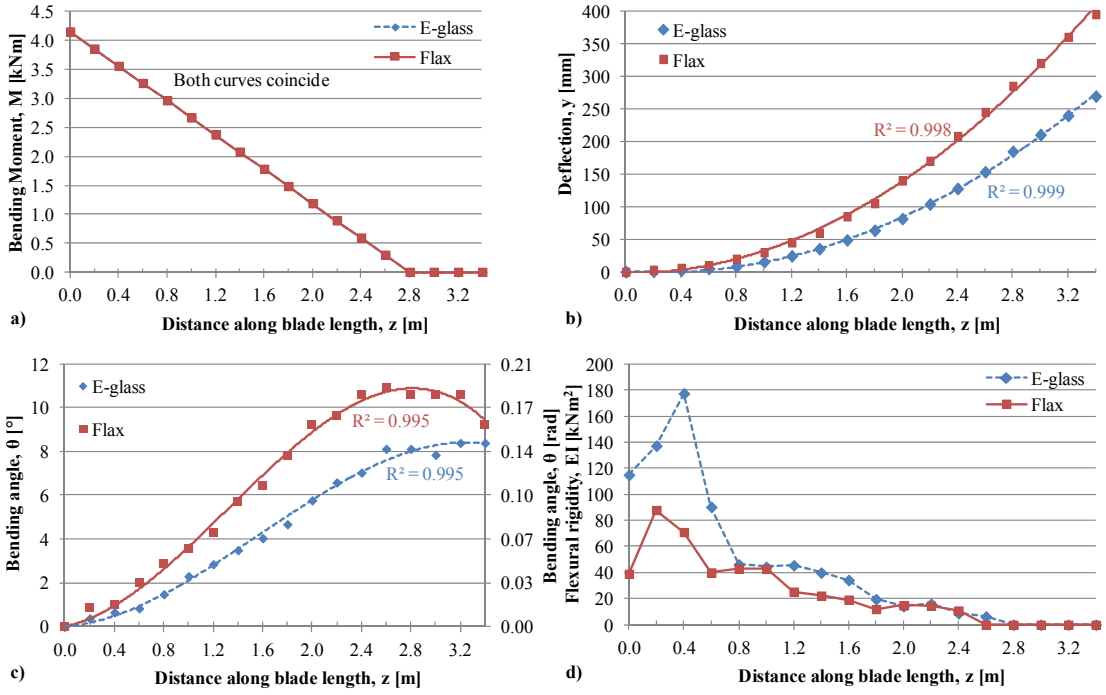


**Fig. 7.13. Graphs showing the variation in *a)* applied moment, *b)* vertical deflection, *c)* bending angle and *d)* flexural rigidity, along the blade length, for the E-glass and flax blades, when subjected to normal operating test loads (*F* = 1.48 kN).**

Fig. 7.13a) shows the applied bending moment $M$ along the blade length $z$, due to the point load at $l$ m from the blade root. Note that the applied bending moment $M$ is null beyond the load application point. In addition, the bending moment $M$ at the blade root is the required $M_{yB}$ of 4.15 kNm. The resulting vertical deflection along the blade length of the E-glass and flax blades can be observed in Fig. 7.13b). The deflection profile for both blades is observed to follow a quadratic equation ($R^2 > 0.99$). It is clearly observed that the flax blade deflects more than the E-glass blade. The calculated bending angle along the blade lengths for the two blades is presented in Fig. 7.13c). The bending angle is observed to increase fairly linearly up to $z = 2.6$ m, after which it becomes constant. This is because the load is being applied at $l = 2.80$ m from the blade root, and beyond this point there is no bending moment (Fig. 7.13a)).

Fig. 7.13d) illustrates the variation in estimated flexural rigidity $EI$ along the blade length for both the blades. The higher flexural rigidity at close to the blade root is due to the higher bending moment of area and presence of more layers of unidirectional reinforcement. Sudden dips in the flexural rigidity along the blade length are possibly due to step-changes in the stacking sequence of the blade.

It is observed that the E-glass blade exhibits a higher flexural rigidity at almost all points along the blade length. In particular, the flexural rigidity of the E-glass blade is 2-3 times more than the flax blade, along the first meter of the blade. Using the trapezium rule, an indicative value of the mean flexural stiffness for the blades can be determined. $EI_{mean}$ is found to be 43.4 kNm$^2$ for the E-glass blade and 24.6 kNm$^2$ for the flax blade. These values are fairly similar to those calculated previously through the simple static analysis method.

#### 7.3.3.3 Comparison of mechanical properties obtained via testing of laminates and full-scale components

Firstly, in comparing the mechanical properties of flax and E-glass composites in Table 7.1, it was found that the tensile and compressive stiffness' of flax composites are between 54-65% that of E-glass composites. The mean flexural rigidity of the flax blade is 57% that of an identical construction E-glass blade. As the flax blade

failed via compressive buckling, perhaps the low absolute compressive stiffness of flax composites in comparison to E-glass composites (also reported in [45]) limits the flexural rigidity of the flax blade. Secondly, the specific stiffness (material performance index) of flax composites is between 80-100% that of E-glass composites (Table 7.1). Comparing the specific flexural rigidity of the flax blade with the E-glass blade (using the density of the composite part of the blades from Table 7.2), it is found that the specific flexural rigidity of the flax blade ($24.6^{1/3}/1.28$ = 2.27 $(kNm^2)^{1/3}/gcm^{-3}$) is ~100% that of the E-glass blade ($43.4^{1/3}/1.59$ = 2.21 $(kNm^2)^{1/3}/gcm^{-3}$).

These two observations not only show that the absolute and specific properties of the composites (*i.e.* flat laminate plaque) are transferred to the blade (*i.e.* component/structure), but also hint at two important implications. Firstly, the flax blade experiences more deflection than the E-glass blade for the same load due to the comparatively lower absolute stiffness of flax composites. Secondly, the former is the case as the flax blade is 10% lighter than the E-glass blade (fibre mass saving of 45%). Indeed, if the blades were of identical mass and thus density (as blade volume is constant), the stiffness of the flax blade would be comparable to that of the E-glass blade. In essence, there is a critical trade-off between component weight savings and component stiffness; for similar stiffness performance of a flax blade to an E-glass blade, weight savings cannot be achieved. In addition, due to the large difference in densities of flax fibre and E-glass fibre, to achieve the same blade mass (and thus blade density), a considerably higher, and possibly unattainable, flax fibre mass (and thus fibre weight content) would need to be used. For instance, the current fibre mass and blade densities of the flax and E-glass blade are tabulated in Table 7.2. The (composite part of the) flax blade will achieve a maximum density of 1.57 $gcm^{-3}$ for 100% fibre weight fraction (*i.e.* no resin); the current density (of the composite part) of the E-glass blade, with a fibre weight fraction of only 44.3% is already 1.59 $gcm^{-3}$. It is also noteworthy that using a larger quantity of flax reinforcement would not only reduce weight savings, but would also imply a substantially larger economic cost and eco-impact of the flax blade than is currently the case.

Nonetheless and importantly, this case study demonstrates that despite the well-documented poor strength properties of flax composites in comparison to GFRPs (ratio of 32-37%, Table 7.1), the flax blade, like the E-glass blade, is able to withstand the worst case loads. This shows that more studies are required to critically understand the behaviour of PFRPs when employed in specific applications and structures, rather than limiting materials analysis to data extracted from coupon testing. Indeed, certain applications may be suitable for even low-strength (relative to GFRPs) PFRPs.

#### 7.3.3.4 Failure modes of blades

The E-glass and flax blades failed under different modes, as is depicted by Fig. 7.14 and Fig. 7.15. The E-glass blade failed due to crack formation at the root-hub junction. Upon further loading, the crack grew across the blade cross-section causing extensive delamination. Fig. 7.14 shows how the composite laminates have peeled from the core. The crack eventually grows to such an extent that the trailing edge, along the maximum chord length, split open.

**Fig. 7.14. The E-glass blade, failing at the blade root, exhibited extensive delamination.**

On the other hand, the flax blade failed ~1 m along the blade length from the blade root (Fig. 7.15a)) which corresponds to a step-change in the stacking sequence. This point of step-change is a possible stress-raiser. Hence, as the load exceeded 4 kN and the tip deflection approached 70% of the blade length, the stress concentration increased substantially. Initially, matrix cracking/peeling was observed (Fig. 7.15b)) – a sign of resin richness. Then, the top surface, experiencing compressive loads,

buckled. The wrinkles and delamination resulting from the compressive failure of the composite laminate can be seen in Fig. 7.15b). Further loading led to complete buckling, delamination and eventually collapse of the blade. The low compressive stiffness and strength of flax composites (Table 7.1) makes compressive buckling an understandably likely source of failure for the flax blade.

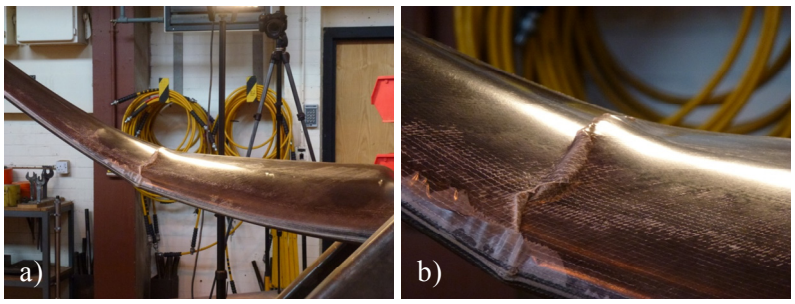


**Fig. 7.15. Images of the fractured flax blade during static flap-wise testing showing *a)* the region of failure, and *b)* wrinkle formation due to buckling.**

## 7.4 CONCLUSIONS

The objective of this chapter was to demonstrate whether plant fibre composites are potentially structural replacements to E-glass composites. This chapter detailed a novel comparative case study looking at the manufacture and mechanical testing of 3.5 m composite rotor blades (suitable for an 11 kW turbine) built from flax/polyester and E-glass/polyester.

Firstly, this chapter compared the weight, cost, eco-impact and manufacturing properties of the two blades. It is found that although the flax/polyester blade is 10% lighter than the E-glass/polyester blade (fibre mass saving of 45%), the materials cost of the former is almost 3 times that of the latter. Furthermore, comparing the estimated cumulative embodied energy of the flax and E-glass blade, it is found that the flax blade has an up to 15% larger eco-impact than the E-glass blade. Hence, currently, aligned flax reinforcements are a light weight, but not low-cost or sustainable, alternative to conventional aligned E-glass reinforcements.

Secondly, through static testing of the blades (in accordance to certification standards), their mechanical properties were compared. It is confirmed that like the

E-glass/polyester blade, the flax/polyester blade satisfies the design and structural integrity requirements for an 11 kW turbine, under normal operation and worst case loading. Hence, flax is a potential structural replacement to E-glass, particularly for small rotor blade applications.

While the displacement-load curve is linear for the E-glass blade, it is non-linear for the flax blade. This is consistent with the fact that plant fibres and their composites have a non-linear stress-strain curve, while E-glass and its composites have a linear stress-strain curve. This highlights the differing stress-strain accumulation mechanisms in natural materials. The flax and E-glass blades are also found to fail in a different manner. The failure load and corresponding tip displacement of the flax blade is 4.14 kN and 2300 mm, respectively. The substantially higher tip deflection of the flax blade is proof of its flexibility. The mean flexural rigidity of the flax and E-glass blades is 24.6 $kNm^2$ and 43.4 $kNm^2$. While it is demonstrated that the absolute and specific properties of the composites (*i.e.* flat laminate plaque) are transferred to the blade (*i.e.* component/structure), it is argued that there is a critical trade-off between component weight savings and component stiffness; for similar stiffness performance of a flax blade to an E-glass blade, weight savings cannot be achieved. Furthermore, while increasing the flax fibre content to enhance the stiffness of the flax blade stiffness may be an attractive option, this would have a substantial detrimental impact on the economic cost and eco-impact of the flax blade.

In conclusion, it is proposed that flax is a suitable structural replacement to E-glass for similar composite small wind turbine blade applications. In view of the findings of this research, it is suggested that *i)* the development of low-cost sustainable aligned plant fibre semi-products is a limiting factor to the industrial uptake of PFRPs in structural applications, *ii)* more ambitious studies are required to understand the behaviour of PFRPs when employed in specific applications/structures, rather than limiting materials analysis to data extracted from coupon testing, and *iii)* the development of bio-based high-performance matrix materials and core materials is a critical step in the wide acceptance of PFRPs as sustainable materials.

## 7.5 REFERENCES


1. Reux F. Worldwide composites market: Main trends of the composites industry, in *5th Innovative Composites Summit - JEC ASIA 2012*. 26-28 June 2012. Singapore.
2. Pickering K, ed. *Properties and performance of natural-fibre composites*. 2008. CRC Press LLC: Boca Raton.
3. Carus M. Bio-composites: Technologies, applications and markets, in *4th International Conference on Sustainable Materials, Polymers and Composites*. 6-7 July 2011. Birmingham, UK.
4. Carus M, Gahle C. Natural fibre reinforced plastics - material with future, 2008. nova-Institut GmbH: Huerth.
5. Staiger M, Tucker N. *Natural-fibre composites in structural applications*, in *Properties and performance of natural-fibre composites*, Pickering K, 2008. CRC Press LLC: Boca Raton.
6. *Auto body made of plastics resists denting under hard blows*, in *Popular Mechanics Magazine*, Dec 1941, Vol 76 No. 6. p. 12.
7. -. A Fighter Fuselage in Synthetic Material, Vol. 34, October 1945. Aero Research Limited: Duxford, Cambridge.
8. *BS EN 61400-2:2006*, *Wind turbines - Part 2: Design requirements for small wind turbines*, 2006. British Standards Institution: London.
9. Goutianos S, Peijs T, Nystrom B, Skrifvars M. Development of flax fibre based textile reinforcements for composite applications. *Applied Composite Materials*, 2006, 13(4): p. 199-215.
10. Baets J, Plastria D, Ivens J, Verpoest I. Determination of the optimal flax fibre preparation for use in UD-epoxy composites, in *4th International Conference on Sustainable Materials, Polymers and Composites*. 6-7 July 2011. Birmingham, UK.
11. Miao M, Finn N. Conversion of natural fibres into structural composites. *Journal of Textile Engineering*, 2008, 54(6): p. 165-177.
12. Jensen F. *Ultimate strength of a large wind turbine blade*. PhD, 2008. Technical University of Denmark: Lyngby, Denmark.
13. Brøndsted P, Lilholt H, Lystrup A. Composite materials for wind power turbine blades. *Annual Review of Materials Research*, 2005, 35: p. 505-538.
14. Brøndsted P, Holmes JW, Sørensen BF, Jiang Z, Sun Z, Chen X. Evaluation of a bamboo/epoxy composite as a potential material for hybrid wind turbine blades, 2008. Chinese Wind Energy Association.
15. Qin Y, Xu J, Zhang Y. Bamboo as a potential material used for windmill turbine blades - A life cycle analysis with sustainable perspective, 2009. Roskilde University Center: Denmark.
16. Frohnapfel P, Muggenhamer M, Schlögl C, Drechsler K. Natural fibre composites for innovative small scale wind turbine blades, in *International Workshop on Small Scale Wind Energy for Developing Countries*. 15-17 November 2010. Pokhara, Nepal.
17. Mikkelsen L, Bottoli F, Pignatti L, Andersen TL, Madsen B. Material selection and design aspects of small wind turbine blades, in *Indo-Danish Workshop on Future Composites Technologies for Wind Turbine Blades*. 2012. Delhi, India.
18. Bottoli F, Pignatti L. Design and processing of structural components in biocomposite materials - Rotor blade for wind turbine cars, ed. Madsen B, Mikkelsen LP, Brondsted P, Andersen TL, 2011. Technical University of Denmark: Roskilde, Denmark.
19. , Small Wind Systems - UK Market Report, 2011. RenewableUK (BWEA): London.

20. Hogg P. Wind Turbine Blade Materials, 2010. SUPERGEN WindWind Energy Technology.
21. *BS-EN 61400-23:2002*, *Wind turbine generator systems - Part 23: Full-scale structural testing of rotor blades*, 2002. British Standards Institution: London.
22. Shah D, Schubel PJ, Clifford MJ, Licence P. Fatigue characterisation of plant fibre composites for small-scale wind turbine blade applications, in *5th Innovative Composites Summit - JEC Asia 2012*. 26-28 June 2012. Singapore.
23. Shah D, Schubel PJ, Clifford MJ, Licence P. *Fatigue characterisation of plant fibre composites for rotor blade applications*, in *JEC Composites Magazine, No. 73: Special JEC Asia*, June 2012. JEC Composites: Paris. p. 51-54.
24. Aziz S, Gale J, Ebrahimpour A, Schoen MP. Passive control of a wind turbine blade using composite material, in *ASME 2011 International Mechanical Engineering Congress & Exposition (IMECE2011)*. November 11-17, 2011. Denver, Colorado, USA.
25. Harris B. *Engineering composite materials*, 1999. London: The Institute of Materials.
26. Bos H, van den Oever MJA, Peters OCJJ. Tensile and compressive properties of flax fibres for natural fibre reinforced composites. *Journal of Materials Science*, 2002, 37: p. 1683-1692.
27. Lewin M. *Handbook of fiber chemistry*. Third ed, 2007. Boca Raton: CRC Press LLC.
28. Dittenber D, Gangarao HVS. Critical review of recent publications on use of natural composites in infrastructure. *Composites Part A: Applied Science and Manufacturing*, 2012, 43: p. 1419-1429.
29. Madsen B. *Properties of plant fibre yarn polymer composites - An experimental study*. PhD, 2004. Technical University of Denmark: Lyngby, Denmark.
30. Andserson J, Jansz A, Steele K, Thistlethwaite P, Bishop G, Black A. Green guide to composites - an environmental profiling system for composite materials and products, 2004. Building Research Establishment (BRE) and NetComposites: Watford, UK.
31. Joshi S, Drzal LT, Mohanty AK, Arora S. Are natural fiber composites environmentally superior to glass fiber reinforced composites? *Composites Part A: Applied Science and Manufacturing*, 2004, 35: p. 371-376.
32. Dissanayake N, Summerscales J, Grove SM, Singh MM. Life cycle impact assessment of flax fibre for the reinforcement of composites. *Journal of Biobased Materials and Bioenergy*, 2009, 3(3): p. 1-4.
33. Dissanayake N, Summerscales J, Grove SM, Singh MM. Energy use in the production of flax fiber for the reinforcement of composites. *Journal of Natural Fibers*, 2009, 6(4): p. 331-346.
34. Summerscales J, Dissanayake N, Virk AS, Hall W. A review of bast fibres and their composites. Part 2 – Composites. *Composites Part A: Applied Science and Manufacturing*, 2010, 41(10): p. 1336-1344.
35. Steger J. Light weight! No matter what the costs? Plant fibres for light weight automotive applications. *Journal of Biobased Materials and Bioenergy*, 2010, 4(2): p. 181-184.
36. Le Duigou A, Davies, P, Baley, C. Environmental impact analysis of the production of flax fibres to be used as composite material reinforcement. *Journal of Biobased Materials and Bioenergy*, 2011, 5(1): p. 153-165.
37. Duflou J, Deng Y, Acker KV, Dewulf W. Do fiber-reinforced polymer composites provide environmentally benign alternatives? A life-cycle-assessment-based study. *MRS Bulletin*, 2012, 37: p. 374-382.

38. Shah D, Schubel PJ. *Full-scale structural testing of a rotor blade*, 2012. The University of Nottingham: Nottingham.
39. Wacker G. Requirements for the certification of rotor blades, in *SAMPE 2003 - Advancing materials in the global economy - Applications, emerging markets and evolving technologies*. May 11-15, 2003. Long Beach, California.
40. Kalia S, Kaith BS, Kaur I. Pretreatments of natural fibers and their application as reinforcing material in polymer composites - a review. *Polymer Engineering and Science*, 2009, 49(7): p. 1253-1272.
41. Wambua P, Ivens J, Verpoest I. Natural fibres: can they replace glass in fibre reinforced plastics? *Composites Science and Technology*, 2003, 63: p. 1259-1264.
42. Hughes M, Carpenter J, Hill C. Deformation and fracture behaviour of flax fibre reinforced thermosetting polymer matrix composites. *Journal of Materials Science*, 2007, 42: p. 2499-2511.
43. Baley C. Analysis of the flax fibres tensile behaviour and analysis of the tensile stiffness increase. *Composites Part A: Applied Science and Manufacturing*, 2002, 33: p. 939-948.
44. McKittrick L, Cairns DS, Mandell J, Combs DC, Rabern DA, van Luchene RD. *SAND2001-1441*, Analysis of a composite blade design for the AOC 15/50 wind turbine using a finite element model, 2001. Sandia National Laboratories: Livermore, California.
45. Bos H, Molenveld K, Teunissen W, van Wingerde AM, van Delft DRV. Compressive behaviour of unidirectional flax fibre reinforced composites. *Journal of Materials Science*, 2004, 39: p. 2159-2168.

# 8 CONCLUSIONS

Structural composites are required to reliably sustain external loads in addition to self-support or play a principal role in supporting the structure of the final component. The overall objective of this research was to investigate the potential of plant fibre reinforced composites (PFRPs), as a prospective alternative to E-glass composites (GFRPs), in structural applications. This would not only demand that the macro-mechanical behaviour of PFRPs is well-studied/documented for various composite parameters, but also obliges that the mechanical properties of PFRPs are well-predicted under various loading conditions. Hence, this thesis is mainly concerned with characterising, optimising, and achieving an improved understanding, of the macro-mechanical properties of aligned PFRPs.

The aim of this chapter is to present the major conclusions established from the work described in this thesis, with reference to the overall theme described in *Chapter 1*. In addition, several recommendations are made for future work.

## 8.1 THESIS CONCLUSIONS

Through an up-to-date critical review of the literature in *Chapter 2*, an overview of key aspects that need consideration when developing PFRPs for structural applications was obtained. This included recommendation on the selection of *i)* the fibre type, fibre extraction process and fibre surface modification technique, *ii)* fibre volume fraction, *iii)* reinforcement geometry and interfacial properties, *iv)* reinforcement packing arrangement and orientation and *v)* matrix type and composite manufacturing technique, was achieved. The review identified long bast fibres converted into minimally-processed well-aligned semi-products as the most suitable composite reinforcement, prepregging, compression moulding and vacuum infusion were identified as the most suitable composite manufacturing techniques, and thermosets were identified as the most suitable matrix material.

In this section, the contents of each chapter are summarised and assessed to evaluate their implications on the mechanical performance of aligned PFRPs, and eventually their suitability for load-bearing applications.

### 8.1.1 *Chapter 3*: Effect of reinforcing fibre/yarn and matrix type

Screening the mechanical properties of various unidirectional plant bast fibre yarn reinforced thermoset matrix composites, it is found that they offer three to five times better tensile stiffness and strength in comparison to conventional non-woven randomly-oriented short-fibre PFRPs (Fig. 8.1). The marked improvements in mechanical properties are not only attributable to enhanced reinforcement alignment but also to increased reinforcement length efficiency factors. It is shown that due to low critical fibre lengths ($l_c$ = 0.28-0.52 mm) and high fibre aspect ratios ($l_f/d_f$ > 100), length efficiency factors for plant fibre yarns/rovings are effectively unity. This indicates good load transferring capability in yarn reinforced PFRPs, without any fibre surface modification to enhance interfacial properties. Indeed, even multiaxial PFRPs exhibit better mechanical properties than conventional non-woven randomly-oriented short-fibre PFRPs (Fig. 8.1) due to the higher efficiency factor (particularly related to length) in the former.

Aligned PFRPs were manufactured through a vacuum infusion process. The yarn bundles in the PFRPs were found to be uniformly distributed and well-impregnated, and the fabricated laminates have low void content (typically in the range of 0.5-2%). No correlation is found between yarn structure and composite void content. However, yarn construction does seem to affect the type of voids that form; for instance, high-twist yarn reinforced PFRPs are susceptible to impregnation-related intra-yarn voids. While single plant fibres have highly variable mechanical properties, PFRPs reinforced with yarns were found to have consistent quality, indicated by the small coefficient of variation in mechanical properties (typically less than 6%). Hence, aligned PFRPs can provide highly controlled properties, which is essential for structural applications.

Considering the effect of matrix type, it is found that epoxies form a stronger interface with plant fibres than polyesters do. While the fracture surfaces of epoxy-based PFRPs are flat (indicating brittle failure), polyester-based PFRP specimens present a serrated fracture surface with greater fibre pull-out lengths and even delamination. However, the effect of matrix type on the longitudinal tensile properties of aligned PFRPs is unclear.

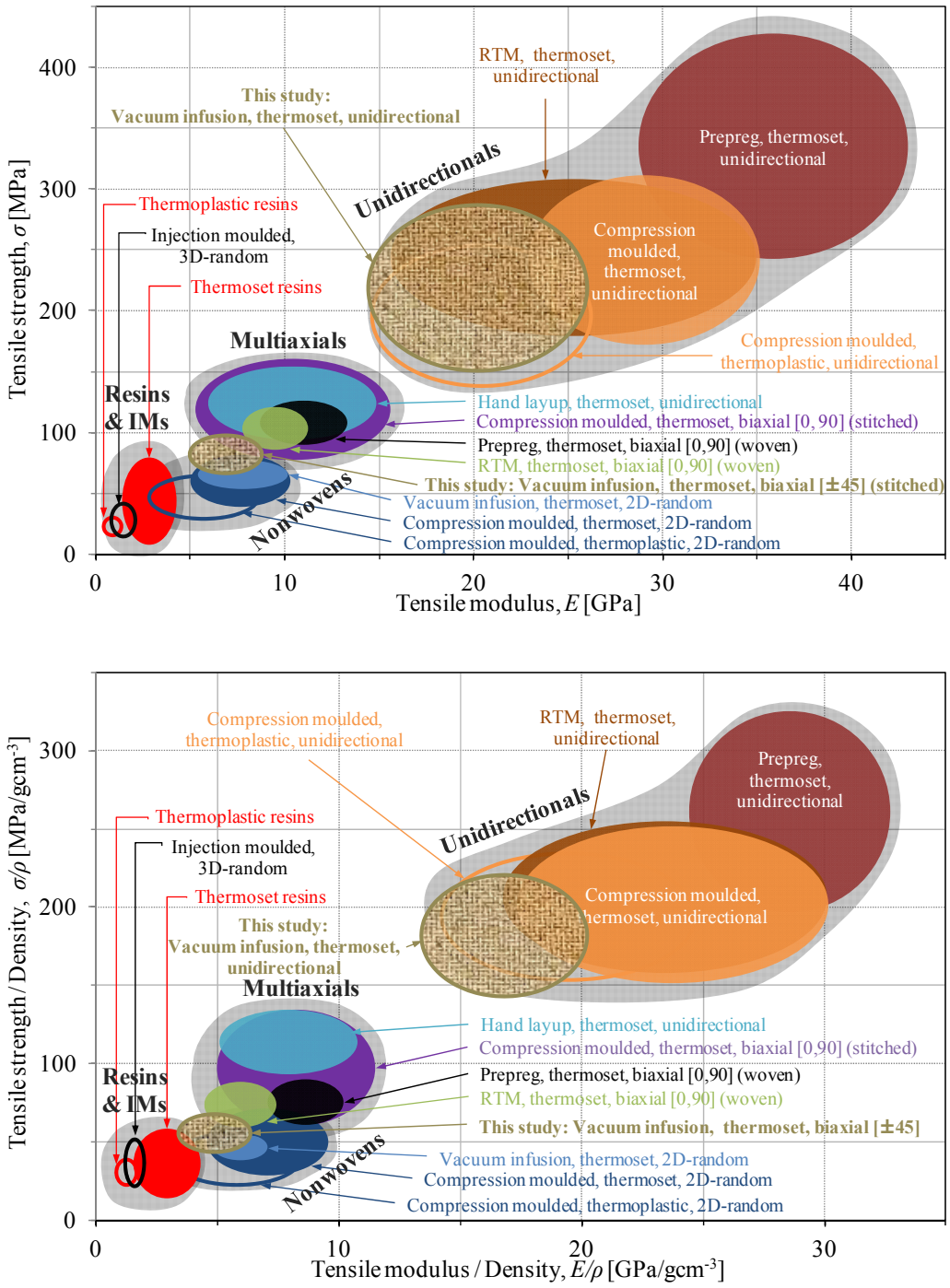


**Fig. 8.1. Materials selection chart (reconstructed from Fig. 2.6 in *Chapter 2*) comparing the mechanical properties of various PFRPs studied in literature and this thesis.**

The low void content and consistency in properties of aligned PFRPs is comparable to that of aligned GFRPs. However, PFRPs exhibit considerably lower fibre volume fractions than GFRPs, due to the low packing-ability of plant fibre preforms. This is thought to be a critical set-back for PFRPs as composite mechanical properties generally improve with fibre volume fraction. Apart from the expected (30-40%) lower density of PFRPs, they have 20-30% lower interlaminar shear strength, 5-10 times lower impact strength, 60-80% lower tensile strength and 30-60% lower tensile stiffness than GFRPs. Hence, unidirectional GFRPs clearly outperform unidirectional PFRPs in terms of absolute mechanical properties. Nonetheless, the specific tensile stiffness performance of high-quality aligned PFRPs is found to be comparable to aligned GFRPs. Hence, where high stiffness and low weight are the key materials selection criteria, high-quality plant fibre rovings can replace E-glass reinforcements in composites.

Amongst the various yarn reinforced PFRPs studied, composites reinforced with flax rovings demonstrated exceptional mechanical properties, with a back-calculated fibre tensile modulus in the range of 65-75 GPa (comparable to that of E-glass) and fibre tensile strength of about 800 MPa (almost half that of E-glass). This is proof of the reinforcing potential of plant fibres for structural composites, without the use of any active fibre surface treatment. Not only the bast fibre type, but yarn structure (twist level and packing fraction) and fibre/yarn quality were also found to have a significant effect on the mechanical properties of the resulting composite.

Reinforcing the recommendations from the critical review in *Chapter 2* and the constructed materials selection chart in Fig. 8.1 (or Fig. 2.6), through the findings of this chapter it is proposed that using minimally-processed flax rovings/slivers, processed specifically for composites applications rather than textile applications, as reinforcements in an epoxy matrix is a good starting point for producing high-quality PFRPs. Furthermore, employing prepregging technology or vacuum-assisted resin transfer moulding could enable the production of PFRPs with higher fibre content and thus better mechanical performance. Alternatively, using (press) consolidation upon resin impregnation may be necessary to produce higher fibre volume fractions.

### 8.1.2 *Chapter 4*: Effect of fibre volume fraction

To identify the processing window which produces PFRPs with useful properties, the effect of fibre volume fraction on the physical and tensile properties of aligned PFRPs has been investigated. Vacuum-infused PFRPs were producible with low local variations in fibre/matrix volume fractions and low void content (typically in the range of 0.3-1.4%). Importantly, there is no clear correlation between fibre content and void content. Furthermore, a void content of up to 4% is found to have negligible effect on the tensile properties of PFRPs. Fibre content and tensile properties are found to be linearly related, as per the rule of mixtures, similar to conventional brittle-fibre ductile-matrix fibre reinforced plastics (FRPs).

It is demonstrated that plant fibre assemblies (particularly in the form of twisted yarns) will inherently produce lower fibre volume fractions than conventional synthetic fibre assemblies. Aligned synthetic fibre reinforced composites have a low critical fibre volume fraction (~2.5% for carbon/polyester) and a high maximum (practical and theoretical) fibre volume fraction (of the order of 75-80%), implying that the range of fibre volume fractions that produce composites with useful properties is 70-75%. The study finds that PFRPs utilising staple fibre twisted yarns as reinforcements have a small window of fibre volume fractions which produce composites with useful properties. A high critical fibre volume fraction (on the order of 10%), low maximum (practical) fibre volume fraction (of the order of 45-55%) and low maximum (theoretical) fibre volume fraction (of the order of 45-60%) implies that the possible range of employable fibre volume fractions for such PFRPs is only 35-50%. Importantly, randomly-oriented short-fibre PFRPs have a much higher critical fibre volume fraction (of the order of 25%) and lower maximum (practical) fibre volume fraction (of the order of 30-45%) implying that the useable range of fibre volume fractions is even lower. This significantly limits the maximum exploitation of the mechanical properties of plant fibres in FRPs.

### 8.1.3 *Chapter 5*: Effect of reinforcement orientation

In aligned PFRPs, (mis)orientation manifests itself in various forms at every length scale: *a)* microfibril angle in a single plant fibre, *b)* twist angle in a processed staple

fibre yarn, and *c)* off-axis loading angle in a composite laminate. The effect of these misorientations on the tensile properties of plant fibres and their composites is reviewed and studied.

#### 8.1.3.1 Yarn structure

Due to the discontinuous length of technical plant fibres, the manufacture of aligned PFRPs requires the reinforcement to be in the form of staple fibre yarns/rovings, which have a twisted structure. Although twist facilitates yarn processability, it has several detrimental effects on the composites produced from such twisted yarn reinforcements; one of which is fibre obliquity and misalignment. This results in a drastic drop in composite mechanical properties.

In this study, a novel mathematical model is developed to predict the influence of yarn structural parameters (twist level, compaction, density) on composite tensile strength. The model is based on *i)* the modified rule of mixtures for PFRPs, *ii)* well-defined structure-property relationships in an idealised twisted staple fibre yarn, and *iii)* the Krenchel reinforcement orientation efficiency factor. The developed model includes a corrected orientation efficiency factor of $\cos^2(2\alpha)$, where $\alpha$ is the yarn surface twist angle. The model has been validated with extensive experimental data from Goutianos and Peijs [1] and is found to be a near-perfect fit (with $R^2 = 0.950$). Experimental data from other studies (namely [2]) on aligned yarn reinforced PFRPs are also used for further verification. An interesting inference of the derived model is that employing yarns with $\alpha > 26°$ or $\alpha > 32°$ as composite reinforcements will reduce the reinforcement orientation efficiency factor as in a 2D-random and 3D-random composite, respectively.

#### 8.1.3.2 Ply orientation

While unidirectional composites provide optimum mechanical properties in one direction, the highly anisotropic nature of plant fibres and their aligned composites implies that off-axis loads have a significant influence on the mechanical behaviour of aligned PFRPs.

Investigating the response of PFRPs to off-axis tensile loads, conventional composite micro-mechanical models are found to be in good agreement with the experimental data, suggesting that reliable prediction of PFRP off-axis properties is possible. The application of such models has also enabled the determination of, otherwise difficult to measure, material properties, such as the fibre shear and transverse modulus. As observed in conventional FRP's, off-axis loaded PFRPs fail by three distinct fracture modes in three different off-axis ranges, where each fracture mode produces a unique fracture surface.

A key finding of this study is that due to the non-linear stress-strain response of PFRPs, the apparent stiffness of the composite reduces by ~30% in the strain range of 0.05–0.25%. In addition, through cyclic tests on the composites, the elastic strain limit is found to be only ~0.15%. This has major implications on the strain range to be used for the determination of the composite elastic Young's modulus. Consequently, it is proposed that the tensile modulus for PFRPs should be measured in the strain range of 0.025–0.100%. It is argued that the non-linear stress-strain response (decreasing 'apparent' stiffness with increasing strain) of single plant fibres has been transferred to the resulting PFRPs.

### 8.1.4 *Chapter 6*: Evaluation of fatigue performance

There is a noticeable lack of fatigue data on PFRPs which seriously limits their prospective use in fatigue-critical structural components. To provide a complete set of fatigue data on aligned PFRPs, S-N lifetime diagrams were constructed to specifically investigate the effect of *i)* plant fibre type/quality, *ii)* fibre volume fraction, *iii)* textile architecture, and *iv)* stress ratio, on PFRP cyclic-loading behaviour. At each stage, the fatigue performance of PFRPs has been compared to that of GFRPs. To facilitate fatigue design and life prediction of a PFRP component, a complete constant-life diagram has also been generated.

It has been demonstrated that power-law regression lines are a good fit to S-N fatigue data for PFRPs ($R^2 > 0.95$), and thus useful in predicting the fatigue life of PFRPs. While plant fibre type, plant fibre quality, textile architecture and composite fibre content have a significant impact on the static (tensile) properties of the PFRP, they

have little impact on the material fatigue strength coefficient *b* (which dictates the slope of the S-N curve). In essence, higher static properties are a sign of superior fatigue loading capacities throughout the lifetime of PFRPs. Increasing stress ratios lead to improved fatigue performance (increasing *b*) in PFRPs. Fatigue fracture mechanisms and modes are the same for all plant fibre types, but depend on fibre content, textile architecture and load regimes (stress ratios). Although the absolute fatigue performance of GFRPs is far superior to PFRPs, it is a revelation to find that fatigue strength degradation rates are lower in PFRPs than in GFRPs.

### 8.1.5 *Chapter 7*: The potential of plant fibres in structural applications

Using composite small wind turbine blades as a case study, the question is directly addressed: Are PFRPs potential alternatives to GFRPs for structural applications? Two identical 3.5-meter composite rotor blades (suitable for an 11 kW turbine) were built from flax/polyester and E-glass/polyester. It is found that although the flax/polyester blade is 10% lighter than the E-glass/polyester blade (fibre mass saving of 45%), the materials cost of the former is almost 3 times more than the latter. It begs mention that under current market conditions, plant fibre reinforcements, in the form of yarns/rovings, are not a cost-viable alternative to E-glass. Furthermore, comparing the estimated cumulative embodied energy of the flax and E-glass blade, it is found that the flax blade has an up to 15% larger eco-impact than the E-glass blade. This is due to the high embodied energy of aligned flax reinforcements; while the energy required in the cultivation of plant fibres is low (4-15 MJ/kg [3-7]), further processing steps (*e.g.* retting and spinning) can significantly increase the cumulative energy demand to 54-118 MJ/kg for flax sliver and 81-146 MJ/kg for flax yarn [4-6, 8]. Note that conversion from slivers/yarns to fabrics would require further energy inputs. It is also suggested that to truly reduce the eco-impact of the final product, noting the large negative contribution of the matrix and core materials to the eco-impact, developing high-performance bio-based (or at least bio-sourced) matrix and core materials is a critical step in the wide acceptance of PFRPs as sustainable materials.

Through static flap-bending testing of the blades (in accordance to certification standards), the mechanical properties of the two blades were compared. It is confirmed that like the E-glass/polyester blade, the flax/polyester blade satisfies the design and structural integrity requirements for an 11 kW turbine, under normal operation and worst case loading. Hence, flax rovings are a potential structural replacement to E-glass, particularly for small wind turbine blade applications. While the displacement-load curve is linear for the E-glass blade, it is non-linear for the flax blade. This is consistent with the fact that plant fibres and their composites have a non-linear stress-strain curve, while E-glass and its composites have a linear stress-strain curve. This highlights the differing stress-strain accumulation mechanisms in natural materials. The failure load and corresponding tip displacement of the flax blade are ~80% and ~250% that of the E-glass blade, respectively. The substantially higher tip deflection of the flax blade is proof of its flexibility and almost a concern. The mean flexural rigidity of the flax and E-glass blades is 24.6 $kNm^2$ and 43.4 $kNm^2$. While it is demonstrated that the absolute and specific properties of the composites (*i.e.* flat laminate plaque) are transferred to the blade (*i.e.* component/structure), it is argued that there is a critical trade-off between component weight savings and component stiffness; for similar stiffness performance of a flax blade to an E-glass blade, weight savings cannot be achieved. Furthermore, while increasing the flax fibre content to enhance the stiffness of the flax blade stiffness may be an attractive option, this would have a substantial detrimental impact on the economic cost and eco-impact of the flax blade.

It is concluded that currently aligned flax reinforcements are a light weight and structural, but not low-cost or sustainable, alternative to conventional aligned E-glass reinforcements. Hence, despite the fact that yarn reinforced PFRPs demonstrate good potential for structural applications and their properties are well-predicted through (conventional and novel) micro-mechanical models, the development of low-cost sustainable aligned plant fibre intermediate products (yarns/rovings/fabrics) is critical to the commercialisation of the material technologies and its wide acceptance as a high-performance green material in industry and the wider society.

## 8.2 RECOMMENDATIONS FOR FUTURE WORK

In light of the work performed, a number of topics are proposed for future work. Some important improvements or studies that could be undertaken in terms of material and manufacturing process development and characterisation are:

- Develop cost-viable aligned plant fibre intermediate products (such as wrap-spun yarns and prepreg tapes) that are more suitable for composites applications rather than textile applications. Consider the potential of utilising fibres that are extracted from non-standard retting processes (*e.g.* biotechnical retting [9]) with minimal processing. It would also be of interest to conduct life-cycle analyses (such as those conducted by [4, 8, 10, 11]) to determine if processed plant fibre reinforcements (in the forms of yarns, fabrics and so on) are sustainable alternatives to traditional E-glass reinforcements.
- Investigate alternative composite manufacturing techniques (suitable for small wind turbine blade manufacture) that enable production of PFRPs with higher fibre volume fractions, such as vacuum-assisted resin transfer moulding and prepregging technology (as initiated recently by other researchers [12, 13]).
- Investigate the properties of aligned plant yarn/roving reinforced bio-based thermoset matrix composites. Examples of bio-resins that could be considered include plant seed-oil–based epoxies (such as those developed by Prof. Wool's group [14, 15]) and hemicellulose–based furan (polyfurfural alcohol) [16].
- Investigate the properties of hybrid composites (*e.g* carbon/flax reinforcements) to meet certain structural integrity requirements, as demonstrated by Mikkelsen *et al.* [17] in developing a flax/carbon wind turbine blade.

In this thesis, the tensile and fatigue behaviour of aligned PFRPs has been thoroughly investigated for various composite parameters and the structural potential of a plant fibre small wind turbine blade has also been demonstrated. However, to consider PFRPs for structural applications, specifically small wind turbine blades, some aspects that need further research include:

- Water sorption properties of PFRPs and particularly its effect on *i)* component dimensional stability, *ii)* tensile mechanical properties, and *iii)* cyclic-loading behaviour. While there are several studies, including [18-25], have investigated the mechanism of water sorption in PFRPs and its (dubious but) generally detrimental effects on the physio-mechanical properties, it is suggested that future studies should consider the effect of protective coatings that are conventionally applied on components (*e.g.* gel-coats and paints) and the effect of one-sided exposure, to truly assess the impact on the design life of a PFRP component.
- The compressive properties of PFRPs are not well-researched, and where studied [26-28] the properties are found to be impressive for the plant fibre (mean compressive strength of 1200 ± 370 MPa [26]) but poor for the composites (on the order of 80 MPa, similar to the compressive strength of the matrix [27]). These need to be investigated and characterised, particularly as a function of fibre content and textile architecture.
- Due to variations in wind velocity, rotor blades typically experience variable-amplitude (rather than constant-amplitude) fatigue loading. In addition, the fatigue loads are not only acting along the blade length (*i.e.* tension and compression), but are also torsional and flexural. Hence, it is of interest to evaluate the multi-axial fatigue behaviour of PFRPs, particularly under variable-amplitude loading. This has not been studied in literature so far.
- Talreja [29] argued and demonstrated that conventional FRPs follow a strain-controlled model of fatigue (rather than a stress-controlled model). Talreja clarified that the strain-life curves of FRPs, where strain is defined as the maximum strain attained in the first cycle of a load-controlled fatigue test, may be thought of in terms of three regimes (relating to the fibre, interface and the matrix) within which separate mechanisms control fatigue failure. The three regimes are: Region I (low-cycle fatigue) where catastrophic fibre breakage leads to failure within the experimental scatter-band for composite failure strain in a static test; Region II (intermediate cycles) where progressive fibre-bridged

matrix cracking and/or interfacial shear failure is dominant; Region 3 (high-cycle fatigue) where failure initiates in the matrix but is arrested by the fibres. To date, the limited studies on fatigue of PFRPs (including the one conducted in *Chapter 6*) employ a stress-controlled fatigue model. It would be of interest to study the fatigue behaviour of PFRPs through strain-life curves, which may provide more appropriate and accurate fatigue life predictions.

- For structures manufactured through infusion processes, flow modelling is also very relevant. It is of interest to investigate the effect of plant yarn structure on flow front evolution and fill time. Employing various yarn construction and fibre volume fractions (and thus yarn and preform permeability) would also allow studying the formation of voids in PFRPs. This has not been studied for PFRPs specifically, but similar studies have been conducted on conventional FRPs.

For structural applications, it becomes necessary to be able to reliably predict the response of a material/component to specific load scenarios. While this thesis does attempt to develop and validate predictive models (based on the rule of mixtures and conventional micro-mechanical models) on the tensile and fatigue properties of aligned yarn reinforced PFRPs, some aspects that require further research include:

- Developing finite element models to predict PFRP mechanical properties based on the properties of the individual constituents derived from experiments, and comparing it with rule of mixture predictions to validate the applicability of the micromechanics to PFRPs.
- In combination with the above, it may be useful to model the effect of reinforcing yarn construction and mechanical properties on composite mechanical properties. As the effect of fibre mechanical properties on yarn mechanical properties has been studied by several studies, and the effect of yarn mechanical properties on impregnated yarn mechanical properties has also been studied, if a mathematical model is developed to understand the effect of reinforcing yarn properties on composite properties, a complete integrated model can be built, which links the fibre, yarn and composite mechanical properties. Certainly, the models would need to be validated with experimental data.

- Fatigue testing with statistical analysis (and thus many more samples). This will not only improve the accuracy of the S-N regression curves but also improve the confidence in using constant-life diagrams for component fatigue life prediction. The DOE matrix for fatigue testing should also include more test frequencies, stress ratios and composite parameters. It would also be of interest to conduct a fatigue test on the actual component (*i.e.* small wind turbine blade) and compare with the estimated fatigue life obtained from the constant-life diagram.

## 8.3 REFERENCES


1. Goutianos S, Peijs T. The optimisation of flax fibre yarns for the development of high-performance natural fibre composites. *Advanced Composites Letters*, 2003, 12(6): p. 237-241.
2. Baets J, Plastria D, Ivens J, Verpoest I. Determination of the optimal flax fibre preparation for use in UD-epoxy composites, in *4th International Conference on Sustainable Materials, Polymers and Composites*. 6-7 July 2011. Birmingham, UK.
3. Joshi S, Drzal LT, Mohanty AK, Arora S. Are natural fiber composites environmentally superior to glass fiber reinforced composites? *Composites Part A: Applied Science and Manufacturing*, 2004, 35: p. 371-376.
4. Dissanayake N, Summerscales J, Grove SM, Singh MM. Life cycle impact assessment of flax fibre for the reinforcement of composites. *Journal of Biobased Materials and Bioenergy*, 2009, 3(3): p. 1-4.
5. Dissanayake N, Summerscales J, Grove SM, Singh MM. Energy use in the production of flax fiber for the reinforcement of composites. *Journal of Natural Fibers*, 2009, 6(4): p. 331-346.
6. Summerscales J, Dissanayake N, Virk AS, Hall W. A review of bast fibres and their composites. Part 2 – Composites. *Composites Part A: Applied Science and Manufacturing*, 2010, 41(10): p. 1336-1344.
7. Steger J. Light weight! No matter what the costs? Plant fibres for light weight automotive applications. *Journal of Biobased Materials and Bioenergy*, 2010, 4(2): p. 181-184.
8. Le Duigou A, Davies, P, Baley, C. Environmental impact analysis of the production of flax fibres to be used as composite material reinforcement. *Journal of Biobased Materials and Bioenergy*, 2011, 5(1): p. 153-165.
9. Oksman K. High quality flax fibre composites manufactured by the resin transfer moulding process. *Journal of Reinforced Plastics and Composites*, 2001, 20(7): p. 621-627.
10. Le Duigou A, Deux JM, Davies, P, Baley, C. PLLA/flax mat/balsa bio-sandwich - Environmental impact and simplified life cycle analysis. *Applied Composite Materials*, 2012, 19: p. 363-378.
11. Dissanayake N. *Life cycle assessment of flax fibres for the reinforcement of polymer matrix composites*. PhD, 2011. University of Plymouth: Plymouth, UK.
12. Phillips S, Baets J, Lessard L, Hubert P, Verpoest I. Characterization of flax/epoxy prepregs before and after cure. *Journal of Reinforced Plastics and Composites*, 2013, In Press. doi: 10.1177/0731684412473359.

13. Meredith J, Coles SR, Powe R, Collings E, Cozien-Cazuc S, Weager B, Müssig J, Kirwan K. On the static and dynamic properties of flax and Cordenka epoxy composites. *Composites Science and Technology*, 2013, 80: p. 31-38.
14. Wool R, Sun XS. *Bio-based polymers and composites*, 2005: Elsevier Science & Technology Books.
15. Khot S, Lascala JJ, Can E, Morye SS, Williams GI, Palmese GR, Kusefoglu SH, Wool RP. Development and application of triglyceride-based polymers and composites. *Journal of Applied Polymer Science*, 2000, 82(3): p. 702-723.
16. Arnold E, Weager, BM, Hoydonckx HE, Madsen B. Next generation sustainable composites: Development and processing of furan-flax biocomposites, in *17th International Conference on Composite Materials*. 27-31 July 2009. Edinburgh, UK.
17. Mikkelsen L, Bottoli F, Pignatti L, Andersen TL, Madsen B. Material selection and design aspects of small wind turbine blades, in *Indo-Danish Workshop on Future Composites Technologies for Wind Turbine Blades*. 2012. Delhi, India.
18. Madsen B, Hoffmeyer P, Lilholt H. Hemp yarn reinforced composites – III. Moisture content and dimensional changes. *Composites Part A: Applied Science and Manufacturing*, 2012, 43(11): p. 2151-2160.
19. Pickering K, ed. *Properties and performance of natural-fibre composites*. 2008. CRC Press LLC: Boca Raton.
20. Espert A, Vilaplana F, Karlsson S. Comparison of water absorption in natural cellulosic fibres from wood and one-year crops in polypropylene composites and its influence on their mechanical properties. *Composites Part A: Applied Science and Manufacturing*, 2004, 35: p. 1267-1276.
21. Shahzad A, Isaac DH. Fatigue properties of hemp fibre composites, in *17th International Conference on Composite Materials (ICCM-17)*. 2009. Edinburgh, UK.
22. Rautkari L, Hill CAS, Curling S, Jalaludin Z, Ormondroyd G. What is the role of the accessibility of wood hydroxyl groups in controlling moisture content? *Journal of Materials Science*, 2013, 48(18): p. 6352-6356.
23. Madsen B. *Properties of plant fibre yarn polymer composites - An experimental study*. PhD, 2004. Technical University of Denmark: Lyngby, Denmark.
24. Saikia D. Studies of water absorption behavior of plant fibers at different temperatures. *International Journal of Thermophysics*, 2010, 31(4-5): p. 1020-1026.
25. Dhakal H, Zhang ZY, Richardson MOW. Effect of water absorption on the mechanical properties of hemp fibre reinforced unsaturated polyester composites. *Composites Science and Technology*, 2007, 67(7-8): p. 1674-1683.
26. Bos H, van den Oever MJA, Peters OCJJ. Tensile and compressive properties of flax fibres for natural fibre reinforced composites. *Journal of Materials Science*, 2002, 37: p. 1683-1692.
27. Bos H, Molenveld K, Teunissen W, van Wingerde AM, van Delft DRV. Compressive behaviour of unidirectional flax fibre reinforced composites. *Journal of Materials Science*, 2004, 39: p. 2159-2168.
28. Bos H. *The potential of flax fibres as reinforcement for composite materials*. PhD, 2004. Technische Universiteit Eindhoven: Eindhoven, Netherlands.
29. Talreja R. Fatigue of composite materials: damage mechanism and fatigue life diagrams. *Proceedings of the Royal Society of London. Series A, Mathematical and Physical Sciences*, 1981, 378: p. 461-475.

# 9 APPENDICES

## 9.1 APPENDIX A: PHYSICAL PROPERTIES OF THE REINFORCING YARNS*

This appendix is in reference to the plant fibre materials used in this study. Specifically, it details the analysis of the physical properties of the plant fibre yarns.

### 9.1.1 Experimental

#### 9.1.1.1 Materials

Four plant fibre spun yarns/rovings have been used for this research study (Table A.1). Yarns are named according to the fibre type (denoted by first initial) followed by the twist level in turns per meter (tpm); so J190 would be a jute yarn with a twist level of 190 tpm. F50 is a S on Z twist blend of flax and polyester, where the latter is used as a binder yarn (13 wt%). F20 roving is alkali treated during production, while J190 yarn is lubricated with jute batching oil for ease in spinning.

**Table A.1. List of plant fibre materials and their datasheet properties.**

| Yarn ID | Fibre type | Linear density [tex] | Twist level [tpm] | Supplier | Notes |
|---|---|---|---|---|---|
| **J190** | Jute | 250 | 190 | Janata and Sadat Jute Ltd. (Bangladesh) | Z-twist yarn, oil used during spinning |
| **H180** | Hemp | 285 | 180 | Safilin (Poland) | Z-twist yarn, naturally dirty |
| **F50** | Flax | 250 | 50 | Composites Evolution (UK) | Z-twist yarn, plied with S-twist polyester |
| **F20** | Flax | 400 | 20 | Safilin (France) | Z-twist yarn, NaOH treated during production |

* This appendix is based on the peer-reviewed journal article:

Shah DU, Schubel PJ, Licence P, Clifford MJ. Hydroxyethylcellulose surface treatment of natural fibres: the new 'twist' in yarn preparation and optimization for composites applicability. *Journal of Materials Science*, 2012, 47(6): p. 2700-2711.

Preliminary to this study, the mean linear density of each yarn $\bar{\rho}$ (Table A.2) was measured from the average weights of ten 1 m yarn samples using a microbalance. The difference in mean between the datasheet and measured linear density was tested using a t-test ($\alpha = 0.05$). The deviation from the nominal linear density was found to be statistically significant for J190 and F50 ($p << 0.01$ and $p = 0.015$) but insignificant for H180 and F20 ($p = 0.23$ and $p = 0.45$). Plant fibres can hold 5-15% moisture by weight [1], hence moisture content of the yarns could be a reason for the observed differences; particularly for J190 as it was produced in humid country.

**Table A.2. Yarn fineness properties and effect of HEC treatment.**

| Yarn | Linear Density [tex] | | Increase in mass upon HEC treatment [%] |
|---|---|---|---|
| | Datasheet | Measured | |
| **J190** | 250 | 206 ± 21 | 1.555 ± 0.753 |
| **H180** | 285 | 278 ± 17 | 1.346 ± 0.274 |
| **F50** | 250 | 229 ± 22 | 1.959 ± 0.644 |
| **F20** | 400 | 396 ± 16 | 2.460 ± 0.426 |

#### 9.1.1.2 HEC treatment

To study the effect of HEC treatment on yarn characteristics, the yarns were painted with 0.6 wt% aqueous HEC solution (purchased from the Dow Chemical Company under the trade name Cellosize HEC QP-52000H; density of 1.4 $gcm^{-3}$) and then dried in an oven at 60 °C for 30 mins. Although the method of HEC treatment is crude with little control over film thickness, it is effective and commercially applicable, particularly in low technology environments. Before any testing, the yarns were given 24 hours at 20°C ± 1°C to reach equilibrium. The binding agent is used in an identical manner to fabricate unidirectional mats for the production of composites.

To determine the amount of HEC deposited onto the yarn, first the ten 1m sample yarns previously used to measure the yarn linear density were treated with HEC and

the new weights were measured. From this the difference in the weights of the treated and untreated yarns was calculated and the increase in mass upon treatment was determined (Table A.2). HEC treatment is shown to increase the mass of the yarns by 1.35-2.50%.

#### 9.1.1.3 Yarn characterization

There are several techniques which have been used to measure the density of low-density fibres [2, 3]. The use of Archimedes buoyancy principle (ASTM-D3800-99) with different density liquids (particularly oils and ethanol) [1, 4], density gradient columns using mixtures of varying density liquids (ASTM 1505–03), and liquid pycnometry [5] are well documented. However, these either produce inaccurate readings, rely heavily on well calibrated systems or require the test liquid density to be higher than that of the fibre specimen [2]. Additionally, the use of liquids makes the process messy. Often the air cavities in the fibres (lumen) and yarns are not accounted for [6-9] (and references therein) which give overestimates of fibre/yarn cross-sectional areas leading to inaccurate conversion of loads into stresses from mechanical tests.

Here, gas pycnometry and optical microscopy (OM) are used. The pycnometric method allows measurement of the yarn density and indirect calculation of the yarn diameter (or cross-sectional area), whereas the microscopy technique enables measurement of the yarn diameter and indirect calculation of the yarn density. However, microscopy techniques provide apparent (fibres and air) yarn properties, whereas pycnometry provides true (only fibres) yarn properties. A cross-comparative study is performed to suggest a test method dedicated for plant fibre density measurements using pycnometry and to discourage the use of the prevalent OM method to determine yarn/fibre properties such as diameter.

Pycnometry

A calibrated Micromeritics AccuPyc 1330 gas pycnometer, with helium as the displacement gas, was used to measure the true density of the plant fibre yarns $\rho_f$ [3, 10]. This instrument works by measuring the amount of displaced gas (Fig. A.1). The pressures observed upon *i)* filling the specimen chamber (with volume $V_r$) $P_1$ , and

then *ii)* evacuating it into a second empty expansion chamber (with volume $V_e$) $P_2$, allows the computation of the sample solid phase volume $V_s$ (Eq. A.1). The final density reading $\rho_f$ was the mean reading from three samples, where each density reading was an average of five systematic readings from five purges and runs. A purge pressure of $P_1$ = 19.0 psig and equilibrium rate of 0.05 psig/min was used. The mass of the sample is measured on a microbalance.

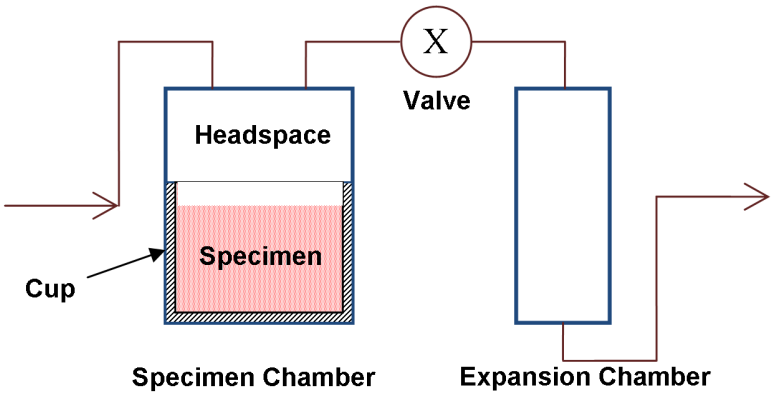


**Fig. A.1. Schematic of a gas pycnometer.**

$$V_s = V_r - \frac{P_2}{P_1 - P_2} V_e \qquad \text{Eq. A.1}$$

The true cross-sectional area $A_t$ of the yarn (no air) was then determined using Eq. A. 2 and the previously measured yarn linear density $\bar{\rho}$ in Table A.2.

$$A_t = \bar{\rho} / \rho_f \qquad \text{Eq. A.2}$$

Optical Microscopy

The other method employed to determine fibre density involves the measurement of the apparent fibre diameter using an OM (10× magnification). The average apparent yarn diameter (fibres and air) $d_a$ was determined by the projection of twenty-five random yarn samples.

The apparent yarn diameter was used to calculate the apparent circular yarn cross-sectional area $A_a$, which was used in conjunction with the measured yarn linear density $\bar{\rho}$ to obtain the apparent yarn density $\rho_y$ (Eq. A.3).

$$\rho_y = \overline{\rho} / A_a \qquad \text{Eq. A.3}$$

The twist angle at the surface $\theta_r$ was also measured. To test for correlation between twist angle and apparent yarn diameter, measurements were recorded pair-wise on the same location on the yarn.

In ring-spun yarns, the twist angle of a fibre is dependent on its location in the yarn cross-section; fibres at the surface are twisted more than fibres in the core of the yarn. Applying reasonable assumptions proves that the mean twist angle $\theta_{mean}$ is a function of the fibre twist angle at the yarn surface only [5] and hence can be easily calculated (Eq. A.4).

$$\theta_{\text{mean}} = \theta_r + \frac{\theta_r}{\tan^2 \theta_r} - \frac{1}{\tan \theta_r} \qquad \text{Eq. A.4}$$

The packing fraction of a yarn $\emptyset$ was determined using the true and apparent yarn densities obtained from pycnometry and microscopy, respectively (Eq. A.5) [11].

$$\phi = V_{fibre} / V_{yarn} \approx \rho_y / \rho_f \qquad \text{Eq. A.5}$$

### 9.1.2 Results and Discussion

#### 9.1.3 Density

The true and apparent densities of the yarns determined by gas pycnometry and OM are presented in Fig. A.2. It is to be noted that yarn cross-sectional views from the microscope confirmed that all yarns, except F20, were circular in cross-section. The F20 roving, was elliptical in cross-section hence an accurate diameter recording could not be made using OM.

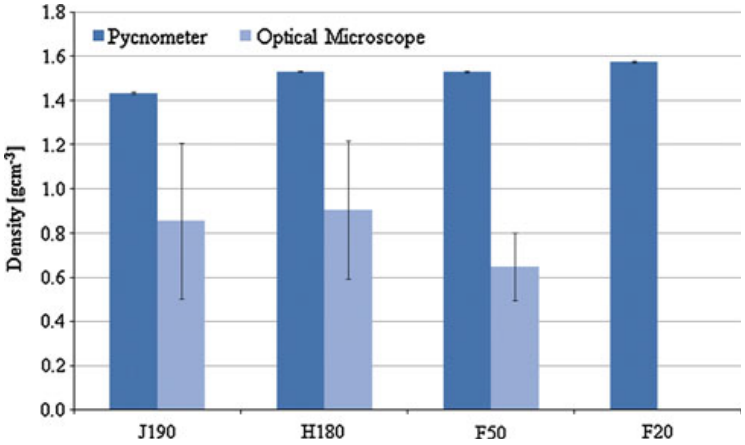


**Fig. A.2. True (through pycnometry) and apparent (through optical microscopy) densities of plant fibre yarns. Error bars denote 1 stdev.**

Quoted literature values for the densities of flax, hemp and jute are usually in the range of 1.4-1.6 $gcm^{-3}$, 1.4-1.6 $gcm^{-3}$ and 1.3-1.5 $gcm^{-3}$, respectively [12]. The density of these cellulose fibres is affected by their chemical composition and is indicative of cellulose content; native cellulose has a density in the range of 1.55-1.64 $gcm^{-3}$ [1, 5, 13]. Jute has a relatively lower content of cellulose and thus displays a slightly lower density. F20 is noticed to have the highest density; this is not only because of high-cellulose content in natural flax, but F20 has undergone NaOH treatment which reduces low-density surface impurities like pectin and wax, thereby increasing the proportion of cellulose in the fibre [14]. The slightly lower density of F50 could be ascribed to the lower density of polyester fibre (~1.4 $gcm^{-3}$) which is used as a binder yarn with flax.

Density measurements from the pycnometer show excellent agreement with literature values for the fibres. The results are also highly repeatable and precise, indicated by the small standard deviation.

Using the indirect method of OM to measure fibre density gives inaccurate readings with large variations. For instance, it suggests that jute has a higher average density than flax. It is to be appreciated that the OM measures the apparent yarn diameter and thus apparent yarn density.

As mentioned earlier, plant yarns have a large amount of air cavities. Firstly, the yarns consist of several fibres each of which is an elongated cell wall with a central air cavity (lumen). Secondly, fibres are twisted together to form a yarn and thus air cavities form between fibres. Helium pycnometry gives high accuracy results by virtue of accurate volume determination of these porous fibres. The gas fills all open-pore air cavities so that the determined volume and density is essentially that of the fibre solid matter. The precision of the results is controlled by the equilibrium rate that is set. OM, on the other hand, relies on accurate diameter measurement for accurate density calculation and hence falls prey to the large variation in diameter along the fibre length, irregularity in cross-sectional shape of plant fibres, and inability to subtract the volume taken up by air cavities in the fibre lumen and between fibres. Despite being laborious, OM still remains a very popular method to determine yarn/fibre diameter due to ease in operation. However, the pycnometric method enables accurate approximation (assuming circular cross-section) of the true yarn diameter.

### 9.1.4 Yarn structure (diameter, twist, compaction)

Measured and calculated yarn structure properties are presented in Table A.3.

**Table A.3. Measured physical properties of the yarns.**

| Yarn | Cross-sectional Area* [$mm^2$] | Yarn diameter* [mm] | Packing fraction | Surface twist angle† [°] | Mean twist angle† [°] |
|---|---|---|---|---|---|
| **J190** | 0.144 | 0.428 | 0.596 | 20.5 ± 5.9 | 14.0 ± 4.2 |
| **H180** | 0.181 | 0.480 | 0.591 | 19.5 ± 4.3 | 13.2 ± 3.0 |
| **F50** | 0.150 | 0.437 | 0.421 | 4.9 ± 3.8 | 3.3 ± 2.5 |
| **F20** | 0.201 | 0.506 | - | 0.3 ± 0.1 | 0.3 ± 0.1 |

***** The cross-sectional area is determined from the pycnometer readings (*i.e.* neglecting air spaces). The yarn diameter is based on the cross-sectional area, assuming circular yarn cross-section.

† The surface twist angles are determined from the OM readings. The mean twist angles are then calculated using Eq. A.4.

The packing fraction of the yarn is determined from the ratio of true and apparent yarn densities. The yarn compaction of J190 and H180 is found to be 0.596 and 0.591, respectively. Conventional twisted (combed) ring-spun yarns have packing densities between 0.50-0.60 [11]. F50 is observed to have a relatively low packing fraction due to less compaction and the fact that it is a plied yarn.

The mean twist angle of the four yarns was determined by OM. The difference in mean twist angles of J190 and H180 is found to be statistically insignificant ($p = 0.44$) but significant for F50 and F20 ($p << 0.01$). Recall that the number in the yarn identity denotes the twist level in tpm. Noting a clear difference in the twist level and mean twist angle of J190/H180 against F50/F20, the yarns can be divided into two categories: high twist (J190 and H180) and low twist (F50 and F20).

The correlation between mean twist angle and packing fraction was also investigated. Although the packing fraction of F20 has not been determined, results from the other three yarns show a very strong positive relationship between the two parameters ($R^2 = 0.999$) indicating that yarn compaction increases with yarn twist. This is concurrent with conventional yarns [11] as fibres in low twist yarns will be loose and have more air gaps between them. Conventional yarns have a packing fraction of 0.5-0.6 [11].

## 9.2 Appendix B: Effect of HEC treatment on composite properties

This appendix is in reference to *Chapter 3.2*, and more specifically addressing the effect of the hydroxyethylcellulose (HEC) binding agent on composite mechanical properties.

### 9.2.1 Experimental

#### 9.2.1.1 Reinforcing materials

250 tex F50 low-twist yarn (flax core yarn with 13 wt% polyester binder; supplied by Composites Evolution (UK)) was chosen as the plant fibre reinforcement. Unidirectional mats from these yarns were to be employed as textile reinforcements for the composites. Unidirectional mats were not only produced using the drum-

winding technique and HEC binding agent described in *Chapter 3.2*, but were also obtained from in the form of stitched fabrics from Formax (UK) Ltd. Both mats have an areal density of about 300 ± 32 gsm.

#### 9.2.1.2 Composite manufacture

Using four layers of the reinforcing mats, composite laminates (250×250 $mm^2$, 3-3.5 mm thick) were fabricated using the vacuum infusion technique described in *Chapter 3.2.* An unsaturated orthophthalic polyester resin (Reichhold Norpol Type 420-100), mixed with 0.25 wt% NL49P accelerator (1% Cobalt solution) and 1 wt% Butanox M50 MEKP initiator, was used as the matrix. Post cure was carried out at 55 °C for 6 h after ambient curing for 16 h.

Making sure that all other parameters were kept constant, the produced composites would allow investigating the effect of HEC treatment on composite mechanical properties.

#### 9.2.1.3 Tensile testing

Longitudinal tensile tests were conducted according to ISO 527-4:1997 using an Instron 5985 testing machine equipped with a 100 kN load cell and a 50 mm extensometer. Six 250 mm long and 15 mm wide specimens were tested for each type of composite at a cross-head speed of 2 mm/min. The tensile modulus $E_c$ (in the strain range of 0.025–0.100%), ultimate tensile strength $\sigma_c$, and tensile failure strain $\varepsilon_c$ were measured from the stress-strain curve.

### 9.2.2 Results and discussion

The tensile properties of the produced composites are presented in Table A.4. Unidirectional composites from both reinforcements, HEC-treated mats and stitched fabrics, were produced at a similar fibre volume fraction of 27.5–27.7 %. The composite tensile strength, stiffness and strain are also very similar at 141-143 MPa, 15.0-15.6 GPa, and 1.55-1.56 %, respectively. In fact, a difference of mean 2-tailed t-test demonstrates that there is no statistically significant difference in the means. Indeed, even the back-calculated fibre tensile strength and modulus is similar at 362-368 MPa and 45-47 GPa, respectively.

**Table A.4. Comparing the properties of F50/polyester composites produced using HEC treated mats and stitched fabrics.**

| Reinforcement | Fibre volume fraction $v_f$ [%] | Composite tensile strength $\sigma_c$ [MPa] | Fibre tensile strength $\sigma_f$ [MPa] | Composite tensile modulus $E_c$ [GPa] | Fibre tensile modulus $E_f$ [GPa] | Composite failure strain $\varepsilon_c$ [%] |
|---|---|---|---|---|---|---|
| **HEC-treated mat** | 27.7 ± 0.1 | 143.0 ± 6.8 | 368.2 | 15.6 ± 0.9 | 47.0 | 1.56 ± 0.04 |
| **Stitched fabric** | 27.5 ± 0.2 | 141.1 ± 9.3 | 361.6 | 15.0 ± 0.7 | 44.9 | 1.55 ± 0.15 |
| **Statistical test**[†] | p = 0.09 | p = 0.70 | - | p = 0.23 | - | p = 0.88 |

[†] Difference of mean 2-tailed t-test ($\alpha = 0.05$). If $p > \alpha$ (i.e. $p > 0.05$), there is no statistically significant difference in the means.

Hence, it can be concluded that composites produced through the HEC-treated mats have similar properties to composites produced through the stitched fabrics.

## 9.3 APPENDIX C: ASSUMPTIONS IN THE IDEALISED STRUCTURE OF A YARN

This appendix is in reference to the assumptions used to develop the idealised structure of a staple fibre yarn in *Chapter 5.3.3*. The idealised structure of a yarn, proposed by Hearle *et al.* [15], is described by the following assumptions:

- The yarn is circular in cross-section (Fig. A.3a)).
- The yarn consists of a very large number of fibres of limited length (Fig. A.3a)).
- The spatial fibre distribution and packing of fibres in the yarn cross-section is uniform. That is, the packing fraction is constant throughout the model (Fig. A.3a)).
- Fibres are assumed to lie on perfect helixes of a constant radius and angle. All those helixes throughout the cross-section have the same number of turns per unit length parallel to the axis of the helix (Fig. A.3a)).
- The radial location of a given fibre is fixed so that the individual fibres are not migrating between the periphery and interior of the yarn, but stay at a given radial location. That is, no fibre migration (Fig. A.3b)).
- A fibre in the centre of the yarn will follow the yarn axis. That is, no fibre micro-buckling (Fig. A.3b)).

- The fibres are assumed to have identical dimensions and properties, are perfectly elastic, and follow Hooke's laws of elasticity and Amonton's laws of friction.
- Transverse stresses between fibres at any point are assumed to be small in all directions perpendicular to the fibre axis.

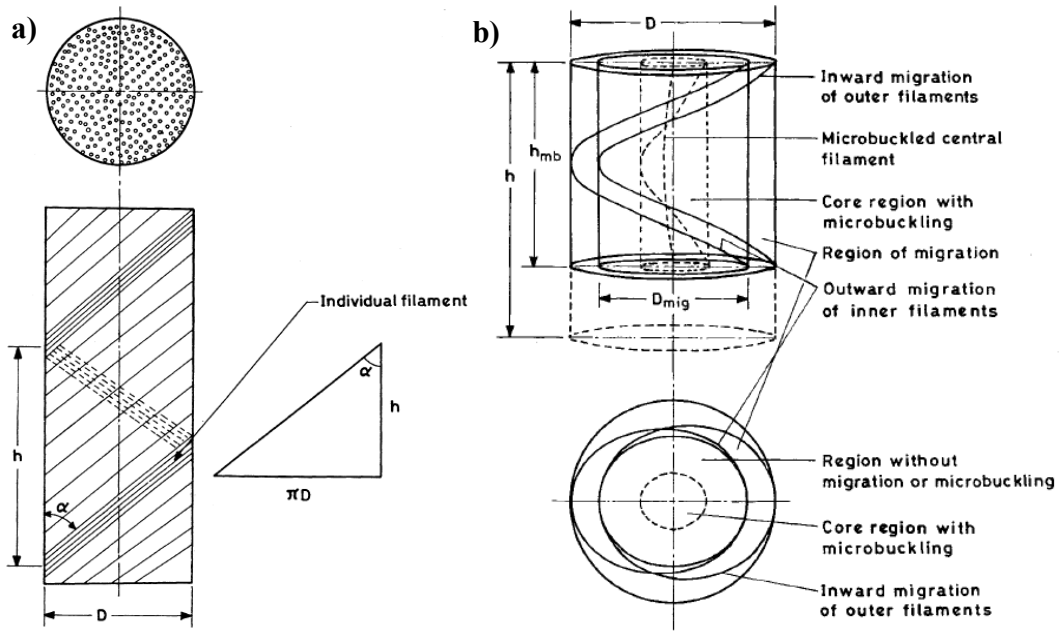


**Fig. A.3. Images (from [16]) showing a) the idealised structure of a staple fibre yarn with a large number of fibres, uniformly distributed in the yarn cross-section and helically located around the yarn axis, and b) the effect of fibre migration and micro-buckling.**

## 9.4 REFERENCES


1. Baley C. Analysis of the flax fibres tensile behaviour and analysis of the tensile stiffness increase. *Composites Part A: Applied Science and Manufacturing*, 2002, 33: p. 939-948.
2. Truong M, Zhong W, Boyko S, Alcock M. A comparative study on natural fibre density measurement. *The Journal of The Textile Institute*, 2009, 100(6): p. 525-529.
3. Rude T, Strait LH, Ruhala LA. Measurement of fiber density by helium pycnometry. *Journal of Composite Materials*, 2000, 34(22): p. 1948-1958.
4. Ghosh I. *Lyocell fiber-reinforced cellulose ester composites - manufacturing considerations and properties*. MSc, 1999. Virginia Polytechnic Institute and State University: Blacksburg, Virginia.
5. Madsen B, Hoffmeyer P, Thomsen AB, Lilholt H. Hemp yarn reinforced composites – I. Yarn characteristics. *Composites Part A: Applied Science and Manufacturing*, 2007, 38: p. 2194–2203.

6. Bonnafous C, Touchard F, Chocinski-Arnault L. Multi scale analysis by acoustic emission of damage mechanisms in natural fibre woven fabrics/epoxy composites, in *14th International Conference on Experimental Mechanics*. 2010. Poitiers, France.
7. Bachtiar D, Sapuan SM, Zainudin ES, Khalina A, Dahlan KZM. The tensile properties of single sugar palm (Arenga pinnata) fibre, in *9th National Symposium on Polymeric Materials*. 2010. Putrajaya, Malaysia.
8. Silva F, Chawla N, Filho RDDT. Tensile behavior of high performance natural (sisal) fibers. *Composites Science and Technology*, 2008, 68: p. 3438-3443.
9. Virk A, Hall W, Summerscales J. Failure strain as the key design criterion for fracture of natural fibre composites. *Composites Science and Technology*, 2010, 70(6): p. 995-999.
10. Pratten N. The precise measurement of the density of small samples. *Journal of Materials Science*, 1981, 16(7): p. 1737-1747.
11. Yilmaz D, Göktepe F, Göktepe O, Kremenakova D. Packing density of compact yarns. *Textile Research Journal*, 2007, 77(9): p. 661-667.
12. Lewin M. *Handbook of fiber chemistry*. Third ed, 2007. Boca Raton: CRC Press LLC.
13. McLaughlin E, Tait RA. Fracture mechanism of plant fibres. *Journal of Materials Science*, 1980, 15: p. 89-95.
14. Mwaikambo L, Ansell MP. Chemical modification of hemp, sisal, jute and kapok fibers by alkalization. *Journal of Applied Polymer Science*, 2002, 84: p. 2222-2234.
15. Hearle J, Grosberg P, Backer S. Structural mechanics of yarns and fabrics. Vol. 1 p. 180, 1969. New York: Wiley-Interscience.
16. Naik N, Madhavan V. Twisted impregnated yarns: Elastic properties. *Journal of Strain Analysis*, 2000, 35(2): p. 83-91.